THE THERMOLYSIS OF ARCHETYPAL NITRATE ESTER AND OXETANE OLIGOMERS

by

Zachary M. Barton

A thesis submitted to the University of Warwick in partial fulfilment

of the requirements for the degree of Doctor of Philosophy

January 1996

Department of Chemistry

University of Warwick

Coventry CV4 7AL

TABLE OF CONTENTS

	Title Page	i
	Table of Contents	ii
	List of Figures	ix
	List of Tables	xv
	Acknowledgements	xvi
	Declaration	xvii
	List of Abbreviations	xviii
	Abstract	xix
	Main Text	1
CHAPTER 1	**INTRODUCTION**	
1.1	The History and Applications of Propellants	1
1.2	The Preparation of PNMMO	5
1.3	The Thermal Degradation of PNMMO	7
1.4	The Effect of Ageing on the Mechanical and Chemical Properties of Polymers	9
1.5	The Thermal Degradation of Nitrate Ester Polymers	11
1.5.1	The Gas Phase Thermolysis Products	11
1.5.2	The Solid Phase Thermolysis Products	14
1.5.3	Kinetic Studies of Nitrate Ester Polymers	15
1.6	The Thermal Degradation of Simple Nitrate Esters	18
1.7	The Photo- and Thermal Degradation of Polyethers	23

1.8 Techniques for Studying the Degradation of Polymers 28

1.8.1 The Application of ESI to the Analysis of Polymers 31

1.8.2 The Electrospray Process 31

1.8.3 The Application of MALDI to the Analysis of Polymers 36

1.9 Column Liquid Chromatography 39

1.10 The Object of this Work 40

CHAPTER 2 EXPERIMENTAL

2.1 Instrumentation 46

2.1.1 Infrared Spectroscopy 46

2.1.1.1 Solution Infrared Spectra 46

2.1.1.2 Infrared Spectra of Polymer Films 46

2.1.1.3 Gas Phase Infrared Spectra 46

2.1.1.4 Heated Infrared Cell 47

2.1.2 Nuclear Magnetic Resonance spectroscopy 47

2.1.2.1 Variable Temperature NMR 48

2.1.2.2 Chemically Induced Dynamic Nuclear Polarisation and Distortionless Enhancement by Polarisation Transfer and 2-D NMR 48

2.1.3 Electron Spin Resonance 48

2.1.4 Electrospray Mass Spectrometry 49

2.1.4.1 The Mass Analyser 49

2.1.4.2 The Electrospray Source 51

2.1.4.3 Sample Introduction 51

2.1.4.4 Data Acquisition 51

2.1.5 Matrix-Assisted Laser Desorption Ionisation 52

2.1.5.1 The Mass Analyser 52

2.1.5.2 Sample Preparation 52

2.1.6 Chemical Ionisation Mass Spectrometry 52

2.1.7 Fast Atom Bombardment 53

2.1.8 Photolysis 53

2.1.8.1 Photolysis of Solutions 53

2.1.8.2 Photolysis of Films 53

2.1.9 Size-Exclusion Chromatography 54

2.1.9.1 Low-Mass Analysis 54

2.1.9.2 High-Mass Analysis 54

2.1.10 Gas Chromatography 55

2.1.11 CHN Analysis 55

2.1.12 Pyrolysis of Polymers in the Oven 55

2.1.13 Photographs of MALDI Samples 56

2.2 Experimental Procedures 57

2.2.1 Electron Spin Resonance 57

2.2.1.1 ESR Spectra of Uncured PNMMO 57

2.2.1.2 ESR Spectra of Cured PNMMO Films 58

2.2.2 Column Chromatography 58

2.2.3 Exposure of PNMMO to Gaseous NO_2 59

2.2.4 Curing of Polymers 60

2.2.4.1 PNMMO 60

2.2.4.2 PEO 60

2.2.5 Addition of Potential Stabilisers to PNMMO 60

2.2.6 Molecular Modelling 61

2.3 Chemicals 62

CHAPTER 3 RESULTS AND DISCUSSION

SPECTRAL ANALYSIS OF UNTREATED PNMMO

3.1 Characterisation of PNMMO by SEC 65

3.2 Characterisation of PNMMO by Infrared Spectroscopy 67

3.3 Characterisation of PNMMO by NMR Spectrometry 69

3.4 Characterisation of PNMMO by ESI 74

3.4.1 ESI Spectra of PNMMO Run at Various cvs 74

3.4.2 ESI Spectra Obtained Using Group I Metal Salts for Cationisation 81

3.4.3 ESI Spectra of PNMMO Obtained Using a DMF/THF Solvent System 90

3.5 Analysis of Untreated Unchromatographed PP260, PP330, PP340 and P-GLYN by ESI 92

3.6 Analysis of PNMMO by MALDI Mass Spectrometry 97

CHAPTER 4 RESULTS AND DISCUSSION

SPECTRAL ANALYSIS OF CHROMATOGRAPHED UNTREATED PNMMO

4.1 Characterisation of the Fractions Obtained from Column Chromatography of Untreated PNMMO by ESI 104

4.2	SEC Analysis of Fractions Obtained by Column Chromatography of Untreated PNMMO	108
4.3	Infrared Analysis of Fractions Obtained by Column Chromatography of Untreated PNMMO	111
4.4	^{1}H and ^{13}C NMR Analysis of Fractions Obtained by Column Chromatography of Untreated PNMMO	112
4.5	SEC and ESI Analysis of the Linear Species Obtained from the Column Chromatography of Untreated PNMMO	125
4.6	Analysis of the Cyclic Tetramer by Chemical Ionisation Mass Spectrometry	131

CHAPTER 5 RESULTS AND DISCUSSION

SPECTRAL ANALYSIS OF PYROLYSED PNMMO

5.1	Characterisation of Pyrolysed PNMMO by SEC	134
5.2	Characterisation of Pyrolysed PNMMO by Solution Infrared Spectroscopy	136
5.3	Characterisation of Pyrolysed PNMMO by ^{1}H and ^{13}C NMR Spectrometry	142
5.4	Characterisation of Pyrolysed PNMMO by ESR	151
5.5	Characterisation of the Pyrolysis Gases of PNMMO by Gas Phase Infrared Spectroscopy	158
5.6	Characterisation of Pyrolysed PNMMO by ESI	166

CHAPTER 6 RESULTS AND DISCUSSION

SPECTRAL ANALYSIS OF PYROLYSED PNMMO AFTER CHROMATOGRAPHY

6.1 Infrared Characterisation of the Fractions Obtained from Column Chromatography of Pyrolysed PNMMO 171

6.2 SEC Characterisation of the Fractions Obtained from Column Chromatography of Pyrolysed PNMMO 174

6.3 ESI Characterisation of the Fractions Obtained from Column Chromatography of Pyrolysed PNMMO 180

6.4 CID Characterisation of the Undegraded Cyclic Tetramer and Low-Mass Thermal Degradation Products of PNMMO 187

6.5 NMR Characterisation of the Fractions Obtained from Column Chromatography of Pyrolysed PNMMO 195

CHAPTER 7 RESULTS AND DISCUSSION

SECONDARY DEGRADATION REACTIONS OF PNMMO AND THE ADDITION OF POTENTIAL STABILISERS TO PNMMO

7.1 The Addition of Potential Stabilisers to PNMMO 208

7.2 Exposure of Untreated PNMMO to Gaseous NO_2 and NO 215

7.3 Exposure of Pyrolysed PNMMO to Gaseous NO_2 227

7.4 Photolysis of Untreated, Cured and Uncured PNMMO 230

7.5 Thermolysis of PP260, PP330, PP340 and P-GLYN 238

CHAPTER 8 RESULTS AND DISCUSSION

MASS SPECTRAL CHARACTERISATION OF THE THERMAL AND PHOTOLYTIC DEGRADATION OF PPO BY ESI AND MALDI

8.1	SEC Analysis of PPO	242
8.2.1	ESI Analysis of Untreated PPO	244
8.2.2	Fragmentation at High cv	247
8.3.1	The Thermal Degradation Mechanisms of PPO	251
8.3.2	ESI Analysis of Pyrolysed PPO	256
8.4	MALDI Analysis of Untreated and Pyrolysed PPO	262
8.5	The Analysis of Photolysed PPO	268
8.5.1	SEC Analysis of Photolysed PPO	268
8.5.2	ESI Analysis of Photolysed PPO	268

CHAPTER 9 CONCLUSIONS AND FUTURE WORK

9.1	Untreated PNMMO	272
9.2	The Pyrolysis of PNMMO	273
9.3	Secondary Reactions of PNMMO	277
9.4	The Pyrolysis and Photolysis of PPO	278
9.5	Future Work	278

APPENDIX: PUBLISHED WORK 281

LIST OF FIGURES

Figure	Title	Follows Page No.
Fig. 1.1	A Schematic Diagram of the Interface of an Electrospray Source to a Triple Quadrupole Mass Spectrometer	33
Fig. 2.1	A Schematic Diagram of the Ion Optics of the Fisons 'Quattro' II Triple Quadrupole Mass Spectrometer	49
Fig. 3.1	SEC Chromatogram of Untreated PNMMO	65
Fig. 3.2	Solution IR Spectrum of Untreated PNMMO	67
Fig. 3.3	250 MHz ^{1}H and ^{13}C NMR Spectra of Untreated PNMMO	69
Fig. 3.4	ESI Spectra of Untreated PNMMO Run at Various cvs	74
Fig. 3.5	A Portion of the ESI Spectrum of Untreated PNMMO	78
Fig. 3.6	ESI Spectra of Untreated PNMMO Obtained Using LiI, NaI and KI	81
Fig. 3.7	ESI Spectra of Untreated PNMMO Obtained Using RbI and CsI	81
Fig. 3.8	The Lowest Energy Conformations of the Na^+ Complexes of the Cyclic Tetramer	86
Fig. 3.9	The Lowest Energy Conformations of the Na^+ Complexes of the Cyclic Pentamer	86

Fig. 3.10	The ESI Spectrum of Untreated PNMMO Obtained Using DMF/THF and KI	90
Fig. 3.11	ESI Spectra of Untreated PNMMO, PP260, PP330, PP340 and P-GLYN	92
Fig. 3.12	ESI Spectra of P-GLYN	94
Fig. 3.13A	MALDI Mass Spectrum of Untreated PNMMO Obtained Using NPOE as a Matrix	98
Fig. 3.13B	MALDI Mass Spectrum of Untreated PNMMO Obtained Using PPO as a Matrix	98
Fig. 4.1	ESI Spectra of the Fractions Obtained During the Column Chromatography of Untreated PNMMO	104
Fig. 4.2	ESI Spectra of the Fractions Obtained During the Column Chromatography of Untreated PNMMO	104
Fig. 4.3	SEC Chromatograms of the Fractions Obtained During the Column Chromatography of Untreated PNMMO	108
Fig. 4.4	250 MHz ^{1}H and ^{13}C NMR Spectra of a Nearly Pure Sample of the Cyclic Tetramer	112
Fig. 4.5	400 MHz ^{1}H and ^{13}C NMR Spectra of Fraction 55 Obtained During the Column Chromatography of Untreated PNMMO	112
Fig. 4.6	400 MHz Narrow Scan ^{13}C NMR Spectrum of Fraction 55	112

Fig. 4.7	The Lowest Energy Conformations Obtained for the Cyclic Tetramer and Pentamer Using the Software Package 'Hyperchem'	120
Fig. 4.8	The ESI Spectrum of Fraction 168 Showing Predominantly Linear Oligomers	125
Fig. 4.9	Portions of the ESI Spectrum of Fraction 168	125
Fig. 4.10	Chemical Ionisation Mass Spectrum of a Sample of the Cyclic Tetramer Obtained from the DRA	131
Fig. 5.1	SEC Chromatograms of Pyrolysed and Untreated PNMMO	134
Fig. 5.2	Solution IR Spectra of Pyrolysed PNMMO	138
Fig. 5.3	IR Difference Spectrum of Pyrolysed PNMMO	140
Fig. 5.4	^{1}H and ^{13}C NMR Spectra of Pyrolysed PNMMO	142
Fig. 5.5	2-D NMR Spectrum of Pyrolysed PNMMO	145
Fig. 5.6	^{13}C NMR Spectrum of Pyrolysed (45 h/145^{0}C) PNMMO Obtained at 90^{0}C	149
Fig. 5.7	ESR Spectrum of Pyrolysed (5 h/150^{0}C) PNMMO Measured at Room Temperature	151
Fig. 5.8	ESR Spectra of a Tempol Labelled Polyurethane (120 - 400 K)	153
Fig. 5.9A	ESR Spectrum of Pyrolysed (15 min/150^{0}C) PNMMO Measured at Room Temperature	155
Fig. 5.9B	ESR Spectrum of Pyrolysed (5 h/150^{0}C) PNMMO After the Addition of Chloroform (l)	155

Fig. 5.10A	Gas Phase IR Spectrum of the Pyrolysis Gases of PNMMO	159
Fig. 5.10B	Gas Phase IR Spectrum of Formaldehyde	159
Fig. 5.11	ESI Spectra of Untreated and Pyrolysed (48 h/130^{0}C) PNMMO	166
Fig. 6.1	Solution IR Spectra of the Fractions Obtained from the Column Chromatography of Pyrolysed PNMMO	172
Fig. 6.2	SEC Chromatograms of the Fractions Obtained from the Column Chromatography of Untreated PNMMO	174
Fig. 6.3	SEC Chromatograms of the Fractions Obtained from the Column Chromatography of Untreated PNMMO	178
Fig. 6.4	The ESI Spectrum of Fraction 43 Obtained from the Column Chromatography of Pyrolysed PNMMO	180
Fig. 6.5	The ESI Spectrum of Fraction 100 Obtained from the Column Chromatography of Pyrolysed PNMMO	185
Fig. 6.6	CID Spectra of the Undegraded and Degraded Cyclic Tetramer	187
Fig. 6.7	^{1}H and ^{13}C NMR Spectra of Fraction 43 Obtained from the Column Chromatography of Pyrolysed PNMMO	195
Fig. 6.8	^{1}H NMR Spectrum of Fraction 38 Obtained from the Column Chromatography of Pyrolysed PNMMO	198
Fig. 6.9	400 MHz ^{1}H NMR Spectrum of the 'Carbonyl Rich' Fraction	202

Fig. 7.1A-H	Plots of Carbonyl and Nitro Absorbance Versus Time for Additive-Containing and Untreated PNMMO Heated at 115, 128, 140 and 147^{0}C	210
Fig. 7.1I	Arrhenius Plot for PNMMO	210
Fig. 7.2	Solution IR Spectra of PNMMO Exposed to NO_2(g) at Room Temperature and 60^{0}C	219
Fig. 7.3	Gas Phase IR Spectrum of the Remaining Gases Obtained after Exposure to PNMMO at 60^{0}C	221
Fig. 7.4	^{1}H NMR Spectra of Pyrolysed PNMMO Before and After Exposure to NO_2(g)	227
Fig. 7.5	A Portion of the ^{1}H NMR Spectrum of Photolysed (350 W Xenon Lamp) PNMMO	231
Fig. 7.6	Solution IR Spectrum of Photolysed (220 W Hanovia Lamp) PNMMO	233
Fig. 7.7	^{1}H and ^{13}C NMR Spectra of Photolysed (220 W Hanovia Lamp) PNMMO	233
Fig. 8.1	SEC Chromatograms of Untreated and Pyrolysed PPO	242
Fig. 8.2	ESI Spectra of Untreated PPO Recorded at Various cvs	244
Fig. 8.3	ESI Spectra of Untreated and Pyrolysed (66 h/155^{0}C) PPO Recorded at a cv of 48	256
Fig. 8.4	Gas Phase IR Spectrum of the Gases Evolved from Pyrolysed PPO	260
Fig. 8.5	MALDI Spectra of Untreated and Pyrolysed (66 h/155^{0}C) PPO Recorded at High and Low Laser Power	263

Fig. 8.6 MALDI Spectra of Pyrolysed (66 h/155^{0}C) PPO Recorded Over 200 Laser Shots and a Single Laser Shot 265

Fig. 8.7 ESI Spectrum of Photolysed (2000 h) PPO Obtained using NH_4Cl to Promote Ionisation 268

LIST OF TABLES

Table	Title	Page No.
Table 3.1	Peak Assignments in the IR Spectrum of PNMMO	67
Table 3.2	Calculated and Experimentally Obtained (cv = 110) Values for the RMM of the Cyclic PNMMO Species ($+NH_4^+$)	77
Table 3.3	Relative Abundances of the Metal Adducts of Cyclic Oligomers in PNMMO	84
Table 3.4	The Relative Energies of the Tetramer and Pentamer Complexes	86
Table 4.1	Table Detailing and Summing the Stereoisomers of the Cyclic Tetramer	119
Table 4.2	Table Detailing and Summing the Stereoisomers of the Cyclic Pentamer	123
Table 4.3	Linear Oligomers in PNMMO and their RMMs	129
Table 6.1	M_n and M_w Values Obtained by SEC for Fractions from Column Chromatography of Pyrolysed PNMMO	174
Table 6.2	CHN Analysis of Untreated PNMMO and Pyrolysed PNMMO Before and After Column Chromatography	177
Table 8.1	Assignments of the Principal Peaks in the ESI Spectrum of Untreated PPO	249/250
Table 8.2	RMM of the Thermal Degradation Products of PPO	253
Table 8.3	Assignments of the Principal Peaks in the ESI Spectrum of Degraded PPO	258/259

ACKNOWLEDGEMENTS

I wish to thank Professor T.J. Kemp, my academic supervisor, for guidance and encouragement throughout this work and for the research studentship.

I express my dearest thanks to all my family for their constant encouragement, especially during my 'write-up'.

I acknowledge Dr. C.J. Samuel and Dr. O.W. Howarth for useful discussion, particularly concerning the interpretation of NMR spectra. Thank-you both.

My thanks go also to Professor K.R. Jennings and Dr. A. Buzy for allowing me to use the electrospray mass spectrometer which proved extremely useful.

Finally my thanks go to my industrial sponsors the Defence Research Agency who funded my work.

DECLARATION

The work described in this thesis is entirely original and my own, except where otherwise indicated.

Parts of this work were presented at conferences in;

1993, 18th Ann. Meeting Polym. Degrad. Discussion Group, Brighton, September.

1995, 17th Ann. Conf. Adv. Stabil. and Polym. Degrad., Lucerne, May.

1995, 20th Ann. Conf. Therm. Degrad. Polym., Glasgow, September.

and selected for oral presentation at the Spring Nat. ACS Meeting in New Orleans (1996).

Parts of the work contained in this thesis have been accepted for, or are awaiting acceptance for publication in the scientific literature:

Barton, Z.M., Kemp, T.J., Jennings, K.R., Buzy, A., *Polymer*, 1995, **36**, 4927. (Research concerning the thermal degradation products and inferred mechanisms of decomposition of poly(propylene oxide) as determined by mass spectrometry).

Barton, Z.M., Kemp, T.J., Jennings, K.R., Buzy, A., *Polymer*, 1996, **??**, ????. (Research concerning the electrospray ionisation mass spectrometric analysis of the untreated PNMMO pre-polymer). Awaiting clearance from the DRA.

Barton, Z.M., Kemp, T.J., Jennings, K.R., Buzy, A., *Polymer*, 1996, **??**, ????. (Research concerning the thermal degradation products and pathways of PNMMO as determined by IR, NMR, ESR and mass spectrometric methods). In preparation.

LIST OF ABBREVIATIONS

amu	atomic mass unit
BDM	1,4-benzenedimethanol
cv	cone voltage
CID	collision-induced dissociation
CIMS	chemical ionisation mass spectrometry
DRA	Defence Research Agency
ESI	electrospray ionisation
ESR	electron spin resonance
GC	gas chromatography
IR	infrared
MALDI	matrix-assisted laser desorption ionisation
NMR	nuclear magnetic resonance
2-NDPA	2-nitrodiphenylamine
NPOE	2-nitrophenyl octyl ether
PEO	poly(ethylene oxide)
PNMMO	poly(3-nitratomethyl-3-methyloxetane)
PPO	poly(propylene oxide)
RMM	relative molecular mass
SEC	size-exclusion chromatography
THN	1,2,3,4-tetrahydronaphthalene
TLC	thin layer chromatography

ABSTRACT

Poly(3-nitratomethyl-3-methyloxetane) (PNMMO) is a nitrate ester pre-polymer which can be cured with an isocyanate and utilised as a binder in solid rocket propellants;

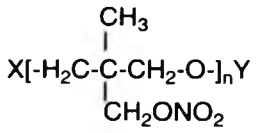

where X and Y are the end groups.

Electrospray ionisation (ESI) mass spectra of untreated PNMMO show that it contains a series of low-mass cyclic and linear oligomers incorporating up to 22 monomer units. Oligomers of higher mass appear not to be detectable by ESI mass spectrometry. The relative abundances of the cyclic oligomer ions in the spectra are affected by various factors but the governing influence is the size of the alkali metal cation used to promote ionisation. The cyclic and linear oligomers can be separated from each other using column chromatography and the cyclic species can be individually characterised by ESI, size-exclusion chromatography (SEC) and ^{13}C nuclear magnetic resonance (NMR) spectroscopy.

Thermal degradation results in the gradual increase in intensity of two main new absorptions around 1729 and 1550 cm^{-1} in the solution infrared (IR) spectrum of PNMMO. The band at 1729 cm^{-1} is attributed to the carbonyl group in a formate ester and the formate proton and carbonyl carbon associated with this compound are clearly visible in the ^{1}H and ^{13}C NMR spectrum at 8.1 and 162 ppm respectively and can be cross-correlated by 2-D NMR. The absorption at 1550 cm^{-1} is attributed to the asymmetric stretch of a nitro group attached to a tertiary carbon. We propose that this nitro species is formed by the recombination of NO_2 following the loss of NO_2 and subsequent elimination of CH_2O from the PNMMO side-chains. The assignment of this nitroalkane was confirmed by ESI and spectroscopic characterisation of a nearly pure sample of the tetrameric nitro species isolated from pyrolysed PNMMO using column chromatography.

The thermal degradation pathways and products of poly(propylene oxide) (PPO) were found to bear some similarities to those of PNMMO. ESI and matrix-assisted laser desorption ionisation (MALDI) mass spectra of thermally and photolytically degraded PPO show that oxidation occurs predominantly at the secondary carbon as opposed to the tertiary carbon.

CHAPTER 1 INTRODUCTION

1.1 THE HISTORY AND APPLICATIONS OF PROPELLANTS

Propellants are explosive materials utilised for the effects of their especially fast combustion for the purpose of propulsion. Propellants are defined as materials which generate a large number of gaseous molecules at high temperature during combustion and which can self-sustain combustion without the presence of added oxidiser; the process features large values for ΔH (exothermic) and ΔS, *viz.*

$$\Delta G = \underset{\text{LARGE (-'VE)}}{\Delta H} - \underset{\text{LARGE (+'VE)}}{T\Delta S}$$

As combustion is a self-sustaining exothermic reaction, both oxidiser and fuel are required to produce a propellant. Propellants are classified by their physical state; thus when a propellant is a liquid, it is termed a liquid propellant and when it is a solid, it is called a solid propellant. Solid propellant rockets have been used in various types of weapons for many years and their history is interwoven with the development of gunpowder, artillery and pyrotechnics. Parchment describing a mixture of honey, saltpetre and sulfur dating back to the 9^{th} century has been found in China, and gunpowder was used by the Chinese as far back as the 10^{th} and 11^{th} centuries and possibly even earlier. It is believed that rocket propellants were first used in the Arab and Western Christian world by the Mongol armies in the early 13^{th} century[1], around the same time as the first recorded description of gunpowder by Andrew Bacon. The development of both rockets and rocket propellants received great interest after they were used to dramatic effect by the Indians against the British at

Travancore at the end of the 18th century and subsequently by the British in the American War of Independence. The constant search to improve the propellants led to the invention of 'smokeless powder' by Vieille in France in 1884 who gelatinised guncotton with ether[2]. Around the same time period nitroglycerine was being developed and manufactured by Alfred Nobel and by the 1880's he had established fifteen factories world wide.

Propellants have uses not only in rockets and guns, but also in gas and pressure generators[3]. Thus the correct choice of propellant is based on its application and different applications require different operating conditions. Both pressure and temperature directly affect the combustion rate of the propellant and these variables must be used to determine the choice of propellant. Rocket propellants operate using gases at high temperatures and pressures (10-300 atm) to generate propulsive forces[3] and the propellant must therefore be chosen with this in mind.

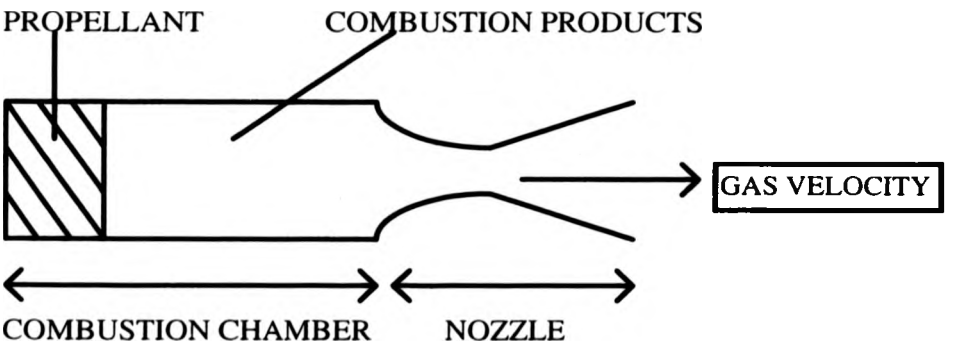

DIAGRAM OF A ROCKET MOTOR[3]

As the propellant burns, gases are evolved into the combustion chamber. The thrust produced by the motor is a direct result of the pressure gradient generated by these gases in

the motor. Thus during 'normal' operation, the flow velocity and pressure of the burned gases is relatively low and approximately constant in the combustion chamber. However as the gases approach the convergent section of the nozzle, the pressure decreases and the flow velocity increases until it becomes approximately sonic in the narrowest region of the nozzle. As the gases flow into the divergent part of the nozzle, the pressure decreases further and the velocity goes supersonic, producing massive thrust.

The solid propellant materials used to power rockets fall into two main categories, namely 'colloidal' and 'composite'. The colloidal propellants were the first to be developed and are based on nitrated organic molecules, such as nitrocellulose (NC). Those utilising a single nitro-organic are termed 'single base'. Those incorporating a distinct pair of materials, as fuel and oxidant, are termed 'double base' propellants. While the single base type of material appeared a century ago, it still finds use today for particular purposes. The principle of this type of propellant is that the organic nitrate provides the 'fuel' in the form of C-H bonds and the powerful oxidant in the form of a nitrate ester, both within a single molecule. This avoids problems of physically intimate mixing of the two necessary ingredients. However, NC and nitroglycerine (NG) were the main energetic components of colloidal propellants for many years and these nitrate esters, particularly nitroglycerine, decompose exothermally at a significant rate even at ambient conditions. While other variables such as temperature and humidity cause this rate to increase, the most dangerous aspect of this process is its autocatalytic nature due to the acidic products formed; thus evolved nitrogen oxides can abstract hydrogen, leading to nitrous and nitric acids. This autocatalysis led to many fires and explosions and it was considered responsible for the loss of many ships and submarines in the first and second World Wars, which led to the development of a second or 'composite' (or double base) class of propellants. This type of

propellant depends on a combination of a fuel (usually aluminium powder) and an oxidant (often ammonium perchlorate), both distributed in an organic matrix, known as a binder, which is normally a flexible polymer. The matrix is then a secondary source of fuel. These materials release greater amounts of energy than the nitro-organics but do present some disadvantages, especially the production of copious clouds of Al_2O_3. The organic matrix is, to some extent, tailorable to specific material requirements, e.g. a specific flexibility (controlled by cross-linking with an isocyanate) and a limiting glass transition temperature, T_g.

Both types of propellant, colloidal and composite, present storage problems especially at sub-tropical or tropical temperatures. The nitrate esters are presumed to decompose via homolysis of the nitrate ester linkage[3], while the composites degrade through denaturing of the rubber of the matrix by cross-linking, oxidation, etc., leading to the development of microcracks and then visually apparent cracks[4,5]. This in turn leads to an increased surface area and undesirably fast burning.

Recent attempts to boost the performance of composite propellants have included the strategy of developing a 'high-energy' binder, which would provide not only the elements of a fuel but also those of an oxidant. Thus the binder would function somewhat like a classical colloidal propellant while acting as a binder. The Defence Research Agency (DRA) decided to produce a hybrid system based on a combustible polymeric binding agent, such as poly(3-nitratomethyl-3-methyloxetane) (PNMMO) which gives energetic rubbery binders. The energy is derived from the nitrate ester groups while the rubbery properties come from the aliphatic backbone. A polyisocyanate, Desmodur N-100, is employed as a curative while ammonium perchlorate is used as the dispersed oxidant. Better performance and higher tailorability are thus obtained. This model of the propellant is somewhat simplified and in

addition to these propellant ingredients many other chemicals are also used to improve performance and tailorability. Thus in its 'ready to use' form, the solid propellant often consists of a 'cocktail' of chemicals including the binder, oxidiser, plasticizer, curing agent, bonding agent, burning rate catalyst, stabiliser, opacifier, flame suppressant and combustion instability suppressant.

Along with their advantages however, it is clear that, like the normal formulations for solid propellants, these hybrid systems possess undesirable features with respect to their environment. In tropical climates, thermal decomposition leads to gas evolution and internal build-up of heat, a process leading to what is known as 'cook-off'. Thus the hybrid system poses the problem of two separate ageing processes; (i) degradation of the nitrate ester group and (ii) changes in the polymer network such as cross-linking or scission resulting from oxidation or hydrolysis. Thus it is clear that an increased thermal stability would be advantageous both in terms of safety and economics; economic requirements favour a shelf life of approximately 20 years, but the DRA suggest that this value is at present considerably lower for PNMMO.

1.2 THE PREPARATION OF PNMMO

PNMMO is prepared by the cationic polymerisation of the monomer, 3-nitratomethyl-3-methyloxetane. The initiator used consists of a mixture of boron trifluoride etherate and 1,4-butanediol.

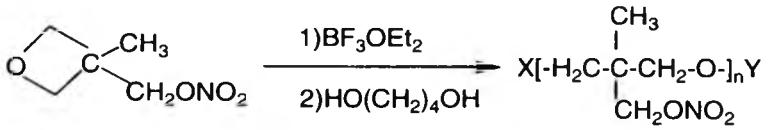

where X and Y correspond to the end groups.

DIAGRAM SHOWING THE PREPARATION OF THE PNMMO PRE-POLYMER

The NMR spectra of PNMMO indicate that both hydroxy and ethoxy end-groups are present in PNMMO[6].

The cure rate for PNMMO is slower than that for conventional polyethers due to a decreased end-group reactivity caused by steric and electronic factors. Dibutyltin dilaurate is found to be an extremely efficient catalyst, reducing the cure time to approximately four days at 60^0C.

2-nitro-diphenylamine (2-NDPA) has been found to be an effective stabiliser when added to cured PNMMO in 1 - 2 % by mass concentrations[1]. The amount of gas produced by cured PNMMO during heating at 100^0C for 40 h was found to be approximately halved on addition of 2-NDPA. This stabiliser of nitrate esters is however thought to act only to reduce the amount of nitrogen-containing species detected by GC/MS and is not thought to influence the rate of carbonyl formation. Clearly a more effective stabiliser is needed.

Prior to the formulation of various potential stabilisers for PNMMO, it is clearly a prerequisite to identify the degradation pathways and products. The extent of the current research in this area is described in the following section.

1.3 THE THERMAL DEGRADATION OF PNMMO

It has been established for many years now that propellants undergo slow thermal decomposition during the course of ageing[7]. Reports obtained from the DRA indicated that little published work was available concerning the degradation pathways and products of PNMMO. However one internal report written subsequent to a conference in Sweden[6] and a paper published by Bunyan *et al.*[1] were acquired from the DRA. Both reports are very similar in content and detail the amounts of various gases evolved during the pyrolysis of cured PNMMO and the effect of the additive, 2-NDPA, on the evolved gases and sol content of cured PNMMO during heating at 100^0C. Only very preliminary results are given, presumably due to the inherent difficulties encountered in the analysis of the cured polymer. However an extensive literature search by us indicated that other published work concerning the thermal degradation of the pre-polymer was available, seemingly originating in a report by Farber *et al.*[8] in 1986 at the Office of Naval Research in Virginia, USA. This report details mass spectrometric investigations performed *in situ* at 150^0C of the pyrolysis mechanisms and low-mass volatile species of 3,3-bis[(methylnitraminomethyl)]oxetane (BMNAMO) and, to a lesser extent, PNMMO. However the mass limit of the spectrometer used was only 100 mass units (mu) and thus the pyrolysis mechanisms are based only on the detectable low-mass volatile species. The scheme proposed for PNMMO is shown over the page.

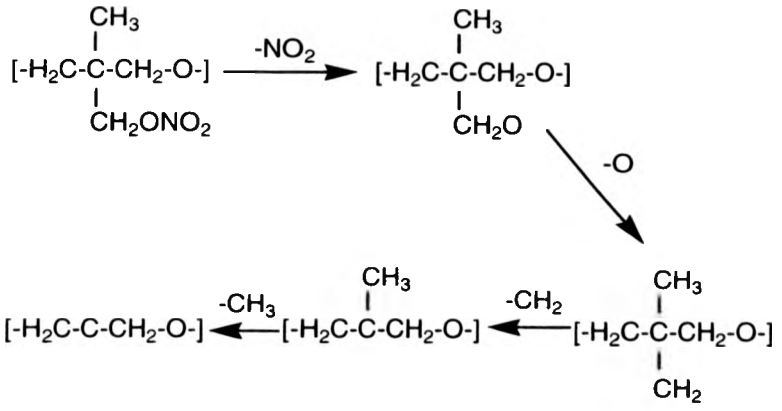

DIAGRAM SHOWING THE SCHEME PROPOSED FOR THE DEGRADATION OF PNMMO BY FARBER[6]

(no free radical symbols were used in this report[6] : the scheme shown is a direct copy from the original)

This scheme clearly reflects the sequential loss of small molecules or radicals comprising the PNMMO side chains and gives no reference to chain scission. Although this mechanism may highlight the degradation products observed *in situ* during mass spectrometric analysis by Farber *et al.*[8], we do not feel this mechanism can truly explain the thermal degradation of PNMMO.

Other reports were also found relating to the thermal degradation of PNMMO but all of these studies[9,10,11] were primarily concerned with the kinetics of weight loss and simultaneous mass and temperature change (SMATCH)/FTIR spectroscopy. SMATCH/FTIR data are generally obtained at heating rates in excess of $100^0C\ s^{-1}$ in order to simulate the combustion of the bulk material in a rocket motor. Rapid-scan FTIR spectroscopy is used to identify the gaseous products near the surface of heated polymer

films (20 - 70 μm) and to determine their relative concentrations in near real-time. The kinetics of mass change can be determined from the mass and temperature change profiles by using a non-isothermal model. The relatively stable gas products, namely CO_2, CO, NO_2, NO, H_2CO and HNO_2 that are detected, indicate that an extensive amount of the decomposition chemistry occurs in the condensed phase. The gaseous products give some indication of the decomposition pathway under fast heating rates although no precise mechanisms are proposed.

Thus it appears that the limited number of publications concerning PNMMO are based nearly entirely on the gas-phase mass spectrometric and IR analyses of the volatile degradation products. No published work appears to be available in many of the areas commonly associated with the degradation studies of polymers such as NMR, photolysis, ESR and solution/solid IR measurements. This is attributed to the relatively recent interest in PNMMO and the greater importance associated with the burn rate and efficiency of the polymer as compared to its slow thermal decomposition.

1.4 THE EFFECT OF AGEING ON THE MECHANICAL AND CHEMICAL PROPERTIES OF POLYMERS

The shape of the solid propellant is based on many factors such as the desired burn rate and its ability to withstand certain pressures, temperatures and mechanical stresses. Thus in addition to the generation of microcracks and then visually apparent cracks in the solid propellant matrix which lead to undesirable burn rates, it is clearly important to realise any chemical and mechanical changes that may occur during the ageing of the propellant. The effect of ageing on the mechanical properties of polymers is reviewed by Verdu[12] who reports that stiffness, modulus, yield stress and rupture properties may all be affected to

varying degrees in different polymers during the course of ageing. Both Verneker *et al.*[13] and Kishore *et al.*[14] have studied the chemical changes during the ageing and decomposition of various composite solid propellants. These authors report that the study of the thermal degradation of propellants is also important from the point of view of the role of the condensed phase reactions during combustion which have been shown to contribute significantly to the combustion process. The build up of both hydrochloric and nitric acids during decomposition of polystyrene/ammonium perchlorate propellants is attributed to an increase in thermal reactivity during the course of degradation. It is proposed[13] that the build up of these acids may influence the thermal degradation rate to a greater extent than the generation of reactive intermediates such as peroxides. This may be particularly important for nitrate ester propellants where the formation of nitrous/nitric acids is possible following the evolution of nitrogen-containing gases such as NO_2.

Accelerated ageing studies of polyurethane- and polybutadiene- based propellants showed that these propellants hardened during ageing and this was attributed to cross-linking reactions. It is also reported that the predominant changes at the exposed surface of the propellant were associated with the binder whereas the oxidiser was the primary component altered in the interior of the propellant. Similarly to many other papers, no degradation mechanisms are proposed, presumably due to the difficulty associated with analysing such a complex mixture of chemicals. Clearly studying the degradation of a propellant consisting of many different chemical substances is inherently complicated and the analysis of the degradation of individual components should be a primary aim.

1.5 THE THERMAL DEGRADATION OF NITRATE ESTER POLYMERS

The thermal degradation of nitrate ester polymers is the subject of only a limited number of reviews and books and most of these, as for PNMMO, report the gases evolved during pyrolysis of the respective polymer. NC, the most extensively researched of all the nitrate ester polymers, appears to be somewhat of an exception and various reports were found concerning both the solid[2,3,15,16,17,18,19] and gas[2,3,20,21,22] phase thermal decomposition products.

1.5.1 THE GAS PHASE THERMOLYSIS PRODUCTS

Many different IR studies of the gases evolved at various pyrolysis temperatures and pressures for nitrocellulose and many other nitrate ester polymers such as poly(vinyl nitrate)[9] (PVN) and poly(glycidyl nitrate)[9] (PGN) often provide conflicting results. The diagram over the page shows the structures of these nitrate ester polymers and some simple nitrate esters namely pentaerythritoltetranitrate[10] (PETN) and triethylene glycol dinitrate (TEGN)[10].

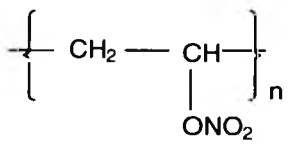

PVN

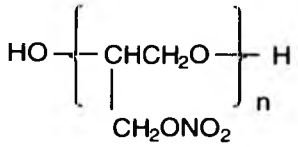

PGN

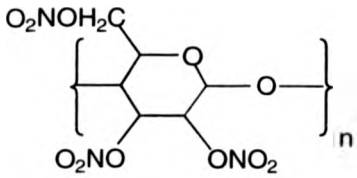

NC

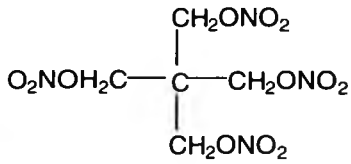

PETN

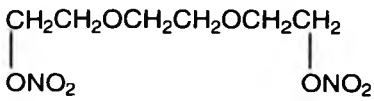

TEGN

DIAGRAM SHOWING THE STRUCTURES OF VARIOUS SIMPLE AND POLYMERIC NITRATE ESTERS

The detection of gaseous NO_2 in the pyrolysis gases of nitrate ester polymers has led researchers to propose drastically different mechanisms to those of other researchers who do not detect NO_2(g). Thus the generally accepted belief that nitrate esters decompose via homolysis of the O-NO_2 bond[11] has been disputed by some authors such as Dauerman and Tajima[3a] and Tranchant[3b] who did not observe NO_2 during the vacuum decomposition of NC. Other authors such as Juhasz and Rocchio[3c] using chromatographic columns to separate gases similarly did not observe NO_2 but attribute this to the reaction of this gas with other

species in the column. Volltrauer *et al.*[22] using chemiluminescence techniques find NO_2(g) to be a major gaseous decomposition product of NC whereas Gelernter *et al.*[18] find only relatively small amounts of NO_2(g). Research in this area is thus fairly intensive but also very contradictory and we attribute this to the extensive condensed phase chemistry that may occur prior to the analysis of the pyrolysis gases using certain analytical methods. A recent paper by Naud *et al.*[23] also shows that the pyrolysis pathways and decomposition rates of various nitramines (octahydro-1,3,5,7-tetranitro-1,3,5,7-tetrazocine, HMX), nitrosamines (6-nitro-1,2-dinitroso-1,2,3,4-tetrahydroquinoxaline) and nitrate esters (cyclohexanol nitrate, NG, propyleneglycol dinitrate and 1-pentanol nitrate) are strongly influenced by the pressures at which thermolysis is performed. The nitramines and nitrosamines studied exhibit significantly different rates of decomposition as the pressure is varied. The reaction rates of most of these compounds decrease with increasing pressure but some exceptions do exist. Secondary nitrate esters are shown to shift their major decomposition pathway from homolysis of the O-NO_2 bond to elimination of HNO_3 in the pressure range 0.4 to 0.8 GPa and as for the nitramines and nitrosamines, most exhibit a decrease in reaction rate with increasing pressure.

Clearly, both the thermolysis conditions and the analytical technique used to detect the pyrolysis gases, greatly influence the relative amounts of gases detected during the thermolysis of nitrate esters; mass spectrometric investigations of the pyrolysis gases performed under reduced pressure will produce significantly different results to gas chromatographic experiments performed at atmospheric pressure. However on the whole the literature concerning NC appears to indicate that significant amounts of NO_2(g) are detected during pyrolysis using the correct experimental conditions and indeed, recent work strongly suggests that the homolysis of the O-NO_2 bond is the primary step during thermal

decomposition of nitrate esters[11,24]. The analysis of the thermolysis gases of nitrate ester polymers such as NC thus gives an indication of the decomposition mechanism of the polymer but clearly does not provide conclusive evidence of reaction pathways as the condensed phase chemistry of the pyrolysis gases is not yet fully understood.

1.5.2 THE SOLID PHASE THERMOLYSIS PRODUCTS

Research concerning the solid phase analysis of the thermal decomposition products of NC also appears somewhat contradictory in some areas. The gradual increase in intensity of a new band around 1740 cm^{-1} in the IR spectrum of NC during thermolysis appears undisputed although the reported wavelength of this band does seem to vary by up to 5 cm^{-1}. The authors of older research papers leave this band either unassigned[17] or tentatively attribute the absorption to an unknown carbonyl species[18]. However more recent work suggests that the absorption around 1740 cm^{-1} is due to both an aldehyde and a carboxyl species seemingly unresolvable in the IR[3]; the presence of a new hydroxyl band around 3400 cm^{-1} is seemingly indicative of the carboxyl species. It is proposed[3] that loss of NO_2 from either of the adjacent O-NO_2 groups results in an oxygen-centred radical which may undergo C-C chain scission to generate an aldehyde. Apparently, good evidence exists to suggest that the loss of NO_2 from one of the two adjacent O-NO_2 groups will result in the subsequent loss of NO_2 from the neighbouring O-NO_2 group[3], producing two aldehyde moieties. The decomposition of the third nitrate ester group in each NC unit is similarly thought to proceed via the loss of NO_2 but the subsequent reactions of the resulting alkoxy radical are thought to be "too complex to be completely understood" [3]. A small proportion (two separate papers) of researchers also document the presence of a band around 1580 cm^{-1} [16] although others report a band around 1560 cm^{-1} [18]. Eisenreich and Pfeil[16] tentatively attribute this

band to a nitrated oxycellulose although neither a structure or a mechanistic scheme is proposed. The fate of the evolved $NO_2(g)$ appears to be unknown although many different reactions are presumably possible including the formation of nitrous/nitric acids. Indeed Oyumi *et al.*[10] propose that the significant quantities of HNO_2 observed in the gas phase IR spectrum of NC pyrolysed at low pressure are indicative of proton transfer reactions involving NO_2 and the polymer.

Batten *et al.*[25] reports the work of various other researchers who have shown that HNO_3 may lead to the acid catalysed hydrolysis of nitrate ester polymers. Clearly, evolved NO_2 and secondary degradation products such as HNO_2/HNO_3 may react with the polymer in a number of different ways and these reactions are most likely dependent on experimental conditions such as temperature and pressure.

1.5.3 KINETIC STUDIES OF NITRATE ESTER POLYMERS

Kinetic studies of weight loss at low heating rates ($dT/dt < 5^0C\ min^{-1}$) for many nitrate ester polymers such as NC[26], PVN[11], PGN[11] and PNMMO[9,11] have been conducted. Similar studies have also been performed to obtain the kinetic constants of weight loss for azide-containing polymers such as GAP[27] and 3,3'-bis(azidomethyl)oxetane (BAMO)[27]. Many kinetic studies have been conducted for NC and generally it is found that the rate laws that describe weight loss from NC at low heating rates are different from those at high heating rates ($dT/dt > 100^0C\ s^{-1}$). Thus a first order autocatalytic model describes NC at low heating rates whereas at high heating rates the rate law is best described by a second order rate law. At low heating rates autocatalysis is attributed to the reactions of $\bullet NO_2$ with $RO\bullet$. After about 50 % weight loss, a discontinuity occurs in the weight loss curve and a second order rate expression better describes the process. This discontinuity is interpreted[9] as the

onset of reactions involving backbone cleavage (although Pfeil *et al.*[15] have measured a significant decrease in molecular weight during the slow thermal decomposition of NC before the decay of nitrate concentration is detected). Like NC, PVN also exhibits first order autocatalytic decomposition at low heating rates whereas PGN and PNMMO exhibit simple first order decomposition. The absence of autocatalytic behaviour for PGN and PNMMO is attributed to both their lower viscosity and lower oxygen balance. Although Chen *et al.*[9] believe the agent of this autocatalytic thermal decomposition to be NO_2, as apparently do many other authors[3], there is some evidence by Batten[25] to suggest that it may be the degradation product formaldehyde. Batten argues that the observation that NO_2, added initially, inhibits the gas-phase thermal decomposition reactions of NG appears inconsistent with NO_2 being the autocatalytic agent. Batten[25] also proposes that as the thermal degradation products of nitramines, such as RDX, are similar to those of nitrate esters, their decomposition mechanisms are also similar. Referring to his previous research which apparently showed that formaldehyde catalysed the decomposition of nitramines, Batten then postulates that this same agent could also be responsible for the autocatalysis of nitrate esters and proposes that the intermediate shown over the page is responsible for the autocatalysis of NG.

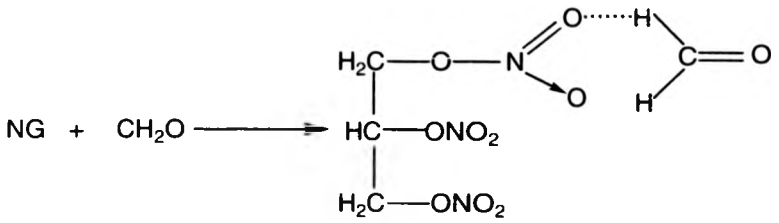

DIAGRAM SHOWING THE INTERMEDIATE PROPOSED TO BE RESPONSIBLE FOR THE AUTOCATALYSIS OF NG[25]

It is suggested that this intermediate increases in concentration and then decomposes, thus accelerating the decomposition rate of NG. These results appear only very preliminary and speculative and unsubstantiated by many other authors and we can find no conclusive evidence to substantiate whether it is NO_2 or CH_2O which promotes autocatalysis of nitrate esters.

Kinetic studies concerning NC are particularly numerous and nearly all the studies of NC previously cited in our work report a value for the activation energy (E_a) of NC. Values fall in the range 155 - 195 kJ mol^{-1} but mostly around 180 - 192 kJ mol^{-1}; presumably autocatalysis may be the cause of some apparently low values (155 kJ mol^{-1}). The values around 180 - 192 kJ mol^{-1} appear to be slightly higher than expected when compared to gaseous methyl and ethyl nitrate (166.4 and 164.7 kJ mol^{-1}) which are thought to undergo unimolecular dissociation[3] and exhibit activation energies very close to the O-NO_2 bond dissociation energy. It is reported[3] that the activation energy for NC should in fact be lower than that for methyl and ethyl nitrate as the stability of a nitrate group is decreased if another nitrate group exists in a vicinal position; this appears to have gone unnoticed by all other

researchers. The occurrence of a cage recombination mechanism is proposed[3] to account for the apparently high E_a of NC. Thus, particularly at low pyrolysis temperatures, NO_2 may recombine to regenerate the nitrate group, resulting in a measured reaction rate slower than the rate at which dissociation is occurring. This seemingly simple explanation would appear to explain the apparent discrepancy in the E_a value of NC.

In summary, research pertaining to the solid phase thermal decomposition products of nitrate ester polymers is apparently associated solely with NC. Although the mechanism of decomposition of NC may bear some similarities with that of PNMMO, such as loss of NO_2, clearly the primary nitrate ester groups present in PNMMO may decompose in a different way from the two secondary nitrate ester groups in NC. The reactions involving the third, primary nitrate ester group in NC are seemingly less well understood although Panina *et al.*[20] have performed kinetic investigations of NC at 167^{0}C under vacuum conditions and have shown that the rate constant for the loss of NO_2 from the primary position is approximately 14 times less than for the secondary position. This implies that the gas and solid phase degradation products resulting from the decomposition of the primary nitrate ester groups in NC may be substantially less significant *in toto* than the products resulting from the decomposition of the secondary nitrate groups. Investigations concerning the thermal decomposition of various simple nitrate esters including some primary nitrate esters have recently been performed by Hiskey *et al.*[28] and the results of this research and that of other researchers is summarised in the following section.

1.6 THE THERMAL DEGRADATION OF SIMPLE NITRATE ESTERS

The kinetics of decomposition of isopropyl nitrate (IPN) have been investigated[29] at temperatures between 200 and 250^{0}C. Like NC, and other nitrate ester polymers, the E_a

obtained from an Arrhenius plot for IPN points to O-NO_2 bond homolysis as the rate determining step. The gaseous decomposition products observed for IPN such as CH_2O and CO_2 were also similar to those observed for many nitrate ester polymers, although NO_2 was observed in the form of nitromethane presumably due to additional reaction of NO_2 in the gas or condensed phase. Extensive research concerning the rates of thermal decomposition and the gas and condensed phase thermal decomposition products of many other simple nitrate esters has been performed by Hiskey *et al.*[28] and this is summarised below.

A variety of solvents including benzene, 1,2,3,4-tetrahydronaphthalene (tetralin) and ether were used by Hiskey *et al.*[28] to dissolve the nitrate esters prior to thermolysis. These hydrogen-donor solvents stabilised radical intermediates, thus allowing their identification and a more detailed analysis of the decomposition pathways of the nitrate esters. Thermolysis of the nitrate esters was generally carried out at approximately 150^0C and product identification was performed using GC-MS and GC-FTIR. The thermal decomposition of each of 13 primary, secondary, tertiary and multiple nitrate esters all followed a first order rate law consistent with O-NO_2 homolytic cleavage in the rate determining step. By varying the concentration of the nitrate ester solutions and thus the viscosity of the resulting solution, Hiskey supports the reversibility of NO_2 loss postulated by Kuo[3]. Thus a significant increase in the rate of reaction is observed following a decrease in the viscosity of the thermolysed solution. This cage recombination mechanism was further substantiated by ^{15}N labelling experiments using ethanol nitrate.

The multiple nitrate esters studied, namely 2,2-dimethyl-1,3-propanediol dinitrate (DPD), nitropentaglycerin (NPG) and pentaerythritol tetranitrate (PETN) all undergo ring closure reactions producing predominantly oxiranes, NO_2 and CH_2O. NPG provides a

representative example of the thermal decomposition of a multiple nitrate ester thermolysed in benzene;

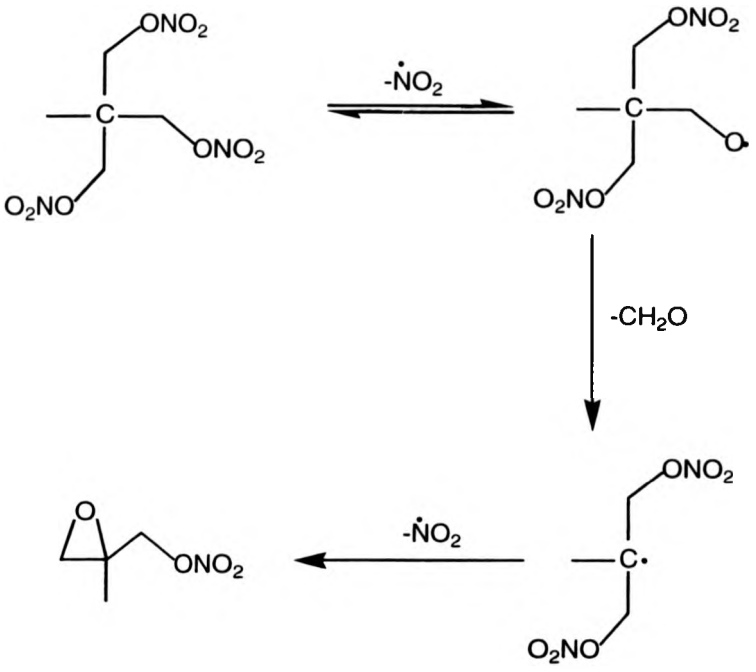

DIAGRAM SHOWING THE THERMAL DECOMPOSITION OF NPG

Following loss of NO_2, an alkoxy radical is formed which decomposes via loss of formaldehyde to give a carbon-centred radical which undergoes a ring closure reaction to give 2-methyl-2-nitroxymethyloxirane. DPD and PETN undergo similar ring closure reactions as do all the multiple nitrate esters studied including 1,4-butanediol dinitrate and 1,5-pentanediol dinitrate.

The thermal decomposition of the primary nitrate ester, neopentanol nitrate, was also studied by Hiskey *et al.*[28] in the gas phase at 175^{0}C and in a variety of solvents at 154^{0}C. The thermolysis product, formed almost exclusively, was shown to be the tertiary nitroalkane, 2-methyl-2-nitropropane and the degradation scheme is shown below;

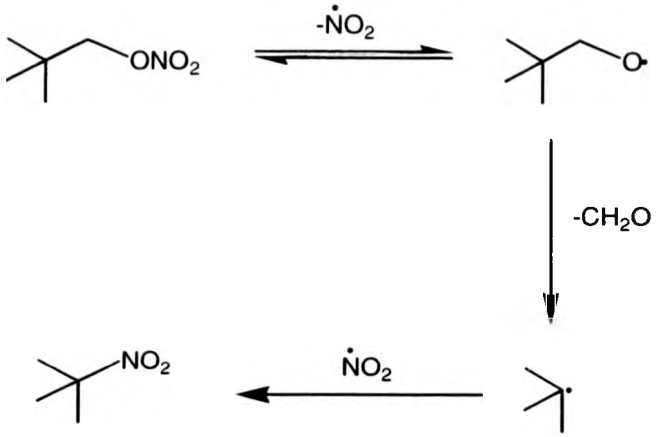

DIAGRAM SHOWING THE THERMAL DECOMPOSITION OF NEOPENTANOL NITRATE

The initial stages of decomposition of neopentanol nitrate involving the loss of NO_2 and subsequent loss of formaldehyde are thus similar to those of NPG. The subsequent recombination of NO_2 is however dissimilar and is presumably due to the relatively high stability of the *tert*-butyl radical and the absence of another nitrate ester moiety which may promote a ring closure reaction as for the previous multiple nitrate esters.

The thermal decomposition mechanisms of tertiary nitrate esters were significantly different from those of the all the other nitrate esters studied[28]. The activation energies for decomposition of both 2-methyl-2-butanol nitrate (MBN) and 2-methyl-2-propanol nitrate (MPN) were substantially lower than for the primary, secondary and multiple nitrate esters, indicating a change in mechanism. Indeed significant quantities of nitric acid were detected during the thermolysis (in ether solvent) of both the tertiary nitrate esters. Hiskey[28] proposes that the tertiary nitrate esters can eliminate nitric acid by a cyclic mechanism somewhat similar to the Cope elimination and Chugaev reaction. Thus for MBN;

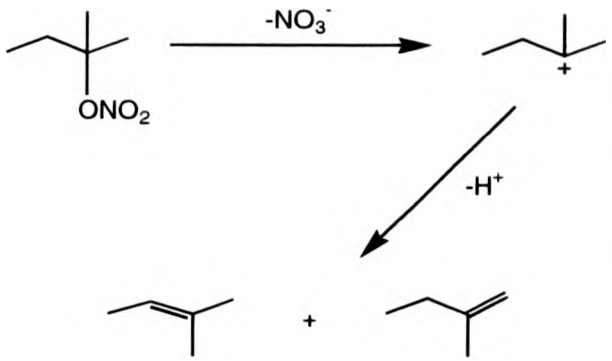

DIAGRAM SHOWING THE THERMAL DECOMPOSITION OF MBN

The decomposition mechanism for simple nitrate esters following homolysis of the $O\text{-}NO_2$ bond is thus strongly influenced by the number of nitrate esters moieties originally present, the substitution on the α and β carbon, and the relative positions of the original nitrate ester groups to each other.

The backbone of PNMMO resembles that of many polyethers and thus although the main degradation pathways of nitrate ester polymers are very dependent on the relationships noted above, some similarities with the degradation mechanisms of more widely researched polymers such as poly(propylene oxide) (PPO) and poly(ethylene oxide) (PEO) are also apparent. A summary of some of the research in this area is given in the following section.

1.7 THE PHOTO- AND THERMAL DEGRADATION OF POLYETHERS

Like the ageing of propellants which is thought to occur via slow thermal decomposition, the ageing of all polymers is thought to be a process which develops with time, thus the study of the degradation mechanism requires a kinetic approach. A better understanding of this mechanism makes it possible to solve intelligently the problem of extending the lifetime of polymeric materials. Consequently, research into this area of chemical kinetics and the pathways of degradation has expanded rapidly over the past decade to encompass a range of widely used polymers including PEO and PPO.

The photo- and thermal degradation of polyethers has been studied for a considerably longer time than has the degradation of nitrate ester polymers. Even so, it appears that the degradation pathways of polyethers such as PEO and PPO are still not completely understood although the degradation products seem to have been more clearly defined.

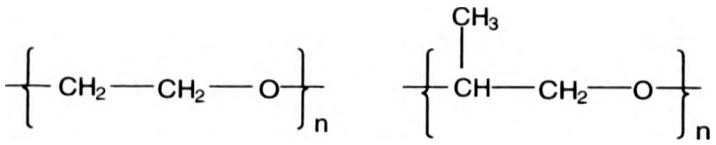

PEO PPO

DIAGRAM SHOWING THE STRUCTURES OF PEO AND PPO

To this extent we have also sought to characterise the thermal degradation products and pathways of PPO in the hope of providing a better understanding of those in PNMMO and for this reason only a brief insight into the degradation of PPO will be given at this point to avoid repetition in the results and discussion section devoted to PPO.

Research papers covering the general aspects of polymer degradation[30,31,32] have been available for many years, but it appears that reports specifically concerning the photo- and thermal degradation products and mechanisms of PPO and PEO have been published only over the past 6 to 7 years. Cameron and co-workers[33,34] has published several papers concerning the thermal degradation of PEO and its complex with metal salts while Fares[35] has characterised the thermal degradation products of PEO by *in situ* pyrolysis mass spectrometry. The photodegradation of PEO has been studied by Lemaire *et al.*[36] and some reference to this is also given in a recently published book by Rabek[37]. Both the photo- and thermal oxidation of PEO are proposed to occur via similar routes involving the formation of the secondary hydroperoxide. Degradation proceeds via hydrogen abstraction as shown over the page.

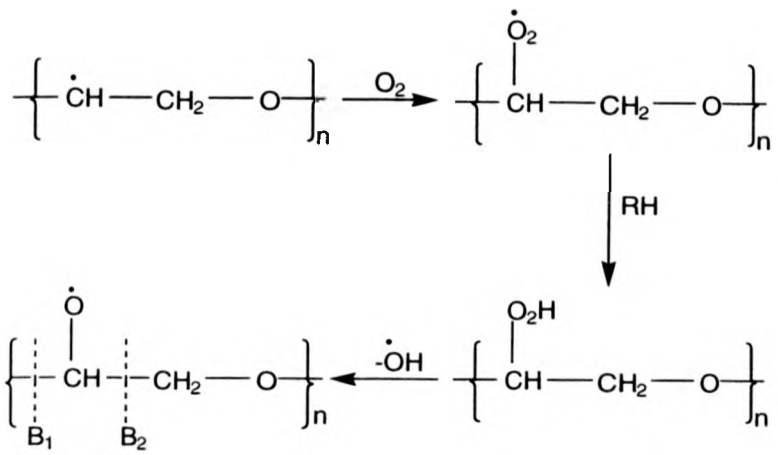

DIAGRAM SHOWING THE THERMAL DEGRADATION OF PEO

The resulting alkoxy and hydroxy radicals may then react in a number of ways although the reactions of the hydroxy radical appear to be less well understood and may be very complex. Four main reaction pathways are apparent for the alkoxy radical and these are summarised as follows;

1) The alkoxy radical may abstract hydrogen from another polymer chain to give a hemiacetal;

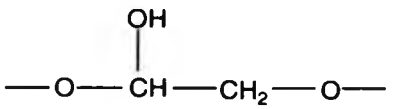

2) A 'cage' reaction involving the abstraction of hydrogen from the alkoxy radical, possibly by a hydroxy radical, to generate an ester;

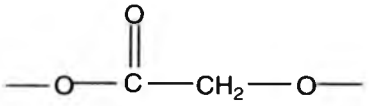

3) The alkoxy radical may undergo β_1 scission to generate an aldehyde and an alkoxy radical;

4) β_2 scission may take place to generate a formate and a carbon-centred radical;

Costa *et al.*[33] comment that the IR spectrum of pyrolysed PEO indicates a high concentration of formate, a lower concentration of ester and no aldehyde. These observations suggest that β_2 scission of the alkoxy radical predominates and that β_1 scission is negligible under the experimental conditions. No explanation for this appears to be given but clearly it is not a direct result of the bond energies as the C-O bond energy is lower (approx. 12.5 kJ mol^{-1}) than the C-C bond energy[33]. The absence of formaldehyde in

the gaseous decomposition products of PEO has led the author to discount the loss of formaldehyde from the alkoxy radical formed in reaction 3 in the scheme above; instead a cyclisation or hydrogen abstraction reaction is invoked. Costa *et al.*[33] note that the gamma irradiation of PEO at room temperature performed by Decker and co-workers produces some different species, such as formaldehyde, not observed during thermolysis. Clearly the experimental conditions may affect the relative concentrations of degradation products observed.

The secondary thermal degradation products of PEO are numerous and it is obvious that many reactions are possible after the formation of significant quantities of primary degradation products. Some attempt to characterise the secondary decomposition products of PEO has however been made by Costa *et al.*[33]

Polypropylene (PP) has been the subject of thermal degradation studies by Lacoste *et al.*[38] and Yang *et al.*[39] and has been shown to yield predominantly the tertiary hydroperoxide via photo- or thermal degradation. As for PP, PPO can yield either a tertiary or secondary hydroperoxide as shown over the page.

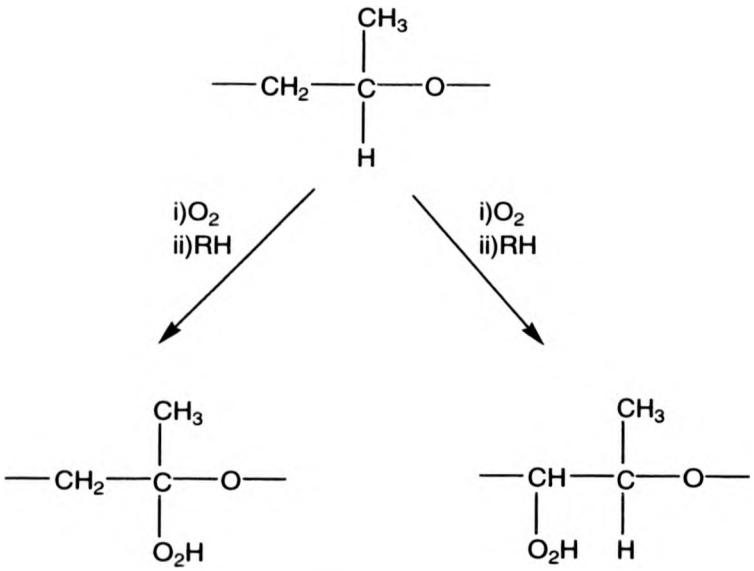

DIAGRAM SHOWING THE PRELIMINARY STAGES OF DEGRADATION OF PPO

Like the mechanism of degradation of PEO, the hydroperoxy radical can decompose via loss of a hydroxy radical to give an alkoxy radical which may then undergo similar reactions to the alkoxy radical produced during pyrolysis of PEO. The formation of a formate ester during pyrolysis (Griffiths *et al.*[40]) or photolysis (Lemaire *et al.*[36]) of PPO appears to be undisptuted, but there is some disagreement as regards the mechanism of its formation and this is more clearly resolved in the results section of our work.

1.8 TECHNIQUES FOR STUDYING THE DEGRADATION OF POLYMERS

We have utilised many of the physical techniques generally applied to the studies of polymers and their degradation. These techniques include infrared (IR) spectroscopy,

nuclear magnetic resonance (NMR) spectrometry and size-exclusion chromatography (SEC) and these analytical methods and their applications to polymers are summarised in books by Bodor[41], Bower[42] and Young[43]. Yinon[44] describes the application of various chromatographic techniques used in conjunction with chemical ionisation (CI) and electron impact (EI) mass spectrometry to analyse various explosives, some with structural similarities to PNMMO.

Synthetic polymers are difficult to ionise owing to their low volatility, thermal lability and general chemical inertness, the qualities which make them so useful for diverse applications. This makes classical ionisation by EI impossible and consequently the application of mass spectrometry to polymers has been restricted to pyrolysis coupled with gas chromatography mass spectrometry owing to the need for extensive heating of the sample to achieve volatilisation[45]. Widely used mass spectrometric techniques such as *in situ* pyrolysis mass spectrometry often provide informative results as regards the degradation of polymers under particular experimental conditions but often these results cannot be applied to the thermal decomposition of polymers in air at ambient temperatures. Consequently mass spectrometric studies of the pyrolysis of polymers[46] or rubbers[47] are often concerned solely with the characterisation of the evolved pyrolysis gases from the sample as opposed to the characterisation of the sample itself. During analysis by pyrolysis mass spectrometry, samples are heated in the absence of air and problems often arise from the ionisation of the thermal decomposition products with energetic electrons which causes further decomposition of the sample, thus resulting in a skewed distribution of degradation products as observed for PEO[35]. Techniques such as direct pyrolysis mass spectrometry have thus become known as 'hard ionisation techniques' as analysis often results in *in situ* reactions leading possibly to additional degradation of the sample. In this respect, we have

sought to apply relatively new mass spectrometric techniques, employing improved ionisation methods, such as electrospray ionisation (ESI) mass spectrometry and matrix-assisted laser desorption ionisation mass spectrometry (MALDI) to the study of undegraded and degraded polymers such as PNMMO and PPO. The primary advantage of using mass spectrometry is that it provides direct observation of oligomer ion distributions, provided that appropriate sample preparation and 'soft' ionisation procedures are used[48]. Both MALDI and ESI are considered to be relatively 'soft ionisation' techniques owing to their ability to ionise samples without causing significant *in situ* degradation of the sample.

In addition to the direct observation of oligomer ion distributions, both ESI and MALDI possess many advantages over the conventional methods of mass analysis such as SEC. Although no quantitative data appear to exist for the sensitivity of the mass spectrometric techniques as regards polymers, proteins can be characterised by ESI in pmol concentrations and by MALDI in nmol concentrations. Apart from the evidently greater sensitivity of the mass spectrometric techniques, many limitations are also associated with the use of refractive index and light scattering detectors in SEC instruments. Careful calibration with specially prepared standards based on the same polymer that is to be analysed is essential to obtain accurate mass measurements and even if these expensive calibrants are available, relatively small concentrations of contaminants can lead to significant mass errors. Clearly many problems are also associated with the SEC analysis of samples with unknown structures, mixtures of polymers and polymers with wide distributions.

PNMMO and PPO consist of a series of polymer molecules with a range of molecular weights. We have used both MALDI and ESI, but predominantly ESI, in conjunction with column chromatography to characterise individually isolated components

of the undegraded and degraded polymer 'mixtures'. A review of the history and the application of MALDI and ESI to the analysis of polymers is given in the subsequent sections.

1.8.1 THE APPLICATION OF ESI TO THE ANALYSIS OF POLYMERS

Mass spectrometry is the single most important technique for the determination of relative molecular masses (RMMs) and has become an integral part of the study of large organic molecules. Commercial mass spectrometers have been available for more than 50 years although it appears that only over the past 20 years have researchers in the field of biosciences realised the potential for mass spectrometry for molecular weight and structural characterisation of biological polymers such as proteins, peptides, polynucleotides and polysaccharides. The application of mass spectrometry to synthetic polymers has similarly grown over the past 20 years, but to a much lesser extent and with the aid of a much smaller number of researchers[49]. This appears surprising considering the advantages that newer mass spectrometric techniques have to offer in terms not only of obtaining RMMs, but also for obtaining structural information by performing collision induced dissociation (CID) experiments by means of a tandem mass spectrometer.

1.8.2 THE ELECTROSPRAY PROCESS

Electrospray ionisation coupled with mass spectrometry was introduced by Malcolm Dole and co-workers in 1968[50]. The pioneering experiment involved the calculation of the kinetic energies of polystyrene (PS) ions after applying a repeller voltage to a collector known as a Faraday cage, in order to deflect unwanted low-mass ions. These calculations led to the determination of the m/z values for the polymer ions. The experiment showed that if a

solution of a polymer in a suitable solvent is pumped through a fine capillary tube, with the aid of a nebulising gas and a high electric field, a fine spray or aerosol, of charged droplets containing solute molecules is produced. Dole's explanation for this process of ion formation is known as the charge residue model. The initial highly charged droplets which emerge from the capillary are desolvated by a combination of heat, gas flow and vacuum. Consequently the diameter of the droplets decreases and the surface charge density increases, resulting in an increase in coulombic repulsive forces. This continues until the repulsive forces overcome the surface tension and at this point the Rayleigh stability limit is exceeded and the droplet ruptures to generate a series of daughter droplets which undergo the same process, thus decreasing in size and breaking apart. This continues until only one solute molecule remains which has retained the charge of the remaining solvent to generate, according to Dole, a singly charged molecular ion.

Yamashita and Fenn[51] continued Dole's research in the mid 1980's by performing similar experiments. Fenn reported that the number of molecules in the electrospray was always 10 to 100 times greater than the number of unit charges and that in order for the ions to desorb from the solvent droplet, the ions must be multiply charged. These observations led Fenn to reject Dole's theory of the formation of a singly charged ion and instead he proposed the ions were in fact multiply charged. Alternative theories have also been put forward to account for the electrospray process although most of these deviate only slightly from the models of Dole and Fenn. Clearly no unifying model to account for the electrospray process has yet been proposed and more research is needed in this area.

Mass spectrometers can only analyse ions in the gas phase and the electrospray technique is an efficient method for transforming ions that are present in a solution into ions in the gas phase. This solution, or mobile phase, usually consists of a mixture of two

solvents (water/methanol or THF/methanol) which essentially 'transport' the sample through a silica tube by means of a liquid chromatograph pump. The mobile phase emerges from a fine steel capillary, which is charged at a potential of between 2 - 3 kV, as a fine spray of droplets. The charged spray of droplets is focused towards a sample cone by an HV lens (see fig.1.1) which also acts to reduce the number of unwanted droplets. The ions are then refocused into a narrow beam by a skimmer lens from where they emerge as a supersonic jet due to the reduction in pressure. This jet can exist in various forms and its appearance has been studied and is thought to directly affect the yield of ions[53]. The ions are then analysed with a quadrupole mass filter which consists of four parallel rods of hyperbolic cross section to which a potential is applied to create an electric field. Mass selection is achieved if the ions follow a stable path between the four rods. The electrospray machine used by us is a triple quadrupole instrument (see experimental section) and the first quadrupole then passes all the deflected ions onto a photomultiplier detector system.

During CID experiments, ions selected by the first quadrupole are deflected into a hexapole collision cell containing argon gas which is used as the collision gas. The second quadrupole is then used to scan the fragment ions generated during CID. A diagram of the hexapole and quadrupoles is shown in section 2.1.4 (experimental section).

With electrospray, ions are typically formed as multiply-charged species and since the nature of the charge formation is dependent on solution conditions such as pH, ions are typically generated with a range of charges[52]. The m/z ratio for the macromolecule is thus some fraction of the molecular weight. The electrospray technique allows the formation of ions with m/z ratios in a relatively low-mass region, around 1 - 4000 mass units (mus), where mass spectrometers operate most efficiently, indeed Nohmi *et al.*[53] have performed mass analysis by ESI with PEO samples of mass 200 to 5,000,000. Polymer ions were

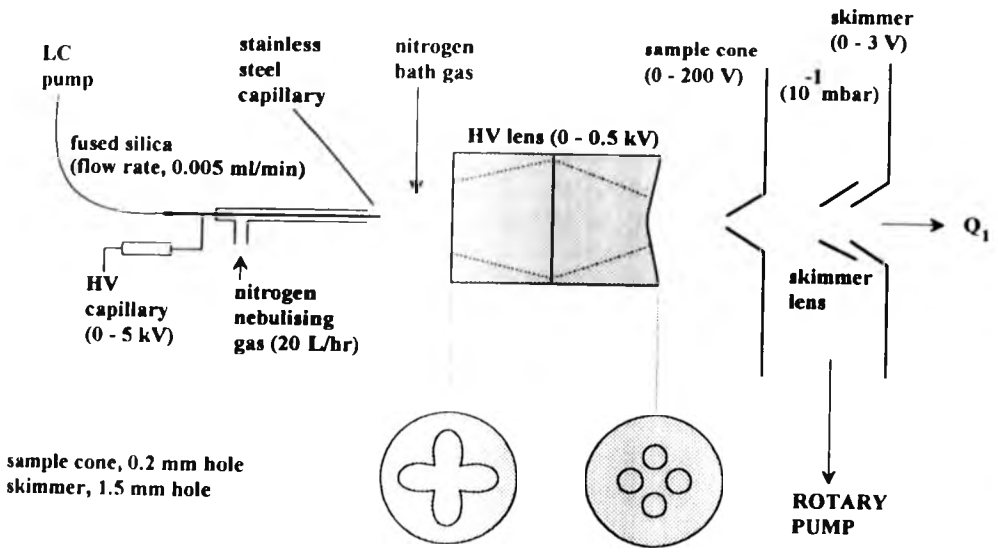

FIG.1.1 A SCHEMATIC DIAGRAM OF THE INTERFACE OF AN ELECTROSPRAY SOURCE TO A TRIPLE QUADRUPOLE MASS SPECTROMETER[54]

observed around 1000 - 1500 mus for all of these PEO samples and it was found that the number of charges per unit length of oligomer decreases with increasing molecular weight in the range below 20 000 mus; above this value the number increases. Other ESI studies of PEO have also been performed[55] but the studies of PPO and other polymers are far less common. This is thought to be due predominantly to the difficulty in finding the correct combination of solvent system and salt. Corless *et al.*[56] have had limited success with low molecular weight PS and singly-charged ions were observed for PS oligomers with masses less than 1000 mus. However for samples of PS with molecular weights greater than the mass limit of their instrument (2000 mus) no ions were observed. They attribute this to the lack of multiple charging of the PS oligomers although we propose that an alternative explanation may be the insolubility of the higher molecular weight PS in the THF/MeOH solvent system. Indeed, owing to the high sensitivity of this mass spectrometric technique and thus the very small masses of sample used, it is usually impossible to visually determine whether the polymer sample has dissolved and consequently extensive solubility testing must be performed prior to sample analysis by ESI. Clearly however both the polymer and the salt must be soluble in the solvent system.

Like PS, low molecular weight oligomers of methyl methacrylate (<500 mus) have also been analysed[57] using ESI but similar problems of solubility were encountered with higher mass samples. In contrast, PEOs of varying molecular weights readily dissolve in a 50 : 50 mixture of water and methanol and give well resolved ESI spectra in the presence of ammonium chloride. Evidently this is not true for many other polymers and extensive testing is required before obtaining an ESI spectrum. The application of ESI to polymers is obviously still in its infancy and significantly more research is needed in this area before

parameters are established to determine the correct choice of solvent system and salt without the need for extensive testing.

The difficulty in finding the correct combination of solvent system and salt for analysis via ESI is directly paralleled with the problem of obtaining the correct choice of matrix for the analysis of polymers via MALDI. A brief summary of the MALDI technique is given in the following section.

1.8.3 THE APPLICATION OF MALDI TO THE ANALYSIS OF POLYMERS

The MALDI instrument used in our studies was the Kratos Kompact III MALDI time-of-flight (TOF) mass spectrometer. This spectrometer is considerably smaller in size (approx.1 m × 1 m × 0.3 m) than the ESI instrument and significantly easier to operate. Samples are prepared as shown in the experimental section.

As for ESI, MALDI is a very recently developed technique and much is still not understood about the desorption process. MALDI was developed by Karas and Hillenkamp[58,59] and Tanaka[60] in the latter part of the 1980's although the method of laser desorption was developed over ten years previously by Hillenkamp[61]. Until this time laser desorption was not considered to be a viable ionisation method for polymers owing to the intense energy of the laser pulse and the fragility of the polymer chains. This generally restricted the mass range to approximately 1000 mus[62]. During laser desorption, the energy from the pulse of a laser focused on a solid sample is absorbed by the analyte molecules which are ionised and vaporised. An important advantage stems from the pulsed nature of the experiment which allows the use of TOF mass spectrometers that can generate a complete mass spectrum for every ionisation event. However it is the sample preparation that is vital to the MALDI process and it was found that the use of an effective matrix

significantly extended the mass limit of the desorption technique. Thus instead of directly irradiating a neat sample, the analyte is deposited from a solution containing a large excess of matrix which absorbs at the wavelength of the incident laser light. After removal of the solvent a residue remains which comprises well separated analyte molecules homogeneously dispersed in a 'sea' of matrix molecules[63]. The energy of the laser pulse is absorbed by the matrix and a small proportion of the matrix vaporises, carrying intact analyte molecules into the gas phase. This part of the process appears to be understood, but it is the next stage involving transfer of a charge to the polymer chains which is not entirely understood. Karas[64] proposes that a shallow surface layer of the matrix is vaporised either by electronic (UV) or vibrational (IR) excitation and forms a gas plume which expands, gaining momentum, into the vacuum against the underlying solid bulk. Multiple collisions in the dense gas plume enhance this effect, thus further increasing the momentum resulting in a jet-like emission with supersonic velocities. Analyte molecules are entrained into the plume by multiple collisions and charged by collisions with reactive photoionised matrix ions, resulting in electron or proton transfer processes (photochemical ionisation). Karas[65] notes that while this proton transfer reaction is likely to occur for proteins and peptides dissolved in aqueous media, it is less likely for polymers dissolved in organic solvents. The lack of understanding of this ionisation process and the fact that most of the matrices used so far are soluble in aqueous solvents and used for water soluble biopolymers, has led to a relatively slow growth in the MALDI analysis of most synthetic polymers over recent years. Clearly polar or more ionic polymers such as PEGs and PPGs may be examined using well-known matrices such as 2,5-dihydroxybenzoic acid and sinapinic acid used for biopolymer analysis, but these matrices do not mix well with non-polar polymers such as PS and polybutadiene. However the recent development of matrices more amenable to the analysis of polymers

insoluble in water has led to a renewed interest in the analysis of synthetic polymers using MALDI. Many of these 'new' matrices are liquids such as 2-nitrophenyl octyl ether[58,62,66] (NPOE), 1,2,4-butanetriol, 2-cyano-5-phenyl-2,4-pentadienoic acid[67] and quinizarin[68] which offer the advantage of providing a homogeneous sample environment, improving sample and thus spectral reproducibility. The intimate mixing of the matrix and analyte (polymer) has been shown to be an essential requirement for the MALDI process and some researchers have integrated microscopes into their MALDI instruments to ensure that efficient mixing has occurred prior to analysis[69]. We have similarly examined mixtures of PNMMO with various matrices prior to MALDI analysis using an Olympus high power microscope and our results are shown in the results section of this thesis. Other new matrices also include solids such as indole acrylic acid[70]. These 'new' matrices have led to well-resolved MALDI spectra of poly(methyl methacrylate) (PMMA)[66,71], PS[70], polybutadiene[68] and poly(vinyl acetate)[70]. The need for the introduction of salts to promote ionisation of many of the less polar synthetic polymers poses an additional problem but, as for the introduction of many 'new' matrices, so has there been considerable research leading to the use of many 'new' salts such as silver, copper and cobalt salts[70].

Clearly the correct choice of matrix and salt to promote ionisation is vital to the MALDI process. Similarly, the relative concentration of matrix versus polymer used to obtain MALDI spectra is also variable and many researchers report many different relative amounts of matrix and polymer. Consequently the application, and thus the correct choice of experimental conditions, of MALDI to a polymer such as PNMMO for which no previous MALDI studies have been performed is unfortunately still somewhat of a 'trial and error' process. However the significant advantages offered by the MALDI technique strongly

suggest that MALDI spectra of PNMMO would facilitate the understanding of the degradation process.

1.9 LIQUID COLUMN CHROMATOGRAPHY

Various types of chromatographic technique are applied to the analysis of both undegraded and degraded polymers[72,73]. Chromatographic methods are among the most widely used methods for the analysis of polymer composition and for the determination of the molecular weight distribution[74,75]. SEC is one of most well utilised of these techniques and it provides quick data pertaining to the molecular weight distribution of the polymer. However the limitations of this technique with respect to its accuracy and the difficulties associated with calibration have been discussed in section 1.8. In addition to these difficulties some researchers[76] also propose that the mechanism of separation employed by SEC may involve solute-solvent-packing interactions that are not strictly dependent on molecular size. However, many researchers have successfully used SEC to analyse thermally degraded polymer samples such as PMMA and poly(alpha-methyl styrene)[77] and photolytically degraded samples such as PMMA and poly(methyl vinyl ketone)[78]. As a result of the apparent limitations of the SEC technique, over the past 2 or 3 years researchers have coupled techniques such as SEC and ESI[76] to separate and to analyse mass spectrometrically the various oligomeric components of polymers. In this way, the problems associated with the calibration of the SEC instrument are overcome. This technique is very much still in its infancy, but it has been successfully applied to the separation of a polydisperse mixture of octylphenoxypoly(ethoxy)ethanol[76].

Although both ESI and SEC were locally available to us separately, it was not possible to couple these techniques as both instruments were in frequent demand. It was also

impossible to perform preparative SEC experiments with the SEC instrument available to us, i.e. the polymer sample could not be recovered for further characterisation during SEC analysis. Thus in an attempt to simulate the coupling of the SEC and ESI techniques, we used column liquid chromatography employing a 1 m column filled with a silica slurry to separate both undegraded and degraded PNMMO and the resulting fractions were analysed using ESI. Clearly this method of chromatographic separation also allows the resultant fractions to be analysed using IR, NMR and SEC. This appears to be the first time that this classical method of chromatographic separation has been coupled with ESI and the results of these experiments are summarised in the results and discussion section of this thesis.

1.10 THE OBJECT OF THIS WORK

The object of this work was to investigate the thermal decomposition of a nitrate ester pre-polymer namely PNMMO, the objective being to characterise the thermolysis products and pathways. The analysis and characterisation of the degradation products of all polymers nearly always requires the application of many different physical techniques and we have similarly used a variety of spectroscopic methods to examine degraded and undegraded PNMMO. At approximately the half way stage of the research, i.e. after one and a half years, we were fortunate to gain local access to relatively new mass spectrometric techniques such as MALDI and ESI. ESI and ESI coupled with liquid column chromatography proved to be particularly useful for the characterisation of the degraded polymer and in particular the undegraded polymer, and this led to a more detailed picture of the undegraded material than has been obtained hitherto.

CHAPTER 1 REFERENCES

1 Bunyan, P., Cunliffe, A.V., Davis, A., Kirby, F.A., *Polymer Degradation and Stability*, 1993, **40**, 239.

2 Quinchon, J., Tranchant, J., Nitrocelluloses, Ellis Horwood Ltd., Chichester, England, 1989.

3 Kuo, K.K., Summerfield, M., Fundamentals of Solid Propellant Combustion, American Institute of Aeronautics and Astronautics Inc., New York, Ch.4, 1984.

3a Dauerman, L., Tajima, Y.A., *J.American Institute of Aeronautics and Astronautics*, 1968, **6**, 1468.

3b Tranchant, H., *Memorial des Poudres*, 1962, **44**, 11.

3c Juhasz, A.A., Rocchio, J.J., The Fundamentals of Ignition and Combustion, 1974.

4 Griffiths, S.K., Nilson, R.H., *Combustion and Flame*, 1992, **88**, 369.

5 Tseng, I.S., Yang, V., *Combustion and Flame*, 1994, **96**, 325.

6 Cunliffe, A.V., Bunyan, P., Unpublished work obtained from the DRA.

7 Kishore, K., Paiverneker, V.R., Prasad, G., *Combustion and Flame*, 1979, **36**, 79.

8 Farber, M., Harris, S.P., Srivastava, R.D., Mass Spectrometric Investigation of the Thermal Degradation of Several Propellant and Explosive Ingredients, The Office of Naval Research, Virginia USA, 1986.

9 Chen, J.K., Brill, T.B., *Combustion and Flame*, 1991, **85**, 479.

10 Oyumi, Y., Brill, T.B., *Combustion and Flame*, 1986, **66**, 9.

11 Chen, J.K., Brill, T.B., *Thermochim. Acta*, 1991, **181**, 71.

12 Verdu, J., *J.Mass Spectrom.-Pure Appl. Chem.* 1994, ***A31***, 1383.

13 Pai Verneker, V.R., Kishore, K., Varadaraju, U.V., *Combustion and Flame*, 1982, **45**, 137.

14 Kishore, K., Pai Verneker, V.R., Prasad, G., *Combustion and Flame*, 1979, **36**, 79.

15 Pfeil, A., Krause, H.H., Eisenreich, N., *Thermochim. Acta*, 1985, **85**, 395.

16 Eisenreich, N., Pfeil, A., *Thermochim. Acta*, 1983, **61**, 13.

17 Phillips, R.W., Orlick, C.A., Steinberger, R., *J. Phys. Chem.* 1955, **59**, 1034.

18 Gelernter G., Browning, L.C., Harris, S.R., Mason, C.M., *J. Phys. Chem.* 1956, **60**, 1260.

19 Wolfrom, M.L., Frazer, J.H., Kuhn, L.P., Dickey, E.E., Olin, S.M., Hoffman, D.O., Bower, R.S., Chaney, A., Carpenter, E., McWain, P., *J. Am. Chem. Soc.* 1955, **77**, 6753.

20 Panina, E.A., Rafeev, V.A., Sorokina, T.V., Rubtsov, Yu.I., Chukanov, N.V., *Bull. Acad. Sci.* 1990, **39**, 1143.

21 Shafizadeh, F., Wolfrom, M.L., *J. Am. Chem. Soc.* 1958, **80**, 1675.

22 Volltrauer, H.N., Fontijn, A., *Combustion and Flame*, 1981, **41**, 313.

23 Naud, D.L., Brower, K.R., *J. Am. Chem. Soc.* 1992, **57**, 3303.

24 Hiskey, M.A., Brower, K.R., Oxley, J.C., *J. Phys. Chem.* 1991, **95**, 3955.

25 Batten, J.J., *Int. J. Chem. Kin.* 1985, **17**, 1085.

26 Huang, C-C., Ger, M-D., Lin, Y-C., Chen, S-I., *Thermochim. Acta*, 1992, **191**, 74.

27 Chen, J.K., Brill, T.B., *Combustion and Flame*, 1991, **87**, 157.

28 Hiskey, M.A., Brower, K.R., Oxley, J.C., *J. Phys. Chem.* 1991, **95**, 3955.

29 Krause, H., *Thermochim. Acta*, 1989, **149**, 349.

30 Emanuel, N.M., *Russ. Chem. Rev.* 1985, **54**, 817.

31 Emanuel, N.M., *Russ. Chem. Rev.* 1981, **50**, 901.

32 Struik, L.C.E., Physical Ageing in Amorphous Polymers and Other Materials, Elsevier, Oxford, 1978.

33 Costa, L., Gad, A.M., Camino, G., Cameron, G.G., Qureshi, M.Y., *J Am. Chem. Soc.* 1992, **25**, 5512.

34 Cameron, G.G., Ingram, M.D., Qureshi, M.Y., Gearing, H.M., *Eur. Polym. J.* 1989, **25**, 779.

35 Fares, M.M., Hacaloglu, J., Suzer, S., *Eur. Polym. J.* 1994, **30**, 845.

36 Lemaire, J., Gauvin, P., Sallet, D., *Makromol. Chem.* 1987, **188**, 1815.

37 Rabek, J.F., Polymer Photodegradation, Chapman and Hall, London, 1995.

38 Lacoste, J., Vaillant, D., Carlsson, D.J., *J. Polym. Sci.: Part A: Polym. Chem.* 1993, **31**, 715.

39 Yang, C.Q., Martin, L.K., *J. Appl. Polym. Sci.* 1994, **51**, 389.

40 Griffiths, P.J.F., Hughes, J.G., Park, G.S., *Eur. Polym. J.* 1993, **29**, 437.

41 Bodor, G., The Structural Investigation of Polymers, Ellis Horwood, London, 1991.

42 Bower, D.I., Maddams, W.F., The Vibrational Spectroscopy of Polymers, Cambridge University Press, 1989.

43 Young, R.J., Introduction to Polymers, Chapman and Hall, London, 1981.

44 Yinon, J., Zitrin, S., Modern Methods and Applications in Analysis of Explosives, John Wiley & Sons, Chichester, 1993.

45 Schulten, H.R., Lattimer, R.P., *Mass Spectrom. Rev.* 1984, **3**, 231.

46 Yalcin, T., Akbulut, U., Suzer, S., *Macromol. Reports*, 1993, **A30**, 55.

47 Erdogan, M., Yalcin, T., Tincer, T., Suzer, S., *Eur. Polym. J.* 1991, **27**, 413.

48 Kahr, M.S., Wilkins, C.L., *J. Am. Soc. Mass Spectrom.* 1993, **4**, 453.

49 Loo, J.A., Udseth, H.R., Smith, R.D., *Rapid Comm. Mass. Spectrom.* 1988, **2**, 207.

50 Dole, M., Mack, L.L., Hines, R.L., Mobley, R.C., Ferguson, L.D., Alice, M.B., *J. Chem. Phys.* 1968, **49**, 2240.

51 Yamashita, M., Fenn, J.B., *J. Phys. Chem.* 1984, **88**, 4451.

52 Campana, J.E., Sheng, L-S., Shew, S.L., Winger, B.E., *Trends Anal. Chem.* 1994, **13**, 239.

53 Nohmi, T., Fenn, J.B., *J. Am. Chem. Soc.* 1992, **114**, 3241.

54 VG Bio Tech Ltd., VG Quattro II Users Guide.

55 Wong, S.F., Meng, C.K., Fenn, J.B., *J. Phys. Chem.* 1988, **92**, 546.

56 Corless, S., Tetler, L.W., Parr, V., Wood, D., 1994, Paper Presented at the 42nd ASMS Conference on Mass Spectrometry and Allied Topics.

57 Simonsick, W.J., Prokai, L., 1994, Paper Presented at the 42nd ASMS Conference on Mass Spectrometry and Allied Topics.

58 Karas, M., Bachmann, D., Bahr, U., Hillenkamp, F., *Int. J. Mass Spectrom. Ion Proc.* 1987, **78**, 53.

59 Karas, M., Hillenkamp, F., *Anal. Chem.* 1988, **60**, 2299.

60 Tanaka, K., Waki, H., Ido, Y., Akita, S., Yoshida, Y., *Rapid Comm. Mass Spectrom.* 1988, **2**, 151.

61 Hillenkamp, F., Unsold, E., Kaufmann, R., Nitsche, R., *Nature*, 1975, **256**, 119.

62 Bahr, U., Deppe, A., Karas, M., Hillenkamp, F., Giessmann, U., *J. Anal. Chem.* 1992, **64**, 2866.

63 Creel, H.S., *Trends in Polym. Chem.* 1993, **1**, 336.

64 Karas, M., *Analusis*, 1992, **20**, 31s.

65 Karas, M., Deppe, A., Hillenkamp, F., Giessmann, U., 1992, Paper Presented at the 40th ASMS Conference on Mass Spectrometry and Allied Topics.

66 Humphrey, P., Resch, M., Kimber, M.L., Dingley, D.C., 1994, Paper Presented at the 42nd ASMS Conference on Mass Spectrometry and Allied Topics.

67 Williams, J.B., Gusev, A.I., Hercules, D.M., 1994, Paper Presented at the 42nd ASMS Conference on Mass Spectrometry and Allied Topics.

68 Mowat, I.A., Donovan, R.J., *Rapid Comm. Mass Spectrom.* 1995, **9**, 82.

69 Ingendoh, A., Karas, M., Hillenkamp, F., Giessmann, U., *Int. J. Mass Spectrom. Ion Proc.* 1994, **131**, 345.

70 Danis, P.O., Karr, D.E., Holle, A., Mayer-Posner, F., Watson, C., 1993, Paper Presented at the 41st ASMS Conference on Mass Spectrometry and Allied Topics.

71 Larsen, B.S., McEwen, C.N., Simonsick, W., Peacock, P.M., 1994, Paper Presented at the 42nd ASMS Conference on Mass Spectrometry and Allied Topics.

72 Provder, T., Barth, H.G., Urban, M.W., Chromatographic Characterisation of Polymers, American Chemical Society, Washington USA, 1995.

73 Provder, T., Chromatography of Polymers, American Chemical Society, Washington USA, 1993.

74 Cowie, J.M.G., Polymers: Chemistry and Physics of Modern Materials, Intext Educational Publishers, London, 1973.

75 Mark, J.E., Eisenberg, A., Graessley, W.W., Mandelkern, L., Koenig, J.L., Physical Properties of Polymers, American Chemical Society, Washington USA, 1984.

76 Prokai, L., Simonsick, W.J., *Rapid Comm. Mass Spectrom.* 1993, **7**, 853.

77 Chiantore, O., *J. Liquid Chromatography*, 1990, **13**, 2957.

78 Bond, S.G., Ebdon, J.R., *Polymer*, 1994, **35**, 451.

CHAPTER 2 EXPERIMENTAL

2.1 INSTRUMENTATION

2.1.1 INFRARED SPECTROSCOPY

IR spectra were recorded with a Perkin-Elmer 1720X FTIR spectrophotometer (range 5250 - 400 cm^{-1}). The resolution was set at 4 cm^{-1}.

2.1.1.1 SOLUTION INFRARED SPECTRA

Solution IR spectra were recorded using sodium chloride plates and 1 mm spacers. The solvent was normally chloroform-d_1.

2.1.1.2 INFRARED SPECTRA OF POLYMER FILMS

Thin (<0.5 mm) polymer films were mounted between sodium chloride plates and spectra recorded in the normal way.

2.1.1.3 GAS-PHASE INFRARED SPECTRA

All preparations involving the handling of gases were carried out on a vacuum line. Samples of polymer (1.0 g) were placed in a round bottomed flask (25 cm^3) and degassed by repeated freeze(77 K)-pump-thaw cycles. The polymer was then heated at a constant temperature in the range 70 - 155^{0}C for varying amounts of time using an oil bath. Gases were condensed into an IR gas cell equipped with a cold finger held at 77 K. The cold finger was then allowed to warm to room temperature and the IR spectrum measured. A spectrum of the evacuated cell was used as the background. The gas cell was 10 cm in length and 5

cm in diameter. The caesium iodide plates were attached at both ends with Apiezon wax and grease to maintain an air-tight seal.

2.1.1.4 HEATED INFRARED CELL

Electrical heating jacket P/N 20707 with liquid cell holder P/N 20500 and automatic temperature controller P/N 20140 were obtained from Specac Ltd. The apparatus consisted of a jacket capable of heating a pair of sodium chloride windows separated by a spacer of known thickness to 250^0C. Samples of PNMMO were injected between the sodium chloride plates using a syringe (5 cm^3). Constant temperature was maintained up to 160^0C by means of a Cr/Al thermocouple P/N 5935 permanently secured inside the thermocouple well of the cell holder. The backplate of the heating jacket was water cooled by a Churchill chiller thermo circulator to minimise transfer of heat from the accessory to the spectrophotometer. When the desired temperature was reached, IR spectra were recorded at set intervals over a period of 4-5 h.

2.1.2 NUCLEAR MAGNETIC RESONANCE (NMR) SPECTROSCOPY

Spectra were recorded on a Bruker ACF 250 spectrometer operating at 250.13 MHz for ^{1}H and 62.86 MHz for ^{13}C NMR. A Bruker ACP 400 spectrometer operating at 400.13 MHz for ^{1}H, 100.62 MHz for ^{13}C and 28.92 MHz for ^{14}N NMR was also employed for increased spectral resolution and ^{14}N NMR. The NMR tubes used were normally 5 mm in diameter and chloroform-d_1 was the commonly used solvent.

2.1.2.1 VARIABLE TEMPERATURE NMR

The ACP 400 spectrometer was equipped with a Bruker variable temperature unit (vtu). Increased resolution of extensively pyrolysed samples was obtained using high temperature NMR employing a sample temperature of 90^0C. For all experiments involving the vtu, neat samples of polymer were placed inside a 10 mm NMR tube and the reference signal obtained by means of a 5 mm NMR tube filled with D_2O placed inside the 10 mm tube. Scan times of approximately 2 h were needed for well resolved spectra.

2.1.2.2 CHEMICALLY INDUCED DYNAMIC NUCLEAR POLARISATION (CIDNP) AND DISTORTIONLESS ENHANCEMENT BY POLARISATION TRANSFER (DEPT) AND 2-D SPECTRA

^{13}C CIDNP experiments were performed on untreated PNMMO. Experiments involve the production of radicals within the sample and their subsequent detection by ^{13}C NMR. Heat was used as the source of radical formation in this case. ^{13}C NMR spectra were recorded at 60, 80, 100 and 110^0C.

DEPT and 2-D ^1J ^{1}H-^{13}C correlation experiments were also performed to identify the pyrolysis products of PNMMO.

2.1.3 ELECTRON SPIN RESONANCE

All data were obtained using a Bruker ER 200tt X-band ESR spectrometer operating at 9.7 GHz (empty cavity at ambient temperature), using 100 kHz field modulation. All spectra are first derivative and were obtained from samples placed in quartz tubes. Calibration of g-values was based on 2,2'-diphenyl-1-picrylhydrazyl (DPPH) (g = 2.0036)

and potassium nitrosyldisulfonate (Fremy's salt) (g = 2.0070). Fremy's salt was prepared according to the method described by Moser and Howie[1].

2.1.4 ELECTROSPRAY MASS SPECTROMETRY

2.1.4.1 THE MASS ANALYSER

The ESI experiments were carried out in a Fisons' "Quattro II" triple quadrupole mass spectrometer (VG Biotech, Altrincham, UK) equipped with an atmospheric pressure ionisation (API) source operated in the nebuliser-assisted electrospray mode. The "Quattro II" instrument is equipped with two high performance, research grade quadrupole mass analysers (MS1 and MS2) and a hexapole collision cell h between them (see fig.2.1). The source is separated from the first mass analyser MS1 by a series of lenses which serve to focus ions formed in the source into MS1.

After MS1 is the 'Altrincham lens' and its associated photomultiplier detector D_1 which separates MS1 from the collision cell h. In MS1 acquisition mode, the Altrincham lens diverts ions to D_1. This operation provides a simple and sensitive method of performing conventional MS analysis. The detection system of the "Quattro II" consists of a low level noise photomultiplier that is typically operated at a gain of 10^5 to amplify the ion current collected.

The hexapole collision cell h enables ions, generated in the source and selected by MS1, to be collisionally activated causing them to fragment. h is a rf-only device, the rf field within the cell efficiently refocusing ions scattered during the collisionally-induced decomposition (CID) process. A gas pressure of 5 μ bar of argon is used as the collision gas for CID.

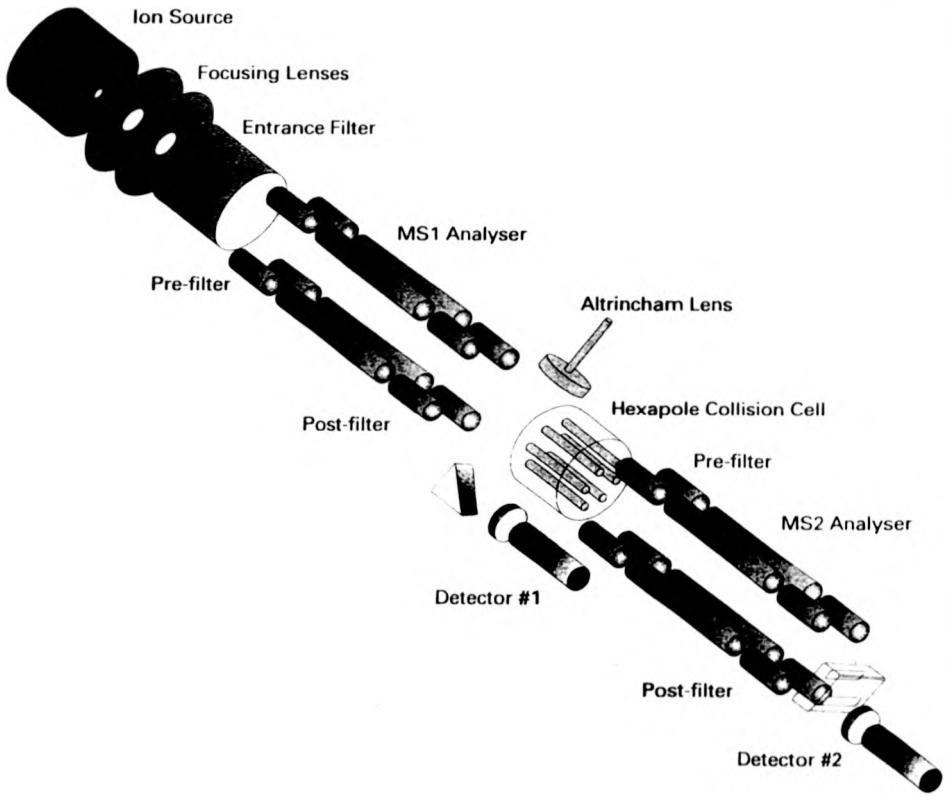

FIG.2.1 A SCHEMATIC DIAGRAM OF THE ION OPTICS OF THE FISONS 'QUATTRO' II TRIPLE QUADRUPOLE MASS SPECTROMETER [2]

The primary purpose of MS2 is to mass analyse the products of fragmentation reactions occurring in h. The detector D_2, situated after MS2 is also a low noise photomultiplier.

2.1.4.2 THE ELECTROSPRAY SOURCE

The potential on the electrospray needle was set at 3.5 kV and the extraction cone voltage was varied between 20 and 100 V.

2.1.4.3 SAMPLE INTRODUCTION

Typically PNMMO/PPO at a concentration of 0.5 $\mu g/\mu l$ were dissolved in a mixture of tetrahydrofuran (THF) and methanol (1:1 by volume) in the presence of 0.5 % ammonium chloride. Aliquots of 20 μl were introduced into the ion source at a flow rate of 5 μl/min. Other solvent systems used were dimethylformamide (DMF)/THF (1:1 by volume) and other salts used were LiCl, NaCl, KCl, RbCl and CsCl. All solvents were dried and distilled under dry nitrogen before use. THF was dried using potassium, and methanol was dried over 4 Å molecular sieves.

2.1.4.4 DATA ACQUISITION

Mass spectra were acquired over the range m/z 3000 - 350 during a 10 s scan and by operating the data system in the multichannel acquisition (MCA) mode, 30 scans were summed to produce the final spectrum. Calibration was carried out using a solution of sodium iodide.

2.1.5 MATRIX-ASSISTED LASER DESORPTION IONISATION (MALDI)

2.1.5.1 THE MASS ANALYSER

All experiments were carried out on a Kratos Kompact III MALDI-TOF mass spectrometer. The instrument is fitted with a nitrogen laser of wavelength 337 nm with a 3 ns pulse duration, and an electron multiplier detector. The spectrometer was operated in the positive ion linear mode with an accelerating potential of 20 kV.

2.1.5.2 SAMPLE PREPARATION

Sample concentrations were approximately 10^{-4} molar in a mixture of methanol and water (1:1) in the presence of 0.5 % sodium chloride. Matrix (2,5-dihydroxybenzoic acid) concentrations were approximately 10^{-1} molar in THF/methanol (1:1 by volume). Equal volumes of matrix and analyte solutions were mixed and 1-2 μ l placed on a stainless steel sample slide. The solvent was evaporated under a cool stream of nitrogen.

Every sample was analysed at various laser powers and spectra were averaged over 200 laser shots. Analysis of the data acquired was carried out using software installed on the Kompact III.

2.1.6 CHEMICAL IONISATION MASS SPECTROMETRY (CIMS)

All experiments were performed on a Kratos MS80 spectrometer incorporating a DS90 data system. The probe temperature was 150^{0}C and ammonia gas was used to promote ionisation.

Experiments combining gas chromatography and mass spectrometry were also performed on the gases evolved from PNMMO on pyrolysis. The column support was Chromosorb WHP and the liquid phase was Carbowax 20M. The column temperature was

set at 100^0C and the carrier gas was helium. PNMMO samples (1.00 g) were placed in glass vials (20.0 ml) and capped with subaseals. The samples were heated for varying lengths of time at 155^0C in an oil bath. Samples (10.0 μ l) of gas were extracted from the vials using a microsyringe and injected directly into the injection port of the GCMS.

2.1.7 FAST ATOM BOMBARDMENT (FAB)

Attempts to evaluate the mass distribution of PNMMO were made on the Kratos 'Concept' 4-sector tandem mass spectrometer employing FAB. Glycerol and meta-nitrobenzyl alcohol, being the most widely used FAB matrices, were both tested.

2.1.8 PHOTOLYSIS

2.1.8.1 PHOTOLYSIS OF SOLUTIONS

PNMMO was dissolved in diethyl ether (0.10 g cm^{-3}) and photolysed using a water-cooled 150 W Phillips medium pressure mercury arc lamp. Samples of solution (10.0 cm^3) were extracted every 50 h and the solvent removed on a rotary evaporator. The photolysate was then dissolved in chloroform-d_1 and examined spectroscopically.

2.1.8.2 PHOTOLYSIS OF FILMS

Polymer films were photolysed using a Eurosep Instruments model no. FOI6000 350 W air-cooled xenon lamp. No filters were used. The films were normally mounted on sodium chloride plates and photolysed directly in air at a distance of approximately 10 cm. The films were photolysed on both sides to ensure more homogeneous photolysis.

2.1.9 SIZE EXCLUSION CHROMATOGRAPHY (SEC)

The SEC system used in this work consisted of a dual piston HPLC pump (ICI instruments LC1110), an injection valve with a 20 μl sample loop (Rheodyne 7125), and a refractive index detector (ICI Instruments LC1240). The data were collected using a Polymer Laboratories (PL) data capture unit (DCU) and analysed using PL Calibre GPC/SEC software.

The SEC eluent was THF with a flow rate of 1.00 ml/min. Toluene (0.2 %wt) was used as an internal standard and flow marker in each sample. All samples were examined at equal concentrations (5 g dm^{-3}), except where stated otherwise. The column set consisted of a PL 5 μm bead size guard column (50 × 7.5 mm) connected to either a Mixed-D or a Mixed-E column depending on the mass range to be examined.

2.1.9.1 LOW MASS ANALYSIS

Analysis of polymer samples with RMM ranges between 100 and 30 000 mus was performed using a PL 3 μm bead size Mixed-E column (300 × 7.5 mm). Data were collected at 1 point per second. The system was calibrated with PPO standards.

2.1.9.2 HIGH MASS ANALYSIS

Analysis of polymer samples with molecular weight ranges between 200 and 400 000 mus was performed using a PL 5 μm bead size Mixed-D column (300 × 7.5 mm). Data was collected at 1 point per second. The system was calibrated with PPO standards.

2.1.10 GAS CHROMATOGRAPHY (GC)

All experiments were performed on a Pye Unicam series 204 gas chromatograph equipped with a flame ionisation detector. The column was 1 m long, 6 mm in diameter and made of glass. The column support was Chromosorb WHP with a mesh range of 100-120 and the liquid phase was Carbowax 20M. The injector and detector temperatures were 150^0C and the column temperature was 100^0C. The flow rate of the nitrogen carrier gas was 30 ml min^{-1}.

Samples were pyrolysed in exactly the same manner as for the GCMS experiments. PNMMO was heated at 150^0C and 10 μl samples of gas were extracted with a microsyringe over varying lengths of time.

2.1.11 CHN ANALYSIS

Pyrolysed and unpyrolysed samples of PNMMO were weighed on a Mettler ultra micro balance (7 d.p.) and sealed in tin capsules. Analysis was performed using a Leeman Laboratories CE440 elemental analyser. Repeat analysis was performed on every sample to ensure the reproducibility of the results.

2.1.12 PYROLYSIS OF POLYMERS IN THE OVEN

Extensive pyrolysis of polymers over a long period of time was carried out in a fan-assisted Gallenkamp Hotbox model oven. The oven temperature was closely monitored with a Cu/Con thermocouple and a stability of $\pm 0.5^0$C was attainable.

2.1.13 PHOTOGRAPHS OF MALDI SAMPLES

MALDI samples of PNMMO and PPO were prepared in the usual manner on stainless steel slides and allowed to dry in a stream of nitrogen. Photomicrographs were taken using an Olympus BH-2 high power microscope incorporating a C-35 AD-4 photographic system. Photographs were taken at $\times 75$ (1 cm $\equiv$ 133.3 μ m) and $\times 150$ (1 cm $\equiv$ 67.7 μ m) magnification.

2.2 EXPERIMENTAL PROCEDURES

2.2.1 ESR

2.2.1.1 ESR SPECTRA OF UNCURED PNMMO

Samples of PNMMO (1.0 g) were placed in glass vials (20.0 ml) and heated at various temperatures in air in the range 100 - 150^{0}C using an oil bath. Samples of the pyrolysate (0.10 g) were then transferred to quartz (6 mm × 100 mm) tubes and the ESR spectrum measured at room temperature.

Spin trap experiments were performed using the spin traps N-tert-butyl-α-(2-sulfophenyl)-nitrone, nitrosodurene and nitrosobenzene. Solutions having a weight composition 0.5 % spin trap, 9.5 % PNMMO and 90 % dimethylsulfoxide-d_6 (water and ca. 0.5 % dimethylsulfoxide-h_6 were present) were heated to 150^{0}C within one minute, maintained at 150^{0}C for one minute and then cooled to room temperature over several minutes. The solutions (2.0 cm^3) were contained in quartz tubes and heated using an oil bath. Similar experiments were also performed with degassed solutions sealed under dynamic vacuum. Standard vacuum-line apparatus was employed for experiments under anaerobic conditions. Solutions were prepared as above and evacuated in quartz tubes. The mixture was frozen under liquid nitrogen (77 K) and "pumped on" for 20 s. The tube was then isolated by means of a Young's tap and allowed to reach 293 K. The mixture was then frozen and the process repeated 4/5 times. Experiments were also performed with neat PNMMO. Samples of PNMMO were mixed with a suitable solvent (chloroform-d_1, dimethylsulfoxide-d_6) to lower the viscosity and evacuated in quartz tubes. Repeated freeze(77 K)-pump-thaw cycles were performed up to 12 times and an oil bath at 60^{0}C was placed around the mixture to ensure removal of all of the solvent and the dissolved oxygen.

The spectrometer was not equipped with a variable temperature cavity. PNMMO could however be heated and very quickly transferred to the ESR cavity where the spectrum could be run at increased temperature. The exact temperature of the polymer was measured with a Cu/Con thermocouple. Efficient preparation ensured that the sample did not cool down more than 4^0C during the spectrum measurement. Low temperature experiments were performed at 77 K by placing the quartz tube containing the polymer sample in a quartz dewar filled with liquid nitrogen.

2.2.1.2 ESR SPECTRA OF CURED PNMMO FILMS

Thin PNMMO films were cured in the usual manner on sheets of PTFE. Films (3 cm × 10 cm) were removed from the PTFE, rolled up and placed inside quartz tubes and heated in the oven at varying temperatures.

2.2.2 COLUMN CHROMATOGRAPHY

Thin layer chromatography (TLC) plates used in conjunction with various solvent systems were employed to find the most appropriate conditions for separation of the components of the unpyrolysed and pyrolysed PNMMO systems (PNMMO was pyrolysed to varying extents at different temperatures). For all chromatographic separations a 'wet column' set-up was employed. A glass column (1 m tall, 5 cm diameter) was filled with a toluene (HPLC grade) and silica slurry. The silica particle size was 0.040-0.063 mm (230-400 mesh ASTM). PNMMO (5.0 g) was dissolved in toluene to give a saturated solution and pipetted on to the top of the silica to a depth of about 3 mm. A layer of sand (2 mm) was placed on top of the PNMMO to avoid disturbance during solvent addition. Toluene was continually added to the column whilst eluting solution was collected as 15 cm^3 fractions.

This extracts the more non-polar constituents of the mixture. A methanol (HPLC grade) and toluene mixture was then used to draw out the more polar constituents of the mixture. The methanol was added in gradually increasing concentration to avoid solvent effects which may disrupt the silica. The methanol concentration did not exceed 10 % v/v. Normally approximately 100 fractions were collected using toluene as the solvent and another 100 were collected using the methanol/toluene solvent system. The solvent was then removed from the various fractions on a rotary evaporator and the resulting polymer analysed via NMR, IR, GPC and ESI.

2.2.3 EXPOSURE OF POLYMERS TO $NO_2(g)$

A cylinder of $NO_2(g)$ (1300 g) was purchased from Chromatography Services Ltd. All experiments using this gas were performed in fume cupboards. Samples of polymer (PNMMO, PPO, PEO) were placed in round bottomed flasks (250 cm^3) and qualitative experiments performed by filling the flasks with $NO_2(g)$ and immediately stoppering and sealing them with PTFE tape. The flasks were left under various conditions (see results section) and samples of polymer examined via ^1H, ^{13}C NMR and IR spectrometry over a period of time. $NO_2(g)$ is dark brown and can be easily observed at room temperature.

Quantitative experiments were performed on a vacuum line. The $NO_2(g)$ cylinder and a round bottomed flask (250 cm^3) filled with PNMMO (2.0 g) were connected to the vacuum line. The line was evacuated and the $NO_2(g)$ cylinder opened very briefly (approx. 1 s), filling the apparatus with $NO_2(g)$. The pressure in the line was measured with an Edwards' pressure gauge. A dewar of $N_2(l)$ was placed under the flask to condense out the $NO_2(g)$. The number of moles of $NO_2(g)$ was thus calculated from the pressure and known volume of the line. The sealed flask was then allowed to reach room temperature and left

under various conditions (see results section). Samples of polymer were examined via ^{1}H, ^{13}C NMR and IR spectroscopy.

2.2.4 CURING OF POLYMERS

2.2.4.1 PNMMO

PNMMO (20.0 g) was heated to $50^{0}C$ in a round bottomed flask and maintained under vacuum for 2 h on a vacuum line. The aliphatic isocyanate curing agent, Desmodur N-100 was added to the PNMMO in a mass concentration of 8.8 %. The mixture was evacuated for a further 15 min and spread as thinly as possible on PTFE sheets which were left in an oven at $70^{0}C$ for approximately 72 h.

2.2.4.2 POLY(ETHYLENE OXIDE)

PEO powder was dissolved in distilled water to give a saturated solution. The resulting solution was spread as thinly as possible on PTFE sheets and left to dry for 24 h at $40^{0}C$.

2.2.5 ADDITION OF POTENTIAL STABILISERS TO PNMMO

The action of three potential stabilisers on the thermal degradation of PNMMO was tested. 1,4-benzenedimethanol and 1,2,3,4-tetrahydronaphthalene were added to PNMMO in a mass concentration of 1.5 and 3 %. 2-nitrodiphenylamine was added in a mass concentration of 1.5 %. Samples of each of the mixtures (5.0 g) were placed in vials (20.0 ml) and heated in the oven at various temperatures in the range 100 - $150^{0}C$. Untreated PNMMO was similarly heated. Six vials of each mixture were prepared so that individual

vials could be removed without excessive cooling of the remaining samples. Samples were analysed by IR, NMR and SEC.

The influence of trace metal ions such as iron and copper was also investigated.

2.2.6 MOLECULAR MODELLING

Molecular modelling was performed using the software package 'Hyperchem'. Both the cyclic and linear species present in PNMMO were modelled. The cyclic species were modelled with and without Na^+ present to calculate the relative stabilities of the adducts formed during ESI. All atom interactions during a simulated heating (and subsequent cooling) process to 4000 K were taken into consideration to produce the lowest energy conformations. A processing time of approximately 48 h on a computer with a 486 DX/2 type processor was needed for each simulation.

2.3 CHEMICALS

2.3.1 POLYMERS

PNMMO was supplied in various batches to the DRA from ICI (Explosives Division). The batches were as follows :

PNMMO: BATCH PP57

PNMMO: BATCH PP260, M_w = 3035, M_n = 1599

PNMMO: BATCH PP330, M_w = 3549, M_n = 1661

PNMMO: BATCH PP340, M_w = 3669, M_n = 2064

P-GLYN: M_w = 2328, M_n = 1769 (ex-ICI)

PPO: M_w = 2000, (ex-ICI)

PPO: M_w = 2000, Janssen. M_w = 4000, Janssen.

PEO: M_w = 100 000, Aldrich.

2.3.2 GASES

NO_2: 98.5 %, Messer Griesheim.

NO: 99.0 %, Argo Int. Ltd.

2.3.3 POTENTIAL STABILISERS

2-Nitrodiphenylamine: 98.0 %, Lancaster.

1,4-Benzenedimethanol: 99.0 %, Aldrich.

1,2,3,4-Tetrahydronaphthalene: 99.0 %, Aldrich.

2.3.4 SOLVENTS

Chloroform-d_1: 99.8 %, Fluorochem Ltd.

$CHCl_3$, CCl_4, THF, $C_6H_5(CH_3)$, MeOH, DMSO, DMF: 99.8 %, HPLC grade, Fisons.

Ethylene glycol dimethyl ether: 99+ %, Aldrich.

2.3.5 ESR STANDARDS

2,2'-Diphenyl-1-picrylhydrazyl: 99.8 %, Aldrich.

Potassium nitrosyldisulfonate: ~99.0 %, synthesised after ref.1,

2.3.6 SALTS FOR ESI/MALDI ANALYSIS

NH_4Cl, LiI, NaI, KI: 99.9 %, Fisons.

2.3.7 MATRICES FOR MALDI /FAB ANALYSIS

2,5-Dihydroxybenzoic acid: 99.0 %, Aldrich.

2-Nitrophenyl octyl ether: 99.5 %, Sigma.

3-β-Indoleacrylic acid: 99.5 %, Sigma.

3-Nitrobenzyl alcohol: 99.0 %, Aldrich.

2.3.8 COLUMN CHROMATOGRAPHY

Silica Gel 60: particle size 0.040 - 0.063 mm (230 - 400 mesh ASTM), Merck.

Sand: low in iron, 40 - 100 mesh, Fisons.

2.3.9 OTHERS

2-Methyl-2-nitropropane: 99.0 %, Aldrich.

Methyl formate: 97.0 %, Aldrich.

Water-d_2: 99.9 %, Fluorochem.

CHAPTER 2 REFERENCES

1 Moser, W., Howie, R., *J. Chem. Soc.(A)*, 1968, 3039.

2 VG Bio Tech Ltd., VG Quattro II Users Guide.

CHAPTER 3

SPECTRAL ANALYSIS OF UNTREATED PNMMO

Untreated PNMMO was characterised by a number of different physical and spectral techniques before and after chromatographic separation. This chapter is concerned with the unchromatographed polymer, while chapter 4 details the results of the chromatographed polymer.

3.1 CHARACTERISATION OF PNMMO BY SEC

SEC shows that PNMMO consists of a material with a molecular weight of several thousand (nominally 5000), and a polydispersity of about 1.5, together with low molecular weight oligomers (fig.3.1). The polymerisation method shown in section 1.2 may be expected to give rise to both linear and cyclic oligomers. Previous to this study however, only the cyclic tetramer of PNMMO has been identified and characterised as a component of PNMMO, by NMR. SEC results suggest that the total oligomer content is about 5 %.

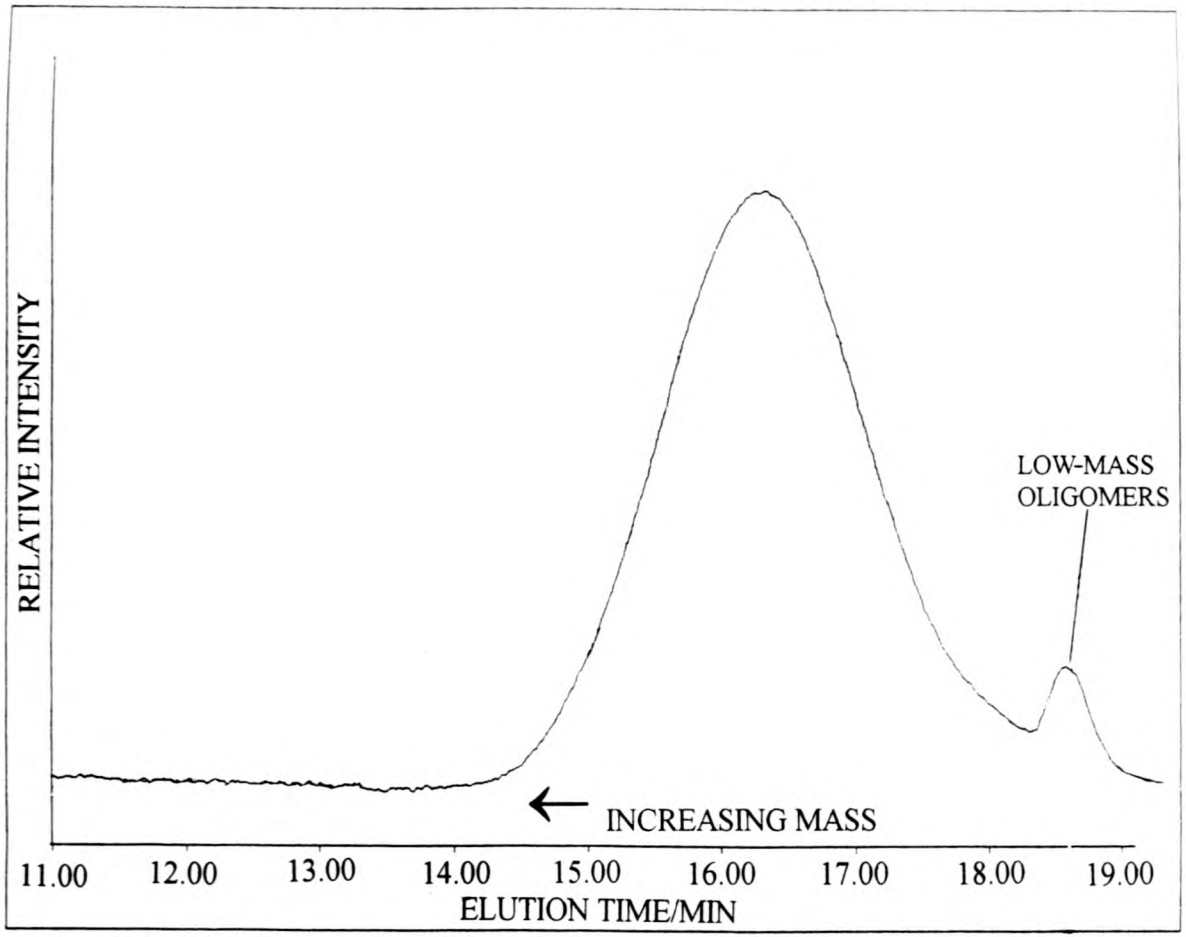

FIG.3.1 SEC CHROMATOGRAM OF UNTREATED PNMMO

3.2 CHARACTERISATION OF PNMMO BY INFRARED SPECTROSCOPY

Fig.3.2 shows the IR spectrum of untreated PNMMO run in chloroform-d_1. The peaks are labelled according to the scheme shown in table 3.1 below. Peak assignments were based on model compounds[1,2,3].

TABLE 3.1

PEAK ASSIGNMENTS IN THE IR SPECTRUM OF PNMMO

ASSIGNMENT	VIBRATIONAL FREQUENCY/cm^{-1}	LABEL
$\upsilon_A(CH_2)$	2972	A
$\upsilon_A(CH_3)$	2938	B
$\upsilon_S(CH_2)$	2889	C
$\upsilon_A(NO_2)$	1636	D
$\delta_S(CH_2)$	1486	E
$\delta_A(CH_3)$	1463	F
$\delta_A(CH_3)$	1368	G
$\upsilon_S(NO_2)$	1280	H
$\gamma_W(CH_2)$	1181	I
υ_A(C-O-C)	1109	J
$\gamma_T(CH_2)$	1051	K
υ(C-C) / $\gamma_R(CH_2)$	987	L
υ (NO)	863	M

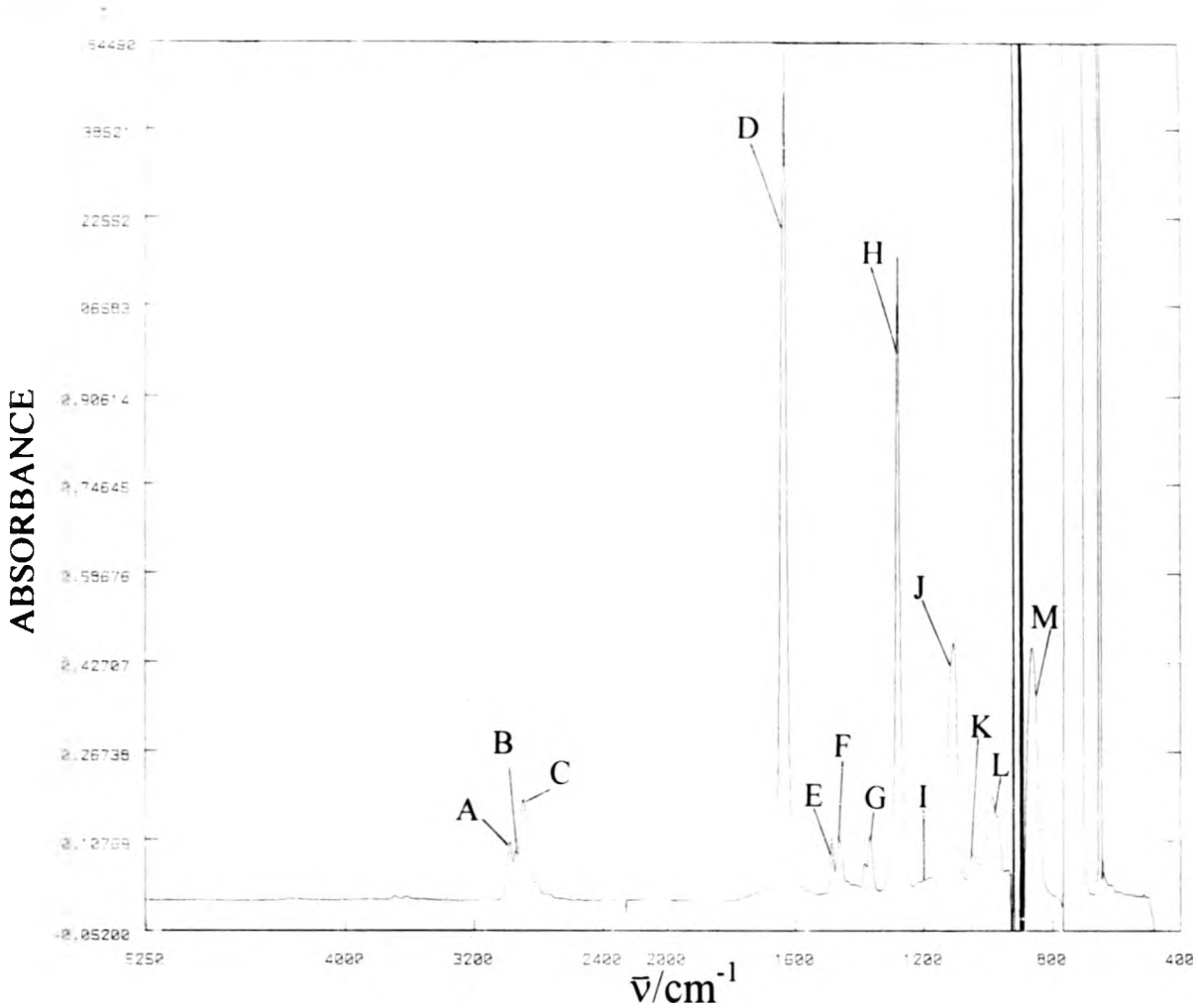

FIG.3.2 SOLUTION ($CDCl_3$) INFRARED SPECTRUM OF UNTREATED PNMMO

All of the expected group frequencies are apparent in the solution IR spectrum of PNMMO (fig.3.2). Spectra run in chloroform-d_1 show poorly resolved regions around 900 and below 800 cm^{-1}. This is due to small differences in path length associated with the background sample. IR spectra of neat PNMMO show only very minor peaks which are difficult to assign in these regions. Assignment of some of the other peaks in the IR spectra of neat PNMMO is also difficult due to their high intensity and thus it is advantageous to run spectra in solution.

3.3 CHARACTERISATION OF PNMMO BY NMR SPECTROMETRY

Untreated PNMMO was characterised by ^{1}H and ^{13}C NMR spectrometry at 298 and 358 K. Spectra run at 358 K showed increased resolution due to the lower viscosity of the polymer at higher temperature. However, as all the peaks in the spectra run at higher temperature were also visible in the spectra at 298 K, and for reasons of comparison with later spectra, the ^{1}H and ^{13}C NMR spectra of untreated PNMMO run at 298 K are shown in figs.3.3A,B. The peaks in the spectra are labelled with letters according to the schemes shown in the diagrams over the page. The assignments are based on PNMMO oligomers designed to contain the appropriate end group[4], and on 2-D NMR spectroscopy[5]. Unassigned peaks in the NMR spectra of PNMMO are not labelled. These peaks are of similar intensity and occur in the same region as the peaks for the end groups in PNMMO. We propose that these peaks are associated with unidentified end groups. ESI results confirm this (see section 4.5).

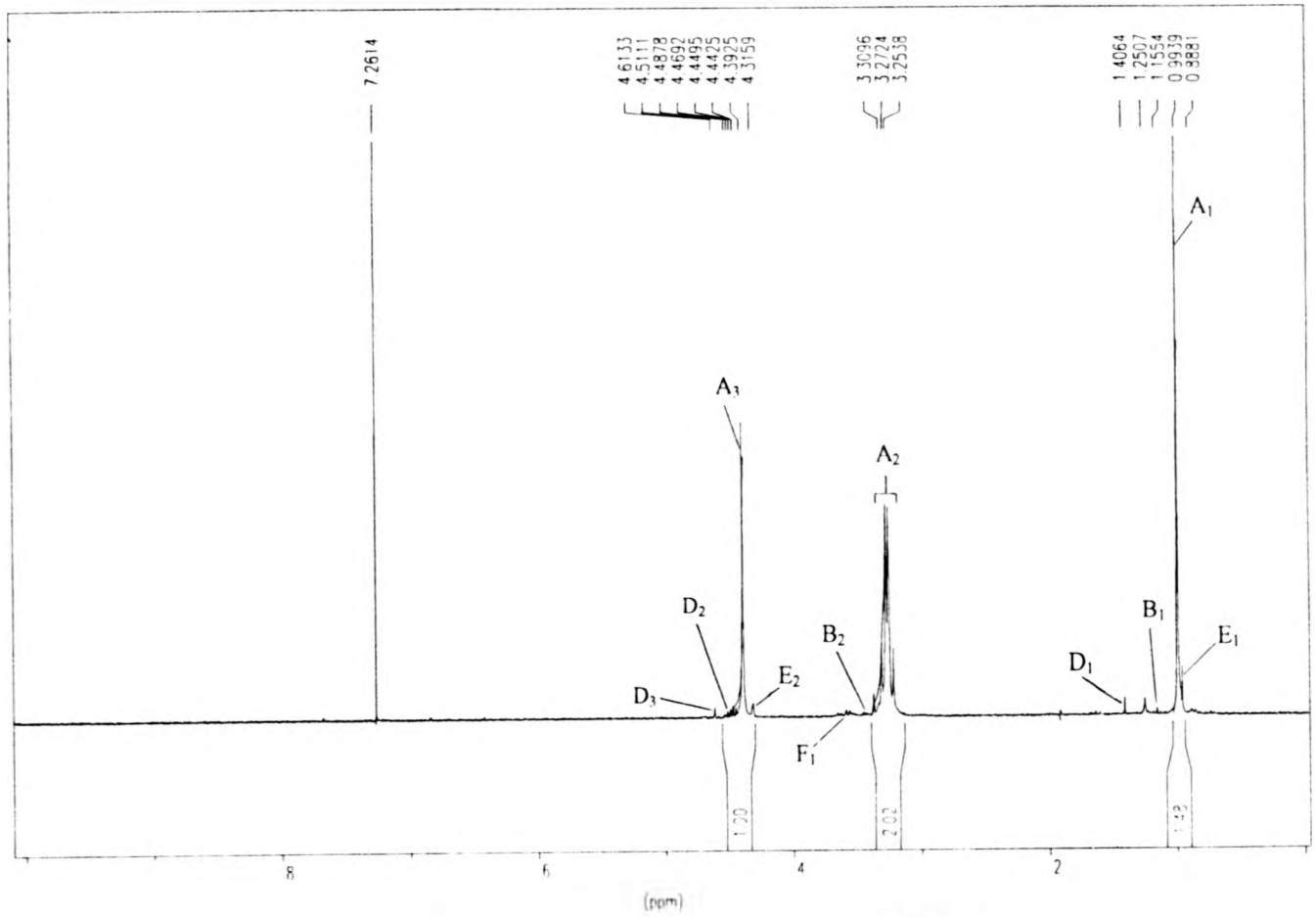

FIG.3.3A 250 MHz ^{1}H NMR SPECTRUM OF
UNTREATED PNMMO OBTAINED USING $CDCl_3$

UNTREATED PNMMO OBTAINED USING $CDCl_3$

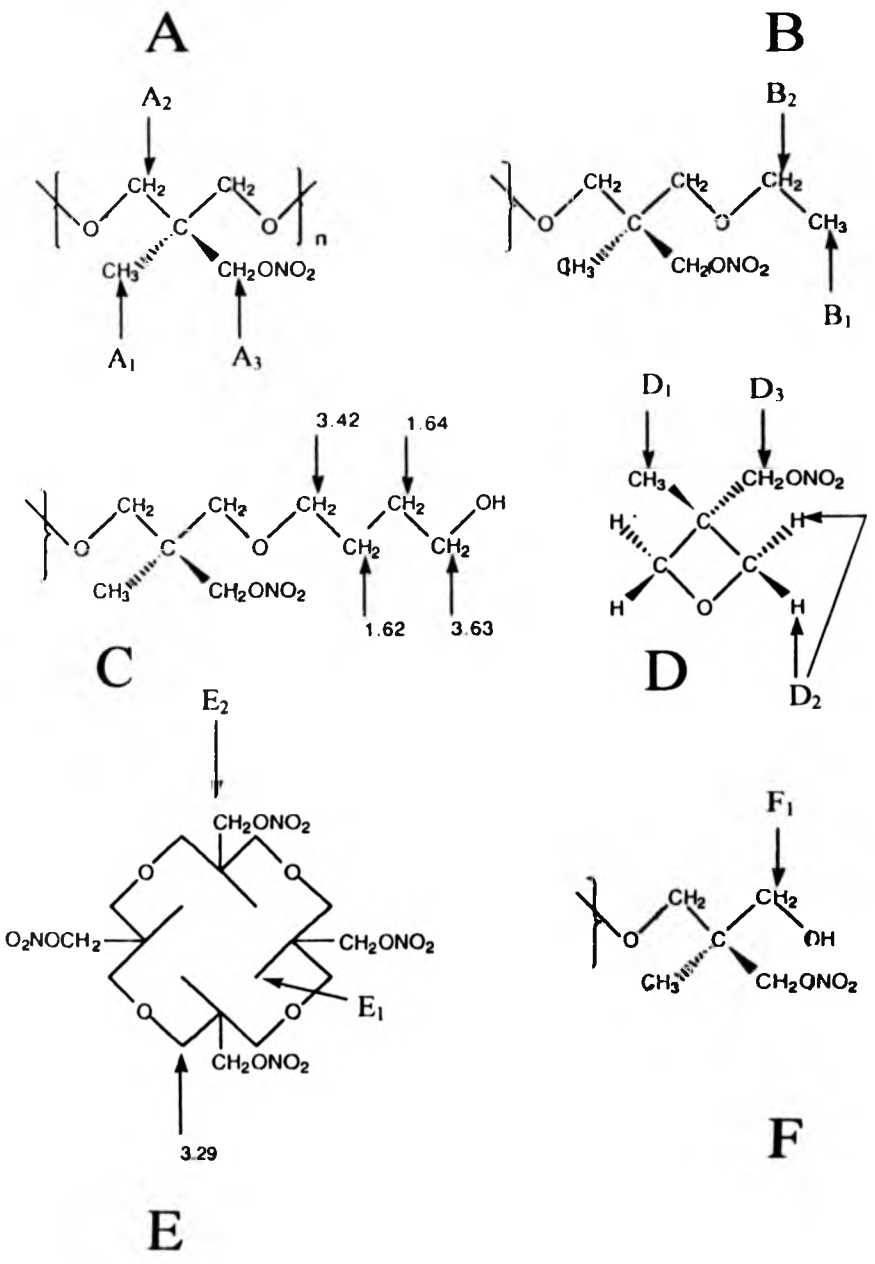

KEY TO THE PEAK ASSIGNMENTS IN FIG.3.3A

(HYDROGEN ATOMS LABELLED WITH THEIR CHEMICAL SHIFT ARE KNOWN TO EXIST FROM NMR MEASUREMENTS[4], BUT ARE NOT EASILY IDENTIFIABLE IN FIG 3.3A)

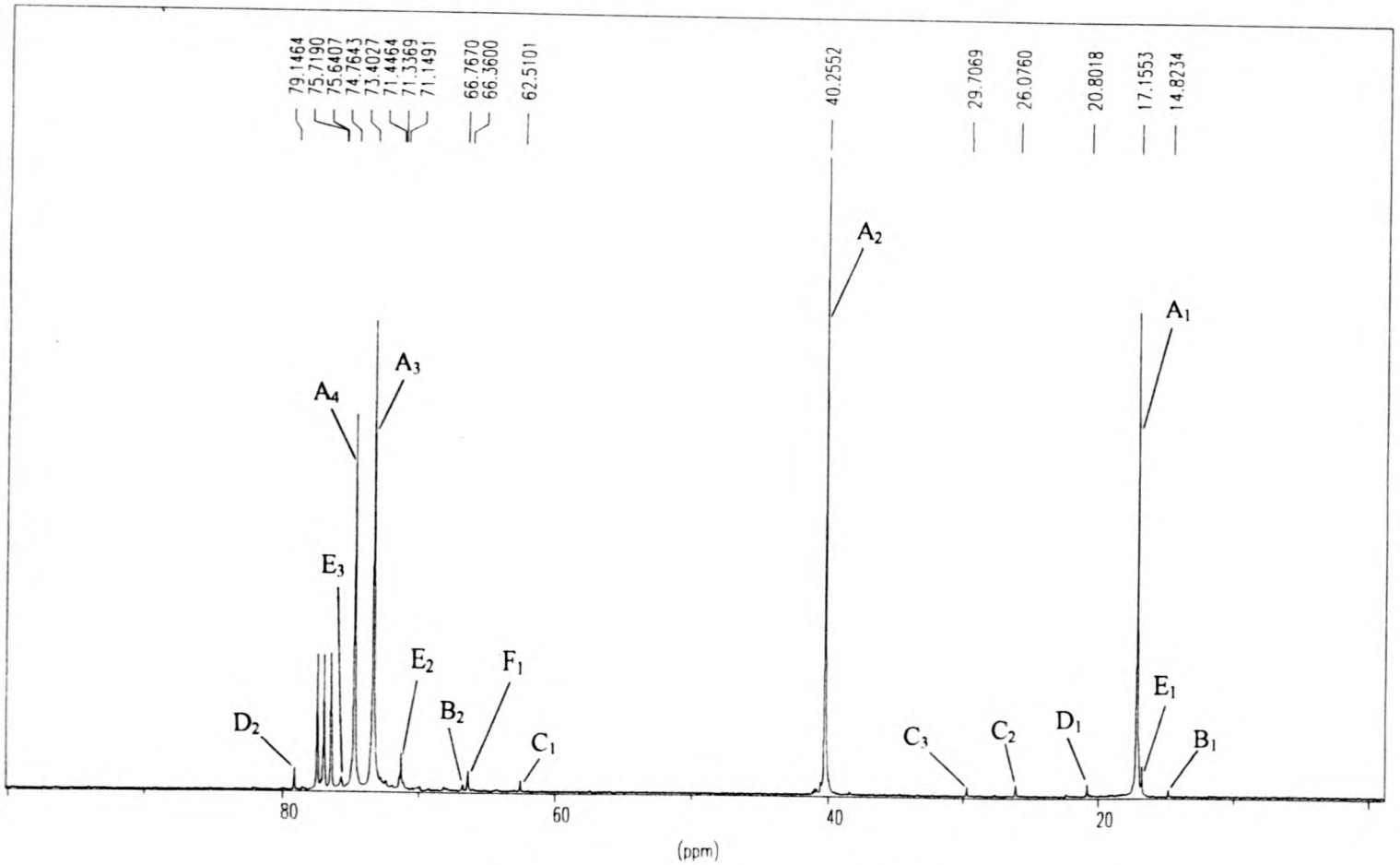

FIG.3.3B 250 MHz ^{13}C NMR SPECTRUM OF UNTREATED PNMMO OBTAINED USING $CDCl_3$

UNTREATED PNMMO OBTAINED USING $CDCl_3$

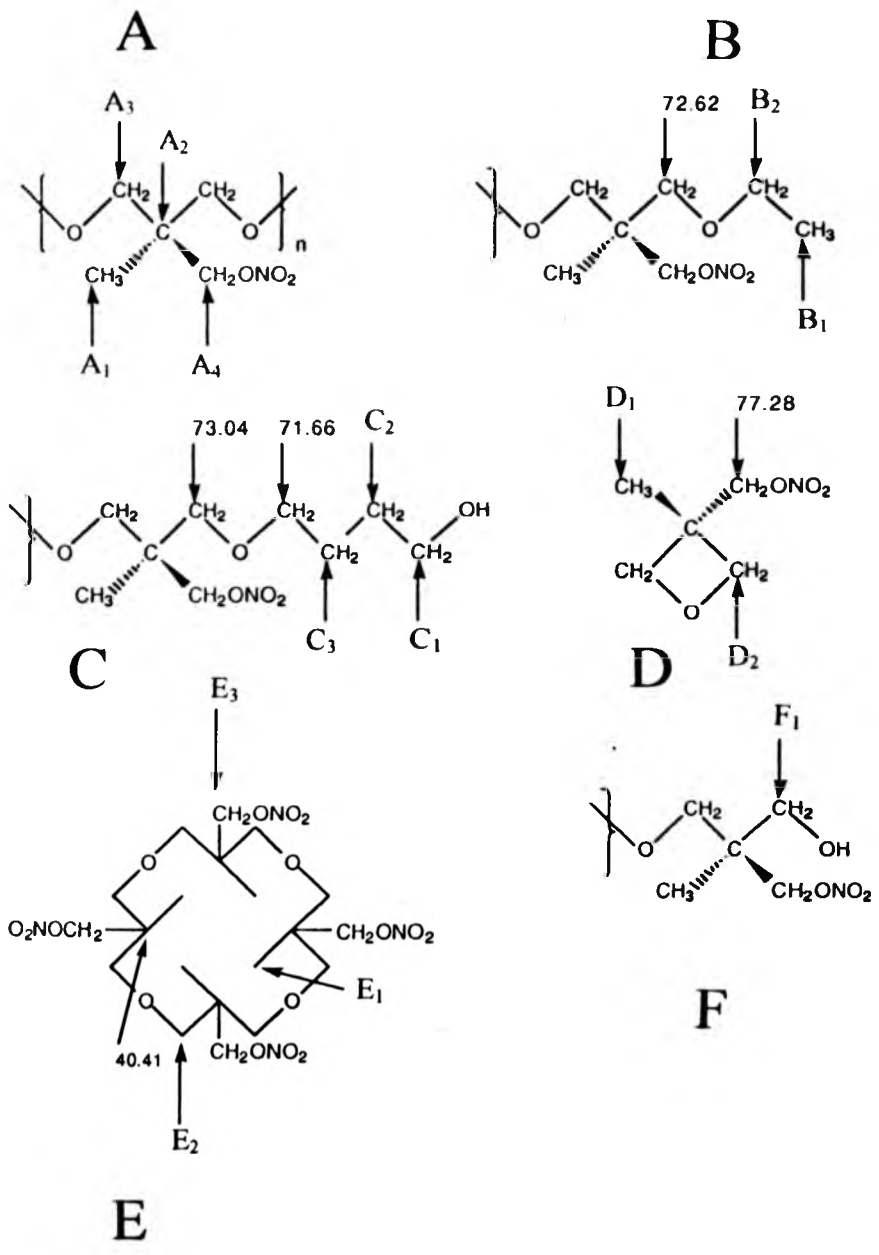

KEY TO THE PEAK ASSIGNMENTS IN FIG.3.3B

(CARBON ATOMS LABELLED WITH THEIR CHEMICAL SHIFT ARE KNOWN TO EXIST FROM NMR MEASUREMENTS[4], BUT ARE NOT EASILY IDENTIFIABLE IN FIG 3.3B)

3.4 CHARACTERISATION OF PNMMO BY ESI

The correct solvent system in combination with an appropriate salt to promote cationisation is essential for the ESI process to occur to an acceptable level[6]. The literature concerning the ESI of polymers is largely based on widely used polymers such as poly(ethylene glycols) (PEGs), polystyrene[7] (PS) and poly(methyl methacrylate)[8] (PMMA). PPO has many structural similarities to PNMMO, but is however far less well characterised than PEGs by ESI. The ESI of PEGs is generally performed using a solvent system containing a 50:50 mixture of methanol and water with either a Group I salt, acetic acid or ammonium chloride to promote cationisation[9,10]. PNMMO is insoluble in either water or methanol but dissolves well in THF. Thus PNMMO (5 g dm^{-3}) was dissolved in a 50:50 mixture of methanol and THF to which an aqueous solution of ammonium chloride (0.5 %) was added (the ammonium chloride dissolved only very sparingly in the absence of water).

3.4.1 ESI SPECTRA OF PNMMO RUN AT VARIOUS CVS

The spectrometer has an upper mass limit of 3500 mass units (mus) and thus for heavier ions to be detected, they must be able to accept more than one charge to lower the m/z ratio. Fig.3.4 shows the ESI spectra of PNMMO obtained at cvs of 20 (A), 50 (B) and 110 (C). In 1988, Loo *et al.*[11] demonstrated that the charge distribution for large molecules such as polypeptides was sensitive to a parameter which they termed the nozzle-skimmer voltage bias. This is the same as the cv. They found that decreasing the cv led to an increase in the abundance of more highly charged molecular ions. This effect of the cv is also well documented for PEGs[12] and proteins[11] and section 8.2 of this thesis also reports the same effect for PPO. PPO shares many structural similarities with PNMMO and it was hoped that multiple charging of PNMMO would produce ions in the mass range of the spectrometer.

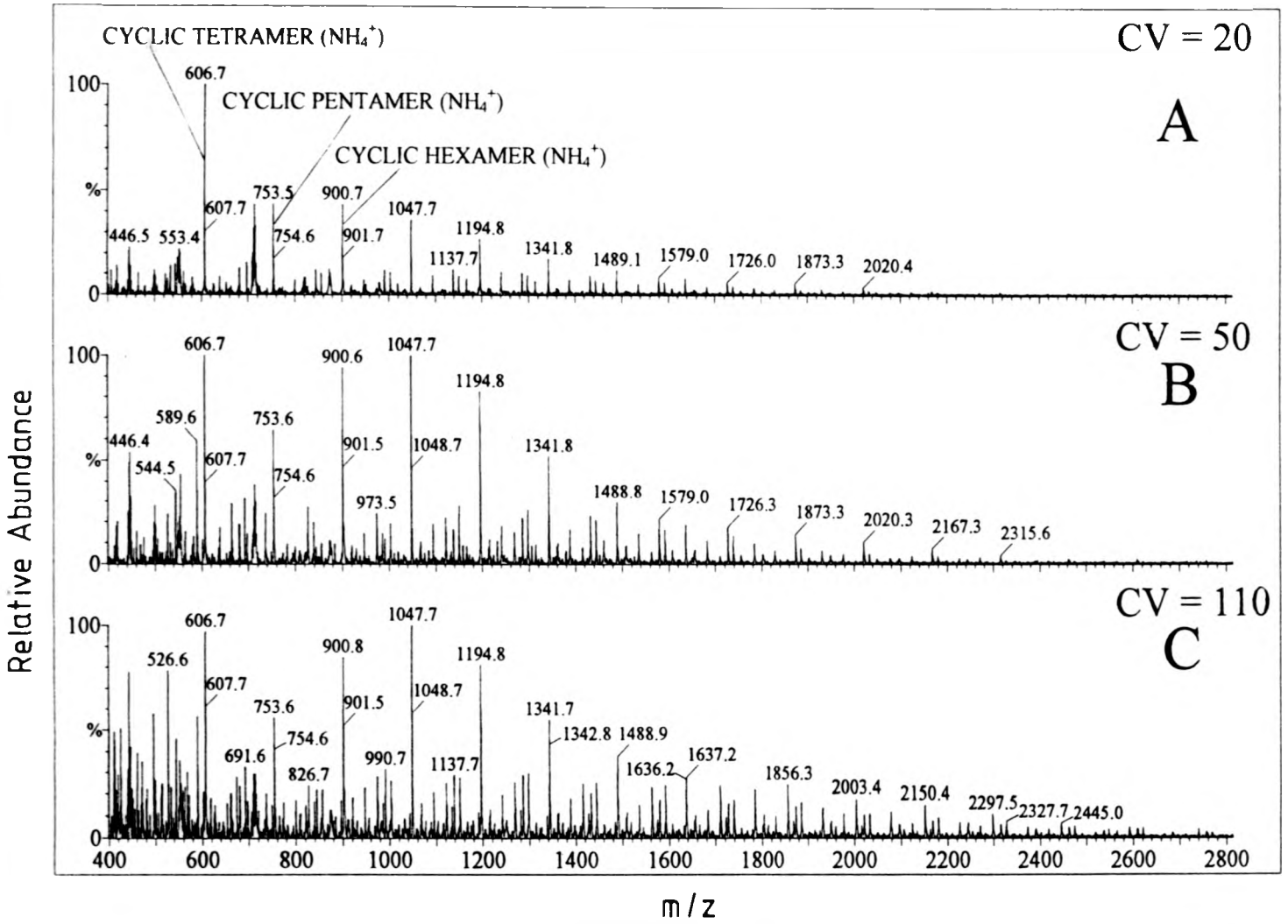
CYCLIC TETRAMER (NH_4^+)
CYCLIC PENTAMER (NH_4^+)
CYCLIC HEXAMER (NH_4^+)
CV = 20
A
606.7
753.5
900.7
1047.7
607.7
754.6
901.7
1194.8
446.5
553.4
1137.7
1341.8
1489.1
1579.0
1726.0
1873.3
2020.4
CV = 50
B
606.7
900.6
1047.7
1194.8
589.6
753.6
446.4
901.5
1048.7
1341.8
544.5
607.7
754.6
973.5
1488.8
1579.0
1726.3
1873.3
2020.3
2167.3
2315.6
CV = 110
C
606.7
1047.7
900.8
1194.8
526.6
607.7
753.6
901.5
1048.7
1341.7
754.6
1342.8
1488.9
691.6
990.7
1137.7
1637.2
826.7
1636.2
1856.3
2003.4
2150.4
2297.5
2327.7
2445.0
100
%
0
400
600
800
1000
1200
1400
1600
1800
2000
2200
2400
2600
2800
Relative Abundance
m/z

FIG.3.4 ESI MASS SPECTRA OF UNTREATED PNMMO OBTAINED AT CV's OF 20 (A), 50 (B) AND 110 (C) USING NH_4Cl TO PROMOTE IONISATION

Decreasing the cv does not however appear to have any effect on the magnitude of the ion charge for PNMMO. For all the species present, the ^{13}C isotopic splitting pattern clearly shows a ^{13}C isotope peak one mu higher than the ^{12}C isotope peak, as expected for a singly charged species. The ^{13}C isotope peak for a doubly charged species would always appear one half of one mu higher than the ^{12}C peak. Under the experimental conditions used here, it does not appear that PNMMO molecules will accept more than one charge.

A series of singly charged ions are observed below 3000 mus in all the ESI spectra of PNMMO (fig.3.4). Ions are not however detectable above 3000 mus, which contrasts with the picture of the polymer distribution from the SEC data. Thus it appears that the main polymer distribution around 5000 mus is not detectable under the experimental conditions used here. This is thought to be due to the insolubility of the higher mass oligomers in the solvent system and the difficulty in obtaining multiply charged species; similar problems of insolubility were also encountered during the ESI analysis of PS[7] and PMMA[8] samples with molecular weights greater than approximately 1000 mus. Other factors such as the cation size are also thought to be important but later experiments with PNMMO show that the use of larger cations is of limited use for the production of higher mass oligomer ions of PNMMO.

The singly-charged ions observed in all the ESI spectra of PNMMO can thus be assigned to the low-mass oligomers detected by SEC. The most intense ion peaks in the spectra appear at multiples of the monomer unit (147.1 mus) plus 18 mus, i.e. 606.7, 753.5, 900.7, 1047.7, 1194.8 and 1341.8 mus. It was later established by CID (see chapter 6) that these ions were ammonium adducts. The 18 mus were thus attributed to the mass of the ammonium ion and the peaks appearing at multiples of the monomer unit were assigned to the cyclic oligomers of PNMMO as the value of the RMM ruled out the presence of any end

group. Table 3.2 shows the calculated and experimentally found values for the RMM of the cyclic species in PNMMO.

TABLE 3.2

CALCULATED AND EXPERIMENTALLY OBTAINED (CV 110) VALUES FOR THE RMM OF THE CYCLIC PNMMO SPECIES ($+NH_4^+$)

RMM (EXPERIMENTAL)	RMM (CALCULATED)	NO. OF REPEAT UNITS
g mol^{-1}	g mol^{-1}	
not observed	459.2	3
606.7	606.3	4
753.6	753.3	5
900.8	900.4	6
1047.7	1047.4	7
1194.8	1194.5	8
1341.7	1341.5	9
1488.9	1488.6	10
1636.2	1635.6	11
1783.1	1782.7	12
1930.2	1929.7	13
2076.8	2076.8	14
2224.9	2223.8	15
2370.7	2370.9	16
2517.8	2518.0	17
2665.9	2665.0	18
2813.6	2812.1	19
2960.3	2959.1	20
3106.7	3106.2	21
3254.8	3253.2	22

The calculated values are in very close agreement with those obtained experimentally, and the greatest error of 0.07 % occurred around 600 mus.

Cyclic oligomers containing up to 22 monomer units are observed at a cv of 110 (88 atoms in the ring). The peaks observed at relatively lower intensity between adjacent cyclic oligomer ion peaks were attributed to linear species of PNMMO and this was confirmed by chromatography and end group analysis. The spectra (fig.3.4) clearly show that use of a higher cv results in the enhanced appearance of larger mass species. Conversely at low cv (20), the peak for the tetramer is twice as intense as any other peak. This phenomenon has not been documented previously for synthetic polymers. Loo *et al.*[11] have demonstrated that the abundances of all ions in the ESI spectra of melittin, a 26-residue polypeptide, drop uniformly as the cv is decreased below 170. This is attributed to collision processes which desolvate ions more efficiently at higher cv. The drop in intensity of the PNMMO ions is not uniform but, unlike the polypeptide sample, the PNMMO sample contains a wide range of different species which may be solvated to varying degrees at a particular cv. It seems likely that the larger mass species are more highly solvated as more sites exist for solvation. Thus the relative favouring of larger mass species at higher cv could be attributed to their relatively greater ease of desolvation as compared to the adducts of the lower mass species. Similarly for the ammonium adducts, larger mass ammonium adducts may be more stable at higher cv, producing the same mass bias seen in fig.3.4.

Fig.3.5 shows a portion of the ESI spectrum of PNNMO between 460 and 610 mus obtained at cvs of 20, 36, 50, 84 and 110. The spectra clearly show that as the cv is increased, the peak around 607.6 mus due to the ^{13}C isotope of the cyclic tetramer increases in intensity. Clearly the cv cannot affect the relative isotopic concentrations and so the

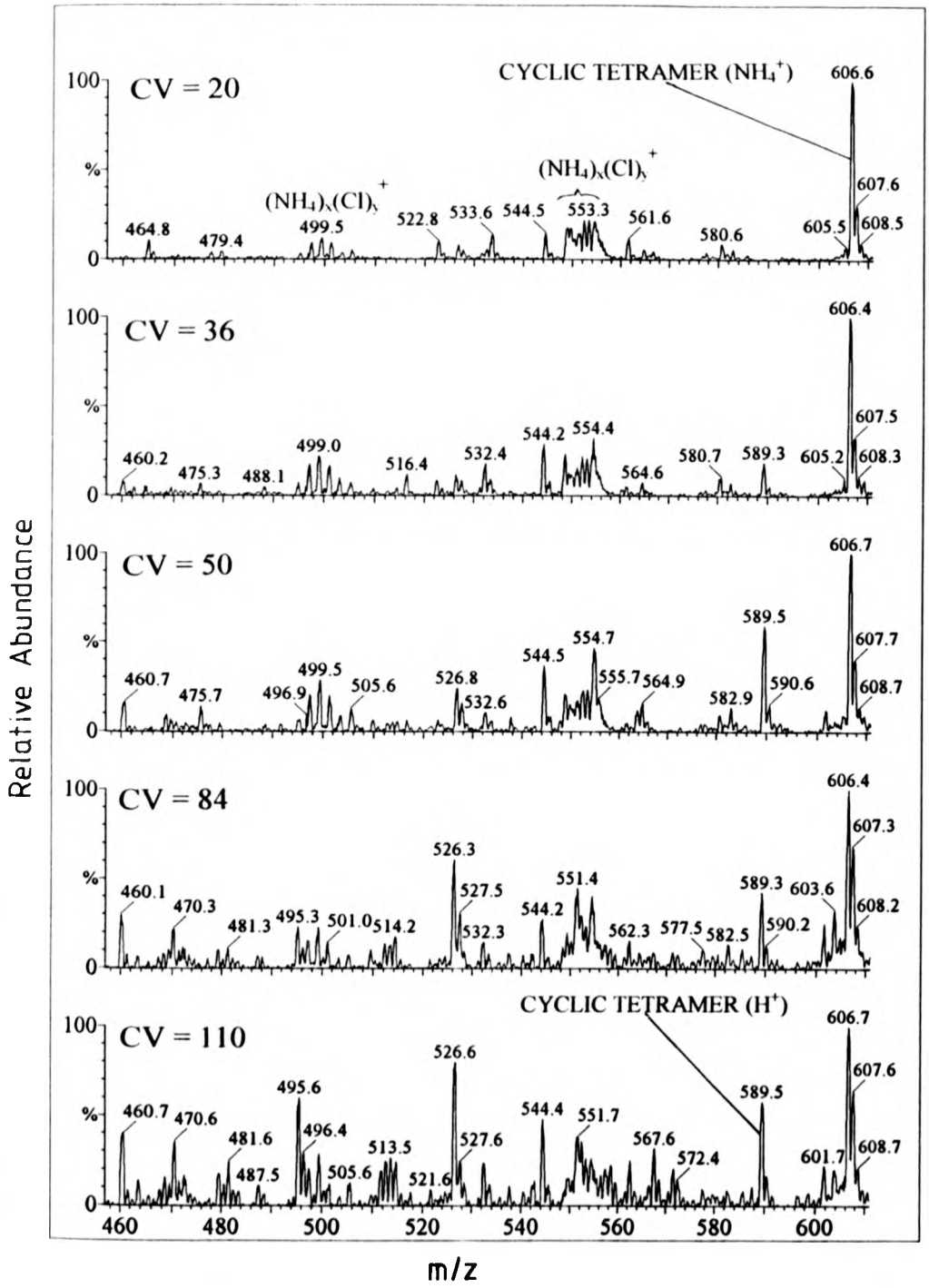

FIG.3.5 A PORTION OF THE ESI MASS SPECTRUM OF UNTREATED PNMMO OBTAINED AT VARIOUS CV's USING NH_4Cl TO PROMOTE IONISATION

increase in intensity of this peak must be due to the formation of a new ionic species at higher cv. The various end groups thought to be present in PNMMO are shown below[13].

A

HO-[PNMMO]-H

B

CH_3CH_2O-[PNMMO]-H

C

$HO(CH_2)_4O$-[PNMMO]-H

The tetramer of species A would give a peak due to the ammonium adduct at 624.3 mus. A very low intensity peak is observed at 624.5 mus. At high cv, loss of NH_3 could occur from the ammonium adduct leaving behind the protonated species at 607.3 mus. Thus at low cv (20), the peak at 607.7 mus is solely attributed to the ^{13}C isotope of the cyclic tetramer as confirmed by the relative intensities of the monoisotopic peaks at 606.7 and 607.7 mus obtained by calculation. At higher cv the H^+ ion of species A is formed and thus the peak at 607.7 mus represents 2 different species. This effect of the cv is clearly shown by the H^+ adduct of the cyclic tetramer at 589.5 mus; the peak is absent at a cv of 20 but is clearly visible at a cv of 36, and gradually increases in intensity as the cv is further increased.

Although the ammonium ion peak of the tetramer of species A gives rise to only a very low intensity peak, higher homologues exhibit more intense ion peaks. This is thought to be due to the increase in stability of the ammonium adduct as the oligomer size increases.

Thus at any particular cv, the H^+ adduct becomes relatively more stable as the mass of the oligomer decreases. The opposite is true for the NH_4^+ adduct. Similarly the H^+ adduct becomes relatively more stable and the NH_4^+ adduct less stable as the cv is increased. This is true for the linear oligomers but, as shown later, the cyclic oligomers behave in a more complex manner.

The tetramer and higher oligomers of species B and C are readily observable. The trimeric species do not however seem representative of the mixture as a whole. At low cv few ion peaks are observed below 600 mus. This may be due to the low concentration of oligomers present or a consequence of the low stability of the ammonium adduct of the trimeric species. A series of peaks due to $[(NH_4)_x(Cl)_y]^+$ can also be seen in the spectra (fig.3.5). These peaks make identification of some oligomers difficult and thus the linear oligomers are more easily identified at higher mass where $[(NH_4)_x(Cl)_y]^+$ clusters are not visible (see section 4.5).

3.4.2 ESI SPECTRA OBTAINED USING GROUP I METAL SALTS FOR CATIONISATION

Various salts were used in an attempt to promote cationisation of higher mass ions. The cation size did not however have a marked effect on the relative stability of the linear oligomers. Figs.3.6 and 3.7 show the ESI spectra of PNMMO obtained at a cv of 36 using Li^+I^- (fig.3.6A), Na^+I^- (fig.3.6B), K^+I^- (fig.3.6C), Rb^+I^- (fig.3.7A) and Cs^+I^- (fig.3.7B) to promote ionisation and a THF/MeOH (50 : 50) solvent system. All of the spectra show peaks due to the formation of salt clusters such as $[Rb_4I_3]^+$ at 722.5 mus (fig.3.7A) and $[Cs_4I_3]^+$ at 912.3 mus (fig.3.7B). These ions are easily identifiable and are particularly abundant for the larger cations such as Rb^+ and Cs^+. All of the ESI spectra were run using

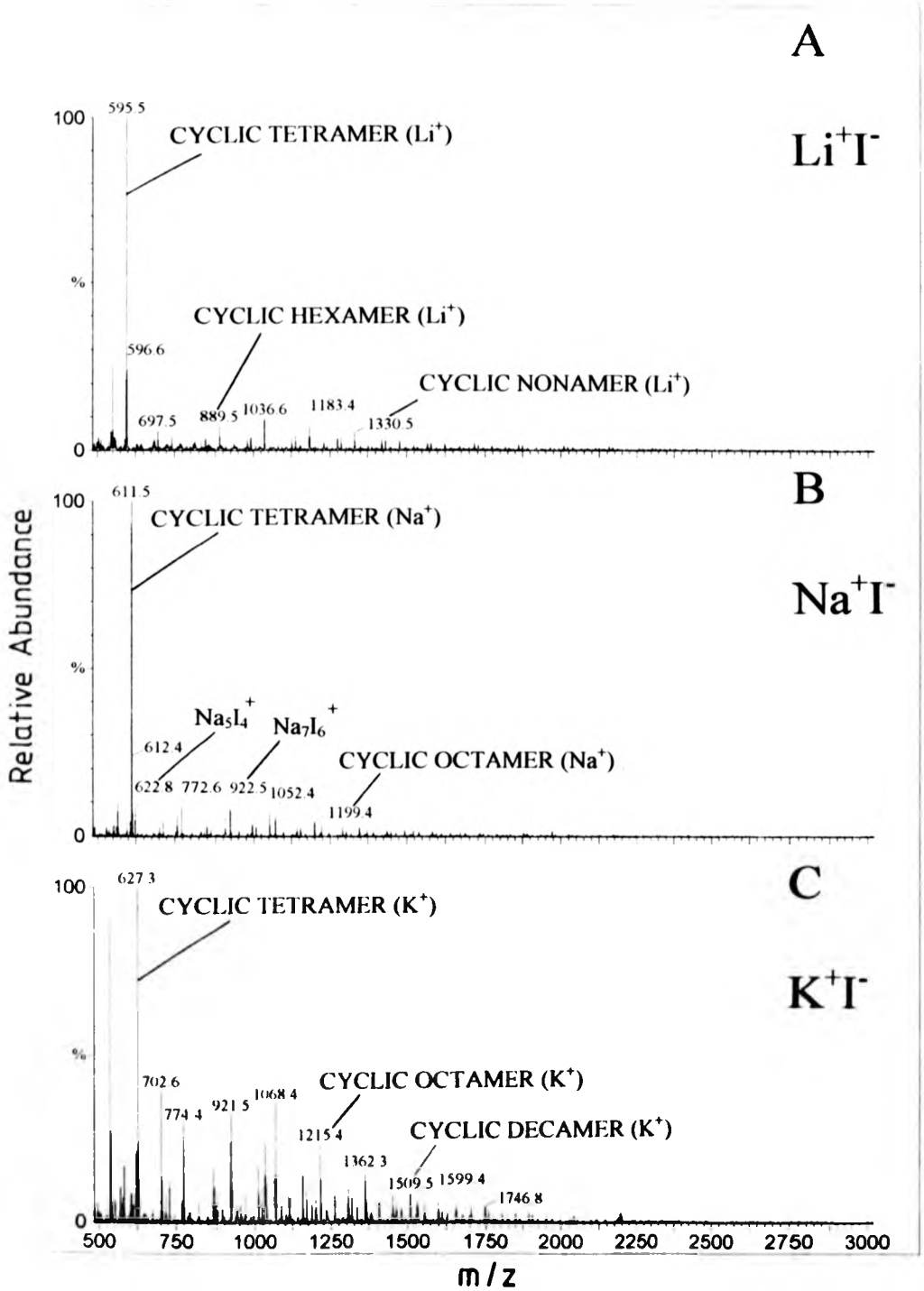

FIG.3.6 ESI MASS SPECTRA OF UNTREATED PNMMO OBTAINED USING LiI (A), NaI (B) AND KI (C) TO PROMOTE IONISATION

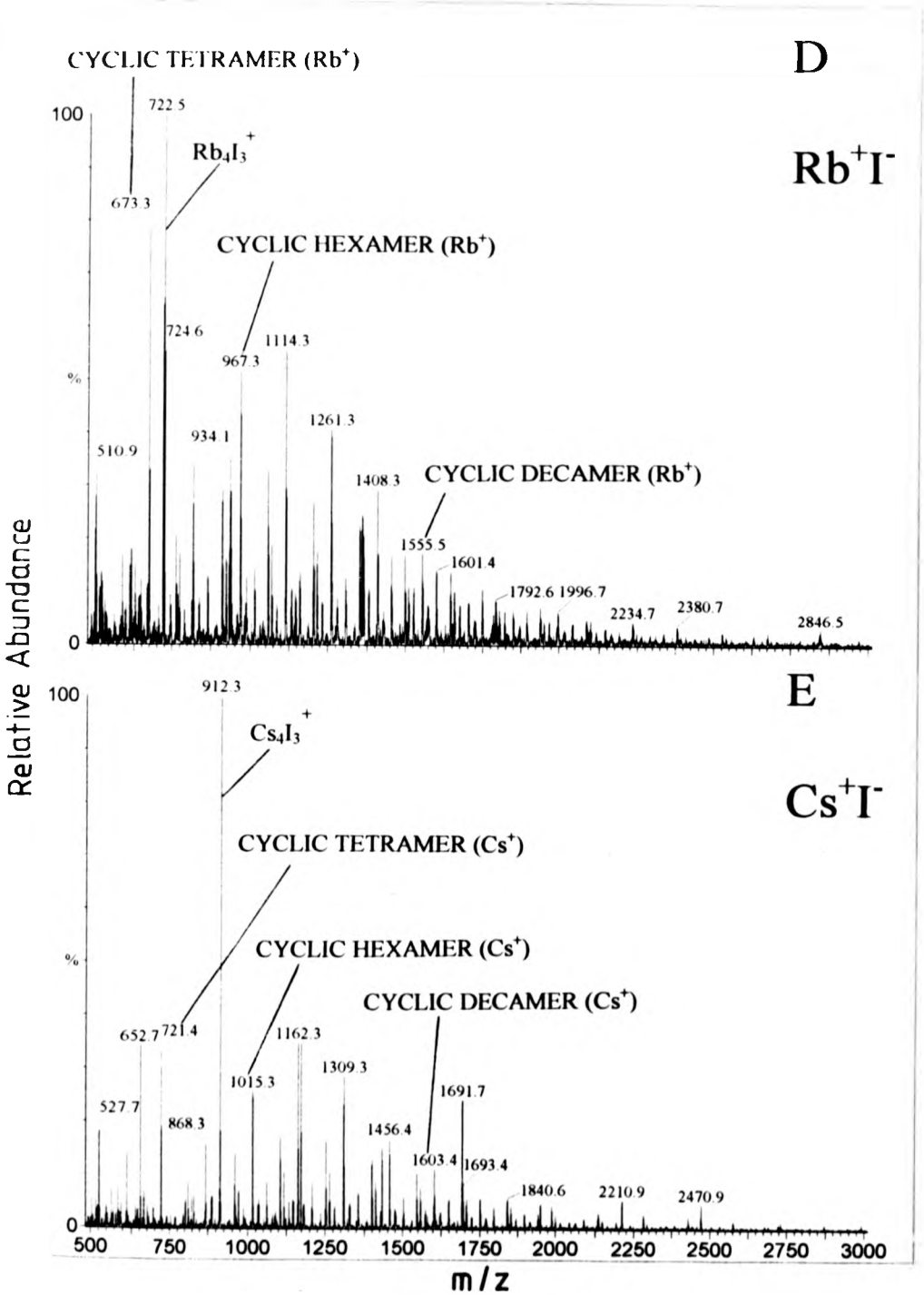

FIG.3.7 ESI MASS SPECTRA OF UNTREATED PNMMO OBTAINED USING RbI (A) AND CsI (B) TO PROMOTE IONISATION

identical concentrations of PNMMO and salt. The five spectra (fig.3.6A, B, C and 3.7A, B) clearly show the strong influence of cation size on the stability of the cyclic oligomer adducts. The spectra obtained using Li^+I^- and Na^+I^- exhibit peaks for the Li^+ (595.5 mus) and Na^+ (611.5 mus) adducts of the cyclic tetramer ten times as intense as any other peak. By contrast, the spectrum obtained using K^+I^- shows a peak for the K^+ adduct of the cyclic tetramer (627.3 mus) only three times as intense as those for the cyclic pentamer, hexamer, heptamer and octamer. Similarly, as the cation size increases further, the spectra obtained using Rb^+I^- and Cs^+I^- show that the peaks for the Rb^+ and Cs^+ adducts of the cyclic hexamer, heptamer and octamer are of approximately equal intensity to those for the corresponding adduct of the cyclic tetramer; indeed, the peak due to the Cs^+ adduct of the cyclic heptamer is of greater intensity than that for the cyclic tetramer. The relative intensities of the peaks due to the metal adducts of the cyclic oligomers in individual spectra are shown in table 3.3 below. In all cases, the metal adduct of the cyclic tetramer is attributed a relative intensity of 100. The cyclic oligomers are denoted by the number of monomer units they contain, thus the cyclic pentamer is denoted by the number **5** in the top row.

TABLE 3.3

RELATIVE ABUNDANCES OF THE METAL ADDUCTS OF CYCLIC OLIGOMERS IN PNMMO

	4	**5**	**6**	**7**	**8**	**9**	**10**	**11**
Li^+	100	4	8	10	8	5	3	2
Na^+	100	6	5	6	4	2	1	0.5
K^+	100	30	32	35	25	15	8	5
Rb^+	100	43	65	69	51	36	22	9
Cs^+	100	48	75	105	84	51	33	10

Clearly, as the cation size increases so the relative abundance of the ions attributed to the higher cyclic homologues increases relative to the ions due to the lower cyclic homologues. This is explained by likening each cyclic species to a crown ether of similar size. The metal ion bonds to the ether oxygens in the cyclic oligomer rings and thus the relatively high abundance of the ion due to the Na^+ adduct of the cyclic tetramer is due to the relatively high stability of the Na^+ complex (16 crown 4). As the cyclic species increase in size, so the Na^+ complex decreases in stability. Conversely, the larger Cs^+ ion forms more stable complexes with the higher mass cyclic homologues. Without a knowledge of the stability constants or the relative concentrations of cyclic oligomers present, it is impossible to calculate which oligomer forms the most stable complex with which cation. Similar experiments performed with the chloride salts of the group I metals showed, as expected, that the influence of the anion on the relative abundances of the adducts of the cyclic oligomers was negligible. Increasing the cv (above 36 V) led to an apparently uniform decrease in the abundance of all ions in the ESI spectra. This was attributed to the lower stability of the metal adducts of the cyclic and linear oligomers at higher cv.

The influence of the cation on the stability of the cyclic oligomer adducts can be confirmed with the aid of molecular modelling[14]. The Na^+ ion usually prefers a six co-ordinate geometry and thus the relatively high stability of the tetramer adduct cannot be fully explained as there are only four ether oxygens available in the tetramer ring. Both the cyclic tetramer and pentamer were modelled with and without Na^+ present to calculate relative stabilities. Both oligomers were initially modelled without Na^+ present by being subjected to simulated heating to 4000 K followed by cooling to 298 K to produce the lowest energy conformation. The Na^+ ion was then introduced and bonds added between the ion and the oxygen atoms in the oligomer ring. Consequently four new bonds were created for the

tetramer and five for the pentamer. The Na^+ to oxygen bond distance was estimated by averaging ten values of the same bond distance obtained (Daresbury data base) from the Na^+ complexes of 16 crown 4 ethers. The Na^+ to oxygen bond distance is not fixed during the modelling process, but with the input of an experimentally obtained value for this bond distance the modelling process is considerably faster and more accurate. The oligomeric adducts were then again subject to the simulated heating-cooling process outlined above. Consequently, the interatomic distances show that the Na^+ ion achieves its six co-ordinate configuration by binding to all the ring oxygens and the appropriate number of oxygens in the nitrate ester side chains. Figs.3.8 and 3.9 show the lowest energy conformations produced for the Na^+ complexes of the tetramer and pentamer respectively. The table below shows the relative energy values obtained from the simulation.

TABLE 3.4

THE RELATIVE ENERGIES OF THE TETRAMER AND PENTAMER COMPLEXES

STRUCTURE	ENERGY/kJ MOL^{-1}
TETRAMER	178.6
TETRAMER + Na^+ (CIS) FIG.3.8B	273.5
TETRAMER + Na^+ (TRANS) FIG.3.8A	202.7
PENTAMER	203.6
PENTAMER + Na^+ FIG.3.9A	398.2
PENTAMER + Na^+ FIG.3.9B	356.0

A

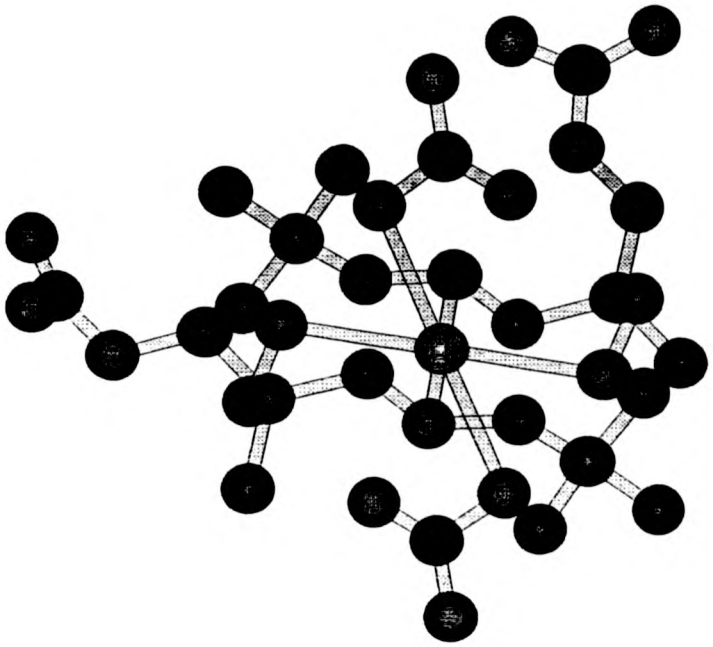

B

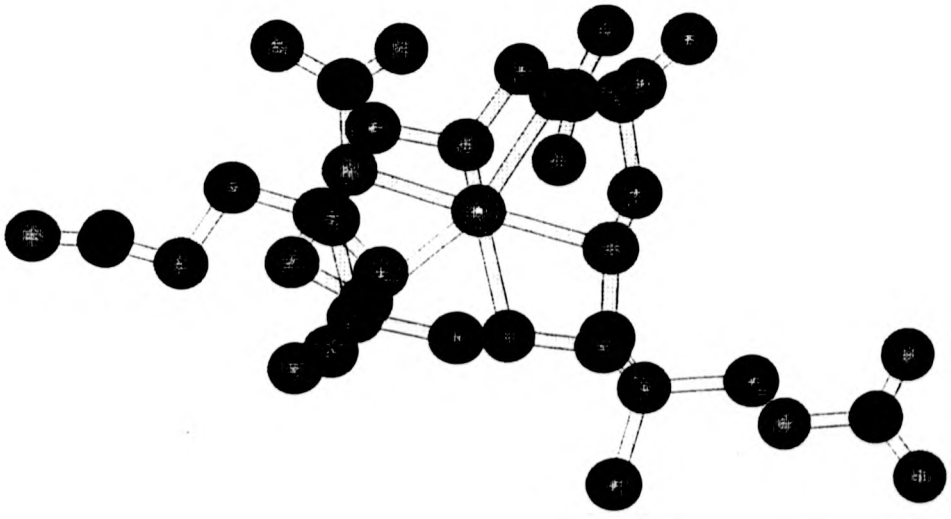

FIG.3.8 THE LOWEST ENERGY CONFORMATIONS OBTAINED USING THE SOFTWARE PACKAGE 'HYPERCHEM' FOR THE Na^+ COMPLEXES (TRANS (A) AND CIS (B)) OF THE CYCLIC TETRAMER

COLOUR SCHEME

RED ≡ OXYGEN
BLUE ≡ NITROGEN
PURPLE ≡ CARBON
GREEN ≡ SODIUM

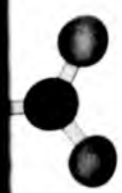

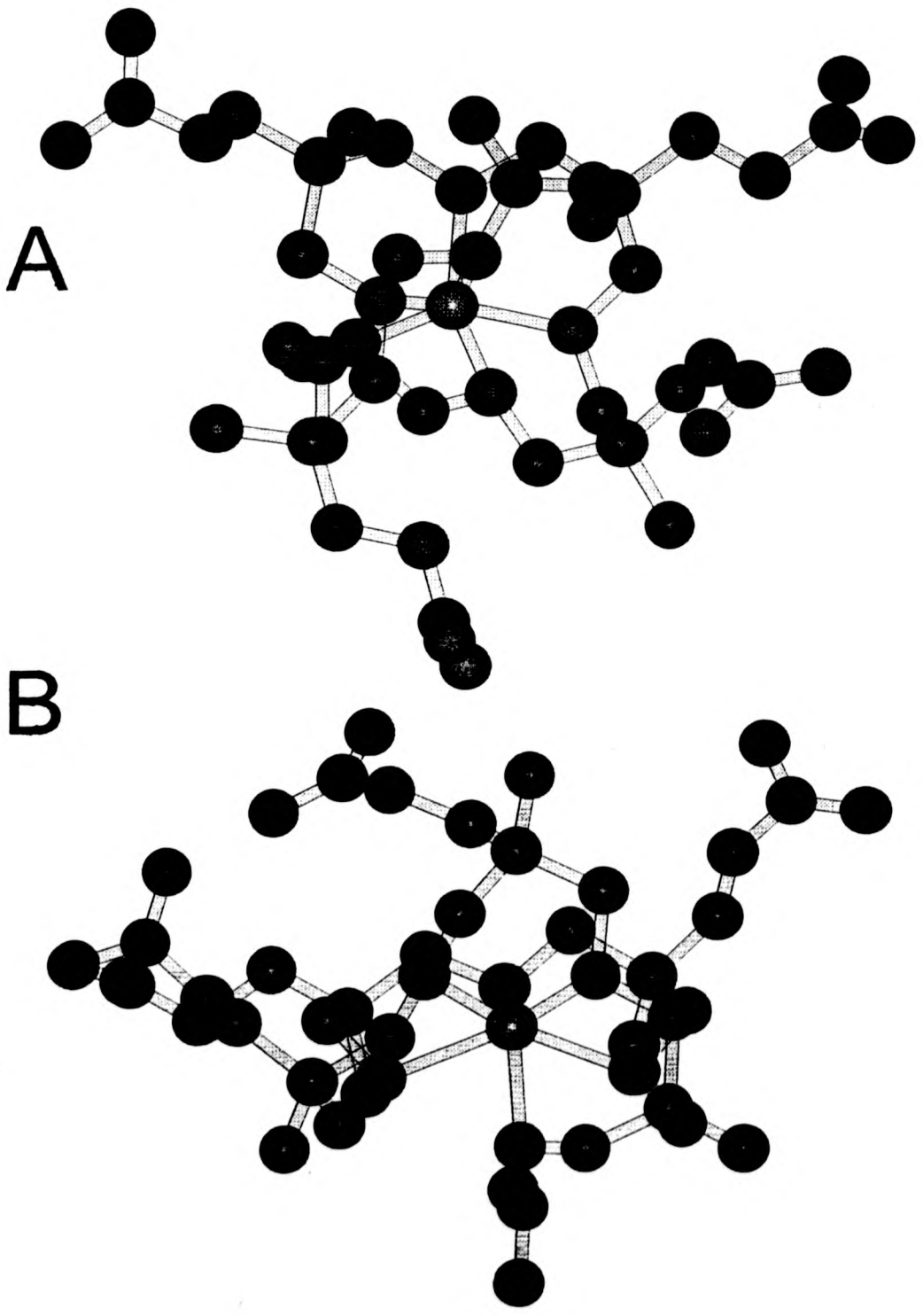
A
B

FIG.3.9 THE LOWEST ENERGY CONFORMATIONS OBTAINED USING THE SOFTWARE PACKAGE 'HYPERCHEM' FOR THE Na^+ COMPLEXES OF THE CYCLIC PENTAMER

COLOUR SCHEME

RED ≡ OXYGEN
BLUE ≡ NITROGEN
PURPLE ≡ CARBON
GREEN ≡ SODIUM

This type of simulation produces energy values which are relative to an arbitrary zero. Thus the energies of the conformers of a particular complex can be compared, but two structurally different complexes cannot.

After the first stage of modelling of the Na^+ adduct of the tetramer had been completed, the tetramer had achieved a conformation such that two of the nitrate ester side chains were in bonding distance and *trans* to the Na^+ ion. Although the *trans* conformation seemed more stable, the cis conformation could not be excluded. The energy values show that the *trans* conformation is substantially more stable than the cis and that the addition of a Na^+ ion and six bonds has resulted in a complex with a relatively small percentage increase in energy. Similarly the cyclic pentamer achieves a conformation such that two nitrate ester side chains are within bonding distance of the Na^+ ion. The lowest energy conformations of both complexes are shown (fig.3.9A,B). Lindoy[15] and other authors[16,17] show that crown ethers which possess additional binding sites on flexible chains attached to the crown ring usually show additional stability relative to those of the simple crowns. Many factors may thus influence the stability of the oligomer ions.

Three main types of complex exist between crown ethers and metal ions[15]. The first group is characterised by the presence of a reasonable match of the metal ion for the radius of the cavity in the crown. Usually a 1:1 (metal:ligand) complex is formed. The second group results when the cavity of the crown, in a non-folded configuration, is too large relative to the radius of the metal ion. In this case, the crown will normally wrap around the cation, again normally producing a 1:1 complex. The third group arises when the metal ion is too large to fit inside the crown cavity. Typically sandwich complexes showing stoichiometries of 1:2 and 2:3 (metal:ligand) then occur. The first and second groups of complexes presumably account for all the cyclic oligomer ions in the ESI spectra of

PNMMO. The third group may however be responsible for producing complexes with the same masses as the individual cyclic oligomers. For instance, two cyclic tetramer oligomers may form a sandwich complex with the metal ion producing a complex with the same mass as the adduct of the cyclic octamer. Thus it is possible that the ions in the ESI spectra due apparently to higher mass cyclic oligomers may in fact be due to the formation of sandwich complexes. To eliminate this possibility, we considered it necessary to undertake the chromatographic separation of the individual components present in PNMMO (see chapter 4).

3.4.3 ESI SPECTRA OF PNMMO OBTAINED USING A DMF/THF SOLVENT SYSTEM

Spectra obtained using a 50 : 50 mixture of dimethylformamide (DMF) and THF showed increased resolution at higher mass. Fig.3.10 shows the ESI spectrum obtained for PNMMO at a cv of 36 using the DMF/THF solvent system and K^+I^- to promote ionisation. Linear oligomers with up to 23 monomer units are clearly visible around 3500 mus, the mass range of the spectrometer. The peaks due to the K^+ adducts of the higher homologues of the cyclic oligomers also show increased resolution as compared with the equivalent peaks in the spectrum obtained using the THF/MeOH solvent system (fig.3.6C). We attribute this increased resolution to the greater solubility of the higher cyclic and linear homologues of PNMMO in the DMF/THF solvent system as compared with the THF/MeOH solvent system. Thus, as expected, the relative abundances of the K^+ adducts of both the cyclic and linear oligomers in the spectra obtained using the DMF/THF solvent system are different to those observed in the spectra obtained using the THF/MeOH solvent system (fig.3.6C). Clearly, the most abundant ion in the spectrum obtained using the

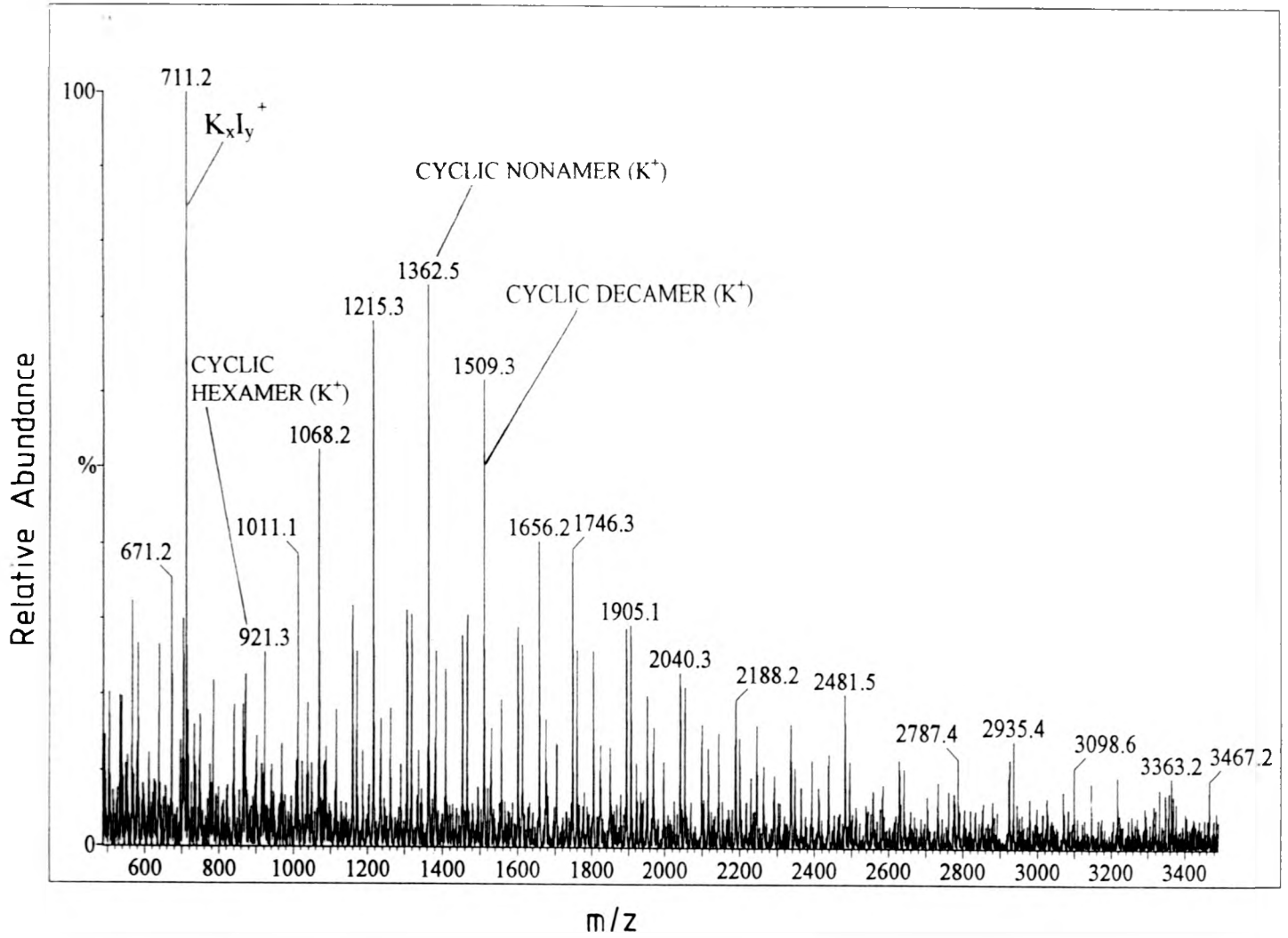
711.2
$K_xI_y^+$
CYCLIC NONAMER (K^+)
1362.5
1215.3
CYCLIC DECAMER (K^+)
CYCLIC HEXAMER (K^+)
1509.3
1068.2
1011.1
671.2
921.3
1656.2
1746.3
1905.1
2040.3
2188.2
2481.5
2787.4
2935.4
3098.6
3363.2
3467.2
100
%
0
Relative Abundance
600
800
1000
1200
1400
1600
1800
2000
2200
2400
2600
2800
3000
3200
3400
m/z

FIG.3.10 ESI MASS SPECTRUM OF UNTREATED PNMMO OBTAINED USING A DMF/THF SOLVENT SYSTEM AND KI TO PROMOTE IONISATION

THF/MeOH solvent system (fig.3.6C) is that due to the K^+ adduct of the cyclic tetramer whereas the most abundant ion in the spectrum obtained using the DMF/THF solvent system is the K^+ adduct of the cyclic nonamer. Clearly therefore the correct choice of both solvent system and cation used to obtain the ESI spectra of PNMMO is vital for the accurate determination of the relative amounts of cyclic and linear oligomers present in PNMMO. Thus, as commented in the previous section, due to the many variables encountered during ESI analysis of PNMMO we considered it necessary to undertake the chromatographic separation of the individual components present in PNMMO (see chapter 4).

3.5 ANALYSIS OF UNTREATED UNCHROMATOGRAPHED PP260, PP330, PP340 AND P-GLYN BY ESI

PP260, PP330 and PP340 were supplied by the DRA. All three polymers are structurally similar to PNMMO, but consist of lower molecular weight oligomers (see section 2.3.1). Figs.3.11A, B, C and D show the ESI spectra (cv = 36) of PNMMO, PP260, PP330 and PP340 respectively. Clearly, the ESI spectra of PP260, PP330 and PP340 are very similar. The ESI spectrum of PNMMO differs only in the relative abundances of the oligomer ions. PP260, PP330 and PP340 contain relatively higher concentrations of lower mass linear oligomers, particularly the dimer, trimer, tetramer and pentamer homologues, as compared to PNMMO. Unlike the ESI spectrum of PNMMO, the intensity of the linear oligomer ions in the spectra of PP260, PP330 and PP340 are greater than those of the cyclic oligomer ions. This is presumably a consequence of the lower molecular weight of the latter three polymers as compared to PNMMO. Thus, as expected, the polymerisation method for PNMMO leads to the formation of a lower concentration of lower molecular weight oligomers as compared to the other three polymers.

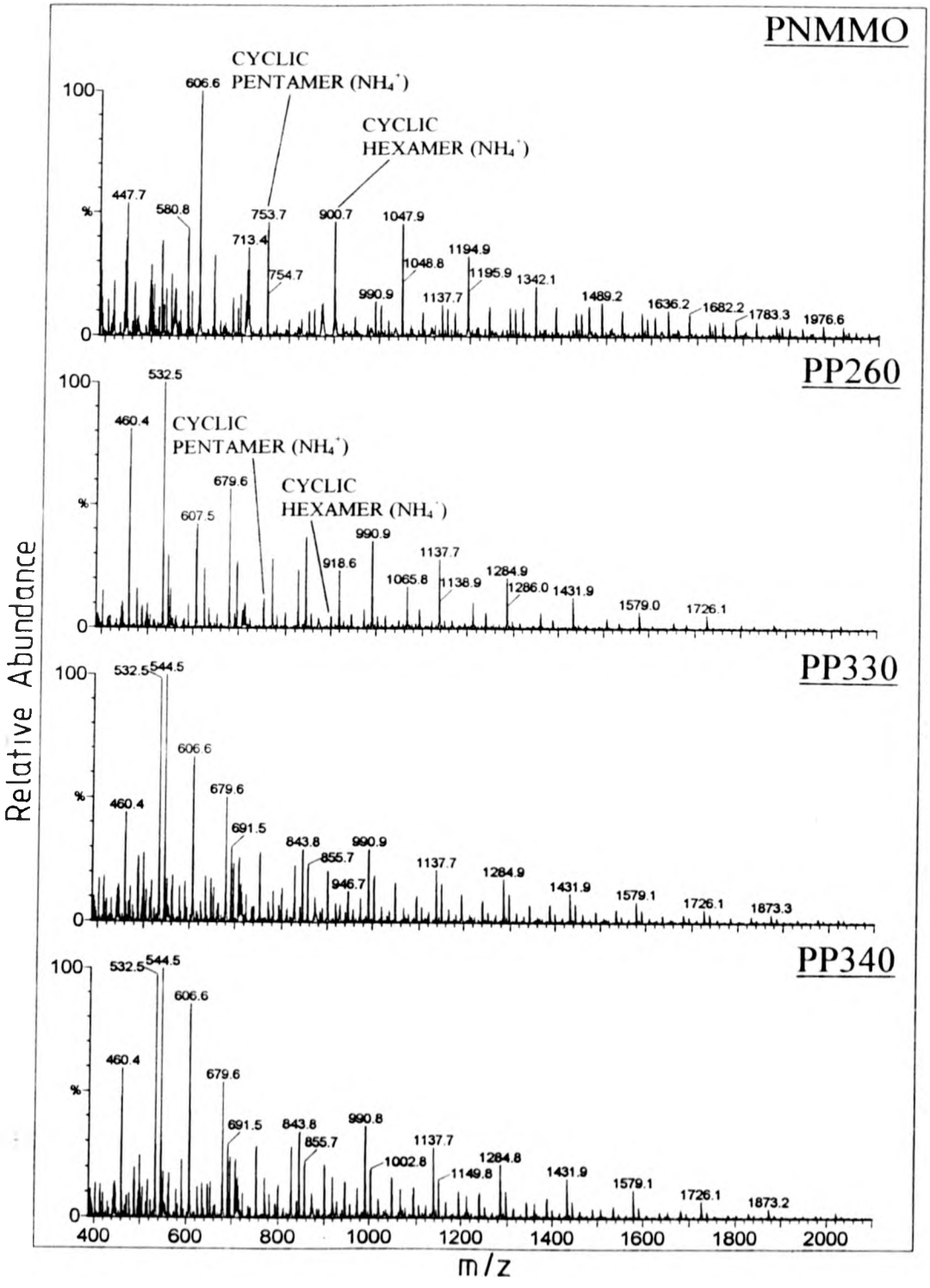
PNMMO
CYCLIC
PENTAMER (NH_4^+)
CYCLIC
HEXAMER (NH_4^+)
606.6
447.7
580.8
753.7
900.7
1047.9
713.4
1194.9
1048.8
754.7
1195.9
1342.1
990.9
1137.7
1489.2
1636.2
1682.2
1783.3
1976.6
PP260
532.5
460.4
CYCLIC
PENTAMER (NH_4^+)
679.6
CYCLIC
HEXAMER (NH_4^+)
607.5
990.9
1137.7
918.6
1065.8
1138.9
1284.9
1286.0
1431.9
1579.0
1726.1
PP330
532.5
544.5
606.6
679.6
460.4
691.5
843.8
990.9
855.7
1137.7
946.7
1284.9
1431.9
1579.1
1726.1
1873.3
PP340
532.5
544.5
606.6
460.4
679.6
691.5
843.8
990.8
855.7
1137.7
1002.8
1284.8
1149.8
1431.9
1579.1
1726.1
1873.2
100
%
0
400
600
800
1000
1200
1400
1600
1800
2000
Relative Abundance
m/z

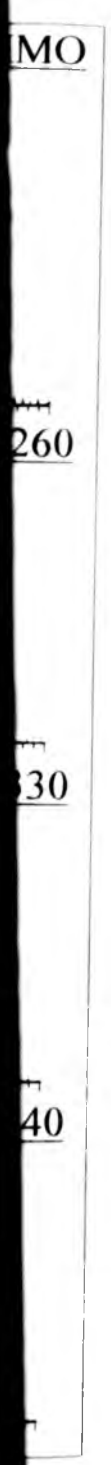

FIG.3.11 ESI MASS SPECTRA OF UNTREATED PNMMO, PP260, PP330 AND PP340 OBTAINED AT A CV OF 36 USING NH_4Cl TO PROMOTE IONISATION

The ESI spectra for PP260, PP330 and PP340 show far greater ion abundances of all the different types of linear trimer as compared to PNMMO. Consequently, the low abundance of these ions in the spectra of PNMMO is most likely due to their low concentration as opposed to their low ammonium adduct stability (see section 3.4.1).

The spectra in fig.3.11 show that the abundance of ions above 2000 mus is not affected by the molecular weight of the polymer as determined by SEC (see section 2.3.1). Thus it appears that the lack of higher mass oligomer ions is due to the relatively low solubility of the higher mass oligomers in the solvent system as opposed to the low stability of their ammonium adducts.

Figs.3.12A, B show the ESI spectra of P-GLYN at cvs of 36 and 110 respectively. The diagram below shows the structure of P-GLYN.

STRUCTURE OF P-GLYN

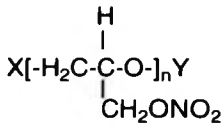

where X and Y are the end groups.

The cv appears to have a dramatic effect on the relative abundances of ions in the ESI spectrum of P-GLYN. The ESI spectra clearly show that use of a higher cv results in the enhanced appearance of larger mass species. This effect is documented for PNMMO in section 3.4.1 and attributed to the relatively greater ease of desolvation of larger mass species as compared to the adducts of the lower mass species at higher cv.

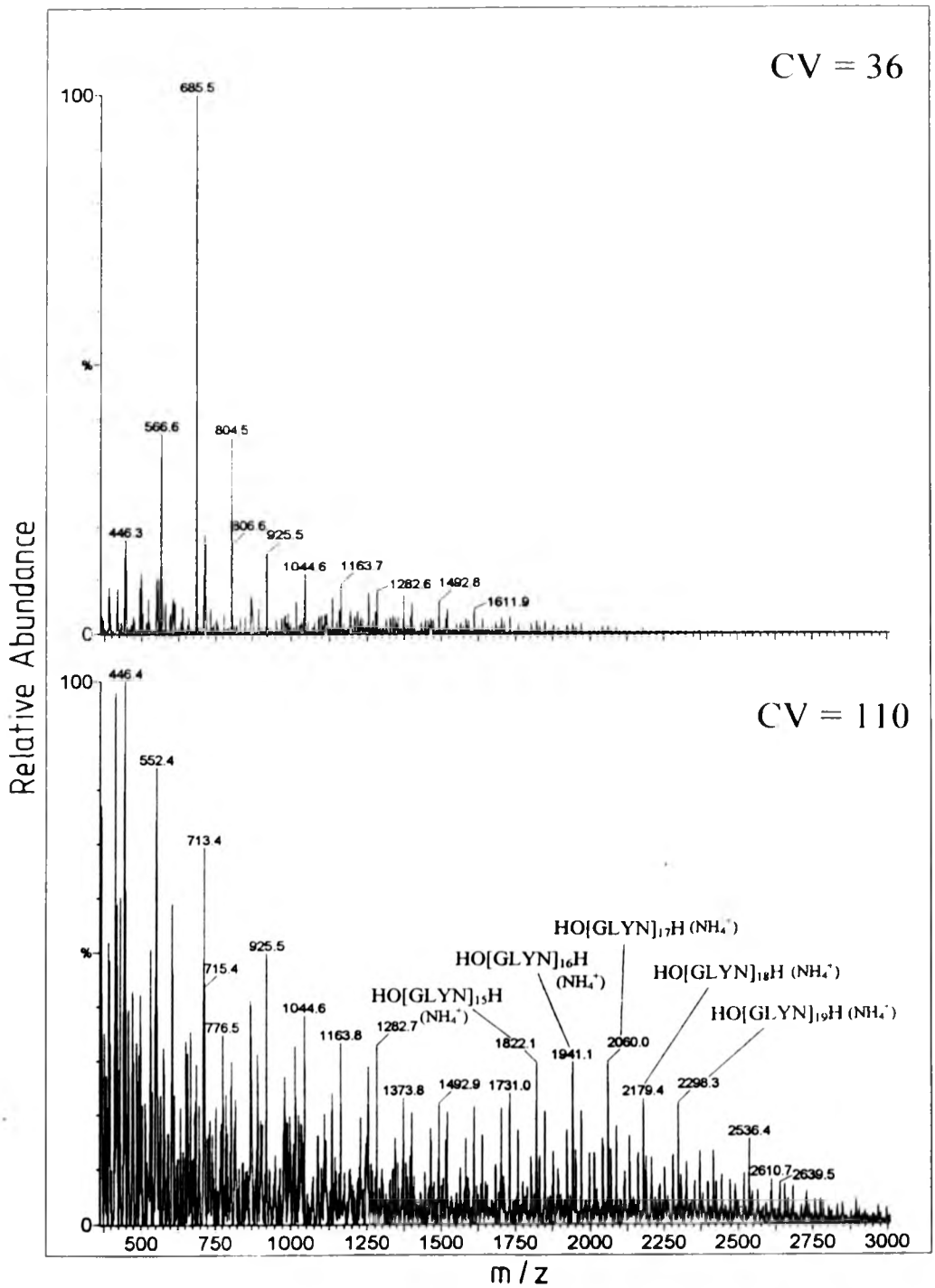
CV = 36
100
%
0
685.5
566.6
804.5
446.3
806.6
925.5
1044.6
1163.7
1282.6
1492.8
1611.9
CV = 110
100
%
0
446.4
552.4
713.4
715.4
925.5
776.5
1044.6
1163.8
1282.7
1373.8
1492.9
1731.0
1822.1
1941.1
2060.0
2179.4
2298.3
2536.4
2610.7
2639.5
HO[GLYN]15H (NH4+)
HO[GLYN]16H (NH4+)
HO[GLYN]17H (NH4+)
HO[GLYN]18H (NH4+)
HO[GLYN]19H (NH4+)
500
750
1000
1250
1500
1750
2000
2250
2500
2750
3000
m / z
Relative Abundance

FIG.3.12 ESI MASS SPECTRA OF UNTREATED P-GLYN OBTAINED AT CV's OF 36 AND 110 USING NH_4Cl TO PROMOTE IONISATION

P-GLYN is polymerised using the same materials as PNMMO (see section 1.2). However, in contrast to the method of polymerisation of PNMMO, the GLYN monomer was added gradually to the reaction mixture in an attempt to reduce the relative concentrations of cyclic oligomers present (polymerisation proceeds via an activated monomer mechanism[18]). Polymerisation reactions were performed by ICI (Explosives Division). The ESI spectra of P-GLYN confirm that the abundances of cyclic oligomer as compared to linear oligomer ions is dramatically reduced in comparison with the spectra of PNMMO (compare with fig.3.4).

All of the end groups thought to be present in PNMMO can also be accounted for in the spectra of P-GLYN. One additional end group is however apparent. The most abundant peaks in the spectrum of P-GLYN obtained at a cv of 36 (fig.3.12A) are visible at 566.5, 685.4, 804.5 and 923.6 mus. By calculating the masses of multiple monomer units of P-GLYN, the mass of the end group is shown to be 72 mus. Considering again the materials used to prepare P-GLYN, these end groups have tentatively been assigned to propyl and ethyl groups.

In contrast to the ESI spectra of PNMMO, the spectra of P-GLYN do not show peaks due to the H^+ adduct of the linear oligomers. Even at a cv of 110, which produced a relatively high abundance of H^+ adducts as compared to NH_4^+ adducts in the spectra of PNMMO, no H^+ adducts are visible in the spectra of P-GLYN. At high cv the NH_4^+ adduct has a relatively low stability (see section 3.4.1) and without subsequent formation of the H^+ adduct by removal of NH_3, a low abundance of ions is observed throughout the spectrum. The relatively low stability of the H^+ adducts of the linear oligomers of P-GLYN as compared to PNMMO is attributed to the lower strength of hydrogen bonding in the P-GLYN adducts. Liou *et al.*[19] have shown that hydrogen bonding interactions in

polyether/NH_4^+ and polyether/H^+ complexes can vary dramatically depending on the structure of the polyether and its adduct. The basicity of the polyether is also shown to play an important role in the stability of its H^+ and NH_4^+ adducts. Conversely, the lower mass (<1000 mus) cyclic oligomers in P-GLYN are visible as NH_4^+ and H^+ adducts. This is thought to be due to the multiple hydrogen-bond interactions that may occur in the lower mass cyclic oligomers (see section 4.1).

At a cv of 110 the spectrum of P-GLYN clearly shows a dispersion of ions centring around 2000 mus resembling a typical polymer distribution. The same ions are also evident at low cv, but their relative ion abundance is much lower due to the high abundance of low mass ions. The most intense ions around 2000 mus are evident at 1822.1, 1941.1, 2060.0 and 2179.4 mus and are due to the hydroxy terminated oligomers. The SEC data for P-GLYN shows a polymer distribution with an M_n of 1800. Some discrepancy is to be expected in the SEC results as the PPO used for calibrating the equipment is substantially different in structure to P-GLYN. Thus it appears that the polymer distribution evident around 2000 mus in the ESI spectrum at high cv is the same polymer distribution observed by SEC, and not solely the lower mass oligomers as observed in the PNMMO spectra. However, the abundance of ions around 2000 mus is still lower than that of ions at lower mass (<1500 mus) and this is again thought to be due to the lower solubility of the higher mass oligomers.

3.6 ANALYSIS OF PNMMO BY MALDI MASS SPECTROMETRY

Extensive research was carried out to obtain MALDI spectra of PNMMO. Samples of PNMMO mixed with various matrices were examined using an Olympus high resolution microscope. As shown in chapter 1, homogeneous mixing of the matrix and polymer is

thought to be a necessary criterion for ion formation. Obtaining a MALDI spectrum proved very difficult, probably owing to the non-polar nature of PNMMO and its insolubility in more polar aqueous solvents. No stable ions were observed with a mass to charge ratio of between 5000 and 8000 using well-known matrices such as 2,5-dihydroxybenzoic acid and sinapinic acid commonly used for MALDI analysis of PEGs and PPGs. Many matrices more amenable to the analysis of polymers insoluble in water have recently been developed and these include viscous liquids such as 2-nitrophenyl octyl ether[20,21,22] (NPOE). Mixtures of PNMMO and NPOE were placed on the metal sample holders used for MALDI analysis and our examination of these mixtures using a high resolution microscope showed that NPOE forms a homogeneous mixture with PNMMO. Consequently PNMMO was dissolved directly into the matrix (5 g dm^{-3}) and MALDI spectra of the resulting mixture were obtained. No peaks were observed in the spectra until the laser power was very high. Fig.3.13A shows the spectrum obtained. The peaks in the spectrum differ in mass by approximately 73 - 74 mus and have been tentatively assigned to doubly-charged PNMMO species as the mass of a single PNMMO monomer unit is 147.06 mus. No singly-charged species are visible and it is not clear which cation is producing the PNMMO ions. The spectrum is only produced on approximately 1 in 10 occasions. Trace amounts of metals in the metal sample holder or the matrix may be responsible for the formation of PNMMO ions.

PPO and PNMMO were mixed in equal concentrations in THF and MALDI spectra were obtained using the matrix 2,5-dihydroxybenzoic acid. Fig.3.13B shows a portion of the spectrum between 3000 and 9000 mus. PPO alone gave no peaks in this region whereas the polymer mixture did so consistently. The masses of the species associated with each peak in

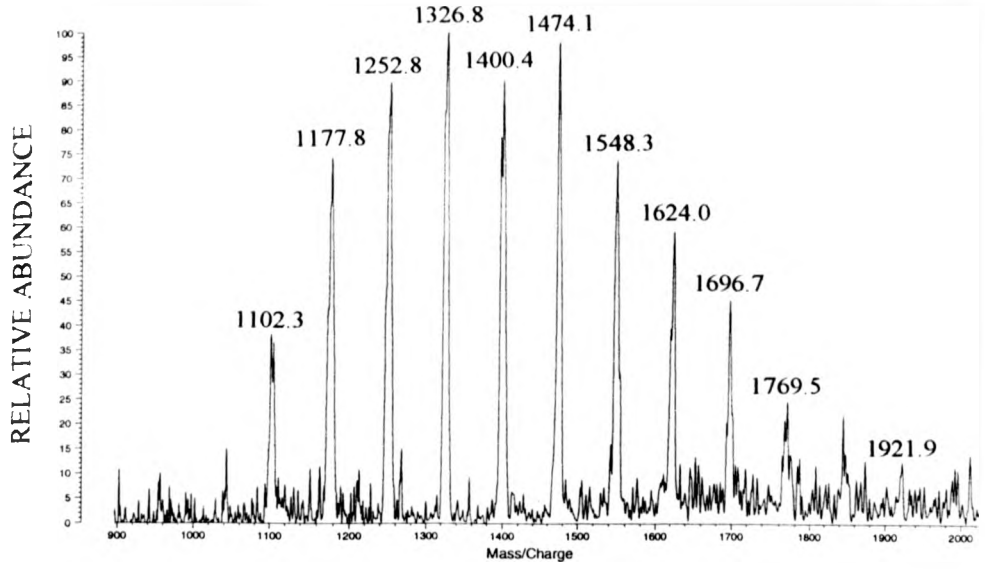

FIG.3.13A MALDI MASS SPECTRUM OF UNTREATED PNMMO OBTAINED USING 2-NITROPHENYL OCTYL ETHER AS A MATRIX

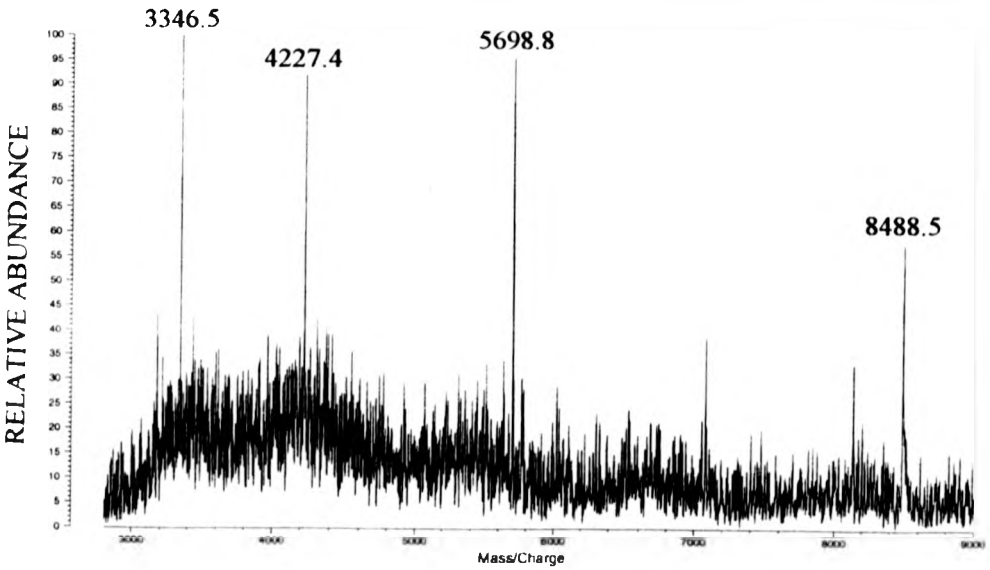

FIG.3.13B MALDI MASS SPECTRUM OF UNTREATED PNMMO OBTAINED USING PPO AS A MATRIX

the spectrum are shown in table 3.5, as is the mass difference of each species as compared to the species showing an ion peak at 3346.5 mus.

TABLE 3.5

RMM (EXPERIMENTAL) X / g mol^{-1}	δ M (X - 3346.5) / g mol^{-1}	δ M ÷ 147.06
4227.4	880.9	5.99
5698.8	2352.3	16.00
8488.5	5142.0	34.98

Again the overall results here are unexplained. The mass difference is however a multiple of the mass of a monomer unit in PNMMO, suggesting that PNMMO ions are indeed observed and that PPO may be acting as a matrix for PNMMO. We were unable to improve on these very preliminary spectra but it does seem that with sufficient ingenuity it should be possible to characterise PNMMO and other nitrated oligomers by MALDI.

CHAPTER 3 REFERENCES

1 Bower, D.I., Maddams, W.F., The Vibrational Spectroscopy of Polymers, Cambridge University Press, 1989, Ch.4.

2 Bellamy, L.J., The Infrared Spectra of Complex Molecules, Vol.1, 3rd ed., Chapman and Hall, London, 1975, Ch.17.

3 Oyumi, Y., Brill, T.B., *Combustion and Flame*, 1986, **66**, 9.

4 Unpublished work concerning NMR spectroscopy obtained from the DRA, Dr.A.V.Cunliffe.

5 Gunther, H., NMR Spectroscopy, 2nd ed., John Wiley & Sons, Chichester, 1994.

6 Campana, J.E., Sheng, L-S., Shew, S.L., Winger, B.E., *Trends in Anal. Chem.* 1994, **13**, 239.

7 Corless, S., Tetler, L.W., Parr, V., Wood, D., 1994, Paper Presented at the 42nd ASMS Conference on Mass Spectrometry and Allied Topics.

8 Simonsick, W.J., Prokai, L., 1994, Paper Presented at the 42nd ASMS Conference on Mass Spectrometry and Allied Topics.

9 Nohmi, T., Fenn, J.B., *J. Am. Chem. Soc.* 1992, **114**, 3241.

10 Wong, S.F., Meng, C.K., Fenn, J.B., *J. Phys. Chem.* 1988, **92**, 546.

11 Loo, J.A., Udseth, H.R., Smith, R.D., *Rapid Commun. Mass Spectrom.* 1988, **2**, 207.

12 McEwen, C.N., Larsen, B.S., Simonsick, W.J., *Abstracts 42nd ASMS Conference on Mass Spectrometry*, Chicago, 1994, 317.

13 Bunyan, P., Cunliffe, A.V., Davis, A., Kirby, F.A., *Polymer Degradation and Stability* 1993, **40**, 239.

14 Cooper, S.R., Crown Compounds Towards Future Applications, VCH Publishers, New York, 1992, Ch.5.

15 Lindoy, L., The Chemistry of Macrocyclic Ligand Complexes, Cambridge University Press, 1989, Ch.4.

16 Weber, E., Toner, J.L., Crown Ethers and Analogs, John Wiley & Sons, New York, 1989.

17 Hiraoka, M., Crown Compounds: Their Characteristics and Applications, Elsevier, Oxford, 1982.

18 Odian, G., Principles of Polymerisation, 3rd ed., John Wiley & Sons, New York, 1991, Ch.7.

19 Liou, C., Wu, H., Brodbelt, J., *J. Am. Soc. Mass Spectrom.* 1994, **5**, 260.

20 Karas, M., Bachmann, D., Bahr, U., Hillenkamp, F., *Int. J. Mass Spectrom. Ion Proc.* 1987, **78**, 53.

21 Bahr, U., Deppe, A., Karas, M., Hillenkamp, F., Giessmann, U., *J. Anal. Chem.* 1992, **64**, 2866.

22 Humphrey, P., Resch, M., Kimber, M.L., Dingley, D.C., 1994, Paper Presented at the 42nd ASMS Conference on Mass Spectrometry and Allied Topics.

CHAPTER 4

SPECTRAL ANALYSIS OF CHROMATOGRAPHED UNTREATED PNMMO

The results of chapter 3 clearly demonstrate that untreated PNMMO comprises a complex mixture of low mass cyclic and linear oligomers. The ion abundance of individual oligomers is strongly dependent on the cation used during ESI, and without a prior knowledge of the stability constants it is impossible to assess the relative concentrations of the oligomers present. It was also possible that *in situ* reactions such as the formation of sandwich complexes or fragmentation were occurring during the ESI analysis of PNMMO. Column chromatography was therefore employed to separate the mixture of oligomers in untreated PNMMO so that SEC, IR and NMR could then be used to validate the ESI results.

Liquid chromatographic separations of mixtures of explosives consisting of HMX, RDX, TNT and NG have been performed by Casetta *et al.*[1] Following separation the explosives were characterised using ESI mass spectrometry. However, the technique of coupling liquid chromatographic apparatus with ESI mass spectrometers to characterise individual polymers[2] or polymer mixtures is still very much in its infancy.

Untreated PNMMO does not fluoresce under uv light and therefore TLC plates cannot be used to follow the separation of the mixture. Various solvent systems were tested in conjunction with glass columns of varying lengths to find the most appropriate conditions for the separation of the components of PNMMO by column chromatography. The best separation of oligomers was obtained using a toluene/methanol solvent system, however the separation was very dependent on the length of the column which needed to be at least 1 m. Normally approximately 220 fractions (each of 15 cm^3) were collected over a period of 15 h.

4.1 CHARACTERISATION OF THE FRACTIONS OBTAINED FROM COLUMN CHROMATOGRAPHY OF UNTREATED PNMMO BY ESI

Figs.4.1 and 4.2 show the ESI spectra (cv = 36) of various fractions obtained from the column chromatography of PNMMO. All spectra were run using NH_4Cl to promote cationisation. The fractions are numbered according to their order of elution from the column. The first 20 fractions contained only virgin solvent. The spectra of fractions 21 to 46 were identical and are represented by the spectra of fractions 35 and 45 (fig.4.1A,B). The peaks at 589.4 and 606.5 mus respectively due to the H^+ and NH_4^+ adducts of the cyclic tetramer are clearly identified in the spectrum. The relative intensity of these two peaks is the same as for the unchromatographed polymer. $[(NH_4)_x(Cl)_y]^+$ clusters account for all the lower intensity peaks in the spectrum. Fig.4.1C, D and E show fractions 50, 55 and 60 respectively. Fraction 50 contains the ion adducts of the cyclic tetramer, pentamer and hexamer whilst fractions 55 and 60 contain apparently increasing concentrations of the ion adducts of the cyclic heptamer but no cyclic tetramer. Thus it appears that the cyclic oligomers are eluted before the linear oligomers and in order of increasing molecular weight. From the relative intensities of the H^+ and NH_4^+ adducts in fig.4.1C it is clear that the H^+ adduct for the cyclic tetramer and pentamer are of approximately equally stabilities. Fig.4.1C, D and E show that, as the size of the ring increases so the stability of the H^+ adduct decreases relative to the NH_4^+ adduct. The H^+ adduct of the cyclic heptamer and higher homologues are of approximately equal stability and show only very low intensity peaks. This is consistent with the ability of the lower mass homologues such as the cyclic tetramer, pentamer and possibly the hexamer to allow the H^+ ion to be sited within the ring. Consequently multiple hydrogen bond interactions with all the ring oxygen atoms occur forming more stable complexes. As the ring size increases, it is more probable that the H^+

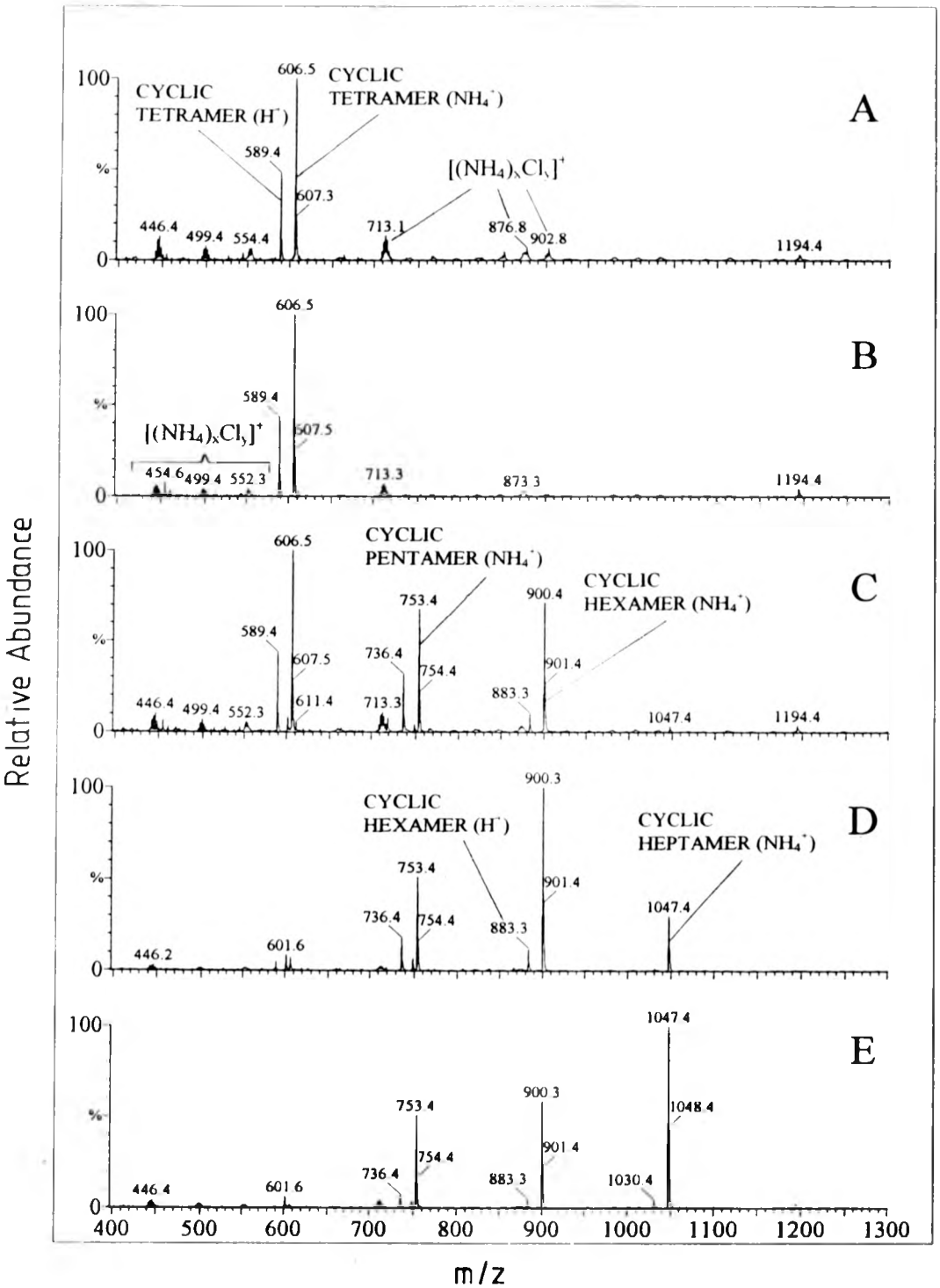
A
CYCLIC TETRAMER (H+)
CYCLIC TETRAMER (NH4+)
606.5
589.4
607.3
446.4
499.4
554.4
713.1
[(NH4)xCly]+
876.8
902.8
1194.4
B
606.5
589.4
[(NH4)xCly]+
607.5
454.6
499.4
552.3
713.3
873.3
1194.4
C
606.5
CYCLIC PENTAMER (NH4+)
753.4
900.4
CYCLIC HEXAMER (NH4+)
589.4
607.5
736.4
754.4
901.4
446.4
499.4
552.3
611.4
713.3
883.3
1047.4
1194.4
D
900.3
CYCLIC HEXAMER (H+)
CYCLIC HEPTAMER (NH4+)
753.4
901.4
1047.4
736.4
754.4
883.3
446.2
601.6
E
1047.4
753.4
900.3
1048.4
754.4
901.4
736.4
883.3
1030.4
446.4
601.6
100
%
0
400
500
600
700
800
900
1000
1100
1200
1300
m/z
Relative Abundance

FIG.4.1 ESI MASS SPECTRA OF REPRESENTATIVE FRACTIONS OBTAINED DURING THE COLUMN CHROMATOGRAPHY OF UNTREATED PNMMO

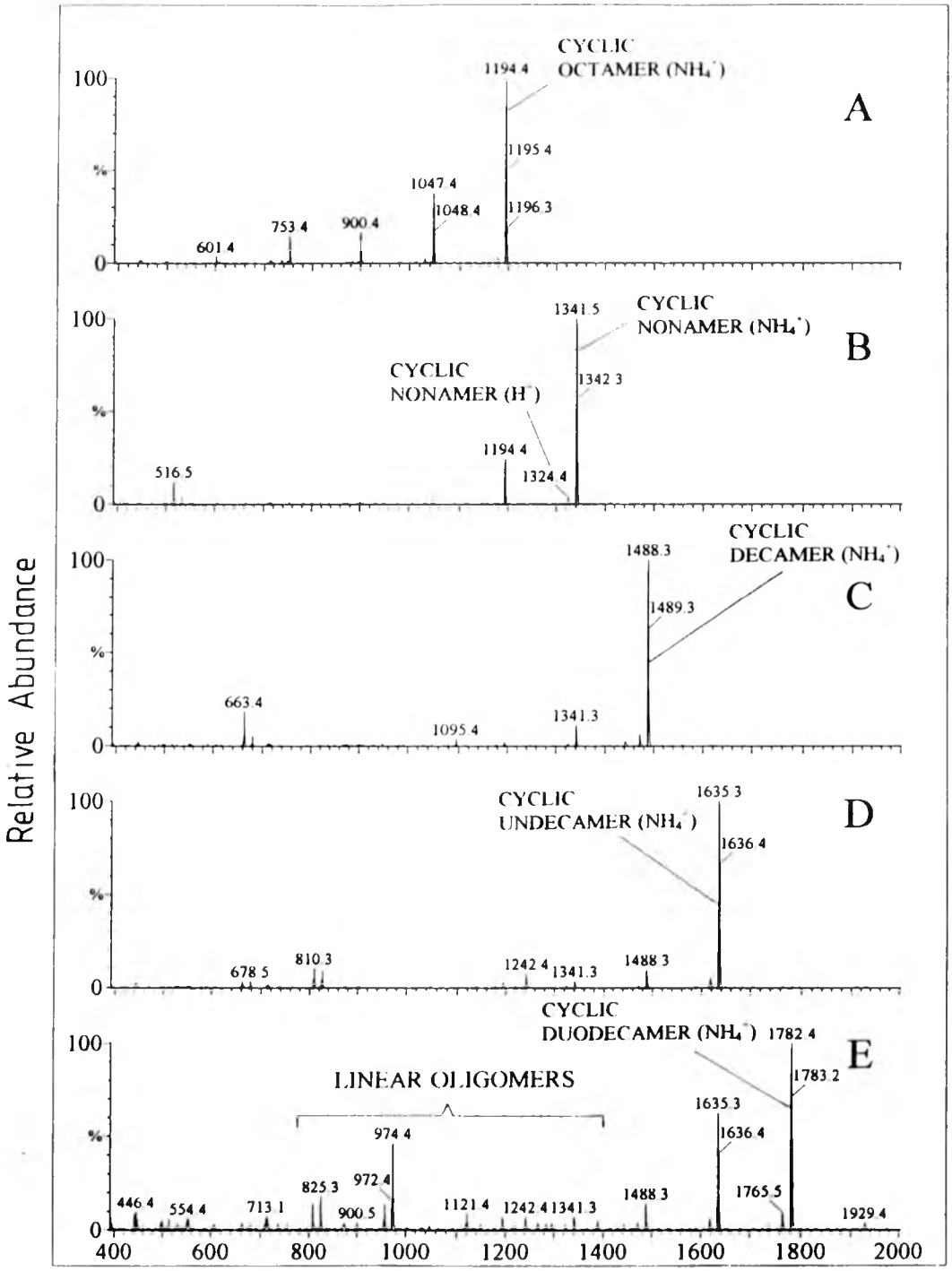
A
CYCLIC
OCTAMER (NH4+)
1194.4
1195.4
1196.3
1047.4
1048.4
753.4
900.4
601.4
B
CYCLIC
NONAMER (NH4+)
1341.5
1342.3
CYCLIC
NONAMER (H+)
1194.4
1324.4
516.5
C
CYCLIC
DECAMER (NH4+)
1488.3
1489.3
663.4
1095.4
1341.3
D
CYCLIC
UNDECAMER (NH4+)
1635.3
1636.4
678.5
810.3
1242.4
1341.3
1488.3
E
CYCLIC
DUODECAMER (NH4+)
1782.4
1783.2
LINEAR OLIGOMERS
1635.3
1636.4
974.4
972.4
825.3
446.4
554.4
713.1
900.5
1121.4
1242.4
1341.3
1488.3
1765.5
1929.4
100
%
0
400
600
800
1000
1200
1400
1600
1800
2000
Relative Abundance
m/z

FIG.4.2 ESI MASS SPECTRA OF REPRESENTATIVE FRACTIONS OBTAINED DURING THE COLUMN CHROMATOGRAPHY OF UNTREATED PNMMO

ion bonds solely with one or two oxygen atoms as the distances are too great for multiple hydrogen bonding to occur. Thus the H^+ adducts of the cyclic heptamer and higher homologues are equally stable.

Fractions 100 to 160 show gradually increasing concentrations of adducts of low-mass linear oligomers. However the ion peak for the respective cyclic oligomer is still strong in every spectrum and the cyclic duodecamer is apparent in fraction 160 at 1782.4 mus (fig.4.2E). Later fractions showed much greater concentrations of linear oligomers, making identification of higher cyclic homologues difficult. Besides this difficulty, the mass of cyclic oligomer obtained from individual fractions was becoming very small. Fraction 147 (fig.4.2D) contained only 1.5 mg of oligomer.

The increased concentrations of individual cyclic species in the fractions obtained by column chromatography thus provide more highly resolved ESI spectra. The H^+ adducts of higher mass cyclic oligomers are now clearly visible and the possibility that *in situ* reactions occur to produce the cyclic species seems very much less likely. A better approximation for the relative amounts of cyclic oligomers present is also obtained from the masses of individual fractions. The mass of cyclic tetramer is approximately 20 times that of the pentamer, hexamer and heptamer. The remaining oligomers show a relatively decreasing concentration. Thus the relative ion intensities in the spectrum of unchromatographed PNMMO obtained using Na^+ for cationisation gives the nearest approximation to the relative masses of cyclic oligomers present. It has been clearly demonstrated however that the exact values and thus relative concentrations of the masses cannot be obtained without prior knowledge of the ion stabilities.

4.2 SEC ANALYSIS OF FRACTIONS OBTAINED BY COLUMN CHROMATOGRAPHY OF UNTREATED PNMMO

Figs.4.3A and B show the SEC chromatograms of the fractions obtained from the column chromatography of untreated PNMMO. The chromatograms were all run using the low molecular weight column system (see section 2.1.9.1) and equivalent concentrations of oligomeric material. Every chromatogram is labelled with the fraction it represents.

The chromatograms of fraction 35 and 45 show a single peak with an M_n = 700. The ESI spectra of the same fractions (fig.4.1A and B) show a single peak for the H^+ adduct of the cyclic tetramer at 589.4 mus. The accuracy of the ESI results has already been demonstrated and thus the value of 700 obtained by SEC seems to be high. Very minor impurities may be responsible for errors in the molecular weight determination, even though the SEC equipment has been calibrated with high purity standards[3]. The PPO used for calibrating the SEC equipment is in any case substantially different in structure from the cyclic oligomers and thus some discrepancy is to be expected.

The chromatogram of fraction 50 shows 3 peaks in decreasing order of intensity. The peaks have M_n values of 700, 800 and 920 respectively. The ESI spectrum (fig.4.1C) of the same fraction also shows 3 peaks for the cyclic tetramer, pentamer and hexamer. Within experimental error, the M_n values of the 3 peaks obtained by SEC correspond to these same three cyclic species. However, the SEC chromatogram shows an intense peak for the cyclic tetramer and much weaker peaks for the cyclic pentamer and hexamer, whereas the ESI spectra show intense ammonium adduct peaks for all the cyclic species, particularly the tetramer. Thus the ESI results appear to emphasise the concentrations of cyclic pentamer and hexamer relative to cyclic tetramer. This can be attributed to the differing stabilities of the ions in ESI, the cv used during ESI and the calibrant used for SEC. The latter two factors are

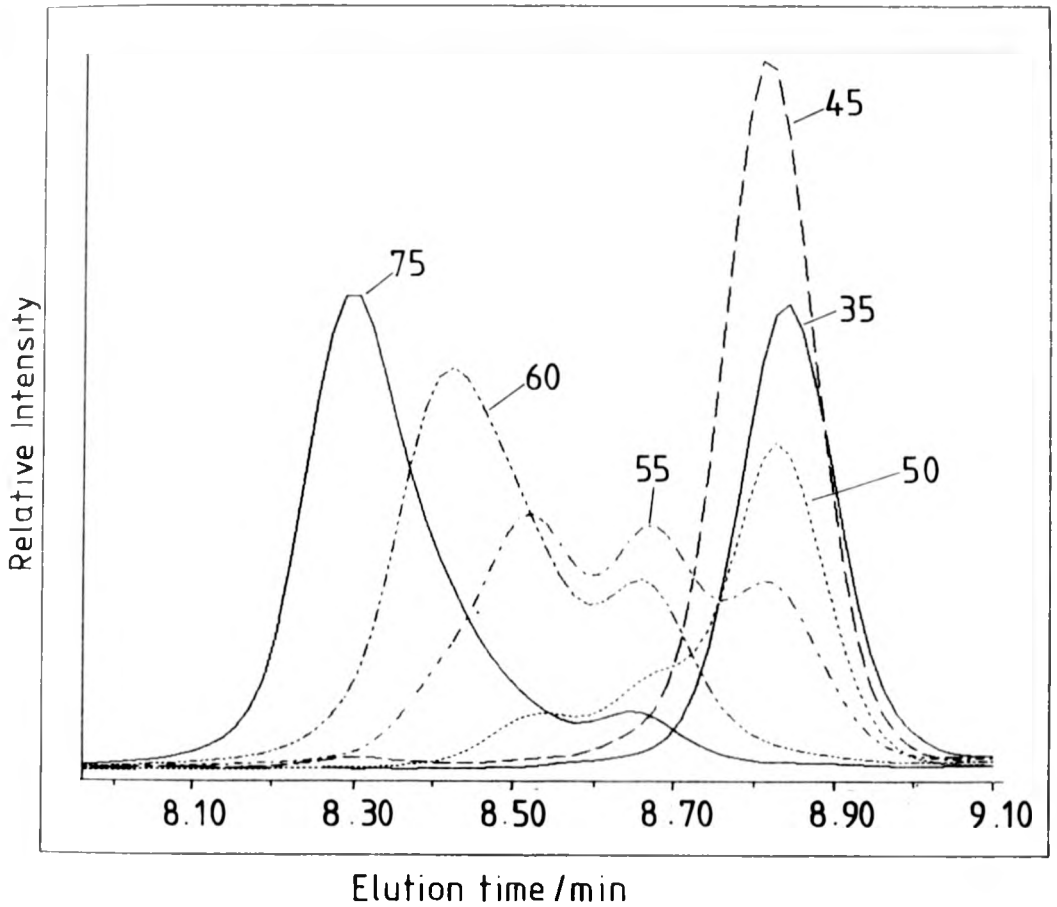

FIG.4.3A SEC CHROMATOGRAMS OF REPRESENTATIVE FRACTIONS OBTAINED FROM THE COLUMN CHROMATOGRAPHY OF UNTREATED PNMMO

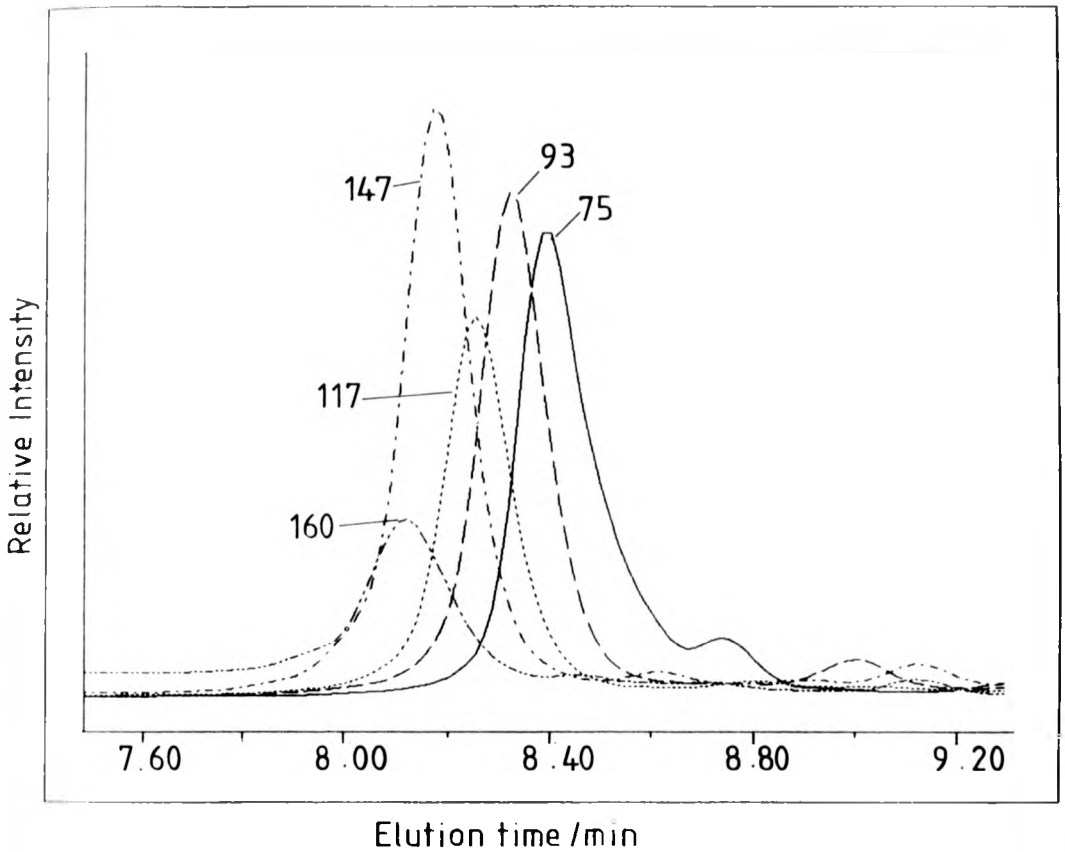

FIG.4.3B SEC CHROMATOGRAMS OF REPRESENTATIVE FRACTIONS OBTAINED FROM THE COLUMN CHROMATOGRAPHY OF UNTREATED PNMMO

thought to have a minimal influence here. The cv was 36, which may have favoured the lower mass cyclic species and not the higher mass as here. Similarly, the calibrant used in SEC would be expected to have little effect on the relative intensities of the cyclic species. The stability of the NH_4^+ adduct is thought to be the most influential factor here. ESI spectra of unchromatographed PNMMO at a cv of 36 show that even though the concentration of cyclic tetramer is approximately 20 times that of either the pentamer or hexamer, its ion intensity is only double. Thus the NH_4^+ adduct of the cyclic pentamer and hexamer is substantially more stable than that of the cyclic tetramer. This explains the apparently high concentrations of cyclic pentamer and hexamer present in the ESI spectra. Similarly, the SEC chromatogram for fraction 55 shows approximately equal concentrations of cyclic tetramer, pentamer and hexamer. The ESI spectrum (fig.4.1D) however shows no NH_4^+ adduct peak for the cyclic tetramer, but relatively strong peaks for the cyclic hexamer and heptamer. By comparing the intensities of the peaks in the SEC and ESI, it appears that the cyclic octamer and nonamer are the most stable ammonium ion adducts, while both higher and lower homologues are somewhat less stable.

4.3 INFRARED ANALYSIS OF FRACTIONS OBTAINED BY COLUMN CHROMATOGRAPHY OF UNTREATED PNMMO

The infrared spectra of the cyclic fractions were very similar to the infrared spectra of the bulk polymer, although subtle differences were visible in the peak shapes. The wavelengths of individual absorption maxima did not differ by more than 2 cm^{-1}.

4.4 ^{1}H AND ^{13}C NMR ANALYSIS OF FRACTIONS OBTAINED BY COLUMN CHROMATOGRAPHY OF UNTREATED PNMMO

The solvent was removed from the eluted fractions using a rotary evaporator. Approximately equal concentrations of oligomeric material were characterised by 250 and 400 MHz ^{1}H and ^{13}C NMR in $CDCl_3$. Previous to this study, only the cyclic tetramer of PNMMO had been characterised by ^{1}H and ^{13}C NMR; these results showed that these samples of cyclic tetramer were impure and contained significant concentrations of PNMMO monomer and unidentified species. Our study shows that the column chromatography of untreated PNMMO produces samples of the cyclic tetramer of higher purity. The cyclic pentamer and hexamer can also be identified in the NMR spectra.

Figs.4.4A, B show the 250 MHz ^{1}H and ^{13}C NMR spectra of fraction 35. Our results using SEC (section 4.3) and ESI (section 4.1) have previously indicated that this fraction contains solely the cyclic tetramer. The NMR results show that a small amount of impurity is also present in the sample (see peaks labelled I in fig.4.4). Low molecular weight oligomers with masses outside the calibration limits used during ESI and SEC analysis may account for these unassigned peaks. The peaks for the cyclic tetramer are clearly labelled (fig.4.4) and closely resemble, in shape and shift, those obtained for the bulk linear polymer.

Figs.4.5A, B show the 400 MHz ^{1}H and ^{13}C NMR spectra of fraction 55. Fig.4.6 shows the ^{13}C NMR spectrum obtained for fraction 55 from a narrow scan range (δ_c = 71 to 76 ppm) experiment. Clearly, the resonance centring around 75.6 ppm due to the nitrate ester methylenes in the cyclic tetramer appears to consist of six separate peaks, whereas only a triplet is observed at 250 MHz. These peaks can be assigned to the various diastereomers of the cyclic tetramer (enantiomers can not be distinguished using NMR). Thus if we consider the stereochemistry around the four quaternary carbons, it is clear that the

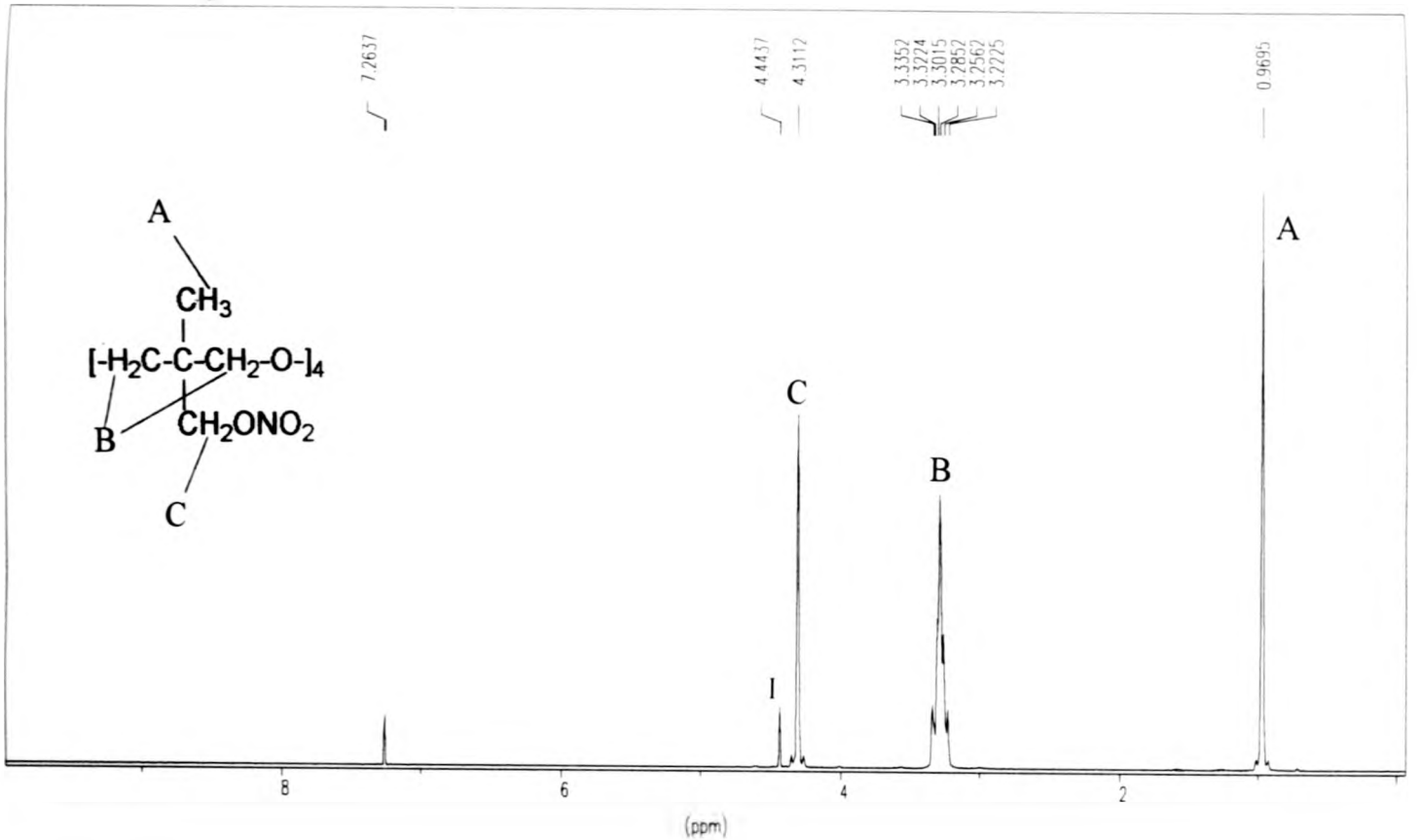

FIG.4.4A 250 MHz ^{1}H NMR SPECTRUM OF A FRACTION CONTAINING PREDOMINANTLY THE CYCLIC TETRAMER ELUTED DURING THE COLUMN CHROMATOGRAPHY OF UNTREATED PNMMO

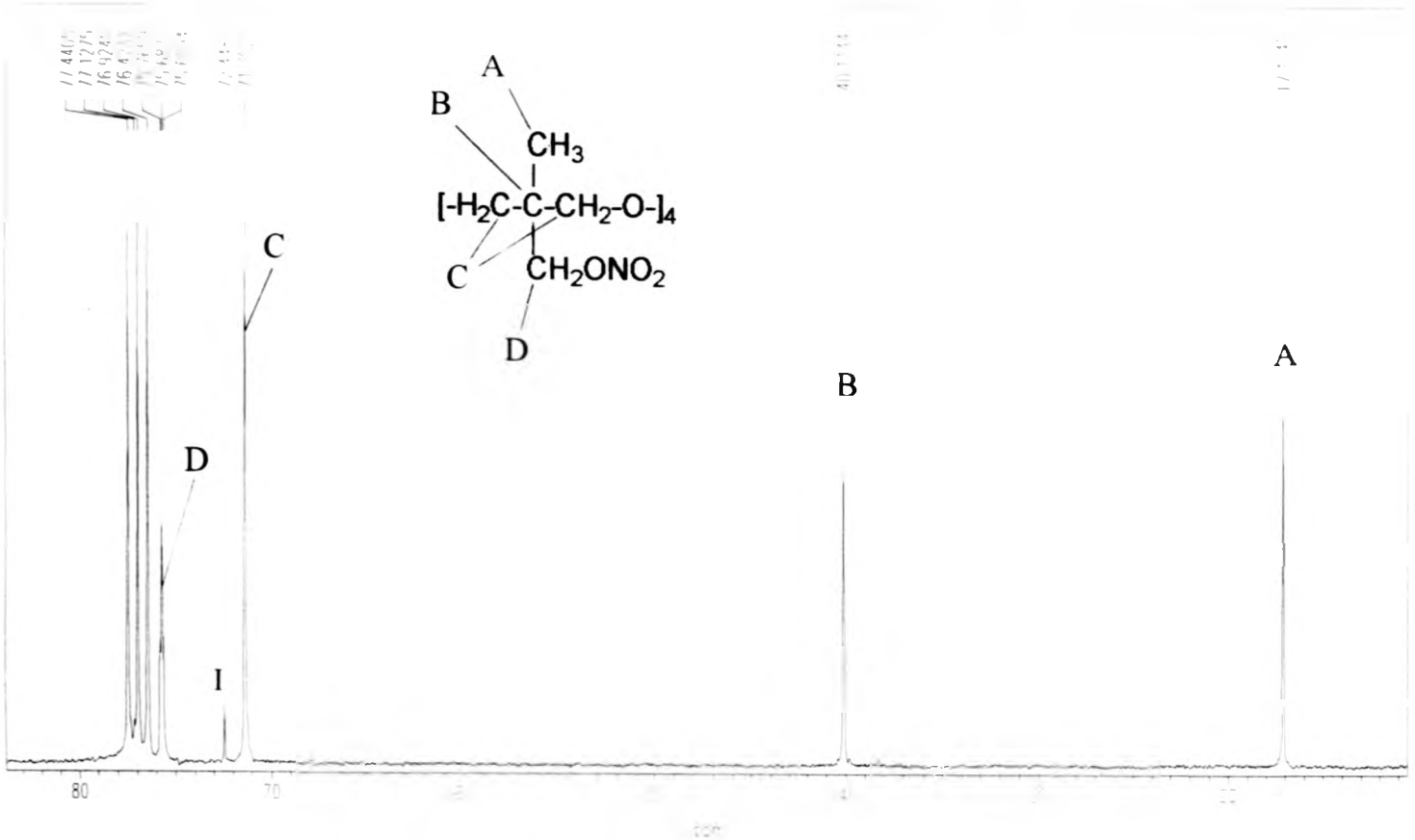

FIG.4.4B 250 MHz ^{13}C NMR SPECTRUM OF A FRACTION CONTAINING PREDOMINANTLY THE CYCLIC TETRAMER ELUTED DURING THE COLUMN CHROMATOGRAPHY OF UNTREATED PNMMO

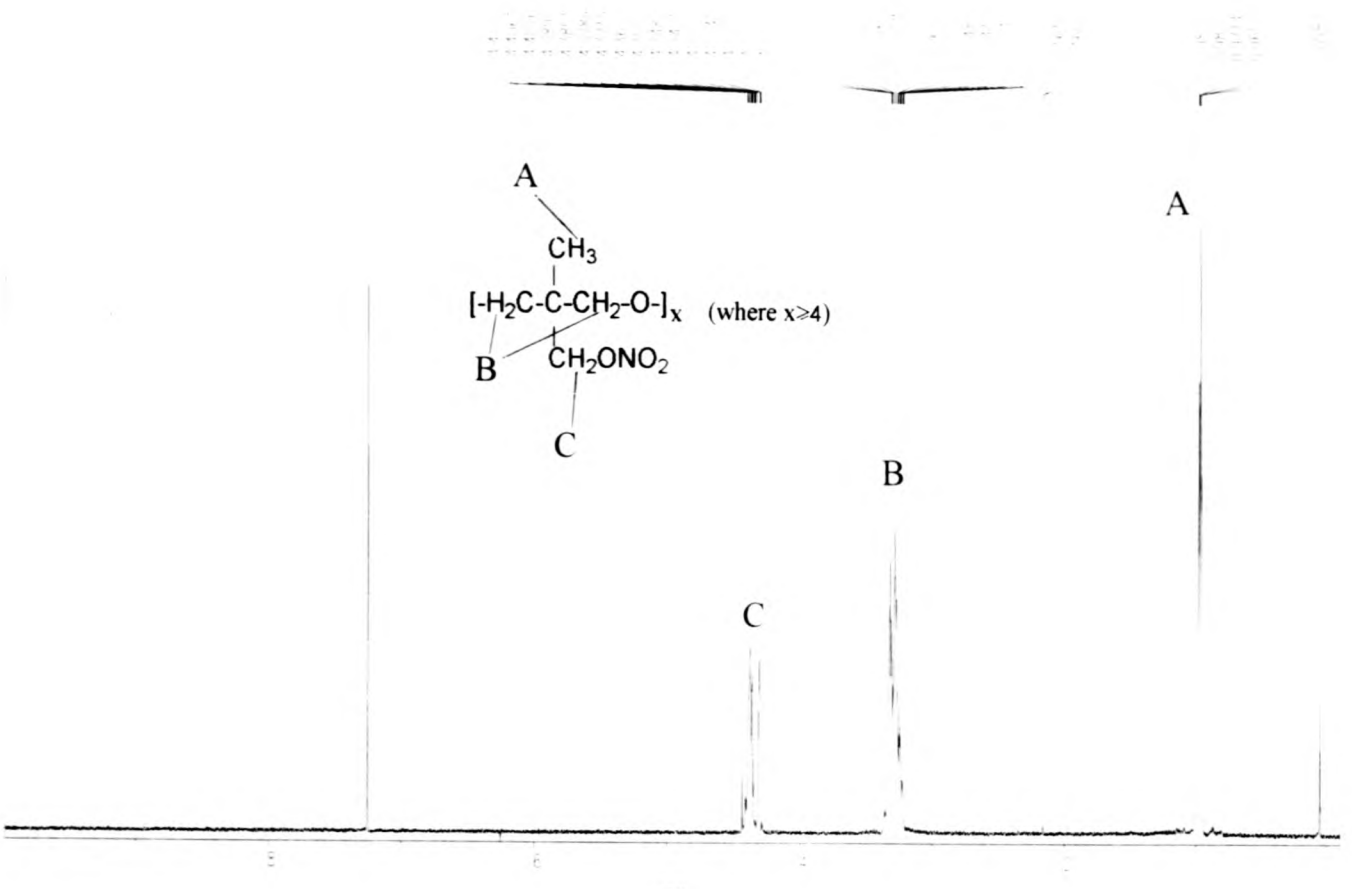

FIG.4.5A 400 MHz ^{1}H NMR SPECTRUM OF A SINGLE FRACTION OBTAINED DURING THE COLUMN CHROMATOGRAPHY OF UNTREATED PNMMO

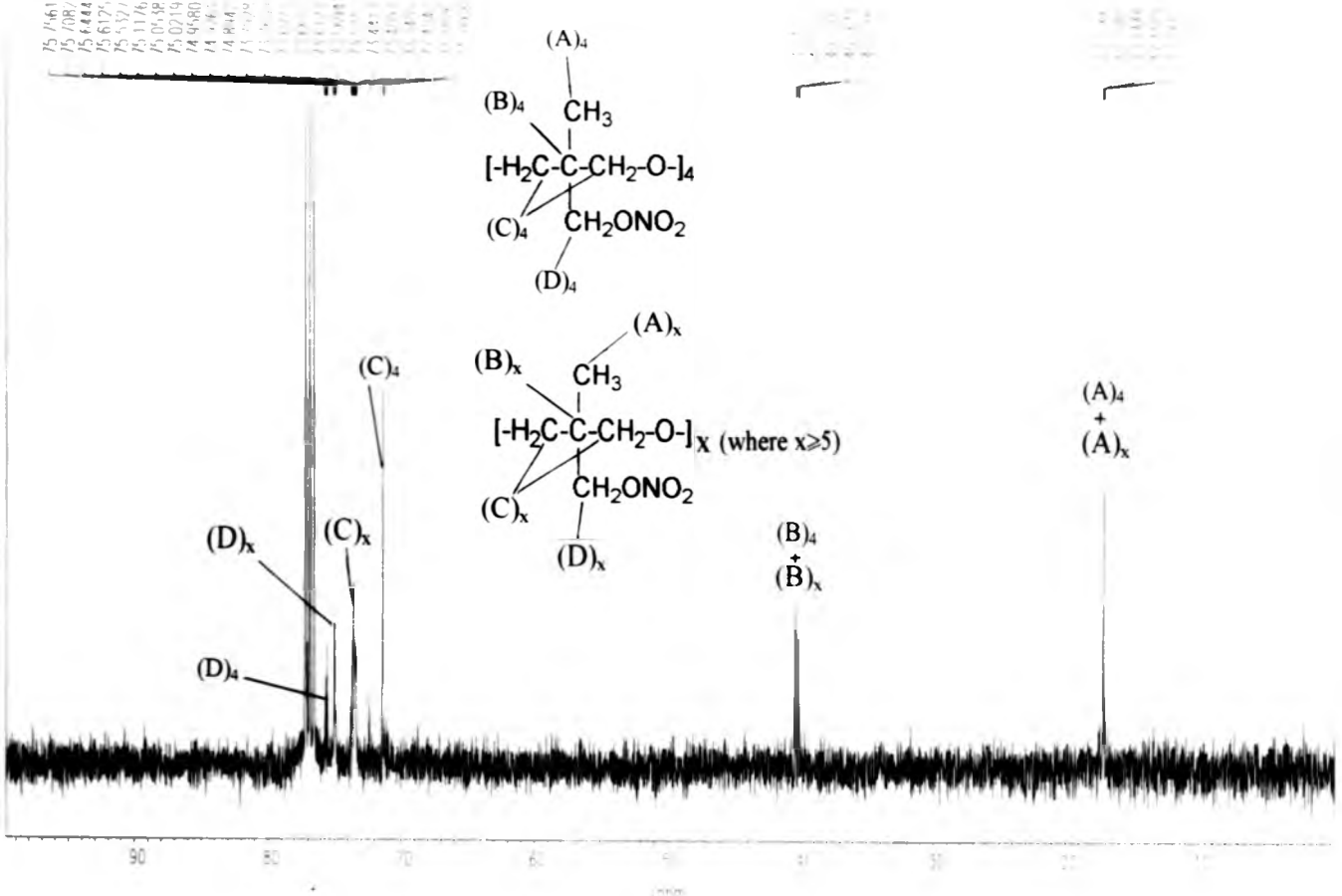

FIG.4.5B 400 MHz ^{13}C NMR SPECTRUM OF A SINGLE FRACTION OBTAINED DURING THE COLUMN CHROMATOGRAPHY OF UNTREATED PNMMO

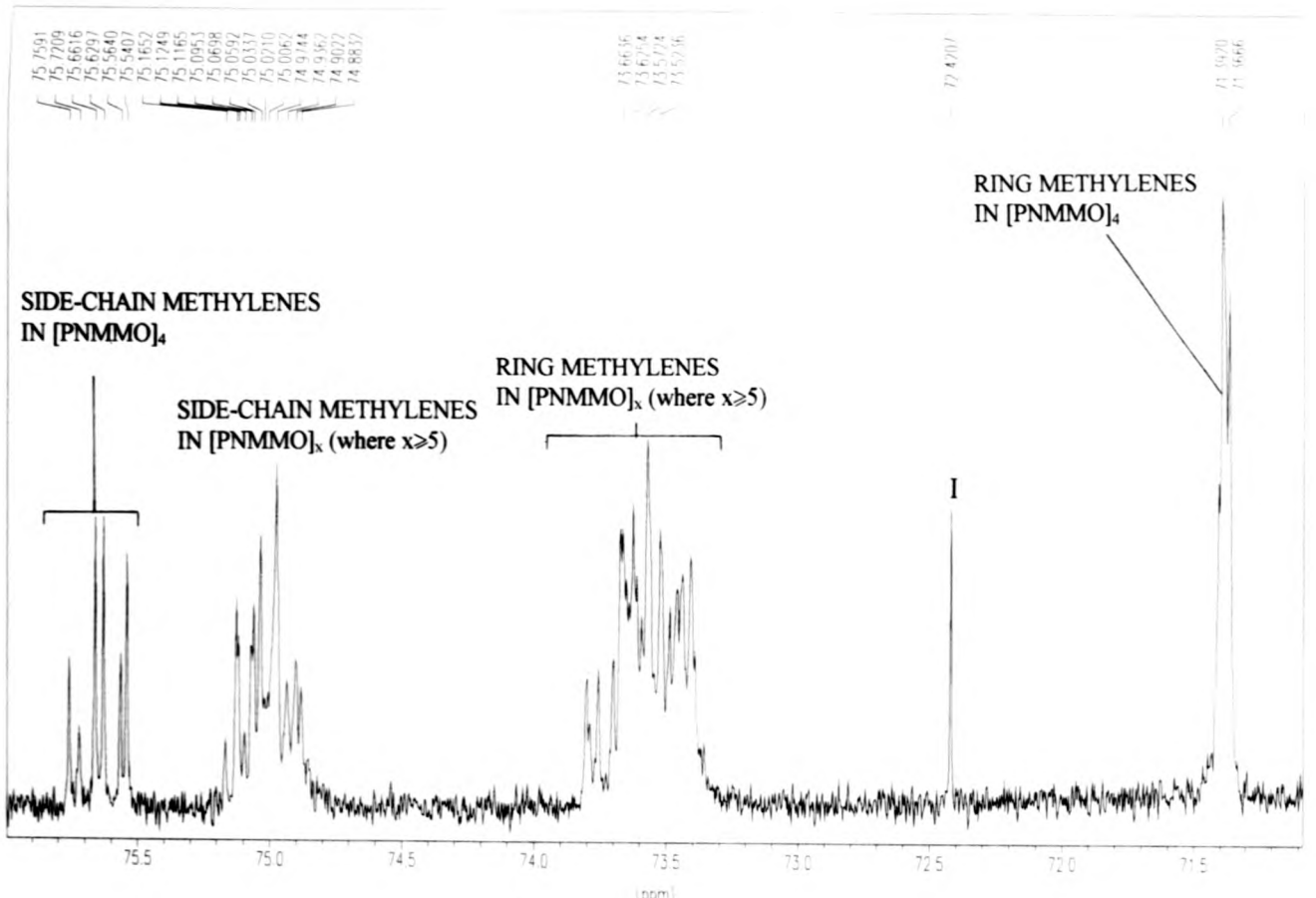

FIG.4.6 400 MHz NARROW SCAN ^{13}C NMR SPECTRUM OF A SINGLE FRACTION CONTAINING PREDOMINANTLY CYCLIC OLIGOMERS ELUTED DURING THE COLUMN CHROMATOGRAPHY OF UNTREATED PNMMO

quaternary carbon can be chiral or non-chiral depending on the orientation of its surrounding groups. To account for the various diastereomers present, the cyclic tetramer can be visualised as a square where the corners represent the quaternary carbons. Clearly the nitrate ester group may be 'up' (+) or 'down' (-) with respect to the ring. If we use r (racemic) to represent neighbouring nitrate ester groups that are either +- or -+ and m (meso) to represent neighbouring nitrate ester groups that are ++ or -- with respect to each other, the following representation of the stereoisomers present is possible.

DIAGRAMATIC REPRESENTATION OF THE STEREOISOMERS OF THE CYCLIC TETRAMER

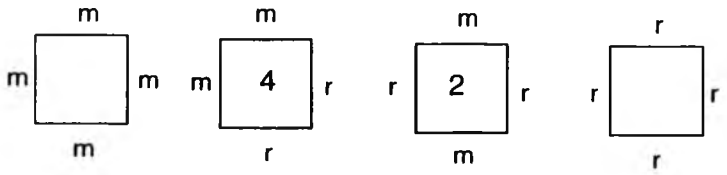

The numbers in the squares refer to the number of distinct orientations of the ring. This model of the cyclic tetramer gives the following possibilities per corner (see table 4.1 over the page).

TABLE 4.1

TABLE DETAILING AND SUMMING THE STEREOISOMERS OF THE CYCLIC TETRAMER

CORNER TYPE	REMAINDER	SUM OF POSSIBILITIES
mm	mm	4
mm	rr	4
mr	mr (≡ rm / rm)	8
mr	rm (≡ rm / mr)	8
rr	mm	4
rr	rr	4
		TOTAL = 32 ($2^4/2 \times 4$)

Thus a multiplet of six peaks with relative intensity 1:1:2:2:1:1 is expected for the nitrate ester methylenes in the ^{13}C NMR (the shift order cannot be defined using the model above). Fig.4.6 shows that this pattern is observed. The diastereomers due to the peaks at 75.54 and 75.56 ppm seem to be favoured slightly as compared to those at 75.72 and 75.76 ppm. This can be attributed to the small differences in energy between the different stereoisomers of the cyclic tetramer and thus the relative predominance of one stereoisomer as compared to another.

New resonances are evident in fig.4.5B and fig.4.6 around 73.5 and 75.0 ppm. The peaks due to the side chain methyls and the peaks for the quarternary carbons in the ring have become more complex, but it is difficult to assign individual peaks as the shift difference between the new peaks and those due to the still present cyclic tetramer is very small (<0.1 ppm). The ESI spectrum (fig.4.1D) and the SEC chromatogram (fig.4.3A) of

fraction 55 show that approximately equal concentrations of cyclic tetramer, pentamer and hexamer are present in the sample. A much lower concentration of cyclic heptamer is also present. The intensity of the new resonances around 73.5 and 75.0 ppm in the ^{13}C NMR increases as the concentrations, as determined by SEC and ESI, of cyclic pentamer and hexamer increase. The new resonances in the NMR are thus assigned to the methylene carbons in the cyclic pentamer and hexamer. However, these new resonances are considerably broader than those seen for the cyclic tetramer. The ring methylenes in the cyclic tetramer give a sharp triplet at 71.4 ppm whereas the two new multiplets at 73.5 and 75.0 ppm are broad and considerably more complex. Thus to assist with the assignment of the new multiplets, both the tetramer and pentamer were modelled using the software package 'Hyperchem' (see section 2.2.6). To shorten the very long processing times needed for this modelling process, the nitrate ester side chains were replaced with methyl groups. Figs.4.7A, B show the lowest energy conformations produced for the cyclic tetramer and pentamer. It is clear from fig.4.7A that the cyclic tetramer achieves a very symmetrical conformation with all the ring oxygens 'facing' inwards. All the ring methylenes are γ-gauche[4,5] to one oxygen and are therefore conformationally equivalent. This accounts for the relatively sharp resonance around 71.4 ppm that is observed for the ring methylenes in the cyclic tetramer. Fig.4.7B shows that the lowest energy conformation of the cyclic pentamer is not as symmetrical as that of the cyclic tetramer. Seven of the ring methylenes are γ-gauche to the oxygen opposite. The other three ring methylenes, labelled with a T, are *trans* to the oxygen opposite and this increases their shift (on average) by $0.3 \times \approx 5$ ppm $\equiv 1.5$ ppm[4]. Consequently, the ring methylenes in the pentamer are expected to show a relative shift of approximately $\delta_c = +1.5$ ppm as compared to the ring methylenes in the cyclic tetramer, i.e. 71.4 + 1.5 ppm = 72.9 ppm. The cyclic hexamer was not modelled as very long

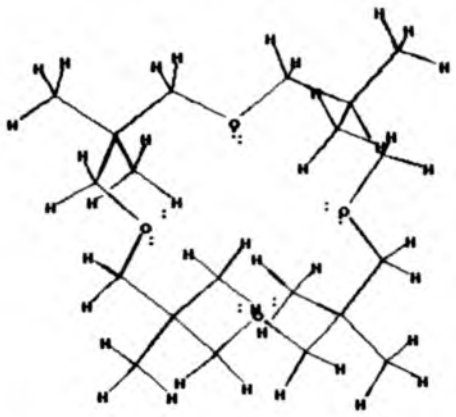

FIG.4.7A THE LOWEST ENERGY CONFORMATION OF THE CYCLIC TETRAMER OBTAINED USING THE SOFTWARE PACKAGE 'HYPERCHEM'

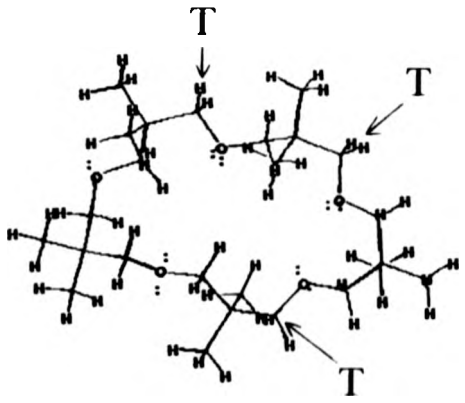

FIG.4.7B THE LOWEST ENERGY CONFORMATION OF THE CYCLIC PENTAMER OBTAINED USING THE SOFTWARE PACKAGE 'HYPERCHEM'

processing times are required for larger molecules. However, similarly to the cyclic pentamer, the cyclic hexamer is not expected to possess the high symmetry of the cyclic tetramer. Thus, the NMR shifts of the ring methylenes in the cyclic pentamer and hexamer are expected to be similar. Consequently, the resonance around 73.5 ppm is assigned to the ring methylenes in both the cyclic pentamer and hexamer. The relatively broad and complex nature of this resonance as compared to the equivalent resonance at 71.4 ppm for the ring methylenes in the cyclic tetramer is attributed to the presence of the additional *trans* relationships that exist between the ring methylenes and the ring oxygens in the cyclic pentamer and hexamer.

The ratio of the peak areas of the resonances around 73.5 and 75.0 ppm as determined by integration is 2:1 respectively. Thus, the resonance around 75.0 ppm is assigned to the nitrate ester methylenes in the cyclic pentamer and hexamer. To confirm this assignment, the number of stereoisomers of the cyclic pentamer were calculated using the same model that was applied to the cyclic tetramer and the following results were obtained;

DIAGRAMATIC REPRESENTATION OF THE STEREOISOMERS OF THE CYCLIC PENTAMER

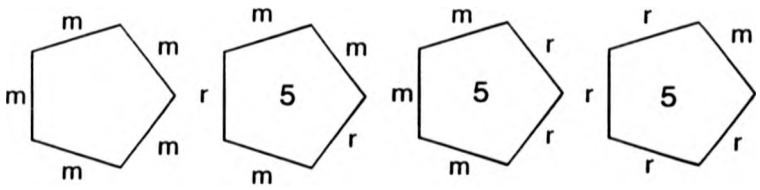

Similarly to the model of the cyclic tetramer, the numbers in the rings refer to the number of distinct orientations of the rings. The data from the diagrams shown on the previous page are tabulated below.

TABLE 4.2

TABLE DETAILING AND SUMMING THE STEREOISOMERS OF THE CYCLIC PENTAMER

CORNER TYPE	REMAINDER	SUM OF POSSIBILITIES	
mm	mmm	5	
mm	rrm	10	T
mm	rmr	5	
mr	mrm (≡ rm / mrm)	10	
mr	rmm (≡ rm / mmr)	10	Q
mr	mmr (≡ rm / rmm)	10	
mr	rr (≡ rm / rrr)	5	
rr	mmm	5	
rr	rmr	10	T
rr	rrm (≡ rr / mrr)	10	
		TOTAL = 80 ($2^5/2\times 5$)	

Thus, the resonance due to the nitrate ester methylenes in the cyclic pentamer is expected to consist of ten peaks of varying intensity. The shift order of these peaks cannot be defined. However, as was the case for the cyclic tetramer, the cyclic pentamer is expected to show separate clusters of peaks each due to the different corner types. Consequently, the multiplet due to the nitrate ester methylenes in the cyclic pentamer is expected to consist of two triplets and one quartet (see table 4.2). Fig.4.6 shows that this resonance (at 75.0 ppm)

does appear to approximate a central quartet with two adjacent triplets. The multiplet is complicated by the presence of peaks due to the cyclic hexamer but, the expected shift pattern for the cyclic pentamer does seem to be observed even though the concentrations of cyclic pentamer and hexamer are approximately equal as determined by SEC. If the splitting pattern of the nitrate ester methylenes in the cyclic hexamer is calculated using the same method as for the cyclic tetramer and pentamer, 17 distinct resonances are expected. The relative intensity of these peaks as compared to those of the cyclic pentamer is expected to be lower as a considerably greater number of distinct stereoisomers are possible. Thus, the intensity of the individual peaks due to the methylenes in the cyclic pentamer are greater than those of the cyclic hexamer. Thus, the model of the cyclic pentamer confirms the assignment of the resonance around 75.0 ppm. As shown previously, three of the ether methylenes are forced *trans* to the gamma oxygen in the cyclic pentamer. This in turn necessitates that an equal number of methyl and nitrate ester side chains that were *trans* now go gauche, thus decreasing their shift. The methyl resonances of the cyclic tetramer, pentamer and hexamer show only very small shift differences (<0.1 ppm). Conversely, the nitrate ester methylenes of the cyclic pentamer and hexamer show a shift difference of approximately 0.7 ppm as compared to the methylenes in the cyclic tetramer. Thus, it appears that it is the nitrate ester methylenes that prefer to be *trans* to the ring oxygens in the tetramer, slightly increasing their shift (on average) with respect to those of the cyclic pentamer and hexamer.

^{1}H NMR spectra of the cyclic fractions are very complex but, similarly for the ^{13}C NMR, small shift differences of the nitrate ester methylenes and the methyls allow the cyclic tetramer to be distinguished from the higher homologues. ^{1}H and ^{13}C NMR spectra of the

cyclic heptamer and higher homologues become progressively more complex as the ring size, and hence the number of different stereoisomers, increases.

4.5 SEC AND ESI ANALYSIS OF THE LINEAR SPECIES OBTAINED FROM THE COLUMN CHROMATOGRAPHY OF UNTREATED PNMMO

Fig.4.3B (shown previously) shows the SEC chromatograms of some of the later fractions obtained from column chromatography of untreated PNMMO, each being labelled with the fraction it represents. The chromatograms were all run using the low molecular weight column system (see chapter 2.1.9.1) and equivalent concentrations of oligomeric material. The chromatogram of fraction 160 represents the cyclic duodecamer. This was the last cyclic oligomer that could be clearly identified from the eluted fractions by SEC. Subsequent fractions were too concentrated in linear oligomers for the individual characterisation of cyclic oligomers. The SEC chromatograms of the linear fractions show that a small degree of separation of the main polymer distribution is possible with the aid of column chromatography, however no differences are apparent in the IR or NMR spectra of these fractions.

Fig.4.8 shows the ESI spectrum of fraction 168 run at a cv of 50 together with two separate enlargements of portions of the spectrum (fig.4.9A and B). Only cyclic oligomers of the nonamer and higher homologues are apparent in the spectrum. Lower homologues were eluted in the previous fractions. The removal of these relatively more highly concentrated cyclic oligomers from the linear oligomers facilitates the identification of the latter species. The ESI spectrum (fig.4.8) shows a series of singly charged, predominantly linear oligomers with molecular weights not exceeding 2800 mus. The SEC chromatogram

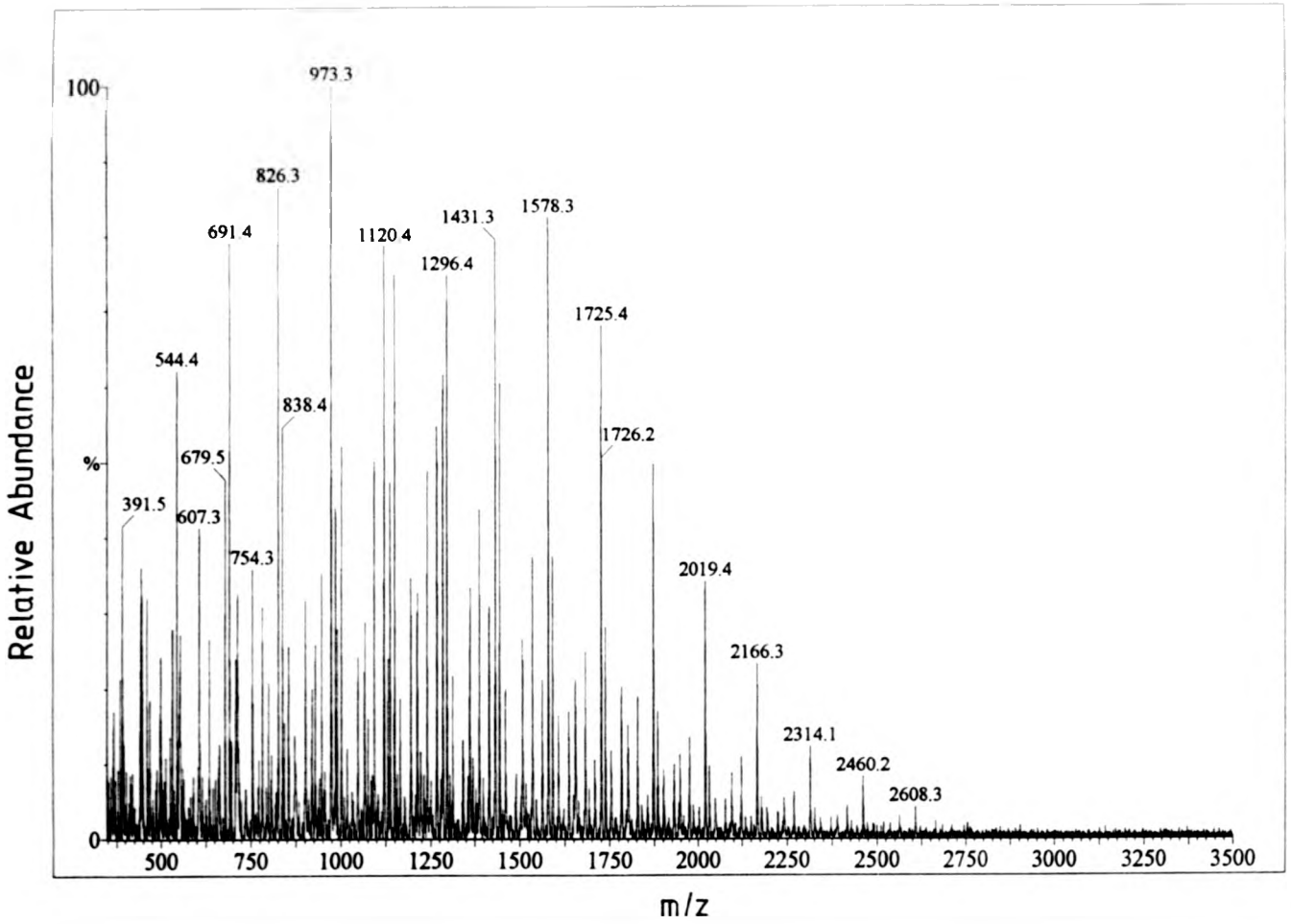

FIG.4.8 ESI MASS SPECTRUM OF FRACTION 168 CONTAINING PREDOMINANTLY LINEAR OLIGOMERS

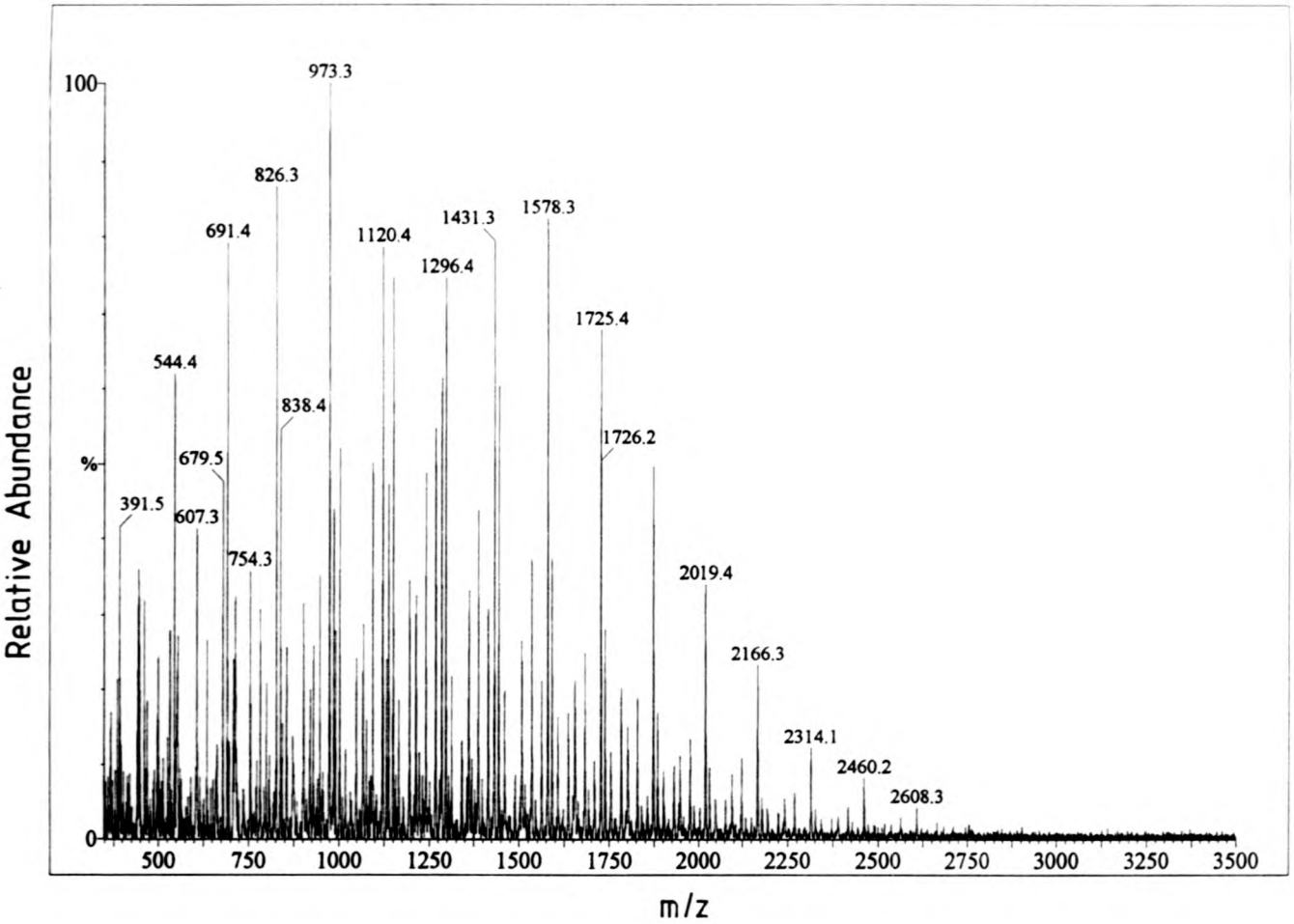

FIG.4.8 ESI MASS SPECTRUM OF FRACTION 168 CONTAINING PREDOMINANTLY LINEAR OLIGOMERS

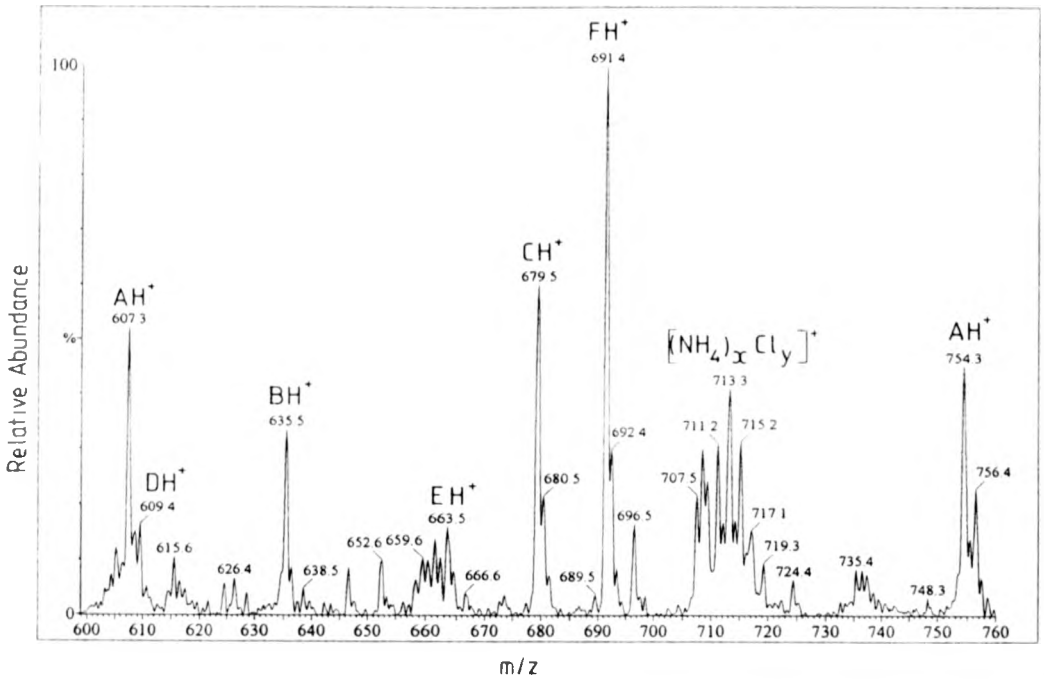
Relative Abundance
100
%
0
AH+
607.3
DH+
609.4
615.6
626.4
BH+
635.5
638.5
652.6
659.6
EH+
663.5
666.6
CH+
679.5
689.5
FH+
691.4
692.4
680.5
696.5
707.5
711.2
713.3
715.2
717.1
719.3
724.4
[(NH4)x Cly]+
735.4
748.3
AH+
754.3
756.4
600 610 620 630 640 650 660 670 680 690 700 710 720 730 740 750 760
m/z

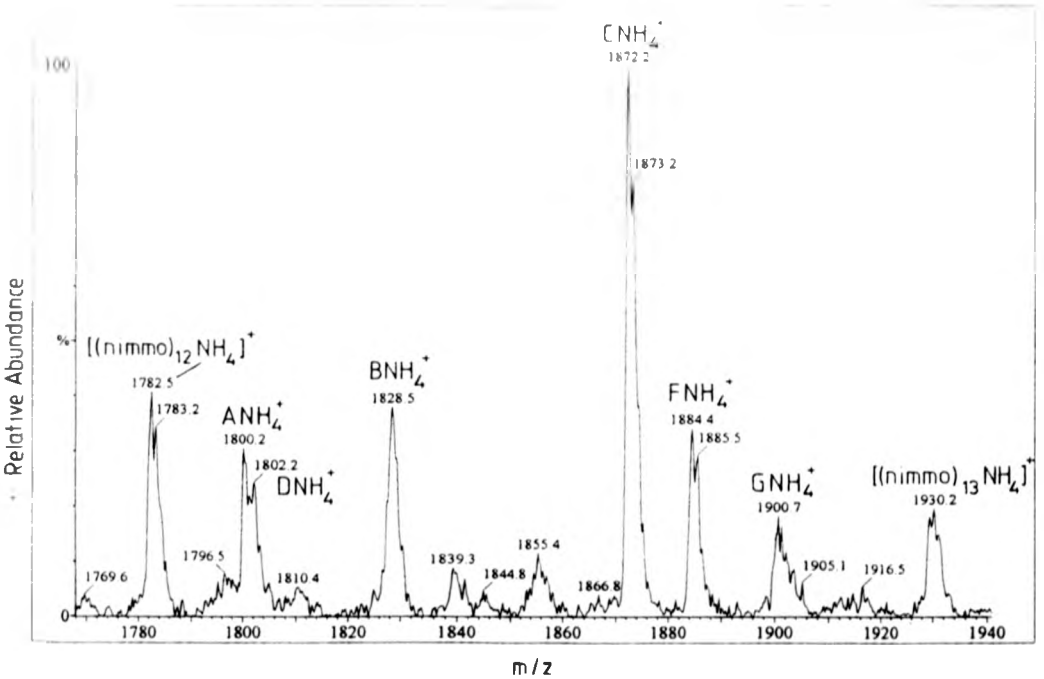
Relative Abundance
100
%
0
[(nimmo)12NH4]+
1782.5
1783.2
ANH4+
1800.2
1802.2
DNH4+
1769.6
1796.5
1810.4
BNH4+
1828.5
1839.3
1844.8
1855.4
CNH4+
1872.2
1873.2
1866.8
FNH4+
1884.4
1885.5
GNH4+
1900.7
1905.1
1916.5
[(nimmo)13NH4]+
1930.2
1780 1800 1820 1840 1860 1880 1900 1920 1940
m/z

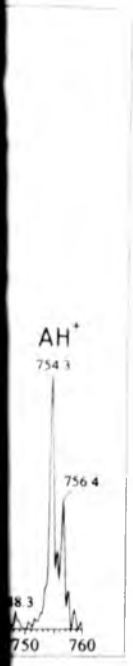

FIG 4 9A A PORTION (600 - 760 MUS) OF THE ESI MASS SPECTRUM OF FRACTION 168 OBTAINED AT A CV OF 50 USING NH_4Cl TO PROMOTE IONISATION

(ION PEAKS IN THE SPECTRA OPPOSITE ARE LABELLED WITH LETTERS ACCORDING TO THE SCHEME SHOWN IN TABLE 4.3 (p.129))

FIG.4.9B A PORTION (1740 - 1940 MUS) OF THE ESI MASS SPECTRUM OF FRACTION 168 OBTAINED AT A CV OF 50 USING NH_4Cl TO PROMOTE IONISATION

of the same fraction shows the main polymer distribution centring around 5000 mus. As shown previously, the main polymer distribution is not visible under the experimental conditions used here (section 3.4.1). Fractions 162 to 170 all gave ESI spectra similar to the spectrum for fraction 168 (fig.4.8). The spectra did vary to a small degree as regards the relative intensities of the various linear oligomers. Different linear oligomers may have slightly different retention volumes in the toluene/methanol solvent system and thus will be eluted from the column at slightly different times. The ESI spectrum shown is however representative of the relative intensities of the low-mass oligomers present in bulk PNMMO. All the subsequent fractions produced only very weak intensity ions.

The three different end groups known to exist in PNMMO have already been described (see section 3.4.1). Linear oligomers with these end groups are apparent in the ESI spectra (fig.4.8). Four different linear species are also visible in the spectra and attempts to identify the end groups have been made by considering the materials used in the preparation of PNMMO;

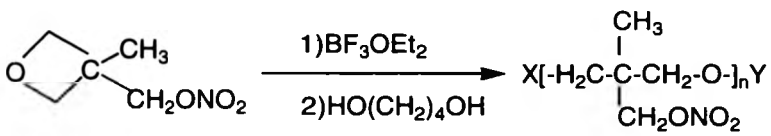

where X and Y are the end groups.

DIAGRAM SHOWING MATERIALS USED IN THE PREPARATION OF PNMMO

Although the loss of fragments characteristic of PNMMO oligomers (see chapter 6) during CID experiments confirmed that all the species attributed to linear oligomers were associated with PNMMO species, it was not possible to identify the various end groups present purely from the CID spectra.

Fig.4.9A shows a portion of the ESI spectrum between 600 and 760 mus. The peaks are labelled with letters according to the scheme shown in table 4.3.

TABLE 4.3

LINEAR OLIGOMERS IN PNMMO AND THEIR RMMs

LABEL	MASS	LINEAR OLIGOMER
A	(147n)+18	HO-[PNMMO]-H
B	(147n)+46	CH_3CH_2O-[PNMMO]-H
C	(147n)+90	$HO(CH_2)_4O$-[PNMMO]-H
D	(147n)+20	unassigned
E	(147n)+74	CH_3CH_2O-[PNMMO]-CH_2CH_3
F	(147n)+102	CH_3CH_2-[PNMMO]-$(CH_2)_4OH$
G	(147n)+118	CH_3CH_2O-[PNMMO]-$(CH_2)_4OH$

The H^+ adduct is considerably more stable than the NH_4^+ adduct for all the different types of linear tetramer. The spectrum (fig.4.9A) clearly shows that in this relatively low mass range, nearly all the peaks are due to H^+ adducts and only very low intensity peaks are visible for the NH_4^+ adducts. No peak is seen for the cyclic tetramer (606.3 mus) or the cyclic pentamer (753.3 mus) and the spectrum clearly shows that the peaks at 607.3 and 754.3 mus are not due to the ^{13}C isotopes of these cyclic species. Linear oligomers A to G, are all visible in the spectrum (fig.4.9A). The peak due to oligomer E is very weak, but is much stronger in the spectrum of unchromatographed PNMMO. Oligomer D is unassigned and is not visible in the spectrum of unchromatographed PNMMO. This oligomer is

however clearly visible in fig.4.9A, particularly for the pentamer at 756.4 mus. The separation and thus increased concentration of the low-mass linear oligomers in the sample of PNMMO makes the identification of relatively low concentration oligomers possible. The relative concentrations of the various linear oligomers present are difficult to calculate as they may have different stabilities with a particular ion. However, the stability of the H^+ adduct would not be expected to vary by a significant amount due to a change in end group. The H^+ ion most probably remains on an oxygen atom in the main chain and is relatively uninfluenced by the end group. Thus the ESI spectrum of unchromatographed PNMMO shows that oligomers A, C, E and F are present in approximately equal concentrations and are roughly five times as concentrated as oligomers B, D and G. However, the peak for oligomer C is thought to be associated with two different species. The oligomer shown below is known to exist from NMR measurements[6] and has the same mass as oligomer C. The relative concentrations of the two oligomers are thus impossible to calculate here.

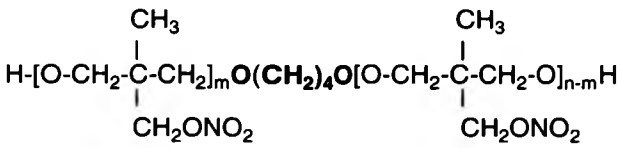

STRUCTURE OF A LINEAR OLIGOMER IN PNMMO

The relative intensities of the H^+ ions for the various linear oligomers remain approximately constant as the mass increases, indicating that their relative concentrations also remain approximately constant.

Fig.4.9B shows a portion of the ESI spectrum of fraction 168 (fig.4.8) between 1740 and 1940 mus. The only peak in the spectrum due to a H^+ adduct is at 1855.4 mus. This very low intensity peak is only visible due to the relatively high concentration of oligomer C. All the other oligomers show only NH_4^+ adducts due to the low stability of the H^+ adduct for oligomers in this mass range. Cyclic oligomers of the nonamer and higher homologues were not separated from the linear oligomers and the NH_4^+ adduct of the cyclic duodecamer is also visible at 1782.5 mus.

4.6 ANALYSIS OF THE CYCLIC TETRAMER BY CHEMICAL IONISATION MASS SPECTROMETRY (CIMS)

Previous to the ESI study in chapters 3 and 4 of this report, CIMS[7] was employed to analyse a sample supplied by the DRA as 'pure cyclic tetramer'. The sample was obtained by soxhlet extraction of untreated PNMMO with hexane. Fig.4.10 shows the mass spectrum obtained using ammonia gas to promote cationisation. Peaks due to the H^+ and NH_4^+ adducts of the cyclic tetramer are clearly visible at 589 and 606 mus. However, the most intense peak in the spectrum at 544 mus has already been assigned to the H^+ adduct of linear oligomer F (section 4.5). NMR results also show additional peaks for the linear oligomers. These additional peaks in the ESI and NMR spectra are not present in the samples of cyclic tetramer obtained by column chromatography in this study. Thus the method of soxhlet extraction using hexane as a solvent does not solely extract the cyclic tetramer. CIMS spectra of higher mass oligomers show very complex spectra as both NH_4^+ and H^+ adducts of all oligomers are present. Analysis by ESI thus provides considerable advantages over CIMS as the variation of the cv during ESI provides a convenient way of identifying H^+ and NH_4^+ adducts.

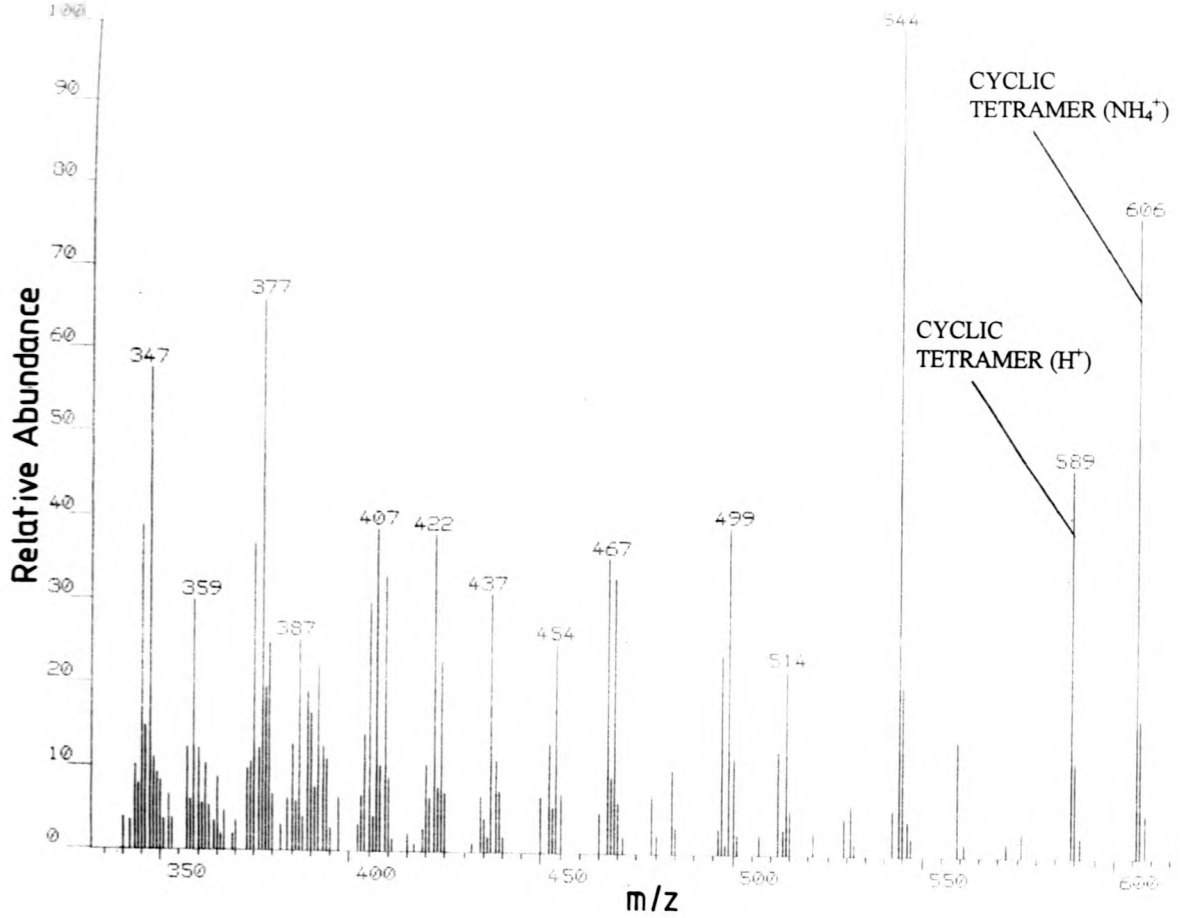

FIG.4.10 CHEMICAL IONISATION (NH_3) MASS SPECTRUM OF A SAMPLE OF THE CYCLIC TETRAMER OBTAINED FROM THE DRA

CHAPTER 4 REFERENCES

1 Casetta, B., Garofolo, F., *Org. Mass Spectrom.* 1994, **29**, 517.

2 Prokai, L., Siminsick, W.J., *Rapid. Comm. Mass Spectrom.* 1993, **7**, 853.

3 Compana, J.E., Sheng, L.-S., Shew, S.L. Winger, B.E., *Trends Anal. Chem.* 1994, **13**, 239.

4 Gunther, H., NMR Spectroscopy, 2nd ed., John Wiley & Sons, Chichester, 1994.

5 Sanders, J.K.M., Hunter, B.K., Modern NMR Spectroscopy, Oxford University Press, 1987.

6 Unpublished work obtained from the DRA.

7 Budzikiewicz, H., Djerassi, C., Williams, D.H., Mass Spectrometry of Organic Compounds, Holden-Day Inc. London, 1967.

CHAPTER 5

SPECTRAL ANALYSIS OF PYROLYSED PNMMO

Pyrolysed PNMMO was characterised by a number of different physical and spectral techniques before and after chromatographic separation. This chapter is concerned with the unchromatographed pyrolysed polymer, while chapter 6 details the results of the chromatographed pyrolysed polymer.

5.1 CHARACTERISATION OF PYROLYSED PNMMO BY SEC

PNMMO (4.0 g) was placed in a glass vial (20.0 cm^3) and pyrolysed in an oven at 130^{0}C for up to 96 h. Samples (0.10 g) of the pyrolysate were removed after 27, 48, 75 and 96 h. The polymer becomes gradually more viscous, darker in colour and harder to dissolve as the heating time is increased. Fig.5.1 shows the SEC chromatograms for the pyrolysed samples and for untreated PNMMO obtained using the high molecular weight column system (see section 2.1.9.1). Clearly pyrolysis has resulted in the formation of both lower and higher mass polymeric material. The shift to lower mass, presumably via a chain scission reaction, appears to be the dominant process at this pyrolysis temperature. The nominal molecular weight of PNMMO decreases from its original value of approximately 5000 to a value of approximately 3000 mass units after 96 h pyrolysis. A substantial amount of higher molecular weight material is also formed, presumably via a cross-linking process, and the weight average molecular weight increases from its original value of 9000 to 24 000 mass units.

The low molecular weight column system gives more accurate results during the first 10 h of pyrolysis as the molecular weight changes of PNMMO are relatively small over this time period. SEC data shows that during the first 3 h of pyrolysis at 130^{0}C, chain scission

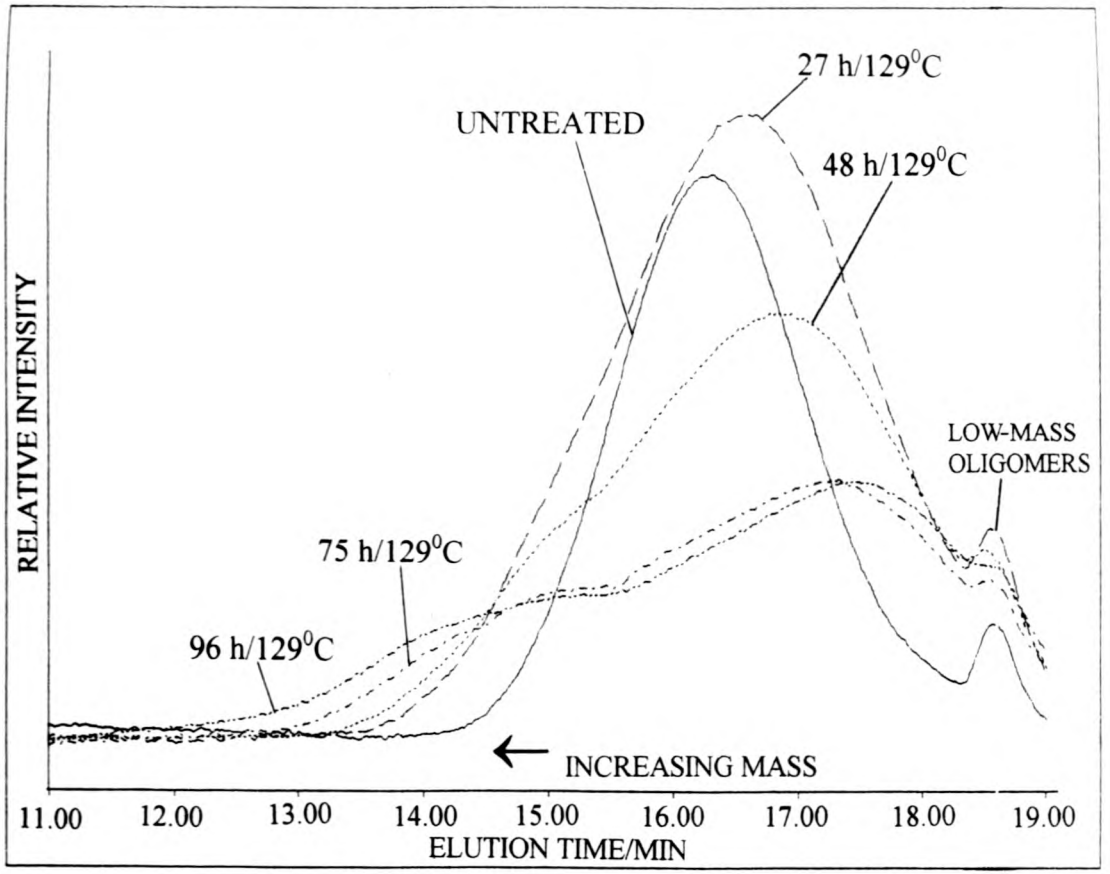

FIG.5.1 SEC CHROMATOGRAMS OF UNTREATED AND PYROLYSED PNMMO

reactions occur to produce lower molecular weight polymer, but no higher molecular weight material is evident. Thus, it appears that there is a inhibition period before cross-linking reactions occur. If the rate of oxygen consumption exceeds the rate of oxygen permeation, as is the case of solid polymers,[1,2] oxidation occurs in the surface layers whereas the bulk core of the polymer remains practically unoxidised. Thus, at 130^0C oxidation proceeds rapidly and the available oxygen is quickly used up. However, during the first few hours of pyrolysis at 130^0C the oxygen levels in PNMMO are relatively high. The thermal oxidation mechanism of PNMMO in section 5.3 shows that thermolysis results in chain scission. Presumably, in the presence of excess oxygen, the rate of oxidation and thus rate of chain scission is far greater than the rate of cross-linking. The importance of this effect depends on several intrinsic parameters such as material geometry (e.g. sample thickness) coupled with oxygen consumption rate, which depends in turn on the reactivity of the polymer, the presence of additives and the oxygen permeability of the material.[1,2]

PNMMO was pyrolysed at temperatures varying between 90 and 150^0C. No significant differences in the distribution of lower as compared to higher mass pyrolysis products were apparent in the SEC chromatograms obtained for PNMMO pyrolysed at temperatures in this range.

5.2 CHARACTERISATION OF PYROLYSED PNMMO BY SOLUTION INFRARED SPECTROSCOPY

Preliminary investigations into the oxidative process were performed using FTIR. PNMMO (5.0 g) was placed in glass vials (20.0 cm^3) and pyrolysed in the oven at 145^0C. New absorptions are visible via solution IR at 1729 and 1550 cm^{-1}. Both peaks appear to increase in intensity at approximately the same rate over a 4 h pyrolysis. The absorption at

1729 cm^{-1} appears in the region for carbonyl compounds[3,4]; as no other new absorptions are observed in this region and as carbonyl formation is expected on thermolysis, this absorption is attributed to a carbonyl species.

Similar experiments using thin films of PNMMO coated on glass plates were subsequently performed. PNMMO was spread as thinly as possible on a glass plate (20 cm $\times$ 20 cm). A glass vial (20 cm^3) was filled with PNMMO (4.0 g) so that a depth of approximately 3 cm was achieved. Both the plate and vial were placed in the oven at 145^{0}C and pyrolysed for a period of 12 h over which time samples were removed and analysed via solution IR spectroscopy. It was found that the relative intensities of the two IR absorptions at 1729 and 1550 cm^{-1} differed substantially between the two sample configurations as summarised below.

GLASS VIAL GEOMETRY

Over the first 4 h of pyrolysis the samples showed nearly identical intensities at 1729 and 1550 cm^{-1}. However, over the next 8 h of pyrolysis the absorption at 1729 cm^{-1} became far more intense until it was approximately twice as intense as that at 1550 cm^{-1}.

FLAT GLASS PLATE GEOMETRY

The most noticeable feature here is the immediate presence during the first 4 h of thermolysis of one absorption at 1550 cm^{-1} and another at 1571 cm^{-1}. The absorption at 1550 cm^{-1} increases in intensity at a slightly lesser rate than its counterpart in the glass vial experiment. However, the peak at 1729 cm^{-1} increases in intensity at a rate nearly double that of its counterpart.

Figs.5.2A,B show the solution IR spectra ($CHCl_3$) obtained for the PNMMO samples from the glass vial and glass plate respectively after 12 h pyrolysis at 145^0C (compare with fig.3.2, IR spectrum of untreated PNMMO). The glass plates were covered in very thin films of polymer and thus it became increasingly difficult to obtain equivalent masses of sample from the glass plate as only very small amounts of polymer could be removed from the plate. Consequently, the concentrations of the samples used to obtain the IR spectra in fig.5.2 were somewhat different.

These results can partly be explained by the limitation of diffusion of oxygen (see section 5.1). Thus, if the rate of oxygen consumption exceeds the rate of oxygen permeation, as it should do for the thicker sample (glass vial), oxidation occurs in the surface layers whereas the core remains practically unoxidised. However, thinner samples should exhibit more rapid carbonyl growth as the surface area of the polymer is relatively larger. Lowering the pyrolysis temperature enhances the relative growth of the 1729 cm^{-1} peak as there is more time for oxygen diffusion to occur. The increased oxygen diffusion at lower temperature also results in the production of a complex mixture of secondary oxidation products absorbing from 1700-1800 cm^{-1}.

The absorption at 1550 cm^{-1} increases in intensity at a slightly lesser rate for the sample on the glass plate. Separate experiments comparing even thinner films to even thicker samples of polymer show that this effect becomes even more pronounced. The absorption at 1550 cm^{-1} could be due to a number of different species. Candidate species include carboxylate, alkene, nitro, nitroso and nitrite compounds. If one of the latter three species is associated with the new absorption, its formation may be expected to result from the loss and subsequent reaction of NO_x. If this process were reduced in significance, i.e. if NO_x is evolved into the atmosphere without reacting, then a lower concentration of product

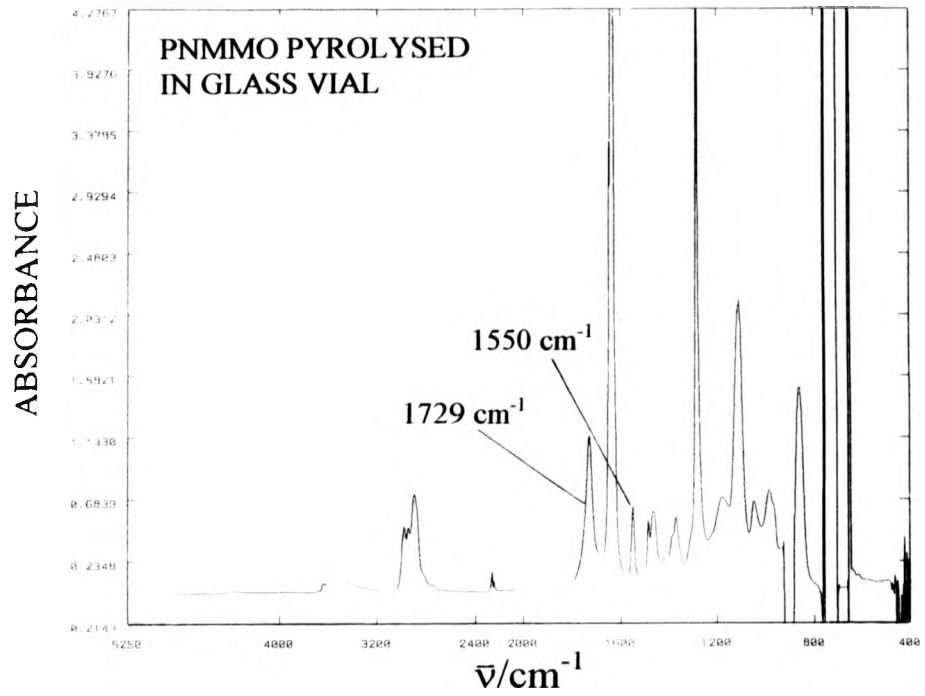

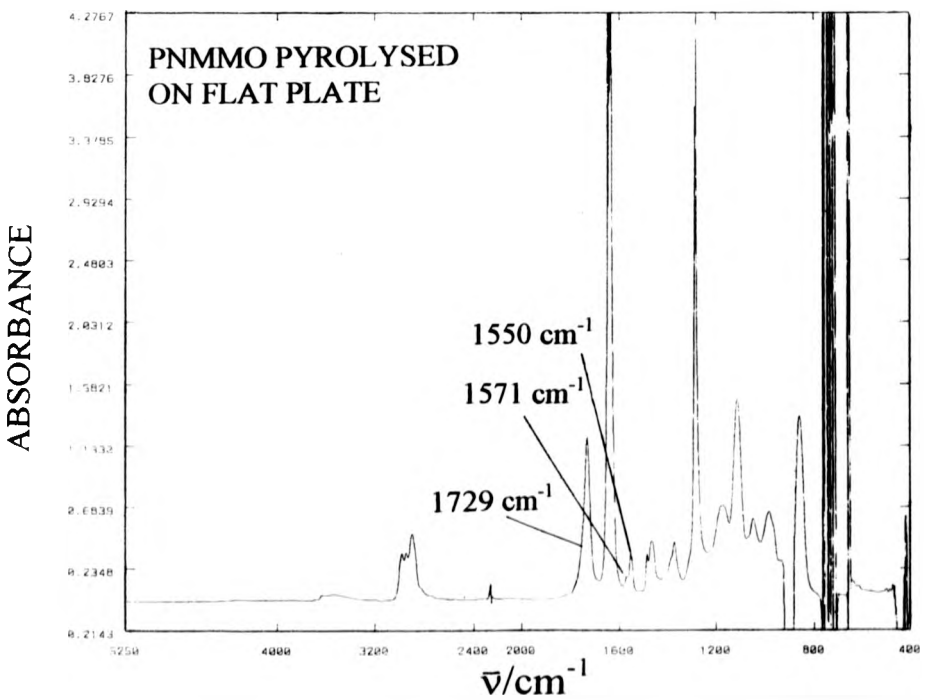

FIGS.5.2A,B SOLUTION IR SPECTRA OF PYROLYSED (12 h/145^{0}C) PNMMO

would be expected. An attempt was made to induce this effect in PNMMO by pyrolysing a thin film; as the surface area is increased and the film thickness decreased, relatively more NO_x is lost without reacting, thus decreasing the amount of product resulting from the polymer's reaction with NO_x. As this was borne out by experiment, it appears likely that the absorption at 1550 cm^{-1} results from the reaction of PNMMO with NO_x and at this stage we tentatively assigned this band to the asymmetric stretching frequency in a nitroalkane. In shape, position and intensity the band at 1550 cm^{-1} strongly resembles those found in nitrobenzene[4], t-nitrobutene[5] and many other nitroalkanes[5].

A comparison of the IR spectra of untreated PNMMO (fig.3.2) and pyrolysed PNMMO (fig.5.2) shows that there is an increase in intensity of the bands in the region around 1000 cm^{-1}. Consequently, IR difference spectra of the pyrolysed PNMMO samples obtained from the glass vial/flat plate experiments were run. Fig.5.3 shows the IR difference spectrum obtained by subtracting the spectrum for untreated PNMMO from that for pyrolysed PNMMO (6 h/145^{0}C). Both spectra were run using identical concentrations of PNMMO. The absorptions at 1729 and 1550 cm^{-1} are clearly visible. Other new absorptions at 3500, 1170, 1085, 1050 and around 1400 cm^{-1} are also visible. The band around 3500 cm^{-1} appears to consist of a sharp unbonded hydroxyl band at 3526 cm^{-1} and a broad bonded hydroxyl band around 3400 cm^{-1}. The absorption around 1170 cm^{-1} appears broad and may consist of multiple absorptions. Many different carbonyl species absorb in this region but the absorption frequency of the carbonyl group (1729 cm^{-1}) suggests that these absorptions may belong to the stretching and bending vibrations of the C-C(=O)-C group in ketone compounds or the stretching vibrations of the C-O-C group in ester compounds. The absorptions around 1085 and 1050 cm^{-1} are consistent with the stretching vibrations of the C-O group of alcohol compounds.

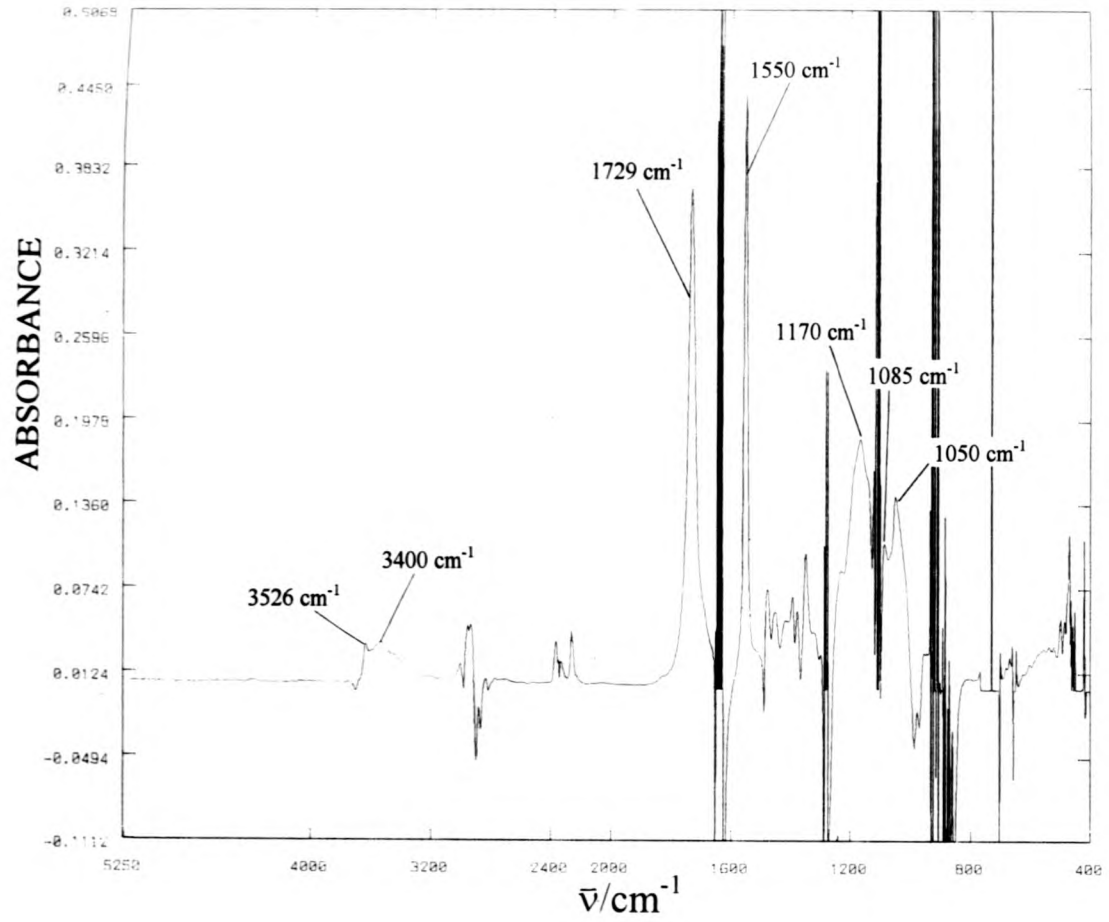

FIG.5.3 IR DIFFERENCE SPECTRUM OBTAINED BY SUBTRACTING THE SPECTRUM FOR UNTREATED PNMMO FROM THAT FOR PYROLYSED (6h/145^{0}C) PNMMO

5.3 CHARACTERISATION OF PYROLYSED PNMMO BY ^{1}H AND ^{13}C NMR SPECTROMETRY

^{1}H and ^{13}C NMR spectra of the pyrolysed samples from the glass vial and glass plate experiments in section 5.2 were recorded. As with IR spectra, the NMR spectra of the PNMMO samples obtained from the glass plate and vial differed only in their relative peak intensities. Figs.5.4A and B show the ^{1}H and ^{13}C NMR spectra of pyrolysed PNMMO. The pyrolysed PNMMO was obtained from the glass vial after 12 h pyrolysis at $145^{0}C$. The peaks due to the original methyl and methylene protons have broadened considerably due to the increased viscosity and thus lowered mobility of the pyrolysed polymer. Many new resonances are visible around 4.0 ppm, making assignments difficult. Column chromatography was employed to separate this complex mixture of pyrolysis products and these peaks are assigned in chapter 6. Two new resonances were observed at low field. The most readily formed of these appears at δ_H = 8.09 ppm and is visible after 5 min at $145^{0}C$. The second appears at δ_H = 9.53 ppm and can be seen after 10 min at $145^{0}C$. The peak at 9.53 ppm increases in intensity over the first 4 h of pyrolysis and then remains at a constant intensity. However, its intensity is very low and this peak is only visible when the spectrum is enlarged (see inset to fig.5.4A). The peak at 8.09 ppm continues to increase in intensity over the course of the pyrolysis. Similarly, a new peak at δ_H = 2.1 ppm increases in intensity during pyrolysis and can be assigned on the basis of published work on the thermal degradation of PPO. PPO has many structural similarities to PNMMO and its degradation products have been characterised by ^{1}H NMR[6]. Similarly to PNMMO, a peak at δ_H = 2.1 ppm is visible in the ^{1}H NMR spectrum of PPO on pyrolysis. Thus, as for PPO, this peak is assigned to a methyl group attached to a carbonyl carbon in a ketone.

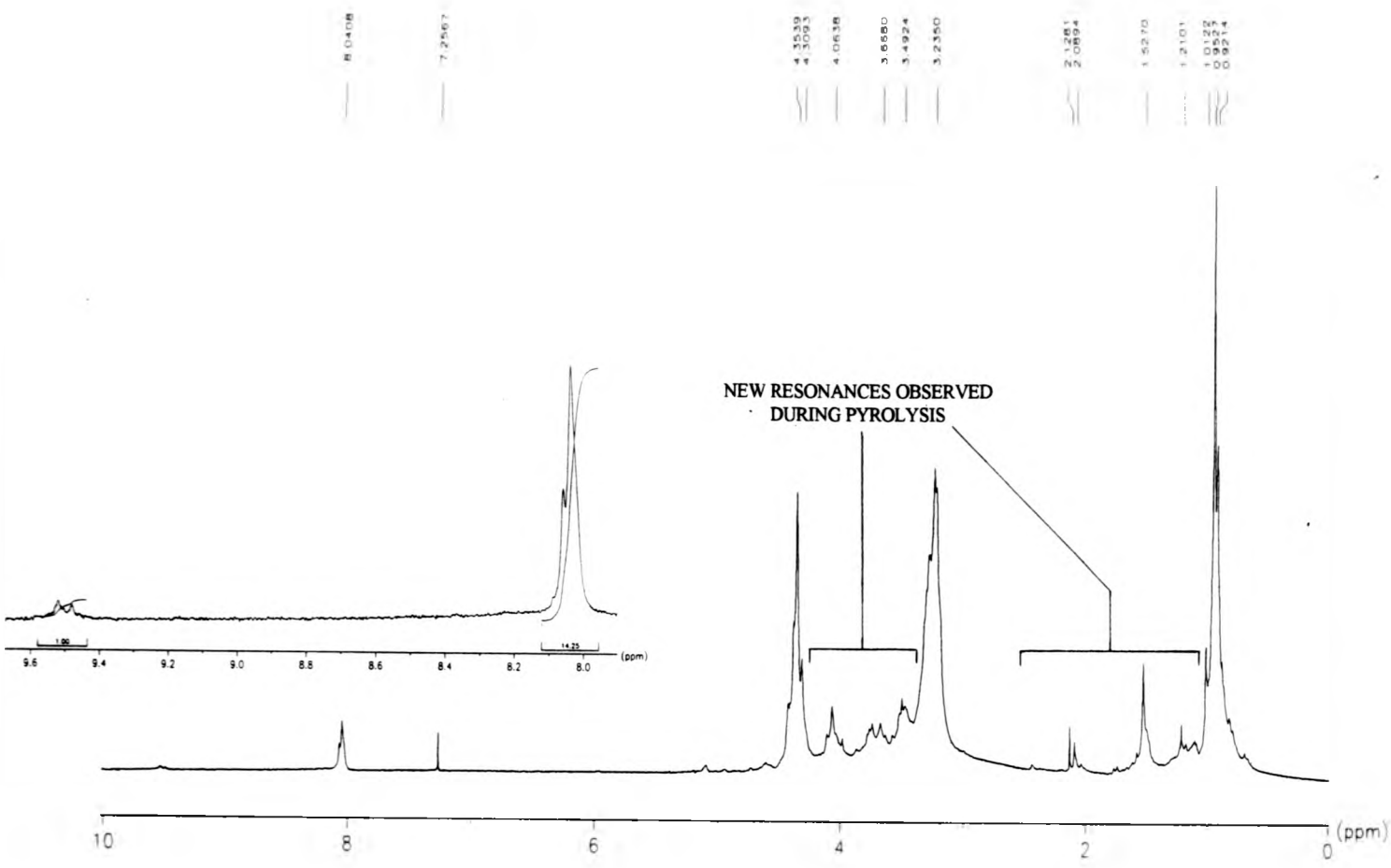

FIG.5.4A 250 MHz ^{1}H NMR SPECTRUM OF PYROLYSED (12 h/145^{0}C) PNMMO

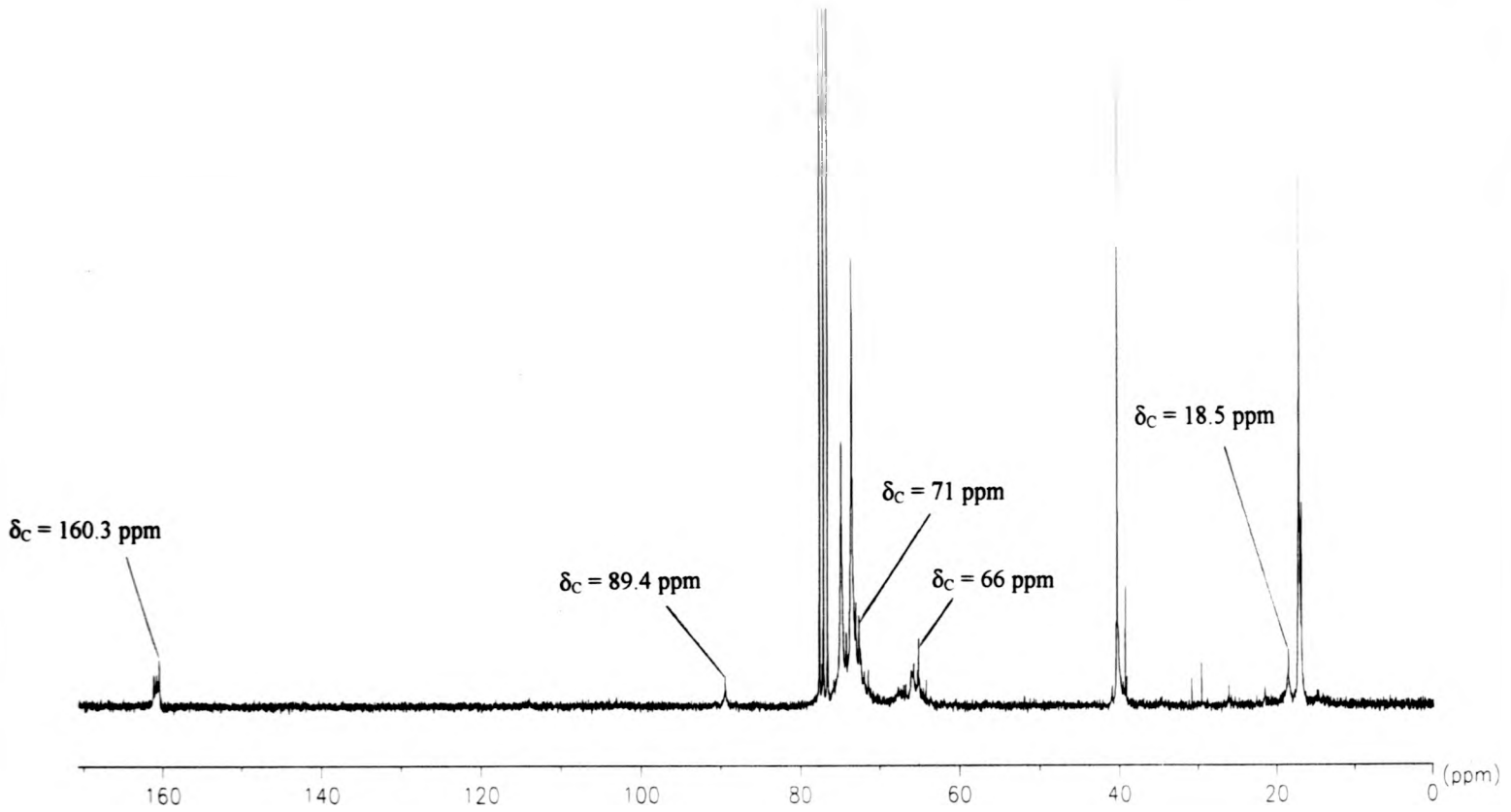

FIG.5.4B 250 MHz ^{13}C NMR SPECTRUM OF PYROLYSED (12 h/145^{0}C) PNMMO

New peaks are visible at δ_C = 160.3 ppm and 89.4 ppm in the ^{13}C NMR spectrum (fig.5.4B) of pyrolysed PNMMO (the latter peak is assigned in chapter 6 of this thesis). Carbonyl formation has already been demonstrated by IR spectroscopy and in the absence of any other new peaks in this region, the peak at δ_C = 160.3 ppm is assigned to a carbonyl group. Due to its field position, this resonance is most likely associated with an ester as opposed to a ketone which would give a resonance at lower field. 2-D NMR was employed to ascertain if this resonance is associated with the peak at δ_H = 8.09 ppm in the ^1H NMR. A 2-D ^1J ^1H-^{13}C correlation experiment (see fig.5.5) showed that the proton associated with the resonance at δ_H = 8.09 ppm is directly attached to the carbonyl group associated with the resonance around δ_C = 160.3 ppm in the ^{13}C NMR. Consequently, the most likely assignment of the carbonyl group is to a formate ester. The position of the carbonyl absorption around 1729 cm^{-1} in the IR spectrum of pyrolysed PNMMO also closely matches the carbonyl absorptions of ethyl, n-propyl and n-butyl formate which absorb around 1725 cm^{-1} [7,8]. Pyrolysis experiments were also performed using degassed solutions of PNMMO sealed under dynamic vacuum. The rates of development of the absorbance at 1729 cm^{-1} in the IR and the associated resonance at δ_H = 8.09 ppm in the ^1H NMR were significantly reduced as compared to those of samples of PNMMO pyrolysed in air, thus substantiating our assignment of the carbonyl compound as an autoxidation product. Exhaustive attempts to inhibit completely carbonyl development were unsuccessful. Indeed, carbonyl development became increasingly difficult to inhibit with increasing concentration of the PNMMO solution due to the difficulty in degassing more viscous solutions.

Other new resonances are also visible around 66.0 and 71.0 ppm in the ^{13}C NMR spectrum of pyrolysed PNMMO. These resonances appear to decrease in intensity in the 2-D NMR spectrum of pyrolysed PNMMO and are consequently thought to be associated, to

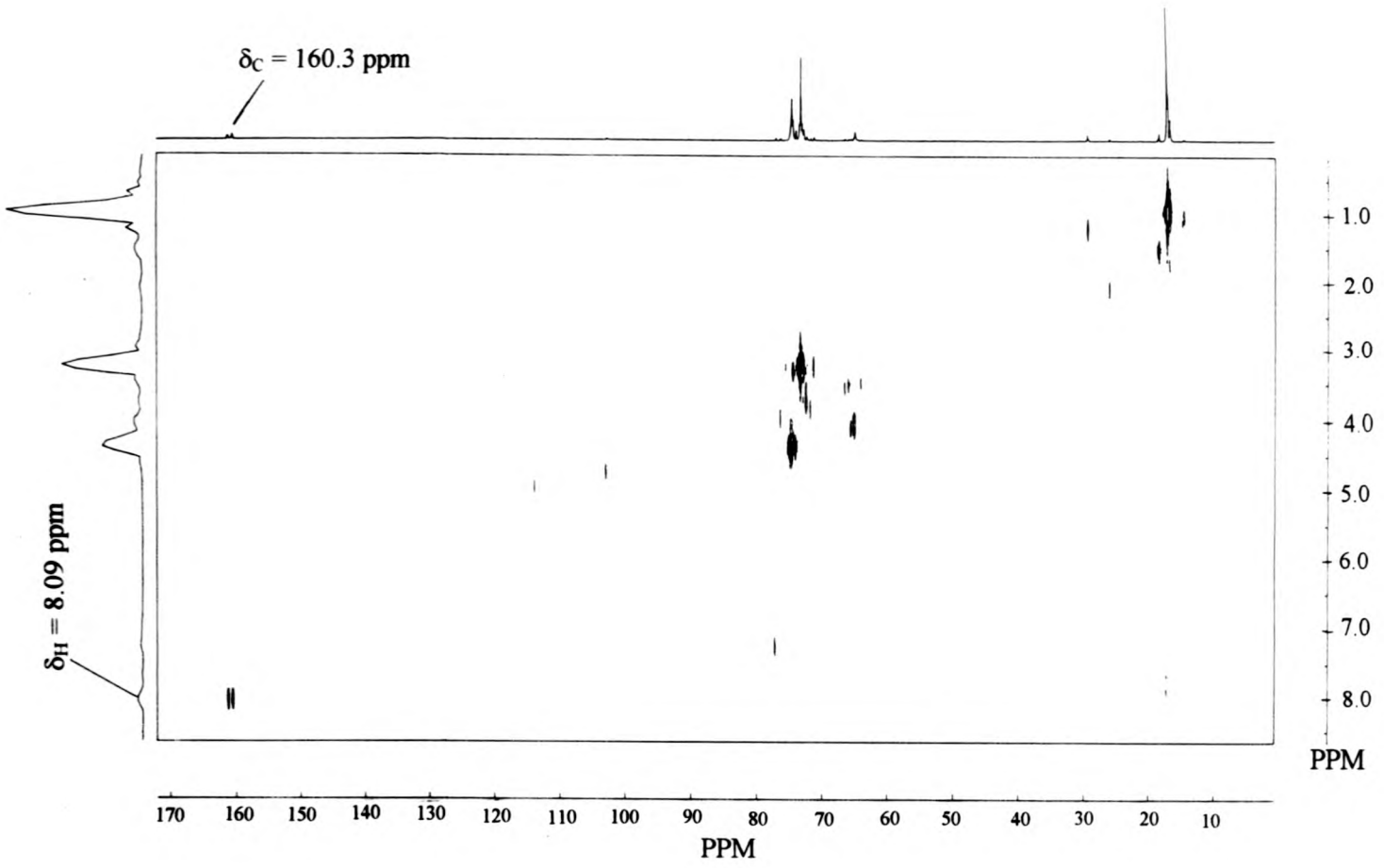

FIG.5.5 2-D (^{1}J, ^{1}H - ^{13}C CORRELATION) NMR SPECTRUM OF PYROLYSED (12h/145^{0}C) PNMMO

some extent, with species possessing a carbon atom with no hydrogens directly attached. Clearly these new resonances around 66 and 71 ppm are complex and consist of many peaks making the assignment of individual peaks very difficult. However resonances around 60 - 80 ppm in the ^{13}C NMR spectrum are often associated with alcohols formed during the thermal degradation of polymers[9]. The mechanism over the page shows the proposed oxidation scheme which leads to the production of the formate ester. We propose that the tertiary, secondary and primary carbon-centred radicals generated during the thermal degradation of PNMMO may lead to the formation of alcohol species via alkoxy radicals (see mechanistic scheme over the page).

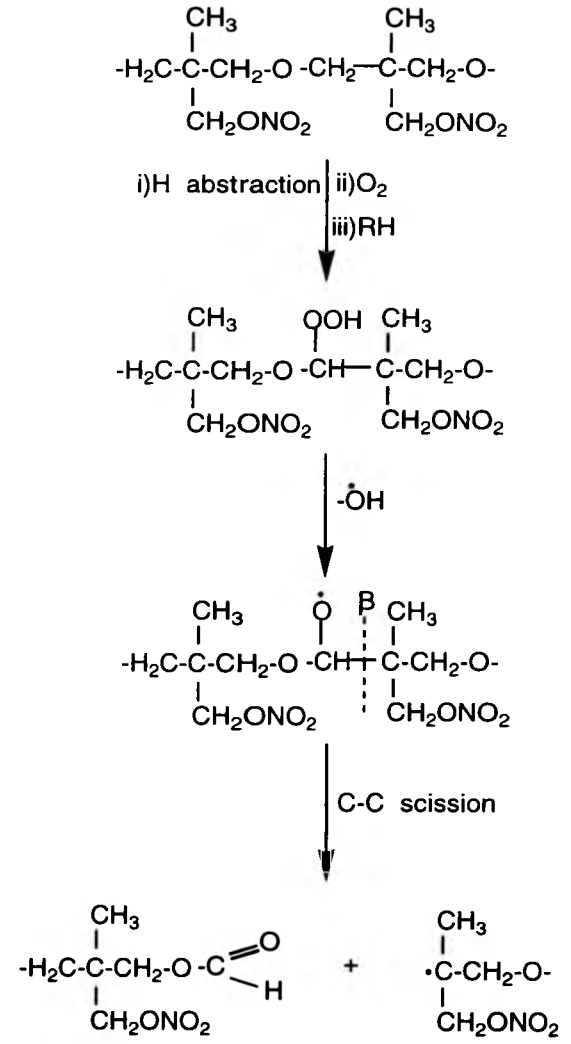

PROPOSED MECHANISM FOR THE FORMATE ESTER DURING PYROLYSIS OF PNMMO

Clearly the formate ester species shown above may be produced by hydroperoxy formation at either of the methylene carbons in each monomer unit in PNMMO. The

resulting alkoxy radical appears to undergo predominantly C-C bond cleavage (β scission), as observed in PEO and PPO (see introduction to this thesis). However low intensity peaks around 9.5 ppm, indicative of an aldehyde species, are also observed in the ^{1}H NMR spectrum of pyrolysed PNMMO and these are discussed in chapter 7.

The tertiary carbon-centred radical generated in the mechanism shown on the previous page may react similarly to the secondary polymer radical to form an alkoxy radical. The alkoxy radical may then undergo a similar β scission (generating a ketone) or, it may abstract hydrogen from another polymer chain to give a tertiary alcohol. Clearly a secondary alcohol will also be formed if the secondary alkoxy radical shown in the scheme above similarly abstracts hydrogen. Any attempt to devise oxidation mechanisms beyond the initial stages of degradation would be speculative but, it is clear that various species of alcohol exhibiting resonances around 60 - 80 ppm in the ^{13}C NMR spectrum may be produced during the thermal degradation of PNMMO.

Due to the lower mobility of the pyrolysed polymer, long scan times were required to obtain well resolved ^{13}C NMR spectra. It was found that far greater spectral resolution was observed when spectra were recorded above room temperature. Consequently, and to avoid any solvent effects, spectra were recorded using neat PNMMO (see section 2.1.2.1) before and after pyrolysis. Due to the gradually increasing viscosity of the polymer with longer pyrolysis times, there exists a limit where the resonances in the ^{13}C NMR spectra become so broad and poorly defined that continued analysis is futile. This seems to occur after approximately 45 h pyrolysis at $145^{0}C$ in a 10 mm NMR tube. Fig.5.6 shows the 400 MHz ^{13}C NMR spectrum obtained at $90^{0}C$ for pyrolysed (45 h/$145^{0}C$) PNMMO. Various new resonances, not previously visible in the solution spectra, appear in the region between 100 and 220 ppm. Only very general attributions can be given to these resonances. New

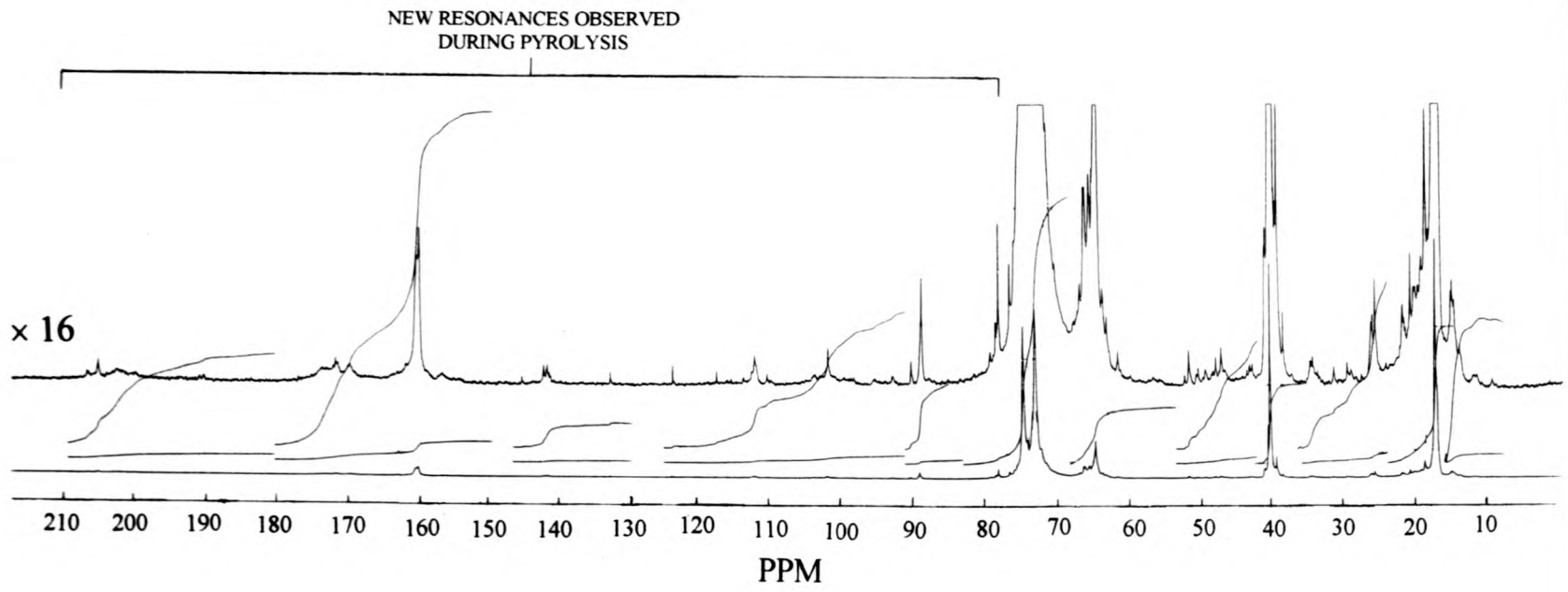

FIG.5.6 400 MHz ^{13}C NMR SPECTRUM OF PYROLYSED (45 h/145^{0}C) PNMMO OBTAINED AT 90^{0}C

resonances around 205 ppm are most probably associated with aldehyde or ketone species. Resonances around 175 ppm are characteristic of ester species produced by direct oxidation at the methylene carbons in the main chain of PNMMO; thus in the absence of chain scission carbonyl formation will result in an ester. Resonances around 100 - 150 ppm are characteristic of alkenes.

5.4 CHARACTERISATION OF PYROLYSED PNMMO BY ESR

PNMMO (0.5 g) was placed in quartz pipette tubes and heated in the oven at temperatures between 100 - 155^{0}C. Preliminary investigations led to the detection of a very clearly defined paramagnetic species. Fig.5.7 shows the ESR spectrum of pyrolysed PNMMO (5 h/150^{0}C) measured at room temperature. Identical spectra were also obtained from the pyrolysis of degassed samples of PNMMO sealed under dynamic vacuum (see section 2.2.1.1) and from the pyrolysis and photolysis of both cured and uncured PNMMO samples in air (see section 2.1.8.2). Heating over various lengths of time produces a gradually increasing concentration of this odd-electron species which remains stable over a period of months. Few such radicals are stable over this time scale; candidate molecules are the nitroxyls, nitrogen dioxide and trapped polymer peroxyl radicals. The two ESR standards, DPPH and Fremy's salt (see section 2.2.1.1) were used to extract the exact anisotropic g-tensors from the spectra. The g-tensor locations were defined in the usual way and are shown on the spectrum.

As high a concentration of the radical species obtained by heating could not be achieved by photolysis, but the g-tensors of the species generated by either method are nearly identical. Samples of PNMMO heated under vacuum and in air gave similarly intense spectra, indicating that oxygen is not a requirement for this free radical formation.

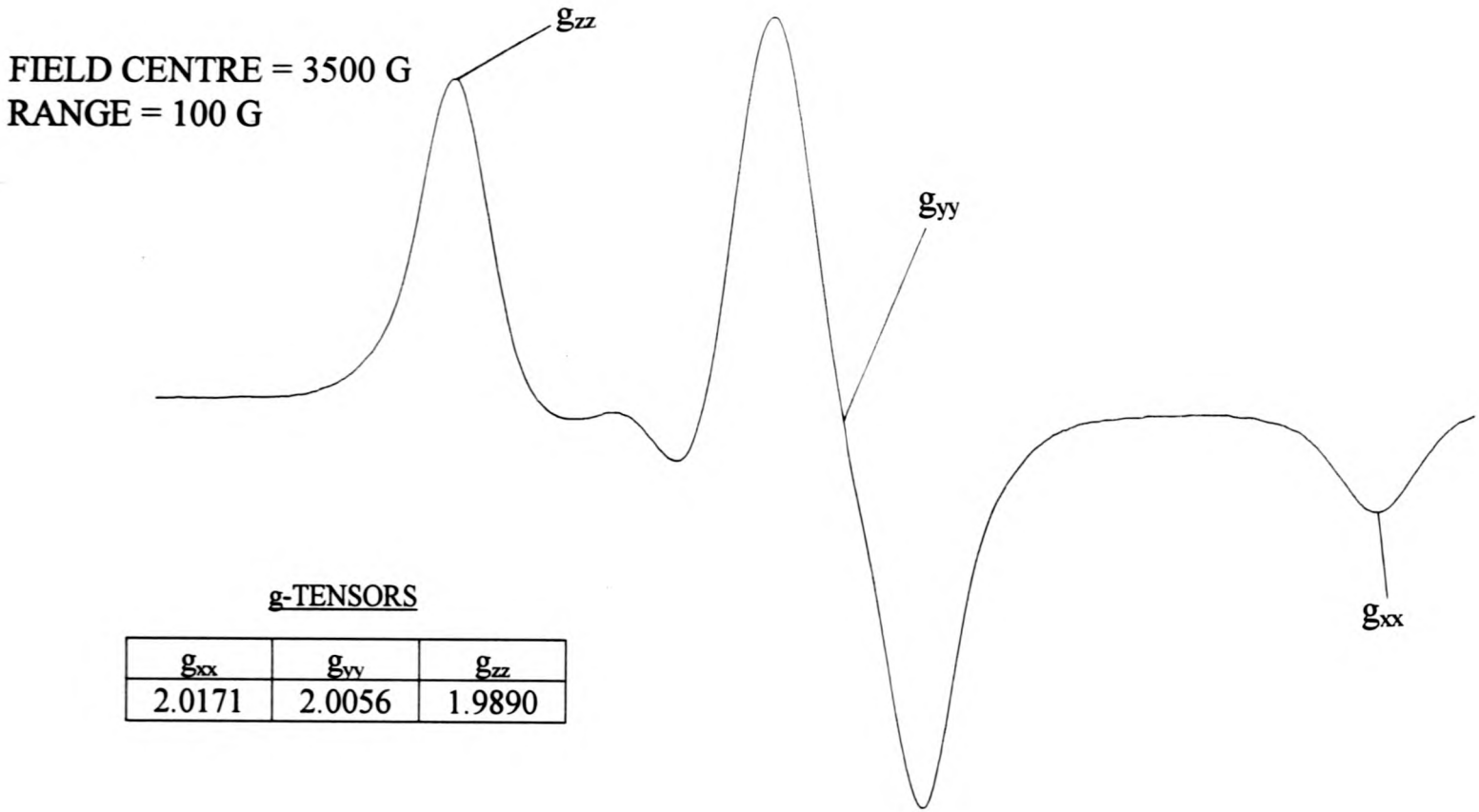

g-TENSORS

g_{xx}	g_{yy}	g_{zz}
2.0171	2.0056	1.9890

FIG.5.7 ESR SPECTRUM OF PYROLYSED (5h/150^{0}C) PNMMO MEASURED AT ROOM TEMPERATURE

Consequently, peroxyl formation seemed unlikely as anaerobic conditions would presumably lead to a lower rate of radical formation. Nitrogen dioxide being paramagnetic and a known product of thermolysis (see section 5.5), seemed a possible attribution to the unknown radical. However, the spectral shape and g-tensors of the unknown radical in pyrolysed PNMMO are substantially different from those observed for NO_2 in various media.[10,11,12,13,14]

A recent paper by Chen *et al.*[15] describes the use of paramagnetic labels to study the motional processes and phase transitions in polyurethanes. The paper although not directly related to the research here, describes the application of the nitroxide probe, 4-hydroxy-2,2',6,6'-tetramethylpiperidine-1-oxyl (TEMPOL). This probe once attached to the polyurethane and examined via ESR displays spectra virtually identical to those obtained for our unknown (fig.5.7). The ESR spectra of the Tempol-labelled polyurethane obtained by Chen *et al.*[15] at various temperatures are shown in fig.5.8. The paper does not give g-tensor values, but the width of Chen's radical measured in gauss (G) and its shape at 120 K are nearly identical to that of the species produced for PNMMO. The g-tensor values for the radical produced from pyrolysis of PNMMO also very closely match those for many other nitroxides[16] and consequently, it is assigned to a nitroxide. To confirm this assignment, a sample of Tempol was dissolved into untreated PNMMO using chloroform as a solvent (10 mg Tempol/g of PNMMO). The spectral shape of the resulting radical was found to differ according to the concentration of the solution added to PNMMO. Thus, the addition of 0.5 cm^3 of chloroform containing 10 mg of Tempol, to 1 g of PNMMO produced a spectral shape that mimics that of Tempol at 260 K while, the addition of less concentrated solutions produced a spectral shape that mimics that at 300 K. Therefore, it appears that the spectra resulting from the increased mobility of the Tempol radical due to the addition of solvent or increased temperature are nearly identical. Consequently, the spectrum of the radical

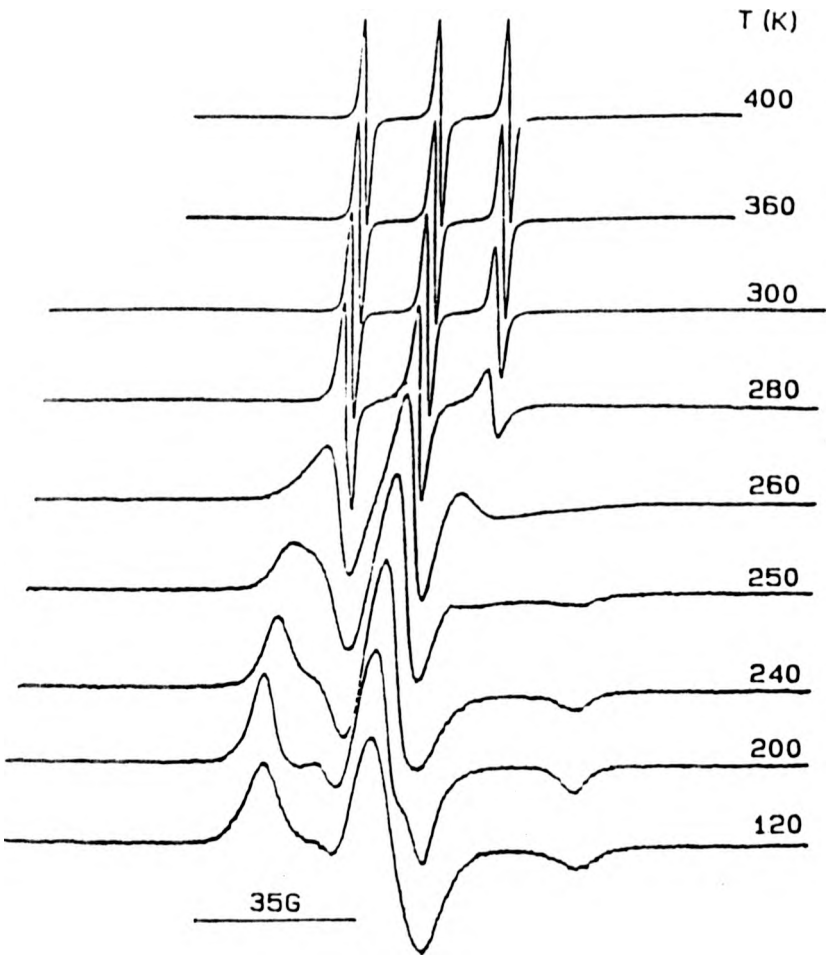

FIG.5.8 ESR SPECTRA OF A TEMPOL-LABELLED POLYURETHANE (120 - 400 K)[15]

attributed to a nitroxide in pyrolysed PNMMO was expected to change in shape similarly. The ESR spectrometer used in our study was not equipped with a variable temperature cavity, but the increased mobility of the radical can be mimicked with addition of solvent to pyrolysed PNMMO. Fig.5.9B shows the ESR spectrum of pyrolysed PNMMO (5 h/150^{0}C) after the addition of 0.5 cm^3 of chloroform, measured at room temperature. As expected, due to the increased mobility of the radical, this spectrum more closely resembles the spectrum obtained for Tempol at increased temperature (260 K). Fig.5.9A shows the ESR spectrum of pyrolysed PNMMO after 15 min pyrolysis at 150^{0}C. Clearly, this spectrum differs from the spectrum obtained at longer pyrolysis time (fig.5.7) in the relative intensity of the peak denoted by the asterisk. The ESR spectra of the Tempol-labelled polyurethane (fig.5.8) show that this same peak appears to increase in intensity on warming from 120 - 200 K and further increases in intensity to become the first line in the spectrum at 260 K. Thus, the relatively greater intensity of this peak in the spectrum of PNMMO after shorter pyrolysis times (fig.5.9A) as compared to longer pyrolysis times (fig.5.7) is attributed to the increase in viscosity and thus reduced mobility of the polymer with increasing pyrolysis times.

Thus, the changes in spectral shape brought about by the differing mobility of the radical produced during pyrolysis of PNMMO exactly mimic those observed for the nitroxide probe Tempol. This re-confirms our assignment of the paramagnetic species in pyrolysed PNMMO to a nitroxide. The first report of a nitroxide radical produced in a nitrate ester polymer during degradation was made in a communication by Yamauchi *et al.*[17] in 1993 during the course of our work. These spectra, produced during the photoirradiation of cellulose nitrate films, are complicated by the presence of alkylperoxyl and alkoxyl radicals not detected in PNMMO; the presence of two different nitroxide radicals further complicates this spectrum. The proposed mechanism of formation of one of these nitroxide

FIG.5.9A ESR SPECTRUM OF PYROLYSED (15 MIN/150^{0}C) PNMMO MEASURED AT ROOM TEMPERATURE

FIG.5.9B ESR SPECTRUM OF PYROLYSED (5 h/150^{0}C) PNMMO DISSOLVED IN CHLOROFORM

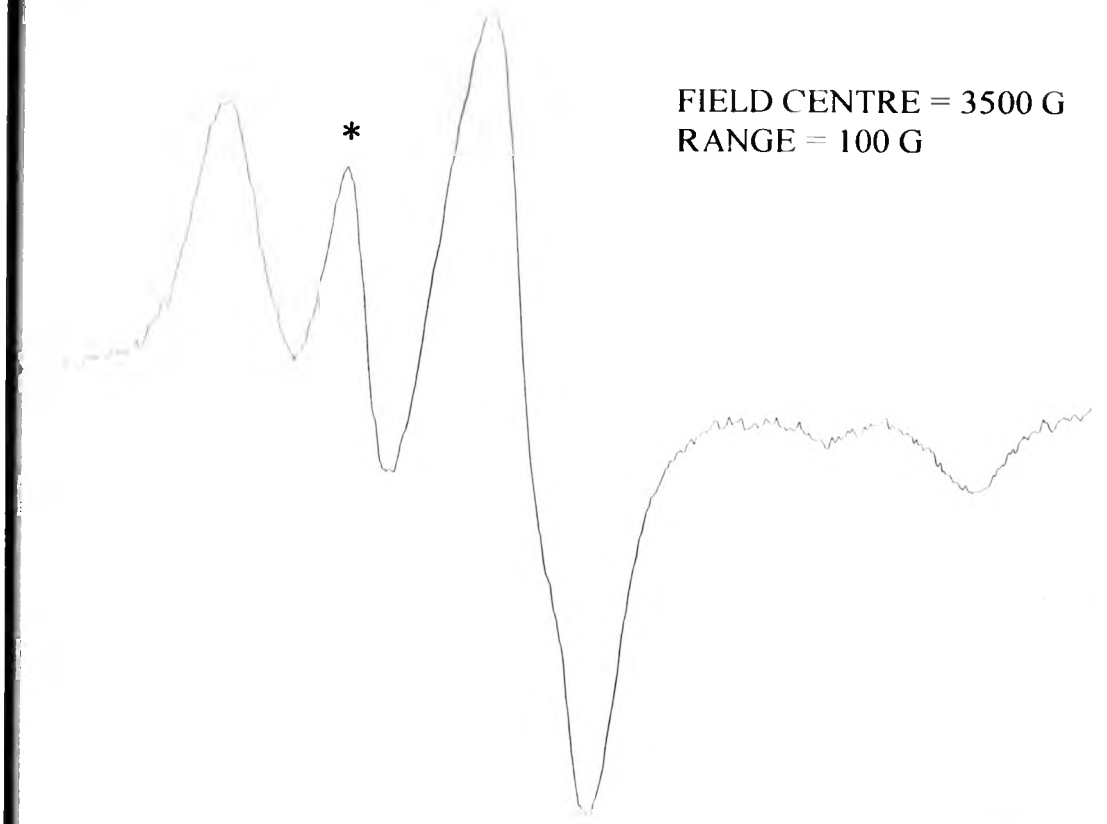

50°C) PNMMO

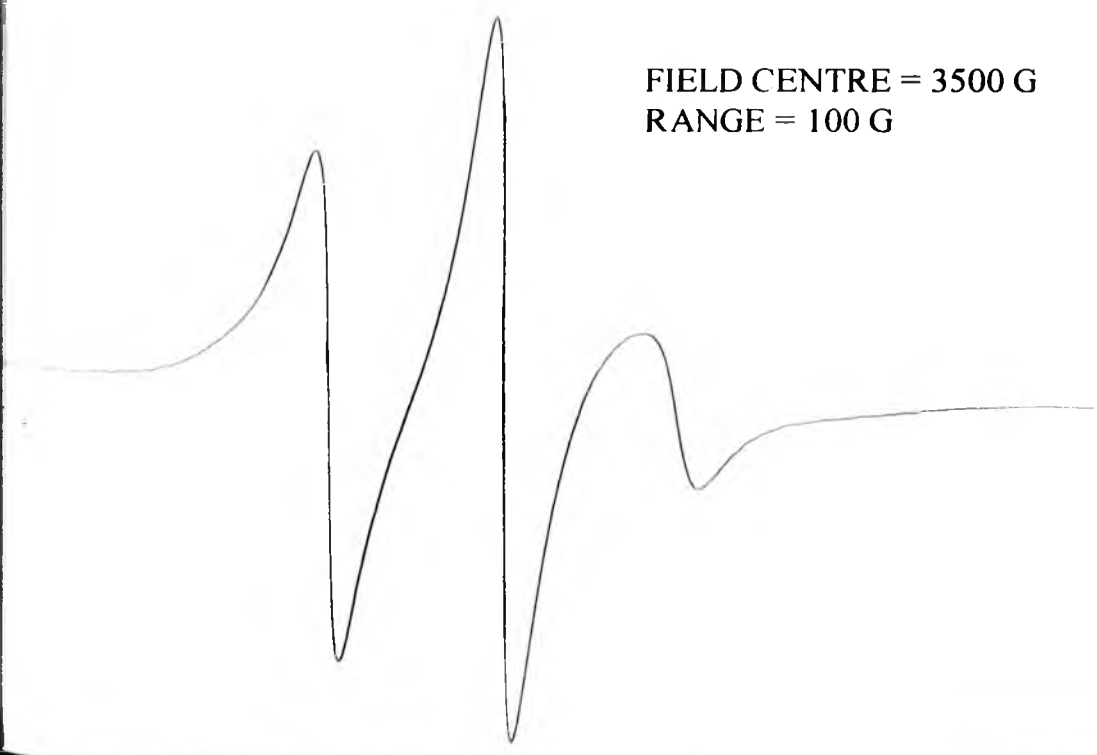

C) PNMMO

radicals during photolysis of cellulose nitrate, shown below, is thought to be the same as that for the nitroxide radical produced during photolysis or pyrolysis of PNMMO. Thus, NO or NO_2 evolved during photo- or thermal degradation of PNMMO may react with alkyl radicals, producing nitroso or nitro compounds which have no unpaired electron. These molecules may then trap other alkyl radicals in a type of spin-trapping process, resulting in nitroxide radicals;

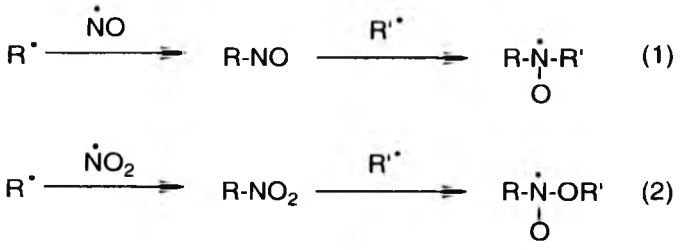

The formation of a nitroalkane during pyrolysis of PNMMO is shown in chapter 6 and thus mechanism (2) appears a likely path to the formation of the nitroxide. Although nitroso species are not detected in the NMR, IR (solution) or ESI (see chapter 6) spectra during pyrolysis of PNMMO, mechanism (1) cannot be completely excluded; nitroso species formed during pyrolysis of PNMMO may not be detected due to their rapid reaction rates with alkyl radicals.

Ranby[18] reports that most polymers show asymmetric singlet-line spectra attributed to ROO• (RO•) radicals, which are generated after the exposure of samples containing R• to air. However exhaustive attempts by us to trap alkylperoxy or alkoxy radicals at either 77 K or at room temperature using spin traps were unsuccessful. We attribute this to the

experimental conditions employed by us, as clearly alkoxy and alkylperoxy radicals are observed in a wide range of polymers, such as PE and PP, during irradiation[18].

5.5 CHARACTERISATION OF THE PYROLYSIS GASES OF PNMMO BY GAS PHASE IR SPECTROSCOPY

Many studies have been conducted on the IR and mass spectrometric analysis of gases evolved from heated samples of various propellant formulations[19,20]. However, all of these studies have employed rapid heating rates in the range 100 - 200^{0}C/s in an attempt to simulate macroscale combustion behaviour. The kinetics of weight loss during programmed heating at 150^{0}C/s have been determined by simultaneous mass and temperature change (SMATCH)/FTIR spectroscopy for PNMMO[21] and other structurally similar propellants[22]. However, in our study of PNMMO, its relatively slow thermal decomposition is monitored at constant temperature in the range 70 - 155^{0}C. At lower temperatures, processes with lower activation energies and greater exothermicity are favoured, while conversely, at higher temperatures, the higher activation energy and more endothermic processes become predominant. However, the products have a shorter time to form and may or may not be the same as products formed at lower temperature. Consequently, descriptions of decomposition processes depend significantly on the temperature and the heating rate.

Experiments were performed according to the method in section 2.1.1.3. PNMMO was heated at temperatures in the range 70 - 155^{0}C using an oil bath and the pyrolysis gases were collected in a IR gas cell and characterised by IR spectroscopy. Preliminary experiments to separate and quantify the relative amounts of pyrolysis gases were performed using gas chromatography. However the chromatograms obtained were unreproducible and this was most likely attributed to the experimental procedure employed by us (see section

2.1.6). GC/MS experiments were also performed as shown in section 2.1.6. PNMMO samples were heated at 155^{0}C in an oil bath and the gases were analysed via GC/MS using an MS80 mass spectrometer. We were not successful in separating the gases, but individual gases could be identified by their ion peaks in the mass spectrum. Thus the relative amounts of individual gases are not accurately known. However, the relative intensities of the peaks in the IR spectrum give an approximate idea of the relative amounts of pyrolysis gases present.

Fig.5.10A shows the gas phase IR spectrum of the pyrolysis gases obtained by heating PNMMO for 15 min at 155^{0}C. The peak assignments shown on the IR spectrum are based on high purity standards[23,24,25,26]. IR-inactive species H_2, N_2 and O_2 may also be present and indeed, in separate experiments run at similar pyrolysis temperatures, significant quantities of both N_2 and O_2 were detected in the electron impact (EI) mass spectrum of the pyrolysis gases.

If the sealed IR cell is left at room temperature for approximately 30 min after collecting the pyrolysis gases, a considerable amount of white solid is visible on the inside of the cell. The cell was re-evacuated and warmed with a hair drier. The white solid sublimed and the IR spectrum of the resulting gas was recorded (see fig.5.10B). The peaks in this spectrum exactly match those expected for formaldehyde. The fundamental frequencies υ_1, υ_2 and υ_3, and the 1st overtone of the υ_2 frequency are clearly visible in this spectrum and in fig.5.10A. Presumably, the original white solid is paraformaldehyde.

The relative intensities of the peaks in the gas phase IR spectrum of pyrolysed PNMMO, and thus the gas composition, appear to vary only in the relative amounts of nitrogen-containing species as compared to formaldehyde present. The peaks due to formaldehyde are similarly or less intense than the peaks due to the nitrogen-containing species when the pyrolysis temperature is less than 120^{0}C. As the pyrolysis temperature is

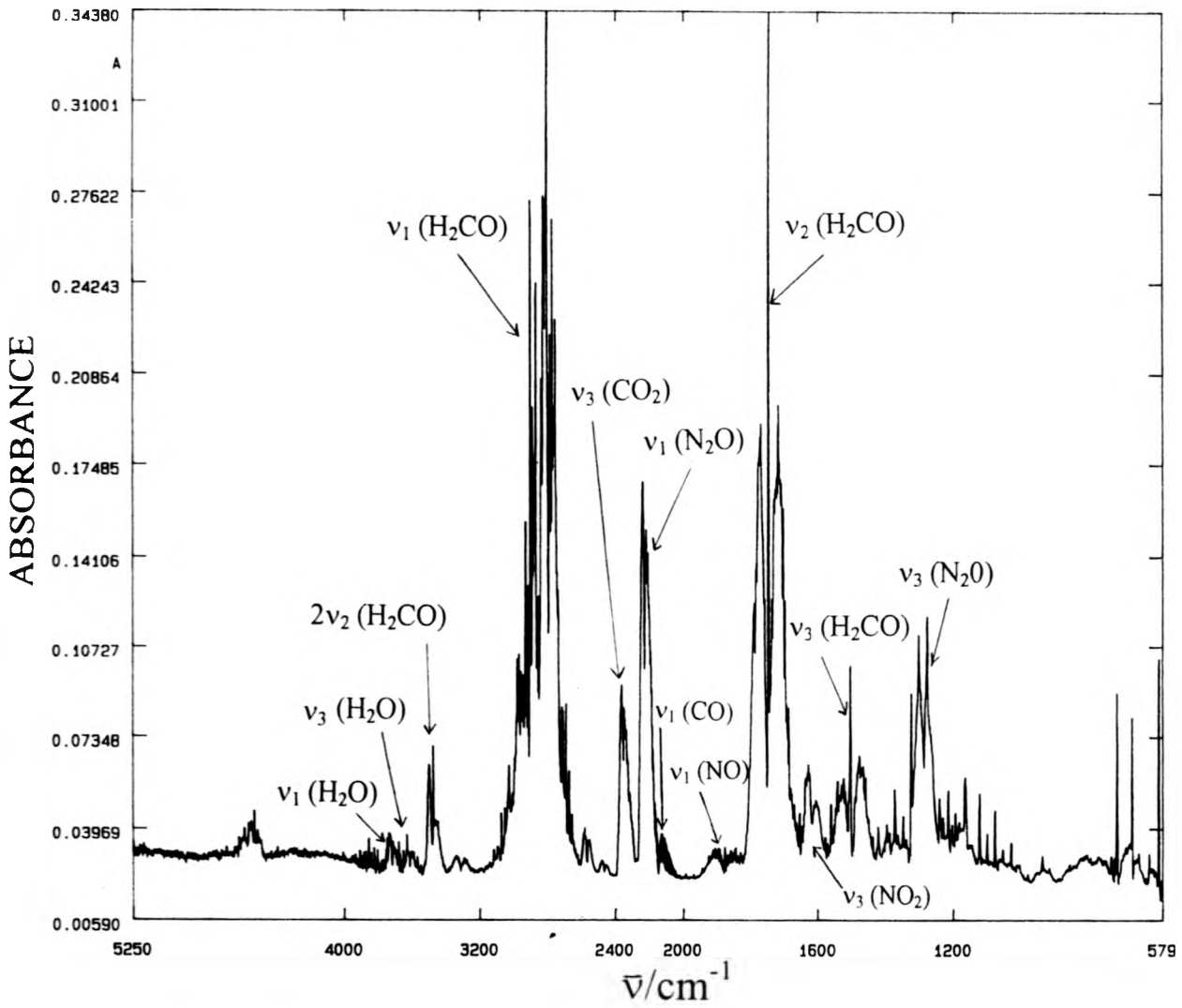
0.34380
A
0.31001
0.27622
0.24243
0.20864
0.17485
0.14106
0.10727
0.07348
0.03969
0.00590
ABSORBANCE
5250
4000
3200
2400
2000
1600
1200
579
$\bar{\nu}$/cm^{-1}
ν_1 (H_2CO)
ν_2 (H_2CO)
ν_3 (CO_2)
ν_1 (N_2O)
$2\nu_2$ (H_2CO)
ν_3 (N_20)
ν_3 (H_2CO)
ν_3 (H_2O)
ν_1 (CO)
ν_1 (NO)
ν_1 (H_2O)
ν_3 (NO_2)

FIG.5.10A GAS PHASE IR SPECTRUM OF THE GASES EVOLVED DURING THE PYROLYSIS OF PNMMO AT 155^{0}C

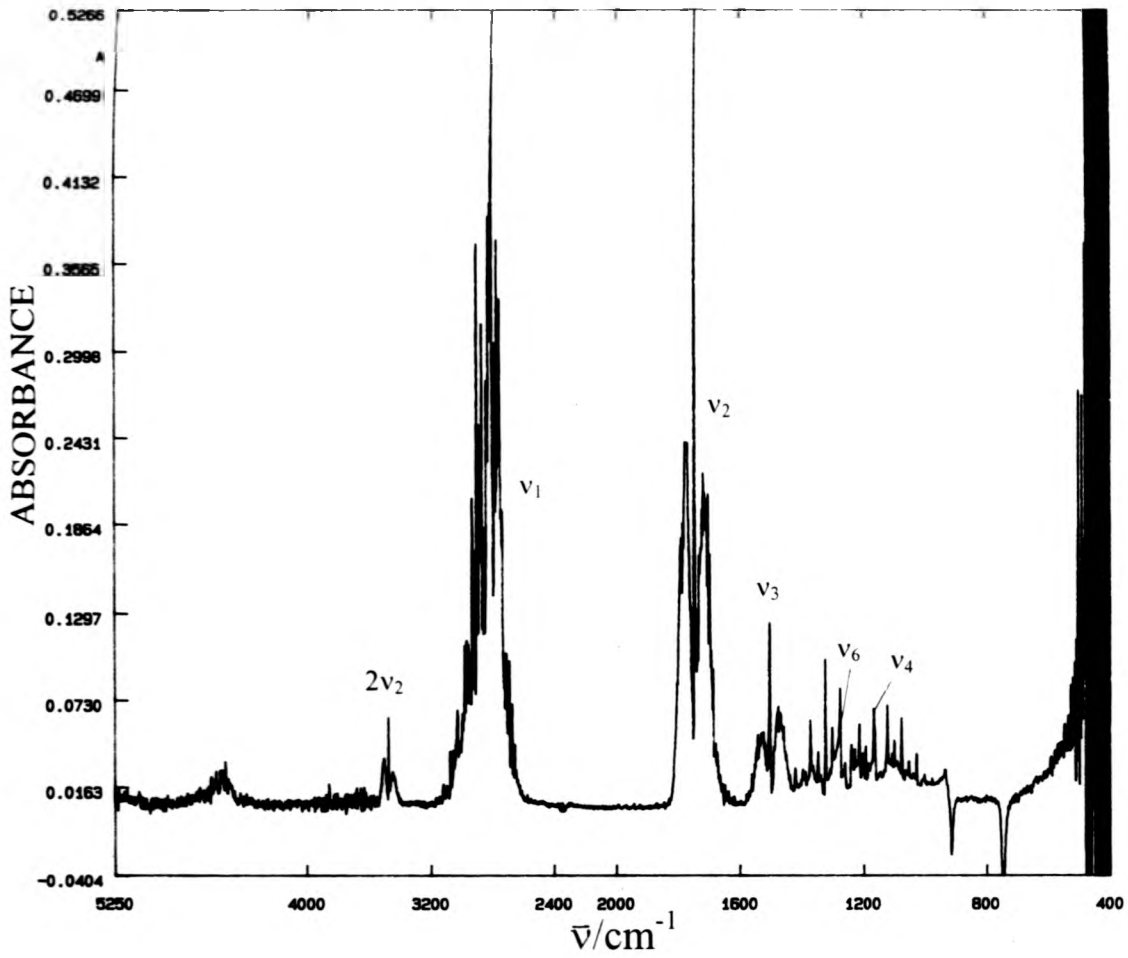

FIG.5.10B GAS PHASE IR SPECTRUM OF FORMALDEHYDE

increased, the formaldehyde peaks gradually become increasingly more intense as compared to the nitrogen-containing species. Pyrolysis temperatures in excess of 140^0C produce gradually increasing concentrations of nitrogen-containing species although the formaldehyde peaks remain more intense (see fig.5.10A). The peaks due to NO_2(g) are only visible in the spectra recorded above 150^0C. NO_2(g) gives strong bands[27] in the IR but, even with pyrolysis temperatures of 155^0C, the intensity of the peaks due to NO_2(g) is very low. This seems curious if we consider that the first step in the thermal decomposition of nitrate esters is generally thought to be the reversible homolysis of the O-NO_2 group[21,28].

$$RONO_2 \rightleftharpoons RO\bullet + NO_2\bullet \quad (3)$$

The presence of NO_2(g) was confirmed by ion peaks at 46, 30 and 16 mus in the EI mass spectrum of the pyrolysis gases of PNMMO although, as for the gas phase IR spectrum, these peaks were relatively weak. Various explanations for the relatively low concentration of NO_2(g) are possible. The first is a result of the effect shown in section 5.2, i.e. NO_2(g) has a relatively greater chance of reacting with the polymer during pyrolysis of thick films as compared to thin films of PNMMO. Except when reaction (3) occurs on the surface, the NO_2(g) must migrate through the polymer matrix. The absorption at 1550 cm^{-1} in the solution IR spectra of pyrolysed PNMMO, due to the reaction of PNMMO with NO_x(g) and later identified as a nitro species (see chapter 6), is relatively more intense for thicker films as compared to thinner films of PNMMO. The intensity of the 1550 cm^{-1} absorption is approximately the same for samples of PNMMO pyrolysed at reduced pressure and PNMMO samples pyrolysed for similar amounts of time and at similar temperatures in air. Thus, because of the high reactivity of NO_2(g) at elevated temperatures, it is not

surprising that much of the nitrogen appears as $N_2O(g)$ and $NO(g)$. Pyrolysis temperatures in excess of 140^0C generate high concentrations of $NO_x(g)$. Consequently, the lower viscosity of the polymer at higher temperature and thus the higher rate of diffusion of $NO_x(g)$ through the polymer matrix results in a greater concentration of nitrogen-containing species being detected. $N_2O(g)$ has been detected during the rapid heating of various nitrate ester polymers[29] but no mechanism for its formation appears to be given. We propose the following mechanisms;

$$2NO_2 \rightleftharpoons N_2O_4 \qquad (4)$$

$$2N_2O_4 \rightarrow 2N_2O + 3\,O_2 \qquad (5)$$

or

$$2\,HNO \rightarrow N_2O + H_2O \qquad (6)^{30}$$

It may be expected that reduced pressure will affect the relative concentration of nitro species produced (1550 cm^{-1}) during pyrolysis of PNMMO. However, the relatively high stability of the nitrogen dioxide radical coupled with the relatively long diffusion times through the viscous polymer matrix suggest that very little difference is actually expected.

Reactions of $NO_2(g)$ with other pyrolysis gases could also account for discrepancies in the relative concentrations of gases observed as it is clear that the increased diffusion rate may compete with an increased reaction rate due to the elevated temperature. These reactions are the subject of much controversy in the field of propellant combustion

chemistry. Various mechanisms have been proposed for the reactions of the pyrolysis gases, which are thought to occur both under high and low pressure depending on the reactivity of the gases produced. In this respect, various energetic polymers have been grouped according to the extent of condensed phase reaction that occurs before gas products are detected[29,31]. PNMMO is grouped at the top of this list of some 30 polymers and it is reported that its decomposition is dominated by intrinsic condensed-phase chemistry irrespective of the pressure in the range 1-1000 psi. Irrespective of whether the pyrolysis gases react in the condensed phase, some reaction may be expected to occur when the IR gas cell is warmed to room temperature. The reactions below have been suggested to account for the low concentration of $NO_2(g)$ in the pyrolysis gases of HMX, RDX[32] and various nitrate ester polymers[21] although, it is difficult to access the extent to which these reactions occur for PNMMO.

$$2NO_2 \rightleftharpoons 2NO + O_2 \qquad (7)$$

$$7\,NO_2 + 5\,CH_2O \longrightarrow 7\,NO + 2\,CO_2 + 3\,CO + 5\,H_2O \qquad (8)$$

Nitro-nitrite isomerisation has long been known to take place on an aliphatic carbon atom[33]. Isomerisation of this kind has been cited as evidence for the low concentrations of $NO_2(g)$ and larger quantities of NO(g) evolved from aliphatic nitro-substituted propellants[34]. Isomerisation of this type is not expected for nitrate esters due to the low stability of the O-O bond, but it will occur for the newly formed nitro species absorbing at 1550 cm^{-1} in the solution IR spectra of pyrolysed PNMMO. Thus, the small amounts of NO(g) in the IR spectrum (fig.5.10A) may result from the thermal decomposition of this nitro species.

It is clear from the structure of PNMMO (see below), that formaldehyde may result from the decomposition of the nitrate ester side chains or the main chain in PNMMO. Loss of $NO_2\bullet$ from the side chain results in the formation of a highly reactive alkoxy radical which may eliminate formaldehyde to produce the more stable tertiary carbon-centred radical. Similarly, if chain scission occurs at the ether linkages along the PNMMO backbone (see below), an alkoxy radical is generated which may undergo the same elimination process.

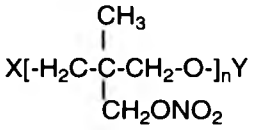

STRUCTURE OF PNMMO

SMATCH/FTIR data for PNMMO[21] and polyvinyl nitrate (PVN)[21], which possesses no primary alkyl nitrate sites, shows that formaldehyde is still detected in the combustion products of PVN although, to a lesser extent than for PNMMO. Similarly 3-azidomethyl-3-methyloxetane (AMMO), which differs from PNMMO only in that it contains an azide side-group as opposed to a nitrate ester side group, also generates significant amounts of formaldehyde during rapid heating[21] (150^0C/s). The fact that formaldehyde forms at all from PVN or AMMO indicates that formaldehyde is not solely formed by these primary alkyl nitrate sites. The SEC data (section 5.1) for pyrolysed PNMMO shows that a considerable amount of chain scission is occurring during pyrolysis, but it is impossible to calculate the relative amounts of formaldehyde produced by the main chain and the side chains.

The gases generated during the pyrolysis of PPO were collected and analysed in the same manner as for PNMMO. Pyrolysis temperatures in the range 100 - 170^0C produced

large quantities of acetaldehyde and much lower concentrations of H_2O and CO_2. This is consistent with the thermal degradation mechanism proposed for PPO by us and is discussed in greater detail in section 8.3.1.

5.6 CHARACTERISATION OF PYROLYSED PNMMO BY ESI

PNMMO (4.0 g) was placed in a glass vial (20.0 cm^3) and pyrolysed in the oven at 130^0C for up to 60 h. Samples of PNMMO were removed over various periods of time and analysed using ESI. Fig.5.11 shows the ESI spectra of pyrolysed (48 h/130 h) and untreated PNMMO run at a cv of 50. Clearly, the thermal degradation of PNMMO has resulted in a far more complex mixture of low-mass oligomers; there are considerably more peaks in the spectrum of degraded PNMMO as compared to untreated PNMMO, thus making the assignment of individual species very difficult. However, the spectra clearly show that the most intense ion peaks in the spectrum of degraded PNMMO are visible at 607.0 + 147n mus. This series of ions was previously assigned (section 3.4.1) to the H^+ adducts of the hydroxy-terminated linear oligomers. Other peaks in the spectrum are similarly attributable to the undegraded linear oligomers. The spectrum of untreated PNMMO shows that the most intense ion peaks are attributed to the cyclic oligomers with masses 606.0 + 147n. Thus, it appears that the thermal degradation of PNMMO has resulted in an increased concentration of low-mass linear oligomers as compared to cyclic oligomers. The greater sensitivity of the latter can most likely be attributed to the strain in the cyclic oligomer ring which confers a lower thermal stability as compared to its linear homologue. The results of SEC have already shown that thermolysis gives rise to a considerable amount of low-mass oligomeric species via chain scission processes. Assuming that cyclisation reactions occur only to a very small degree during thermolysis, if at all, then the increased concentration of

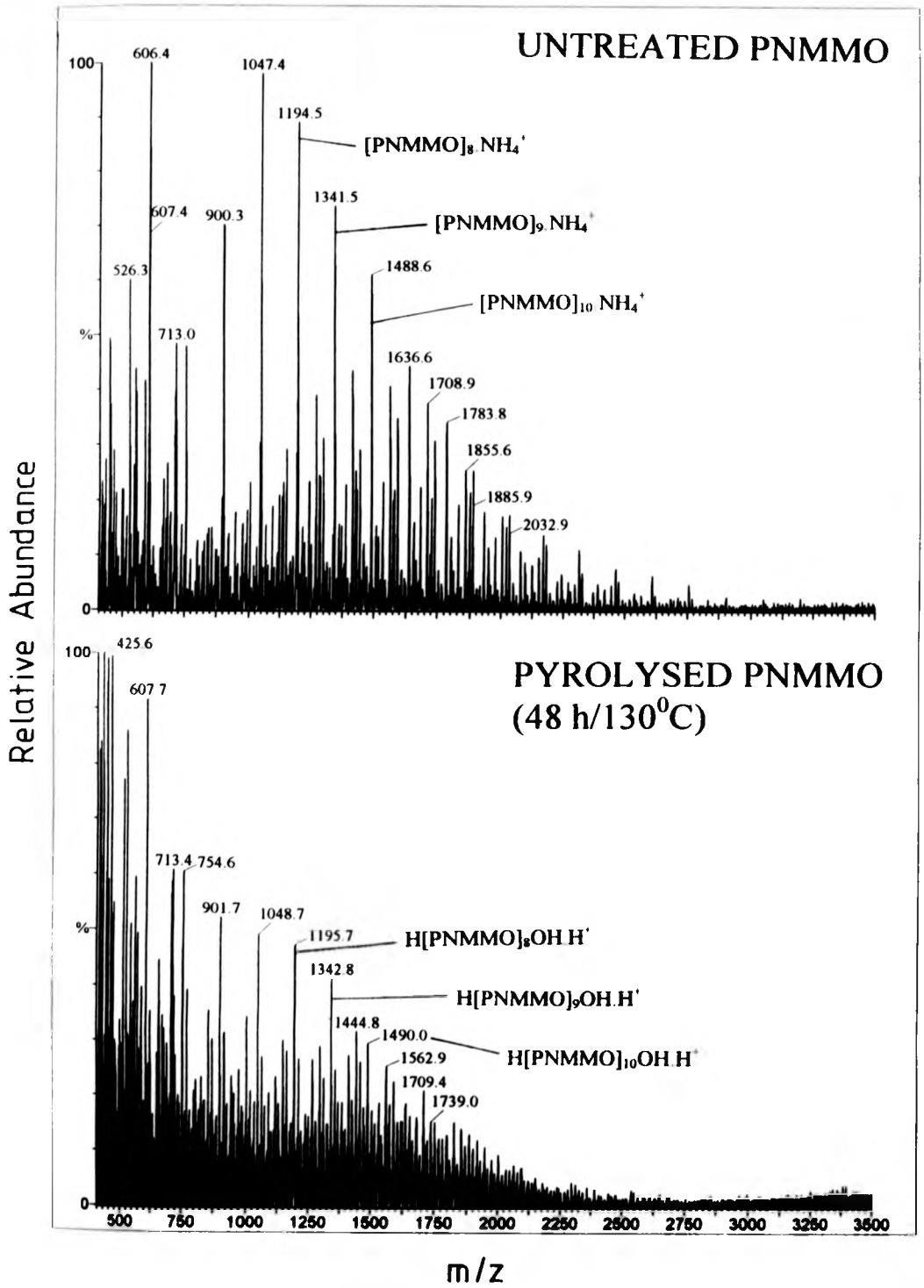

FIG.5.11 ESI SPECTRA OF UNTREATED AND PYROLYSED PNMMO

low-mass linear oligomers (due to chain scission) as compared to cyclic oligomers is to be expected. Increasing pyrolysis times produce increasingly more complex ESI spectra and the polymer distribution as observed by ESI gradually tends towards lower molecular weight. This is presumably not only a consequence of the occurrence of chain scission processes during thermolysis, but also the higher solubility of the lower mass species in the THF/MeOH solvent system (see section 3.5).

Clearly, the assignment of degraded PNMMO species from these ESI spectra (fig.5.11) is impossible due to the complexity of the mixture of ions present. Column chromatography was therefore employed to separate the complex mixture of degradation products, the results of which are given in chapter 6.

CHAPTER 5 REFERENCES

1 Delprat, P., Gardette, J-L., *Polymer*, 1993, **34**, 933.

2 Barr-Kumarakulasinghe, S.A., *Polymer*, 1994, **35**, 995.

3 Bower, D.I., Maddams, W.F., The Vibrational Spectroscopy of Polymers, Cambridge University Press, 1989, Ch.5.

4 Silverstein, R., Bassler, G., Spectrometric Identification of Organic Compounds, 4th ed., John Wiley & Sons, Chichester England, 1991, Ch.3.

5 Pouchert, C.J., The Aldrich Library of Infrared Spectra, Aldrich Chem. Co., 1970.

6 Griffiths, P.J., Hughes, J.H., Park, G.S., *Eur. Polym. J.* 1993, **29**, 437.

7 Thompson, H.W., Torkington, P., *J. Chem. Soc.* 1945, 640.

8 Bellamy, L.J., The Infrared Spectra of Complex Molecules, Vol.1, 3rd ed., Chapman and Hall, 1975, Ch.17.

9 Han, S., Kim, C., Kwon, D., *Polymer Degradation and Stability*, 1995, **47**, 203.

10 Bielski, B.H.J., Gebicki, J.M., Atlas of ESR Spectra, Academic Press, 1967.

11 Alger, R.S., Electron Paramagnetic Resonance, Interscience, 1968.

12 Myers, G.H., Easley, W.C., Zilles, B.A., *J. Chem. Phys.* 1970, **53**, 1181.

13 Poole, C.P., Electron Spin Resonance, Interscience, 1967.

14 Adrian, F.J., *J. Chem. Phys.* 1962, **36**, 1692.

15 Chen, W-P., Kenney, D.J., Frisch, K.C., Wong, S-W., Moore, R., *J. Polym. Sci.: Part B: Polym. Phys.* 1991, **29**, 1513.

16 Berliner, L.J., Spin Labelling, Academic Press, 1976, Ch.3, 6.

17 Yamauchi, J., Ando, H., Yamaoka A., *Makromol. Chem., Rapid Commun.* 1993, **14**, 13.

18 Ranby, B., Rabek, J.F., ESR Spectroscopy in Polymer Research, Springer-Verlag Berlin Heidelberg, New York, 1977, Ch.7.

19 Kinoshita, R., Teramato, Y., Yoshida, H., *Thermochim. Acta*, 1993, **222**, 45.

20 Oyumi, Y., Brill, T.B., *Combustion and Flame*, 1985, **62**, 233.

21 Chen, J.K., Brill, T.B., *Combustion and Flame*, 1991, **85**, 479.

22 Chen, J.K., Brill, T.B., *Combustion and Flame*, 1991, **87**, 157.

23 Pierson, R.H., Fletcher, A.N., Gantz, E.C., *J. Anal. Chem.* 1956, **28**, 1218.

24 Nightingale, R.E., Downie, A.R., Rotenberg, D.L., Crawford, B., Ogg, R.A., *J. Phys. Chem.* 1954, **58**, 1047.

25 Brechignac, C., Johns, J.W.C., McKellar, A.R.W., Wong, M., *J. Mol. Spectroscopy*, 1982, **96**, 353.

26 Fateley, W.G., Bent, H.A., Crawford, B., *J. Chem. Phys.* 1959, **31**, 204.

27 Banwell, C.N., Fundamentals of Molecular Spectroscopy, 3rd ed., McGraw-Hill, 1983, Ch.3.

28 Chen, J.K., Brill, T.B., *Thermochim. Acta*, 1991, **181**, 71.

29 Oyumi, Y., Brill, T.B., *Combustion and Flame*, 1986, **66**, 9.

30 Chen, J.K., Brill, T.B., *Combustion and Flame*, 1993, **94**, 70.

31 Oyumi, Y., Brill, T.B., *Combustion and Flame*, 1987, **68**, 209.

32 Oyumi, Y., Brill, T.B., *Combustion and Flame*, 1985, **62**, 213.

33 Gray, P., Rathbone, P., Williams, A., *J. Chem. Soc.* 1960, 3932.

34 Brill, T.B., James, K.J., *Chem. Rev.* 1993, **93**, 2667.

CHAPTER 6

SPECTRAL ANALYSIS OF PYROLYSED PNMMO AFTER CHROMATOGRAPHY

The results of chapter 5 clearly demonstrate that pyrolysed PNMMO comprises a complex mixture of degradation products. Column chromatography was therefore employed to separate this mixture, with the aim of obtaining either pure or at least enriched samples of individual thermal degradation products for characterisation. In particular we hoped to separate the two main thermal degradation products observed by IR, at 1729 cm^{-1} (formate ester) and 1550 cm^{-1} (nitro-alkane), thus aiding the characterisation of this species, tentatively assigned to a nitro-species, by ESI and NMR.

PNMMO (10.0 g) was placed in a glass vial (25.0 cm^3) and pyrolysed in the oven at 130^0C for 25 h. The pyrolysate (5.0 g) was dissolved in toluene to give a saturated solution, and column chromatography was carried out as shown in section 2.2.2. This eluting solution was collected as 15 cm^3 fractions. Approximately 250 fractions were collected over a 12 h period.

6.1 INFRARED CHARACTERISATION OF THE FRACTIONS OBTAINED FROM COLUMN CHROMATOGRAPHY OF PYROLYSED PNMMO

Section 5.2 shows that new absorptions are observed at 1550 and 1729 cm^{-1} in the solution IR spectra of PNMMO following pyrolysis. Other new absorptions, thought to be associated with the formate ester species at 1729 cm^{-1}, are also visible in the IR difference spectra.

The first 20 fractions obtained from the column chromatography of pyrolysed PNMMO contained solely solvent. The IR spectra of the subsequent 9 fractions showed absorptions characteristic of undegraded cyclic oligomer (see section 4.3). This was further substantiated by the ESI spectra of these fractions which show only a single peak due to the cyclic tetramer ion. The IR spectra of fractions 30 - 41 show a new peak of gradually increasing intensity at 1550 cm^{-1}. This peak, tentatively assigned to a nitro-species, gradually decreases in intensity in fractions 42 - 52. Fig.6.1A shows the solution ($CDCl_3$) IR spectrum of fraction 41. Only one new peak is visible in this spectrum at 1550 cm^{-1}, and thus it appears that this sample contains solely the nitro-species and possibly some undegraded oligomer. Clearly, the isolation of this nitro-species confirms, as expected, that it can exist independently of the carbonyl species absorbing at 1729 cm^{-1}.

The IR spectra of fractions 53 - 150 show absorptions for both the 1550 and 1729 cm^{-1} species. The relative intensities of these peaks vary in each spectrum in a non-uniform manner. Fig.6.1B shows the IR spectrum of fraction 100. The ratio of the intensities of the 1729 to 1550 cm^{-1} absorptions is the greatest in this spectrum; the peak at 1729 cm^{-1} is six times as intense as the absorption at 1550 cm^{-1}. A comparison of the IR spectra of fractions 40 (fig.6.1A) and 100 (fig.6.1B) show that the peak due to the carbonyl species at 1729 cm^{-1} is associated with the absorption around 1170 cm^{-1} which is visible in fig.6.1B but not 6.1A. This confirms the assignment of the carbonyl group to a formate ester (see section 5.2). The IR spectra of fractions 151 - 220 also show absorptions for both the 1729 and 1550 cm^{-1} species and thus it appears impossible to obtain a sample containing solely the formate ester. Unlike the same absorptions for fractions 53 - 150, the ratio of the intensities of the 1729 and 1550 cm^{-1} absorptions appears to vary in a uniform manner for fractions 151 - 220; the intensity of the 1729 cm^{-1} absorption gradually decreases relative to the 1550 cm^{-1}

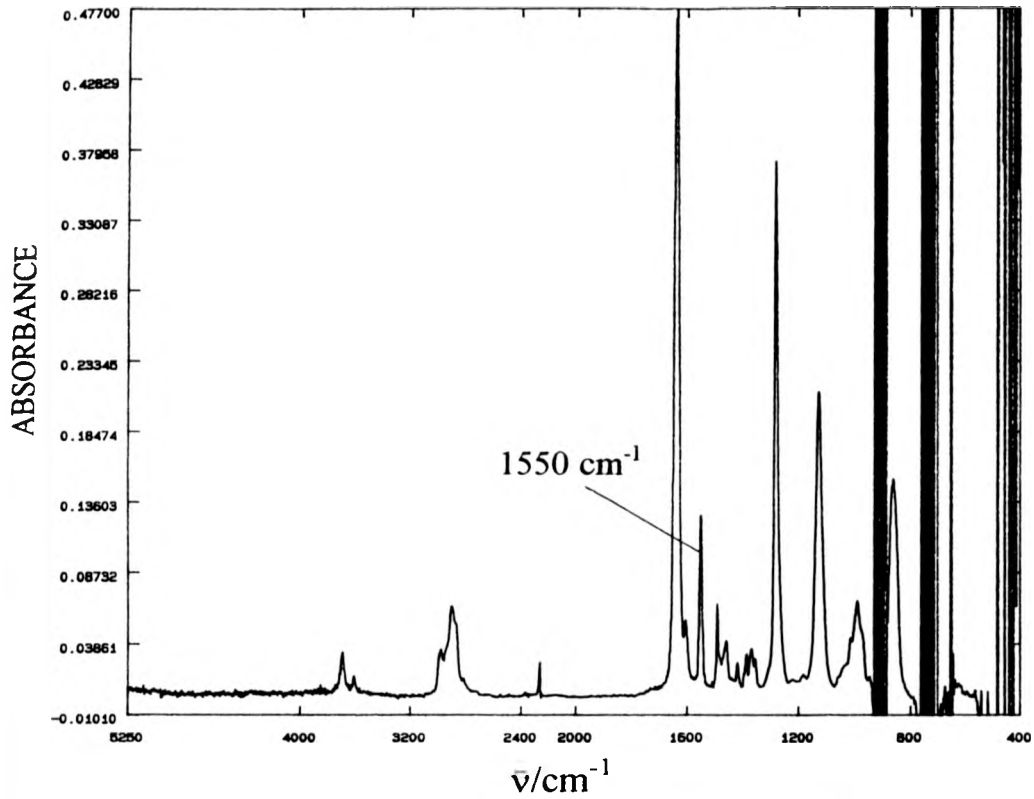
ABSORBANCE
0.47700
0.42829
0.37958
0.33087
0.28216
0.23345
0.18474
0.13603
0.08732
0.03861
-0.01010
5250
4000
3200
2400
2000
1600
1200
800
400
1550 cm-1
ν̄/cm-1

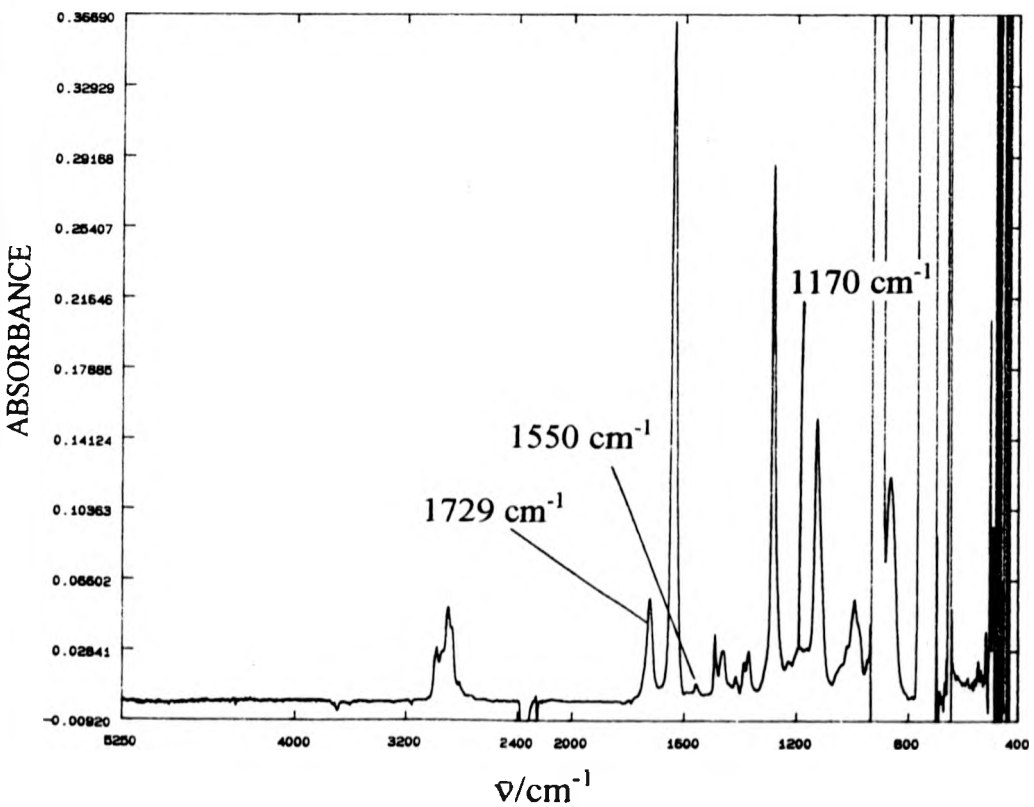
ABSORBANCE
0.36690
0.32929
0.29168
0.25407
0.21646
0.17885
0.14124
0.10363
0.06602
0.02841
-0.00920
5250
4000
3200
2400
2000
1600
1200
800
400
1170 cm-1
1550 cm-1
1729 cm-1
ν̄/cm-1

FIG.6.1A SOLUTION ($CDCl_3$) IR SPECTRUM OF FRACTION 41 OBTAINED DURING THE COLUMN CHROMATOGRAPHY OF PYROLYSED PNMMO

FIG.6.1B SOLUTION ($CDCl_3$) IR SPECTRUM OF FRACTION 100 OBTAINED DURING THE COLUMN CHROMATOGRAPHY OF PYROLYSED PNMMO

absorption with increasing elution order. Explanation of this variation in the relative concentrations of the species absorbing at 1729 and 1550 cm^{-1} in the IR spectra of the eluted fractions is clarified by the SEC and CHN analysis of the fractions, as described and discussed in section 6.2.

6.2 SEC CHARACTERISATION OF THE FRACTIONS OBTAINED FROM COLUMN CHROMATOGRAPHY OF PYROLYSED PNMMO

As with the fractions obtained from the column chromatography of untreated PNMMO, the higher mass linear oligomers in degraded PNMMO are eluted last. Fig.6.2 shows the SEC chromatograms of fractions 154, 160, 169, 182 and 193 obtained from the column chromatography of pyrolysed PNMMO. The chromatograms were run using the high molecular weight column system (see section 2.1.9.2) and equivalent masses of oligomer. Section 5.1 shows that the pyrolysis of PNMMO results in a much wider polymer distribution as observed by SEC. Both fig.6.2 and the molecular weight averages obtained for fractions 154, 169 and 193 (table 6.1) clearly illustrate that a good degree of separation of this polymer distribution is possible by column chromatography.

TABLE 6.1

M_n AND M_W VALUES OBTAINED BY SEC FOR FRACTIONS FROM COLUMN CHROMATOGRAPHY OF PYROLYSED PNMMO

FRACTION	M_n	M_W
154	1000	3400
169	3000	13000
193	8300	28000

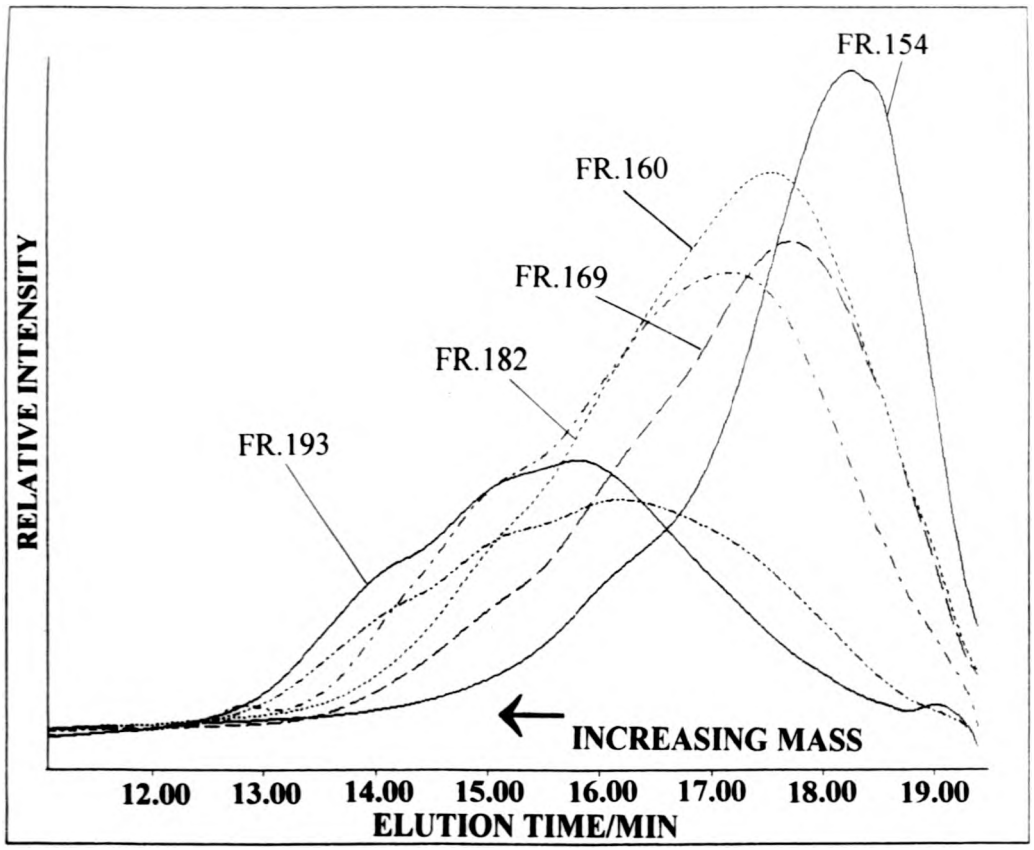

FIG.6.2 SEC CHROMATOGRAMS OF REPRESENTATIVE FRACTIONS OBTAINED DURING THE COLUMN CHROMATOGRAPHY OF PYROLYSED (25 h/130^{0}C) PNMMO

Conversely, the fractions containing the higher mass linear oligomers obtained from the column chromatography of untreated PNMMO (section 4.1) show only very small differences in the M_n and M_w values due to the much narrower polymer distribution.

As shown in section 6.1, the ratio of the intensities of the 1550 and 1729 cm^{-1} absorptions in the IR for fractions 150 - 220 show a trend towards a greater concentration of the species due to the absorption at 1550 cm^{-1} (tentatively assigned to a nitro species) as compared to the species absorbing at 1729 cm^{-1} (formate ester) with increasing elution time. Clearly, SEC analysis of these fractions shows that they contain the linear oligomers of PNMMO, eluted in order of increasing molecular weight. The results of chapter 5 have shown that the production of the formate ester species during thermolysis most likely occurs via scission of the C-C bond in the main chain of PNMMO. Thus on average, the fractions containing relatively lower molecular weight oligomer are expected to contain a higher concentration of carbonyl species as compared to the higher molecular weight fractions. The results in section 6.3 also show that the formation of the species absorbing at 1550 cm^{-1} in the IR does not result in chain scission and therefore its concentration would not be expected to vary with the molecular weight of the oligomer. Consequently, the intensity of the absorption at 1550 cm^{-1} relative to the carbonyl absorption (1729 cm^{-1}) is expected to increase with increasing elution time, as we observe. CHN analysis of the fractions further substantiates this and the results are shown in table 6.2.

TABLE 6.2

CHN ANALYSIS OF UNTREATED PNMMO AND PYROLYSED PNMMO BEFORE AND AFTER COLUMN CHROMATOGRAPHY

SAMPLE	%C	%H	%N	%O[a]
UNTREATED (FOUND)	41.02	6.18	9.20	43.60
UNTREATED (EXPECTED)	40.82	6.17	9.52	43.50
PYROLYSATE (BEFORE CHROMATOGRAPHY)	42.53	6.34	8.53	42.60
FRACTION 154	42.10	6.30	8.51	43.09
FRACTION 160	42.15	6.30	8.55	43.00
FRACTION 169	42.26	6.31	8.63	42.80
FRACTION 175	42.42	6.38	8.57	42.63
FRACTION 180	42.35	6.34	8.64	42.67
FRACTION 187	42.46	6.35	8.61	42.58

[a] Figure obtained by subtraction

The % of C, H and O in untreated PNMMO shows good agreement with expected values (overall % error = 0.5 %). The % of N is however lower than expected (overall % error = 3.5 %) which may result from the influence of the different end groups present. Calculations were based on the % of C,H,N and O in the monomer unit of PNMMO and did not take account of end groups, as the relative amounts of each end group present are impossible to calculate.

As the elution time increases, the % of O in the fractions tends to decrease. This can again be explained by the higher concentration of formate ester present in the lower molecular weight species. Many competing reactions make it difficult to see any particular

trends in the % of C, H and N, although the % of N in the pyrolysate before chromatography and in all the fractions is lower than in untreated polymer, presumably due to the loss of NO_x.

Fig.6.3 shows the SEC chromatograms of fractions 35, 43, 46, 50 and 58 obtained from the column chromatography of pyrolysed PNMMO. Both the IR and ESI spectra of fraction 35 (section 6.1) have shown that this fraction and fractions 21 - 34 contain predominantly the undegraded cyclic tetramer. This is confirmed by the SEC chromatogram for fraction 35 which shows a single peak with a M_n value identical to that for the cyclic tetramer obtained by column chromatography of untreated PNMMO (section 5.1). Thus, as expected, some cyclic tetramer still remains undegraded.

The mass of oligomer recovered from each of the first 150 fractions obtained from column chromatography was usually approximately 5 - 10 mg. Consequently, characterisation of individual fractions using ESI, SEC, NMR and IR was not always feasible, as complete sample recovery was sometimes impossible, particularly for SEC and ESI where the solvents contained added salts and stabilisers. So, although the IR spectra show fraction 41 contains the highest concentration of the putative nitro species, the SEC chromatogram of fraction 43 and not 41 is shown in fig.6.3. In any case, the IR spectrum of fraction 43 shows a strong absorption at 1550 cm^{-1}. The SEC chromatogram of fraction 43 (fig.6.3) consists of three peaks, decreasing in intensity towards higher mass. The most intense peak in this chromatogram appears at a lower mass than that of the cyclic tetramer (see fraction 35). The column chromatography of untreated PNMMO (chapter 4) shows that the cyclic oligomers are eluted in order of increasing molecular weight, starting with the cyclic tetramer, prior to the elution of the linear oligomers. Thus, it appears that a *new species* with a lower molecular weight than that of the cyclic tetramer is present in fraction 43. A comparison of the IR spectra and SEC chromatograms for fractions 30 - 53 shows that

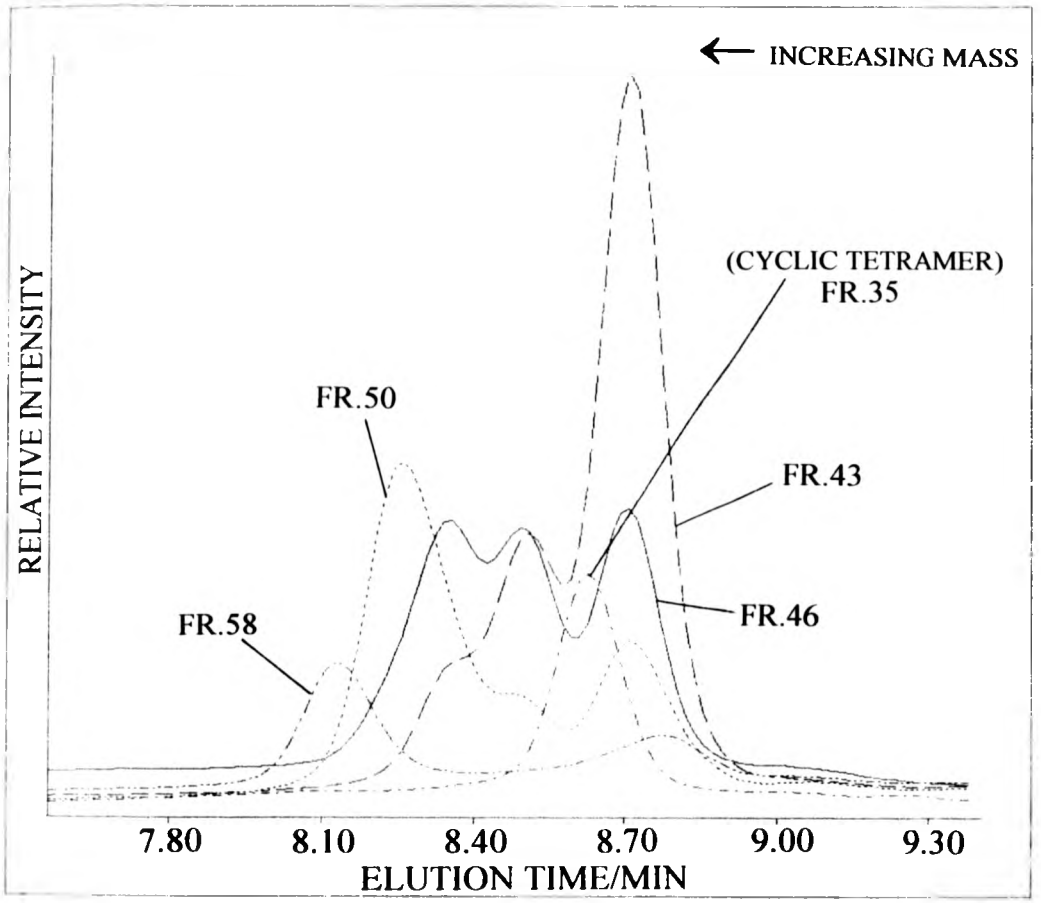

FIG.6.3 SEC CHROMATOGRAMS OF FRACTIONS CONTAINING PREDOMINANTLY LOW-MASS CYCLIC OLIGOMERS ELUTED DURING THE COLUMN CHROMATOGRAPHY OF PYROLYSED (25 h/130^{0}C) PNMMO

this new peak in the chromatograms is present in all the fractions containing the 1550 cm^{-1} peak in the IR, and the variation in intensity of this new peak in the SEC chromatograms exactly mimics the variation in intensity of the new absorption at 1550 cm^{-1} in the IR; the chromatograms of fractions 46 and 50 show that with increasing elution order, the relative intensity of this new peak decreases relative to other peaks as does the absorption at 1550 cm^{-1} in the IR. This new peak in the chromatograms is thus associated with the species absorbing at 1550 cm^{-1} in the IR. This species is characterised and assigned using ESI in section 6.3. Other peaks in the chromatograms can be assigned to undegraded higher mass cyclic homologues by comparing their M_n values to those of the cyclic oligomers obtained by column chromatography of untreated PNMMO.

6.3 ESI CHARACTERISATION OF THE FRACTIONS OBTAINED FROM COLUMN CHROMATOGRAPHY OF PYROLYSED PNMMO

Fractions 30 - 52 obtained from the column chromatography of pyrolysed PNMMO contain varying concentrations of the species absorbing at 1550 cm^{-1} in the IR. The results of section 6.2 show that this species is associated with a new peak in the SEC chromatograms. Clearly, the identification of this species is vital to the elucidation of the thermal decomposition pathway of PNMMO. The ESI spectra of fractions 30 - 52 show a new ion peak which varies in intensity in a manner identical to the new peak in the IR and SEC chromatograms. Fig.6.4 shows the ESI spectrum obtained for fraction 43 using NH_4Cl to promote ionisation. The new ion peak is the most intense peak in this spectrum and is clearly visible at 576.4 mus. Peaks around 446, 552 and 713 mus are attributed to $[(NH_4)_xCl_y]^+$ clusters and the peak at 753.6 mus is assigned to the NH_4^+ adduct of the undegraded cyclic pentamer. The peak due to the cyclic pentamer is also visible in the

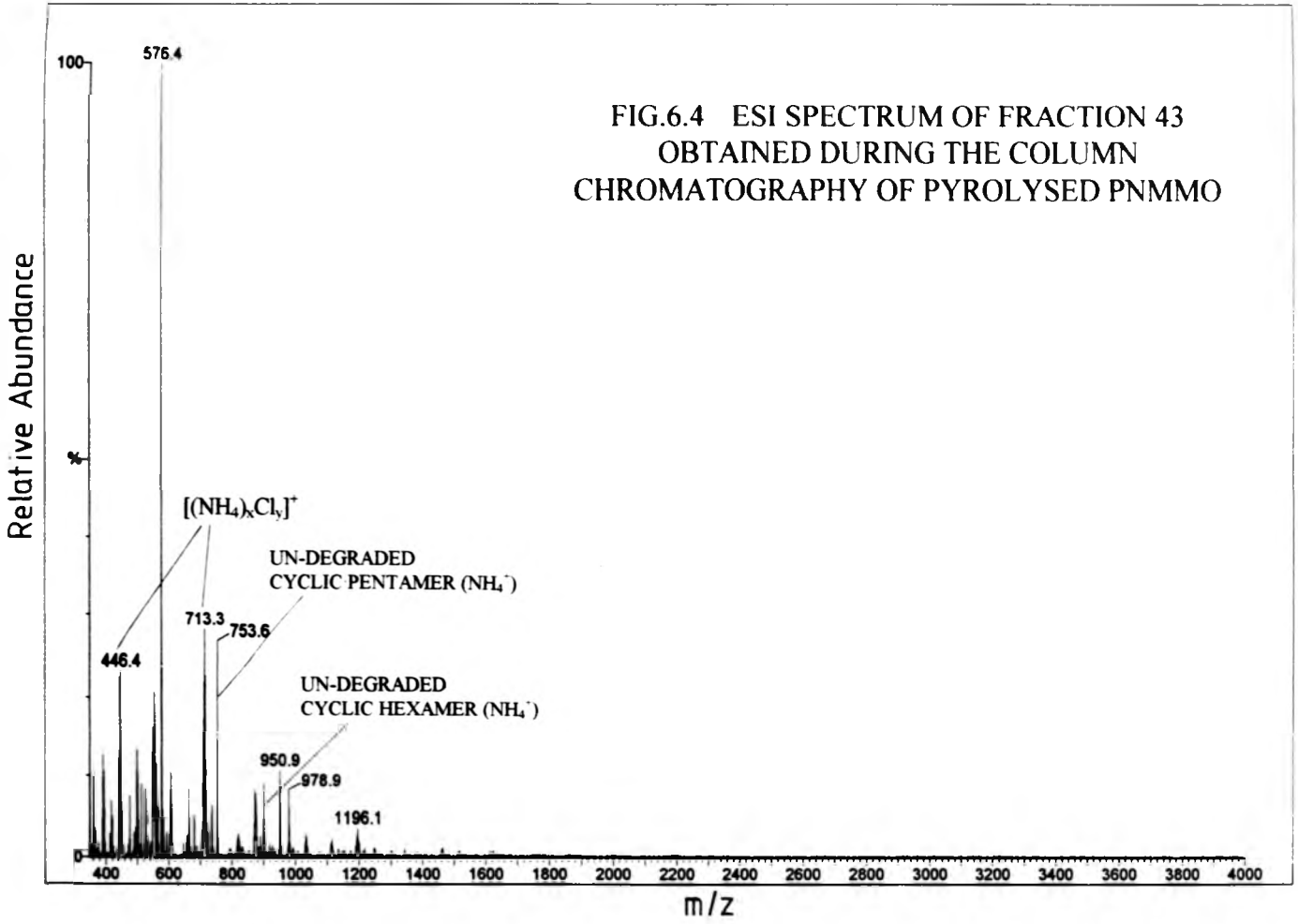

FIG.6.4 ESI SPECTRUM OF FRACTION 43 OBTAINED DURING THE COLUMN CHROMATOGRAPHY OF PYROLYSED PNMMO

chromatogram of fraction 43 (fig.6.3). Other peaks in the ESI spectrum of fraction 43 are less than one tenth as intense as the peak at 576.4 mus and can be assigned to the undegraded linear oligomers of PNMMO by comparison with the ESI spectra of chromatographed untreated PNMMO. The peak at 576.4 mus in the ESI spectrum is later attributed, with the aid of CID, to an NH_4^+ adduct and is thus associated with a species of mass 558.4 mus. The new peak in the chromatograms (fig.6.3) has a mass value just lower than that of the cyclic tetramer (588.4 mus) which strongly suggests that this peak is associated with the new peak at 576.4 mus in the ESI spectrum (fig.6.4). Except for the new peak at 576.4 mus, all the ion peaks in the ESI spectrum can be assigned to the undegraded cyclic and linear oligomers of PNMMO. Consequently, the species absorbing at 1550 cm^{-1} in the IR spectra of fractions 30 - 52 is most likely to be associated with the ion peak at 576.4 mus in the ESI spectrum. Due to the relatively high concentration of this species in fractions 30 - 52 as observed by SEC, IR and ESI, and its relatively short elution time from the column, it was tentatively assigned to a thermal degradation product of the cyclic tetramer. This was subsequently confirmed by NMR spectrometry (see section 6.4). Consequently the ammonium ion peak at 576.4 mus is associated with a compound formed by the loss of 30 mus from the cyclic tetramer. Two candidate molecules of mass 30 mus are NO and CH_2O. However, the abundant loss of formaldehyde from PNMMO during pyrolysis has already been demonstrated using gas-phase IR spectroscopy (section 5.5) and CH_2O thus seems the most likely attribution to the species of mass 30 mus. The loss of NO from a nitrate ester would leave a peroxyl radical, the formation of which would involve an unlikely, highly concerted pathway. Loss of formaldehyde from the main chain in the cyclic tetramer must proceed via scission of at least two bonds in the main chain to produce an unstable molecule which will undergo further reaction. The resulting molecule is expected

to have a different mass from that observed for the degradation product of the cyclic tetramer and thus an alternative degradation route is likely. Loss of formaldehyde can also occur from any one of the four side-chains in the cyclic tetramer via loss of NO_2. Loss of NO_2 via homolysis of the nitrate ester linkage produces a reactive alkoxy radical which will eliminate formaldehyde to give a stable tertiary carbon-centred radical. Re-combination of NO_2 can then occur to produce a nitroalkane as shown below.

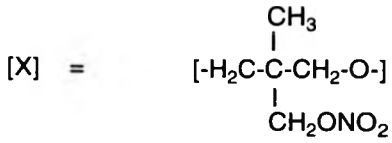

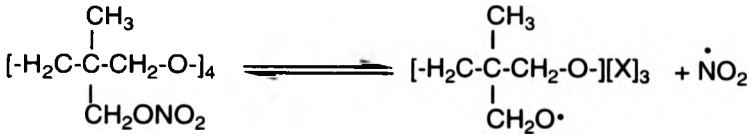

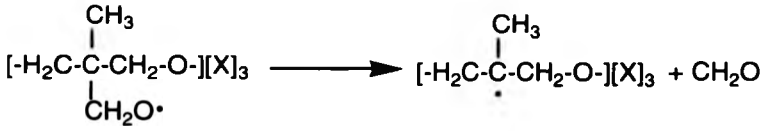

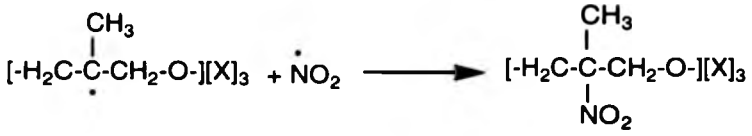

The resulting nitroalkane exhibits an overall loss of 30 mus from the original cyclic tetramer and produces an ion peak due to the ammonium adduct at 576.4 mus as we observe. The strong absorption visible at 1550 cm^{-1} in the IR spectra of fractions 30 - 52 is consistent with the asymmetric stretch of a nitroalkane. However the absence of a similarly intense absorption due to the symmetric stretch of the nitroalkane around 1340 cm^{-1} in the IR spectrum of fraction 41 (fig.6.1A) and IR difference spectrum of pyrolysed unchromatographed PNMMO (fig.5.3) appears at variance with this assignment. Indeed without the ESI results, the absorption at 1550 cm^{-1} could well be attributed to a tertiary nitroso compound which produces only a single absorption around 1600 cm^{-1} in the IR. However the frequency of the asymmetric and symmetric stretching absorptions of the NO_2 group are highly sensitive to the nature of the attached alkyl group; IR studies of nitroalkanes reveal that the absorption band due to the symmetric stretch is particularly sensitive and is less strongly-defined as regards frequency and intensity as compared to the antisymmetric stretch[1]. For this same reason there is no clear overall relationship between the frequencies of these two bands in tertiary alkyl nitro compounds[1]. In general, the symmetric absorption is appreciably less intense than the asymmetric absorption as we observe for the nitro species in our studies. A further complication also arises due to the presence of the methyl group on the α-carbon atom of the nitro species, which causes the symmetric absorption to split such that the total intensity is equally divided between the two bands[2]. These two bands generally appear around 1370 and 1395 cm^{-1} and we do find weak absorptions at 1377 and 1394 cm^{-1} in the IR difference spectrum of pyrolysed unchromatographed PNMMO (fig.5.3). It was not possible to run IR difference spectra of the fractions obtained from column chromatography as it was impossible to calculate the exact relative amounts of oligomer present and thus prepare a background sample. However,

as the frequency of the absorption at 1550 cm^{-1} is exactly the same for both the degraded cyclic tetramer and degraded bulk PNMMO samples, the nitro species formed by pyrolysis of the cyclic tetramer is thought to be structurally identical to that formed during pyrolysis of bulk PNMMO.

ESI spectra were also obtained for fraction 100 which appeared to contain a relatively high concentration of the carbonyl species as observed by IR spectroscopy (fig.6.1B). Fig.6.5 shows the ESI spectrum of fraction 100 obtained using NH_4Cl to promote ionisation. Six new peaks are visible in this spectrum at 572.6, 589.4, 603.4, 620.4, 870.4 and 1164.4 mus. All other peaks in the spectrum can be assigned to undegraded cyclic and linear oligomers such as the cyclic hexamer, heptamer and octamer at 900.4, 1047.3 and 1194.4 mus respectively. Although fraction 100 appears to contain a high concentration of the carbonyl species, a low intensity absorption is also visible for the nitro species at 1550 cm^{-1}. No peak is visible for the partly degraded cyclic tetramer at 576.4 mus, but new peaks are visible at 870.4 and 1164.4 mus attributed to nitro formation in the cyclic hexamer and octamer respectively. Thus as we expect, nitro formation occurs not only in the cyclic tetramer but also in the higher cyclic homologues.

In addition to the ESI, IR and SEC results which all support our assignment of the tertiary nitroalkane in pyrolysed PNMMO, CID experiments were also performed.

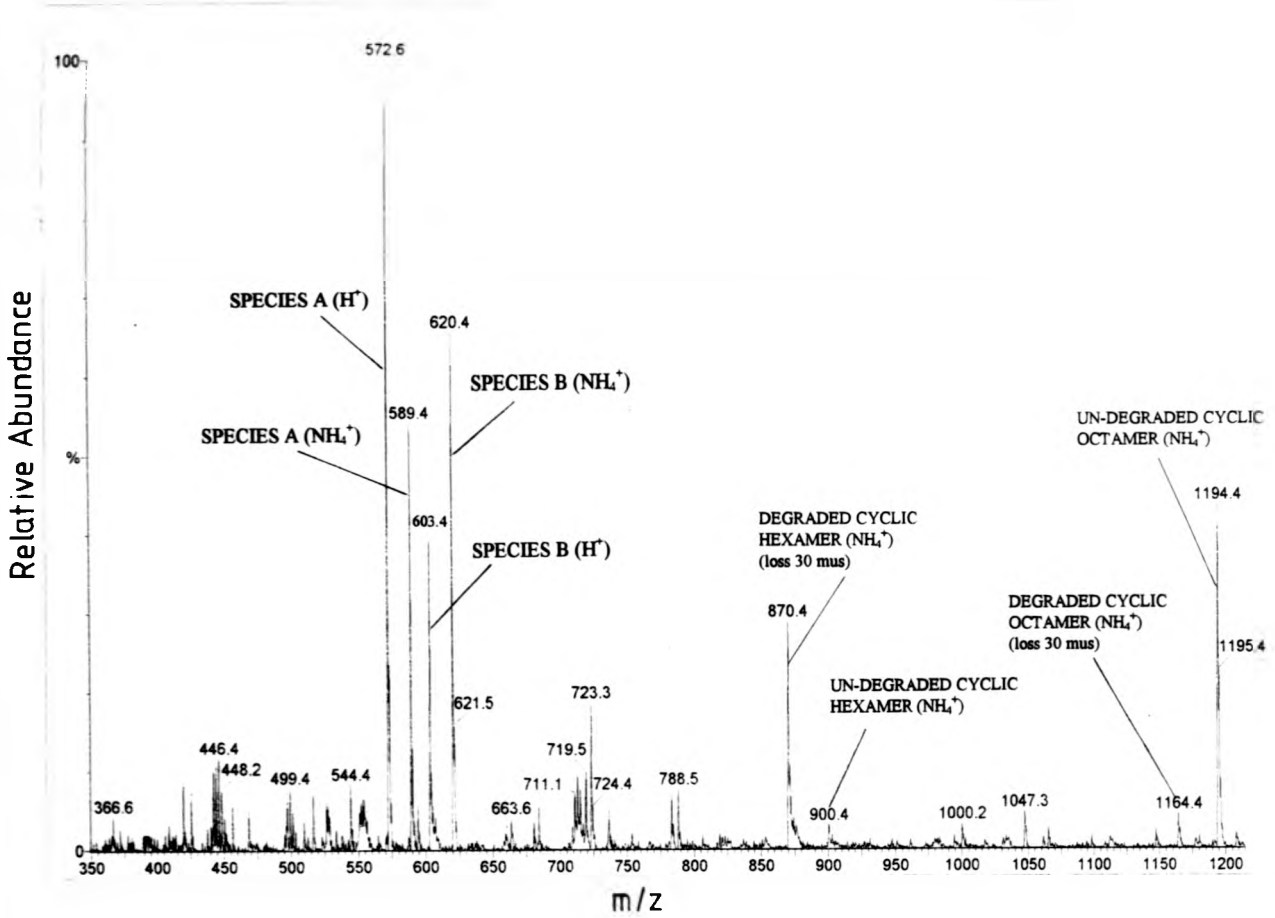

FIG.6.5 THE ESI SPECTRUM OF FRACTION 100 ('CARBONYL RICH') OBTAINED DURING THE COLUMN CHROMATOGRAPHY OF PYROLYSED PNMMO

6.4 CID CHARACTERISATION OF THE UNDEGRADED CYCLIC TETRAMER AND LOW-MASS THERMAL DEGRADATION PRODUCTS OF PNMMO

Fig.6.6 shows the CID spectra of both the H^+ adduct of the undegraded cyclic tetramer (589.4 mus) and the NH_4^+ adduct of the nitro species (576.6 mus) produced during thermolysis of PNMMO. The ESI spectra of the nitro species (section 6.3) show only a very low abundance of the H^+ as compared to the NH_4^+ adduct and thus it was difficult to obtain reproducible CID spectra of the H^+ adduct. However the CID spectra of the H^+ and NH_4^+ adducts of the undegraded cyclic tetramer are nearly identical and differ only to a small extent in the relative abundances of the daughter ions. The daughter ions are considerably more intense in the CID spectrum of the H^+ as compared to NH_4^+ adduct of the cyclic tetramer and thus the CID spectrum of the H^+ adduct of the cyclic tetramer is compared to the NH_4^+ adduct of the nitro species in fig.6.6. The NH_4^+ ion binds more strongly to the cyclic tetramer than does the H^+ ion due to the multiple hydrogen bonds that can exist between the ring and side-chain oxygens in the cyclic tetramer and the hydrogen atoms in the NH_4^+ ion. Therefore as expected, the NH_4^+ adduct of the cyclic tetramer is more difficult to fragment via CID as compared to its H^+ counterpart and thus gives a lower abundance of daughter ions as compared to parent ion; similar observations are also reported for cyclic and linear polyglycols[3,4].

An extensive literature search failed to find any publications relating to the CID of nitrate ester or nitro compounds using ESI. However, various reports concerning the electron impact (EI) mass spectra of aliphatic nitro compounds[5,6], acyclic[7,8] and cyclic[9,10] polyethers and the CID mass spectra of cyclic[11,12,13] polyether compounds do exist. It is reported that acyclic polyglycols, particularly PEG and PPG, show product ions resulting

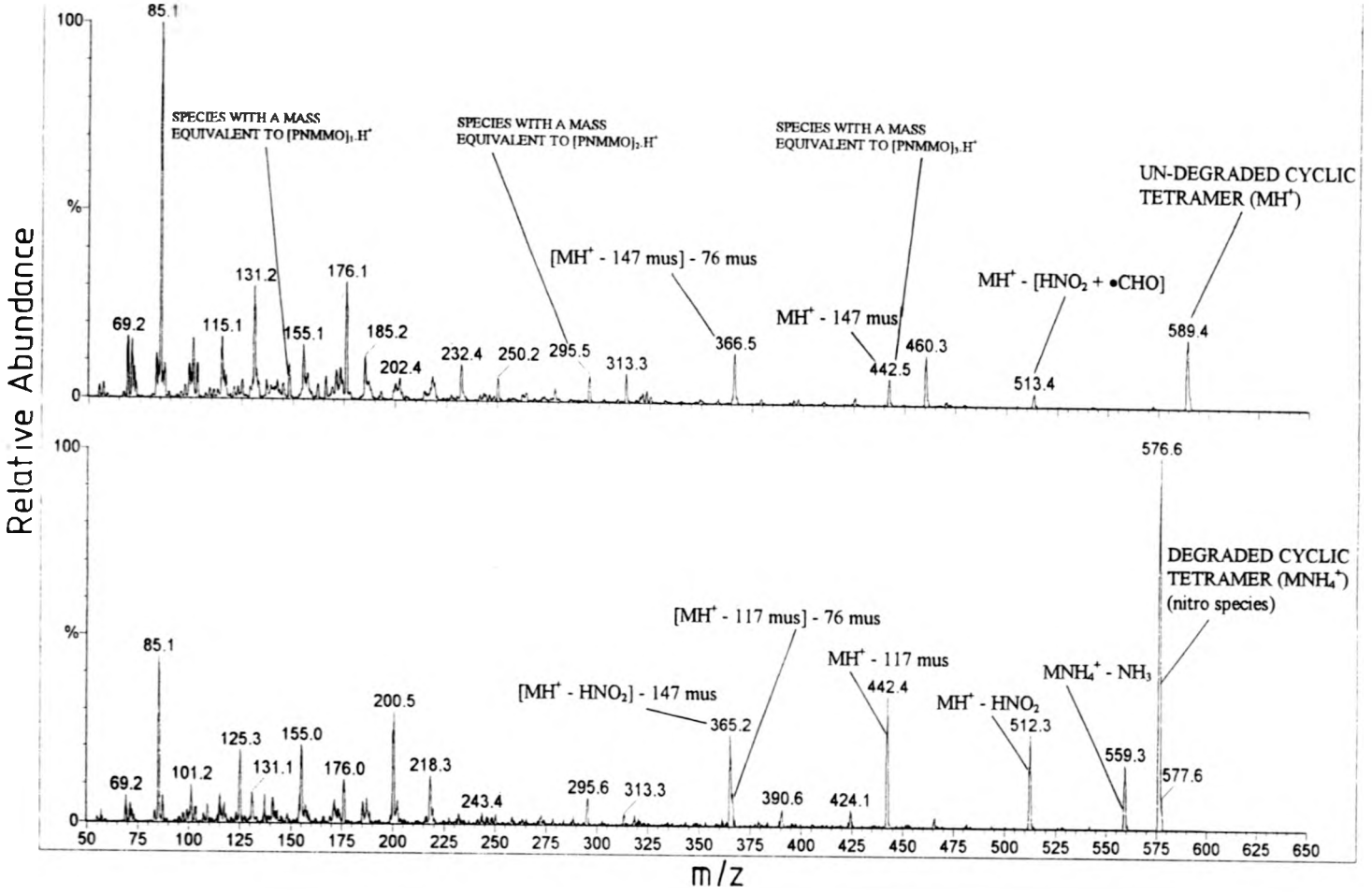
Relative Abundance
100
%
0
85.1
SPECIES WITH A MASS EQUIVALENT TO [PNMMO]1.H+
SPECIES WITH A MASS EQUIVALENT TO [PNMMO]2.H+
SPECIES WITH A MASS EQUIVALENT TO [PNMMO]3.H+
UN-DEGRADED CYCLIC TETRAMER (MH+)
[MH+ - 147 mus] - 76 mus
MH+ - [HNO2 + •CHO]
MH+ - 147 mus
69.2
115.1
131.2
155.1
176.1
185.2
202.4
232.4
250.2
295.5
313.3
366.5
442.5
460.3
513.4
589.4
576.6
DEGRADED CYCLIC TETRAMER (MNH4+) (nitro species)
[MH+ - 117 mus] - 76 mus
MH+ - 117 mus
MNH4+ - NH3
[MH+ - HNO2] - 147 mus
MH+ - HNO2
69.2
85.1
101.2
125.3
131.1
155.0
176.0
200.5
218.3
243.4
295.6
313.3
365.2
390.6
424.1
442.4
512.3
559.3
577.6
50 75 100 125 150 175 200 225 250 275 300 325 350 375 400 425 450 475 500 525 550 575 600 625 650
m/z

FIG.6.6 COLLISION INDUCED DISSOCIATION ESI MASS SPECTRA OF THE UN-DEGRADED CYCLIC TETRAMER AND THE DEGRADED CYCLIC TETRAMER (NITRO SPECIES)

from the loss of consecutive monomer units during FAB[7,8] , EI[13] and CID[4,11] measurements. Cyclic polyglycols similarly undergo loss of consecutive monomer units[7] via C-C or C-O bond cleavage although this process is complicated by the presence of side-groups. The mechanism of loss of monomer units in the cyclic tetramer of PNMMO is thought to differ from that of the simple polyglycols which can eliminate neutral species, such as C_2H_4O in the case of PEG, in a relatively low energy process.

The CID spectra in fig.6.6 show that both the undegraded cyclic tetramer and the nitro species fragment via loss of consecutive monomer units similarly to the cyclic and linear polyglycols described above. Species with the same mass as the monomer, dimer and trimer of PNMMO are labelled on the spectra. The main fragmentation pathways are also labelled along with their respective loss in mass. The NH_4^+ adduct of the nitro species (576.6 mus) initially fragments via loss of NH_3 to give the H^+ adduct at 559.3 mus. The loss of NH_3 is typical of NH_4^+ adducts[3] and confirms our assignment of the peak at 576.6 mus to an NH_4^+ adduct as opposed to an H^+ adduct. As expected, the H^+ adduct of the undegraded cyclic tetramer (MH^+) does not show a fragment ion at MH^+-17. There is however a prominent peak at MH^+-76 which is consistent with cleavage of the C-C bond adjacent to the ONO_2 group in any one of the four nitrate ester side chains in the cyclic tetramer. Minor peaks at MH^+-47 and MH^+-63 suggest that the consecutive elimination of the two neutral species HNO_2 and $\bullet CHO$ may also play a major (and possibly the major) role in the formation of the species with mass MH^+-76 as shown over the page.

DIAGRAM SHOWING THE FRAGMENTATION OF A SINGLE NITRATE ESTER SIDE CHAIN IN THE CYCLIC TETRAMER DURING CID

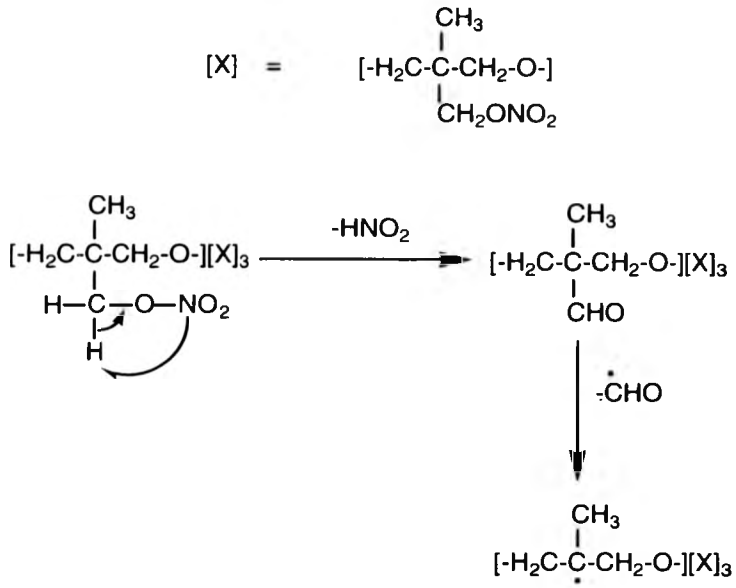

Conversely, the H^+ adduct of the nitro species (559.3 mus) shows a fragment ion peak at MH^+-47. In the EI mass spectra of primary and secondary nitroalkanes the loss of both $\bullet NO_2$ and HNO_2 from the molecular ion (M) is observed but the latter process occurs to a much lesser extent and the M-HNO_2 ion peak is present in only very low abundance as compared to the M-NO_2 ion peak. The EI mass spectra of tertiary nitroalkanes are in most cases different, the main feature being the loss of HNO_2 from the molecular ion giving rise to the highest discernible peaks in the spectra[6]. Clearly, an ion peak at MH^+-47 is observed in the CID mass spectrum of the tentatively assigned nitro species (fig.6.6) thus substantiating our assignment of this thermal degradation product to a tertiary nitro species. The MH^+-46 ion peak is not apparent in this mass spectrum. Aplin *et al.*[5] show that the loss

of hydrogen can occur from either the methylene or the methyl group in 2,4-dimethyl-2-nitropentane. As with the nitro species, loss of hydrogen may occur via either of the routes shown below.

DIAGRAM SHOWING THE FRAGMENTATION OF THE NITRO SIDE CHAIN IN THE DEGRADED CYCLIC TETRAMER DURING CID

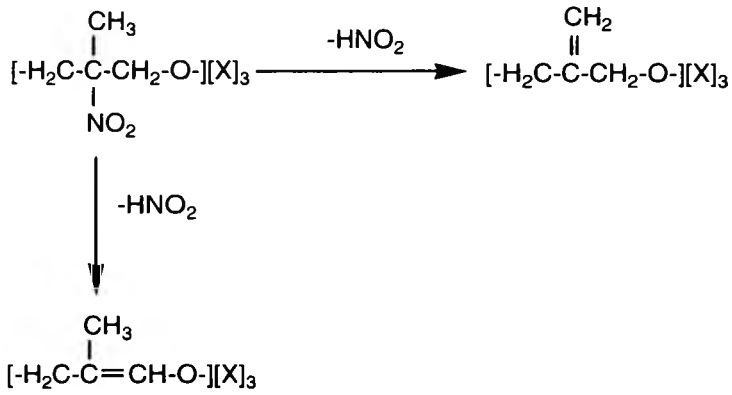

Both the undegraded cyclic tetramer and the nitro species show a prominent ion peak for the trimer of PNMMO at 442.4 mus. This ion is thought to originate from the direct fragmentation of the ions at 589.4 and 559.3 mus respectively, and the following mechanism (see over the page) is proposed.

DIAGRAM SHOWING THE ELIMINATION OF A SPECIES WITH THE SAME MASS AS THE MONOMER UNIT OF PNMMO

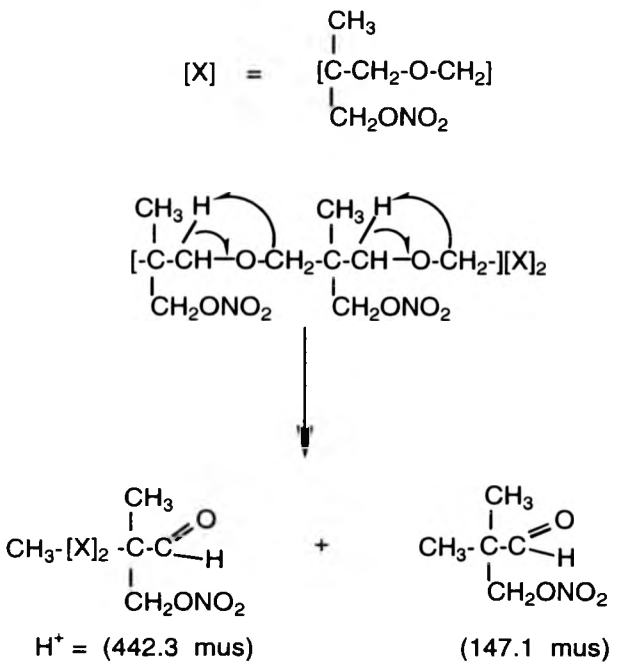

This mechanism is similarly applicable to the H^+ adduct of the nitro species (559.3 mus) although the presence of the nitro group appears to promote the elimination of the nitro-containing monomer unit. Thus instead of the loss of 147 mus, as observed for the undegraded cyclic tetramer, a loss of 117 mus is observed from the nitro species resulting in a species which exhibits an ion peak at 442.3 mus. Clearly the mass of the nitro side-chain is 30 mus lower than that of the other 3 nitrate side chains thus accounting for the loss of 117 mus instead of 147 mus.

The H^+ adduct of a species with a mass equivalent to two PNMMO monomer units is observed at 295.5 mus in the CID spectrum of the undegraded cyclic tetramer and at 295.6

mus in the CID spectrum of the nitro species. We propose that this species is formed by the loss of 147.1 mus from the species with a mass of 442.4 mus in a similar mechanism to that shown on the previous page. The diagram below shows the mechanism of this loss of 147.1 mus although a species with 147.1 mus would also be lost if the same process were to occur in the adjacent monomer unit. Thus two distinct pathways exist both of which generate ions with a mass of 147.1 mus and 295.5 mus.

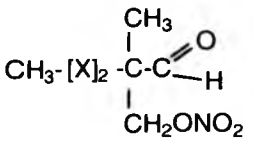

H^+ = (442.3 mus)

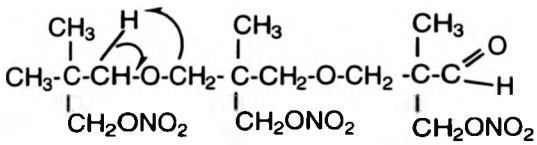

The prominent ion peak at 366.5 mus in both of the CID spectra shows that the species with a mass of 442.4 not only eliminates a fragment of mass 147.1, as shown in the mechanism above, but in a parallel process also eliminates a nitrate ester side-chain in a similar process to that already shown, i.e. loss of HNO_2 followed by elimination of CHO•. The ion peak at 366.5 mus in the CID spectrum of the nitro species is observed only as a shoulder on the peak of mass 365.2 mus, the latter ion formed by the elimination of 147.1 mus from the species with a mass of 512.3 mus. Clearly the CID spectra of both the cyclic tetramer and the nitro species contain many daughter ions but most of these result from the consecutive elimination of fragments of mass 147.1 mus or 76 mus (HNO_2 + CHO•).

The fragment of mass 147.1 which is generated in all the proposed schemes above may then eliminate NO_3^- and rearrange to give the $C_4H_9CO^+$ ion which shows an intense ion peak at 85.1 mus in both CID spectra (fig.6.6), however there are several alternatives.

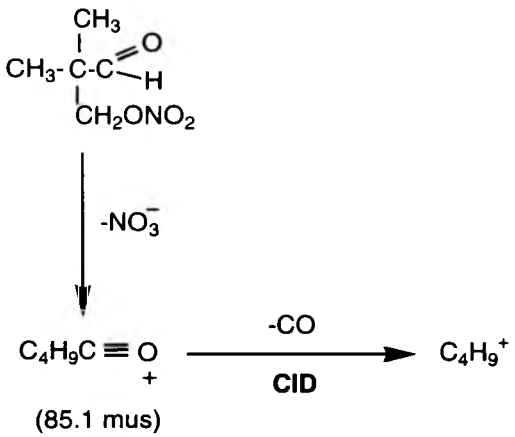

The assignment of the species exhibiting an ion peak at 85.1 mus to the $C_4H_9CO^+$ ion was substantiated by further CID experiments which showed that this ion fragmented initially by loss of 28 mus, attributed to CO. Lower mass fragments at 43, 41 and 29 mus were assigned to the common fragment ions of hydrocarbons[14] namely $C_3H_7^+$, $C_3H_5^+$ and $C_2H_5^+$ respectively.

The fragmentation schemes shown above account for the main fragmentation pathways of both species but are not completely exhaustive. Clearly the importance of the CID experiment was to establish the presence of a nitro group attached to a tertiary carbon and this was substantiated by the preferential loss of HNO_2 (47 mus) from the H^+ adduct at 559.3 mus.

6.5 NMR CHARACTERISATION OF THE FRACTIONS OBTAINED FROM COLUMN CHROMATOGRAPHY OF PYROLYSED PNMMO

Figs.6.7 A and B respectively show the ^{1}H and ^{13}C NMR spectra of fraction 43 which contains a relatively high concentration of the tertiary nitro species as characterised by SEC and ESI. Three distinct new resonances are visible in the ^{13}C NMR spectrum around 20.4, 70.1 and 87.7 ppm. A DEPT experiment reveals that the resonance around 20.4 ppm is associated with a primary carbon, the resonance around 70.1 ppm with a secondary carbon and the resonance around 87.7 ppm with a tertiary carbon. Consequently the resonance at 87.7 ppm was attributed to the tertiary carbon directly attached to the NO_2 group. The chemical shift of this carbon closely matched that for C-NO_2 in 2-methyl-2-nitropropane (85.0 ppm) and the assignment was further substantiated by the ratio of the integrals of the resonances due to the tertiary carbons at 87.7 and 40.1 ppm (the latter refers to the tertiary carbon attached to the unchanged nitrate ester group). This ratio is 0.55 : 0.15 ≡ 3.7 : 1 and is, as expected, slightly greater than the 3 : 1 ratio predicted for the nitro species of the cyclic tetramer due to the presence of much smaller amounts of undegraded cyclic pentamer/hexamer and linear oligomers (as shown by ESI and SEC in sections 6.2 and 6.3). The presence of undegraded cyclic pentamer and hexamer is clearly evidenced in the ^{13}C NMR by the peaks around 73.6 ppm due to the ring methylenes in these two compounds. The new methyl peak at 20.4 ppm is attributed to the methyl group β to the nitro group and, as for the tertiary carbons, the ratio of the integrals of this methyl to the relatively unaltered methyls around 17 ppm is 0.33 : 1.18 ≡ 1 : 3.6. Both the ^{1}H and ^{13}C NMR chemical shifts of the new methyl group closely match those for a methyl attached β to a nitro group[14]. The new set of peaks around 70.2 ppm are attributed to the two perturbed methylenes attached β to the nitro group and like the new methyl and tertiary carbons, the ratio of their integrals

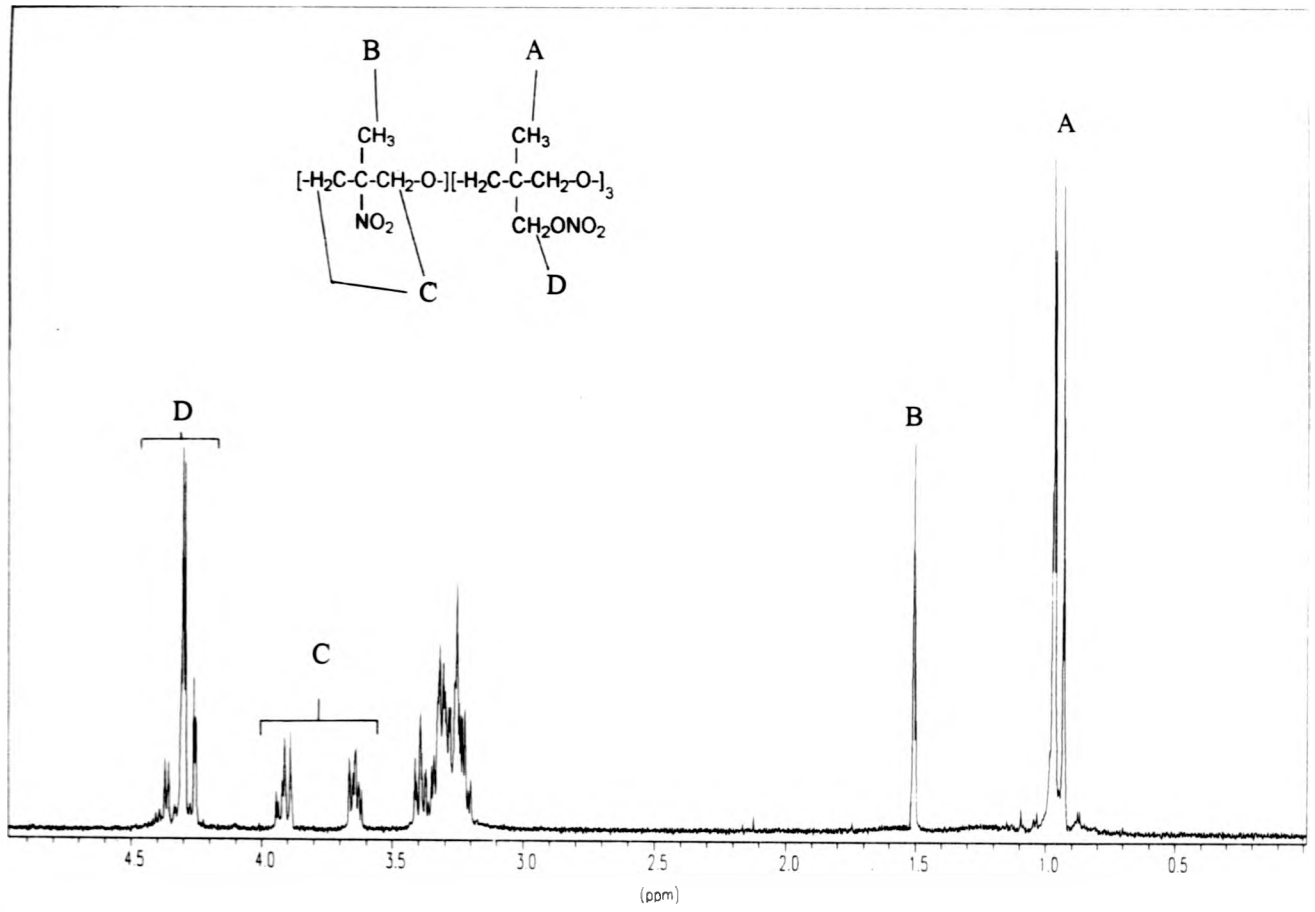

FIG.6.7A 400 MHz ^{1}H NMR SPECTRUM OF FRACTION 43 OBTAINED DURING THE COLUMN CHROMATOGRAPHY OF PYROLYSED PNMMO

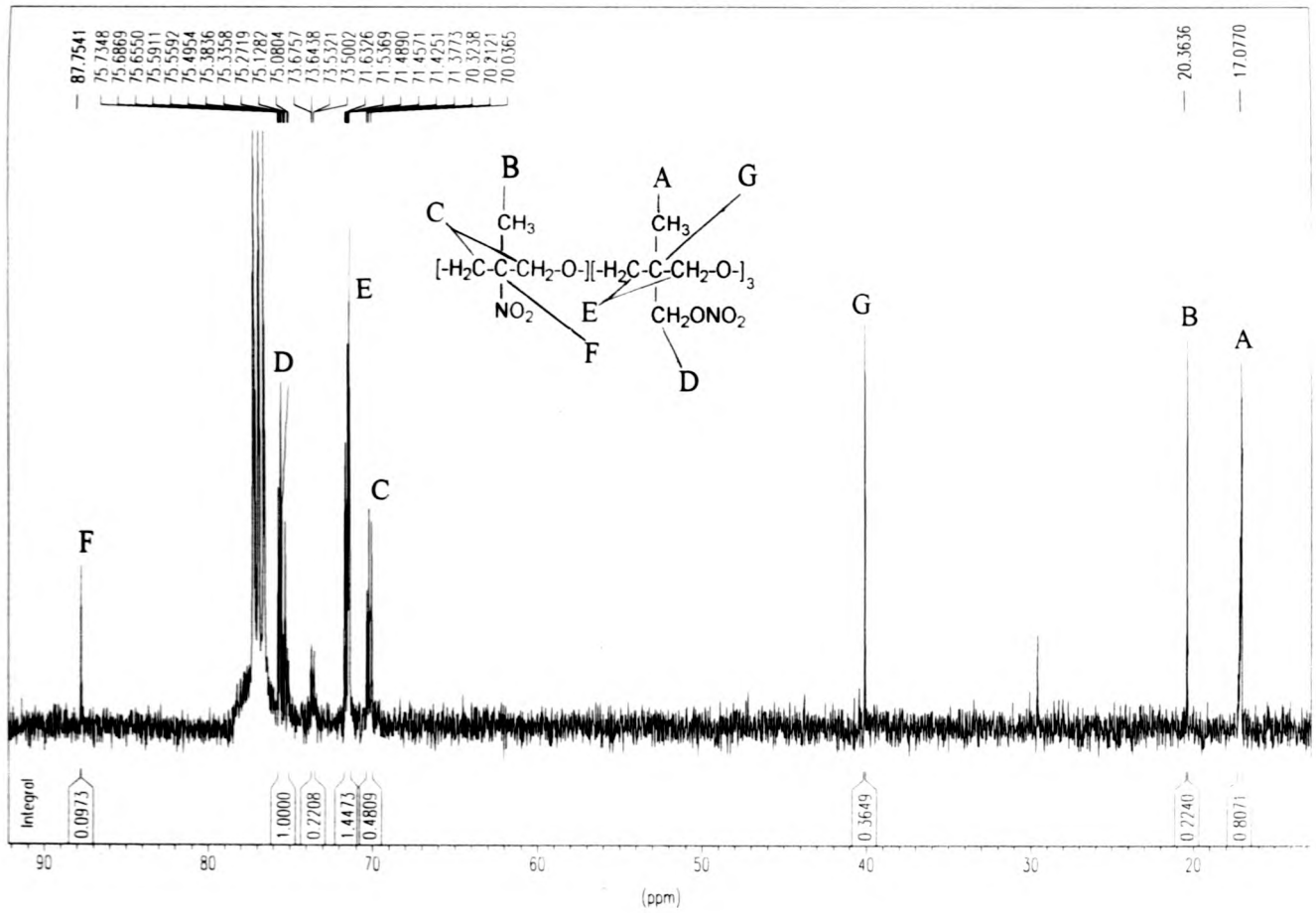

FIG.6.7B 400 MHz ^{13}C NMR SPECTRUM OF FRACTION 43 OBTAINED DURING THE COLUMN CHROMATOGRAPHY OF PYROLYSED PNMMO

to the 6 relatively unperturbed methylenes around 71.4 ppm is approximately 1 : 3.3. Their shift to higher field is attributed to an increased number of γ -gauche effects between the nitro group and the methylene carbons. Thus the two oxygens on the nitro group gamma to these methylene carbons may exert a greater γ -gauche effect than the single oxygen in the original nitrate ester side chains, resulting in a shift to higher field. The nitro species could be modelled in the same manner as the cyclic tetramer and pentamer in section 4.4 to validate this assumption. The four hydrogens on the two perturbed methylenes β to the nitro group are clearly visible in the ^{1}H NMR (fig.6.7A) spectrum of the degraded fraction and exhibit the expected AB system around 3.9 and 3.6 ppm. The coupling constant for this system is more easily extracted from the ^{1}H NMR spectra of fractions containing lower concentrations of the nitro species due to the fewer number of peaks observed for the AB system. There is also a new set of resonances present in the ^{1}H NMR spectrum around 3.4 ppm. Fig.6.8 shows the ^{1}H NMR spectrum obtained for a fraction with a lower elution time than that of the fraction 43 above. The coupling constant measured from the resonances around 3.6 and 3.9 ppm is 8.7 Hz and the chemical shift difference is approximately 0.25 ppm. The ^{1}H NMR spectrum (fig.6.8) also shows that the new set of resonances around 3.4 ppm can be attributed to another AB system. Clearly only one set of peaks are visible for this AB system but the other set are thought to be 'hidden' under the resonances due to the relatively unperturbed methylenes around 3.3 ppm. The coupling constant for this AB system is exactly the same as that measured for the AB system around 3.6 and 3.9 ppm i.e. 8.7 Hz. The chemical shift difference cannot be measured here but it must be less than that observed for the previous AB system (0.25 ppm) as no resonances with a chemical shift difference of more than 0.20 ppm, except those for the methyl hydrogens, are visible at higher field. The ratio of the integrals of each of the 3 new sets of peaks around 3.4, 3.6 and

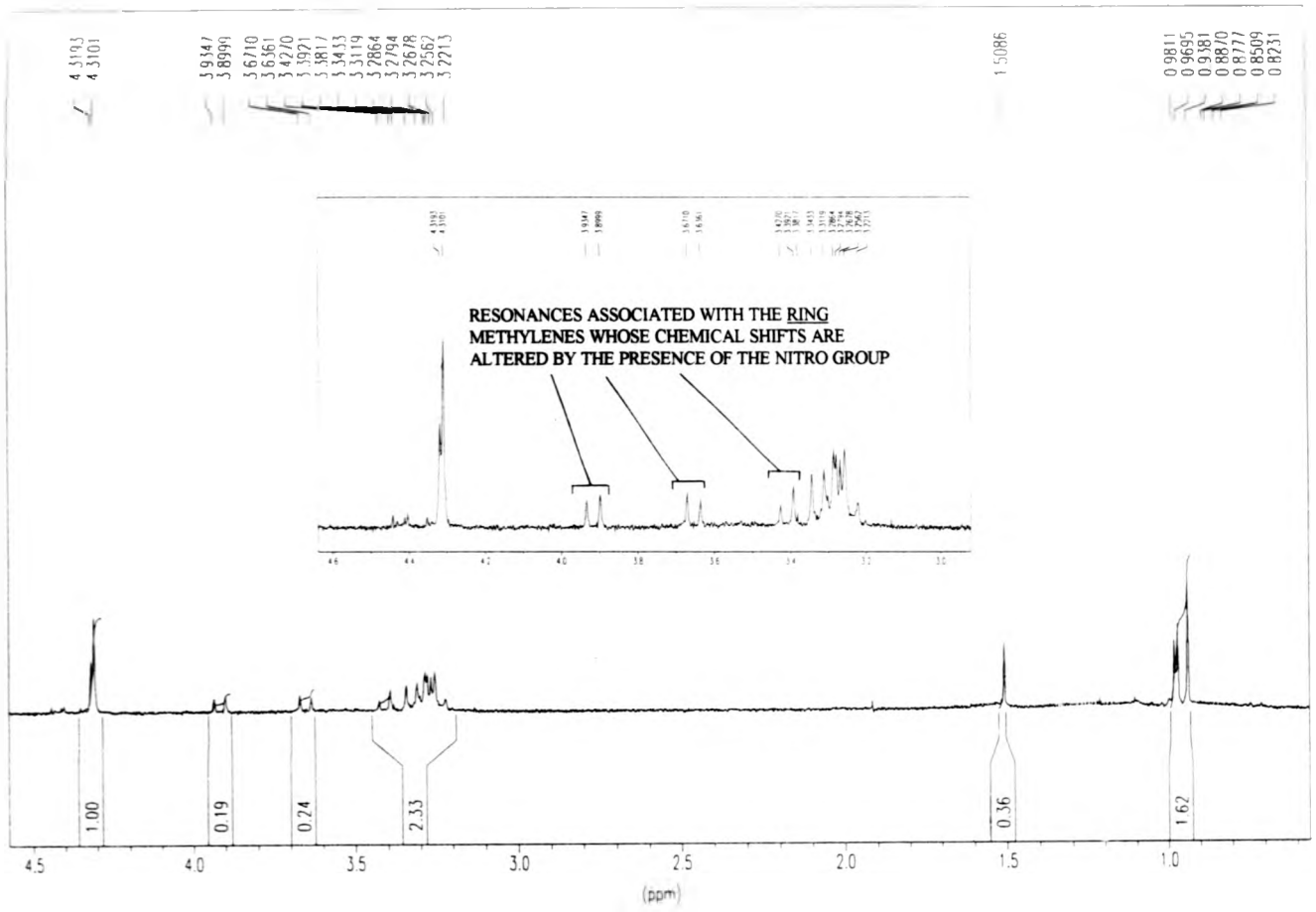

FIG.6.8 250 MHz ^{1}H NMR SPECTRUM OF FRACTION 38
OBTAINED DURING THE COLUMN CHROMATOGRAPHY
OF PYROLYSED PNMMO

3.9 ppm in the ^{1}H NMR spectrum (fig.6.7A) is ca. 1 : 1 : 1 and consequently the resonances around 3.4 ppm and their associated resonances 'hidden' under the methylene protons around 3.3 ppm are attributed to the hydrogens on the methylene carbons four bonds away from the nitro group. These hydrogens will be influenced to a lesser extent than the hydrogens on the methylenes β to the nitro group and thus both their chemical shift and chemical shift separation will be less but their coupling constant is, as expected, the same. All the resonances due to the methyl and methylene carbons and hydrogens and the tertiary carbons over four bonds away from the nitro group show, as expected, a greater number of resonances than in the undegraded cyclic tetramer due to the relative decrease in the symmetry of the tetramer ring and the reduced influence of the nitro group. Thus, the IR, SEC, ESI and NMR results for the nitro species of the cyclic tetramer all substantiate the assignment of the thermal degradation product of the cyclic tetramer to a tertiary nitro species. ^{14}N NMR spectra of untreated PNMMO and the untreated cyclic tetramer were compared with ^{14}N NMR spectra of the fractions containing relatively high concentrations of the nitro species. However due to the very small amounts of oligomer in each fraction, the low sensitivity and the quadrupolar effect of the ^{14}N nucleus[15], the resonances in the ^{14}N NMR spectra of the fractions containing the nitro species were too weak to provide conclusive results. The ^{15}N nucleus is generally used in preference to the ^{14}N nucleus for structural determinations but its low natural abundance (0.37 %) means that experiments are commonly performed with enriched samples where cost is often prohibitive[16,17]. The range of ^{14}N chemical shifts in organic compounds is about 800 ppm. However, similar chemical shifts of around +50 to -50 ppm are observed for both nitrates and nitroalkanes[15] and particularly for tertiary nitroalkanes where the chemical shift is very similar to those for

primary nitrates, thus making the differentiation of these two species very difficult in PNMMO.

The assignment of the tertiary nitro group in the cyclic tetramer of PNMMO is extended to linear PNMMO where the same absorption at 1550 cm^{-1} is observed in the solution IR spectrum of pyrolysed PNMMO. The peak due to the tertiary carbon α to the nitro group in pyrolysed PNMMO is visible around 89.4 ppm (see fig.5.4B) in the ^{13}C NMR spectra instead of at 87.7 ppm as observed for the nitro species of the cyclic tetramer. The shift difference of less than 2 ppm can be attributed to small differences in bond lengths and angles between the linear and cyclic forms of PNMMO. The assignment of this quaternary carbon in linear pyrolysed PNMMO was confirmed by a 2-D ^{1}H-^{13}C correlation experiment which showed that the resonance at 89.4 ppm in the ^{13}C NMR spectrum of pyrolysed unchromatographed PNMMO (figs.5.4B and 5.6) disappears in the 2-D experiment (fig.5.5) as no hydrogens are associated with this carbon atom. The relatively strong intensity of the resonance due to this tertiary carbon can be attributed to relaxation effects which also lead to a resonance of relatively strong intensity for the tertiary carbon in untreated PNMMO (fig.3.3B). The resonance due to the methyl group β to the nitro group in linear PNMMO is clearly visible in the ^{13}C NMR spectrum of pyrolysed PNMMO at 18.5 ppm (see figs.5.4B and 5.6) and similarly to the cyclic nitro species, a 2-D ^{1}H-^{13}C NMR correlation experiment shows that this resonance is associated with the new resonance around 1.5 ppm in the ^{1}H NMR spectrum of pyrolysed PNMMO. The resonance around 18.5 ppm in the ^{13}C NMR spectrum increases in intensity at approximately the same rate as the tertiary carbon at 89.4 ppm. The methylene carbons β to the nitro group in pyrolysed linear PNMMO are tentatively assigned to the new resonances around 65 - 74 ppm in the ^{13}C NMR spectrum of pyrolysed PNMMO (see figs.5.4/5.6). The shift to higher field is attributed, as for the cyclic

nitro species, to increased γ -gauche effects caused by the two oxygens in the nitro group γ to the methylene carbons. 2-D NMR experiments show that all the resonances around 65 - 74 ppm are attributable to methylene and tertiary carbons and consequently it is difficult to assign individual resonances although, as discussed in chapter 5, alcohol species show resonances in this region. The formation of the formate ester species during pyrolysis of PNMMO will also result in a different chemical shift for the methylene carbons γ to the carbonyl oxygen;

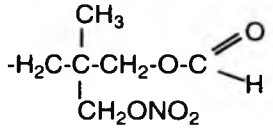

As only a relatively small amount (as determined by integration) of methylenes are shifted to lower field in the ^{13}C NMR spectrum of pyrolysed PNMMO, the new resonances around 65 - 74 ppm are also attributed to the methylene carbons γ to the carbonyl oxygen which are shifted to higher field due to the γ -gauche effect of the carbonyl oxygen.

As we have shown, the solution IR spectrum of fraction 100 (fig.6.1B) shows that this fraction contains a relatively high concentration of the formate ester species (1729 cm^{-1}, 1170 cm^{-1}). The ESI spectrum of this fraction (fig.6.5) shows 4 new peaks at 572.6, 589.4, 603.4 and 620.4 mus. It was only possible to obtain approximately 4 mg of this carbonyl enriched fraction via column chromatography of pyrolysed PNMMO and consequently analysis via SEC or ^{13}C NMR spectroscopy was impossible. However fig.6.9 shows the 400 MHz ^{1}H NMR spectrum of this fraction. The resonance due to the formate hydrogen is clearly visible around 8.05 ppm as are the resonances due to the hydrogens on the methylene

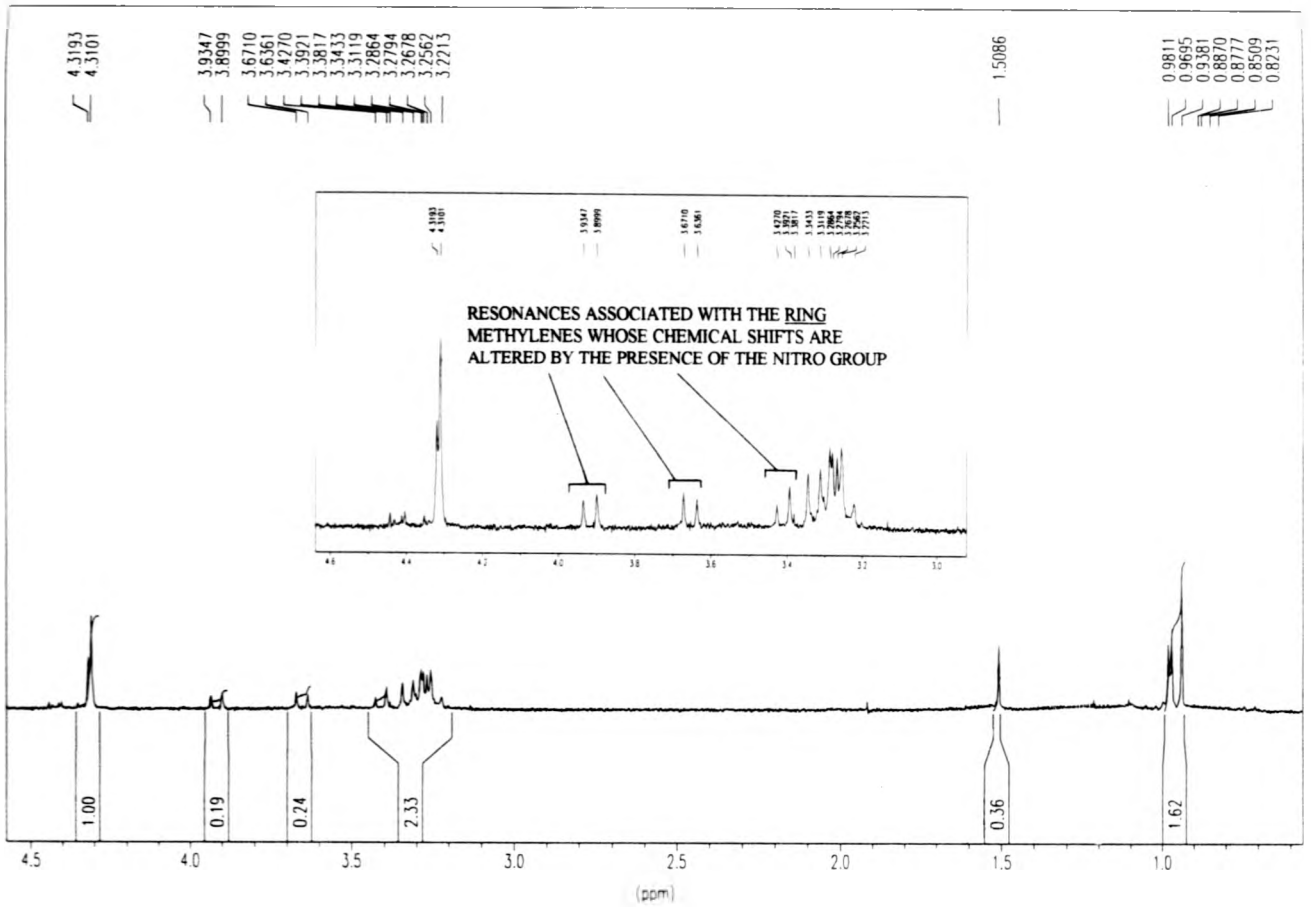

FIG.6.8 250 MHz ^{1}H NMR SPECTRUM OF FRACTION 38 OBTAINED DURING THE COLUMN CHROMATOGRAPHY OF PYROLYSED PNMMO

carbon β to the carbonyl group around 4.0 ppm. As expected, the ratio of the integrals of the methylene to the formate hydrogens is 2 : 1 and the methylene hydrogens show a complex splitting pattern due to their proximity to the carbonyl group and the asymmetric carbon. The resonances due to the methyl, the main chain and the side-chain methylene hydrogens are clearly visible around 1.0, 3.2 and 4.3 ppm respectively. CID experiments show that the four new peaks at 572.6, 589.4, 603.4 and 620.4 mus in the ESI spectrum of fraction 100 (fig.6.5) are associated with the H^+ and NH_4^+ adducts of two different species, namely species A and species B. However, without the aid of ^{13}C NMR spectroscopy it is impossible to positively assign either of these two species to cyclic or linear compounds. The CID spectra of the H^+ and NH_4^+ adducts at 603.4 and 620.4 mus in the ESI spectrum of fraction 100 show some similar fragmentation pathways to those observed for the undegraded cyclic tetramer such as the loss of HNO_2 and HCO. However many dissimilar pathways also exist giving rise to a complex CID spectrum containing numerous ion peaks and making identification of individual species very difficult. However the CID spectra of the H^+ and NH_4^+ adducts at 572.6 and 589.4 mus in the ESI spectrum of fraction 100 contain fewer peaks than the CID spectra of the previous adducts (603.4 and 620.4 mus) and importantly show a fragment ion at MH^+-28. Common fragment ions of mass 28 mus are C_2H_4 and CO. As both the solution IR and ^1H NMR spectra of fraction 100 point towards the presence of a relatively high concentration of formate ester in this fraction, the fragment ion is attributed to the loss of carbon monoxide from the formate ester and indeed acyclic formate esters are reported[13,18,19] to fragment via loss of CO. Although the species associated with the H^+ (572.6 mus) and NH_4^+ (589.6 mus) adducts of the formate ester species eluted from the column in our work cannot be positively assigned to an acyclic species, it is unlikely that a formate ester group can be generated in any one of the cyclic

homologues of PNMMO without the occurrence of chain scission. Thus although complete analysis of the NMR and ESI spectra is not possible, the IR, NMR and ESI (CID) results all suggest that the column chromatography of pyrolysed PNMMO has resulted in the separation and characterisation of a relatively pure sample of one of the major oxidation products of PNMMO, the formate ester.

Analysis of the fractions eluted from the column chromatography of pyrolysed PNMMO using SEC, IR, NMR and ESI (CID) has shown that PNMMO consists of a complex mixture of undegraded and degraded oligomers. Clearly however the presence of low-mass cyclic and linear oligomers (soluble in the THF/MeOH solvent system) in both the degraded and undegraded polymer allows the characterisation of the thermal degradation products of PNMMO via ESI and CID.

We performed several column chromatographic separations of pyrolysed PNMMO and repeat results verified our original assignments of the degradation products in pyrolysed PNMMO.

CHAPTER 6 REFERENCES

1 Bellamy, L.J., The Infrared Spectra of Complex Molecules, Vol.1, 3rd ed., Chapman and Hall, 1975, Ch.17.

2 Eckstein, Glucinski, Sobotka, Urbanski, *J.Chem.Soc.* 1961, 1370.

3 Liou, C.-C., Wu, H.-F., Brodbelt, J.S., *J.Am.Soc.Mass Spectrom.* 1974, **5**, 260.

4 Selby, T.L., Wesdemiotis, C., Lattimer, R.P., *J.Am.Soc.Mass Spectrom.* 1994, **5**, 1081.

5 Aplin, R.T., Fischer, M., Becher, D., Budzikiewicz, H., Djerassi, C., *J.Am.Chem.Soc.* 1965, **87**, 4888.

6 Konopski, L., Grela, K., *J.Org.Mass Spectrom.* 1992, **27**, 741.

7 Jaeger, D.A., Whitney, R.R., *J.Org.Chem.* 1975, **40**, 92.

8 Bose, A.K., Prakash, O., Yuan Hu, G., Edasery, J., *J.Org.Chem.* 1983, **48**, 1782.

9 Lattimer, R.P., *J.Am.Soc.Mass Spectrom.* 1992, **3**, 225.

10 Lattimer, R.P., Munster, H., Budzikiewicz, H., *Int.J.Mass Spectrom.Ion Processes* 1989, **90**, 119.

11 Maleknia, S., Liou, C-C., Brodbelt, J., *J.Org.Mass Spectrom.* 1991, **26**, 997.

12 Curcuruto, O., Traldi, P., Moneti, G., Corda, L., Podda, G., *J.Org.Mass Spectrom.* 1991, **26**, 713.

13 Budzikiewicz, H., Djerassi, C., Williams, D., Mass Spectrometry of Organic Compounds, Holden-Day, California USA, 1967.

14 Silverstein, R., Bassler, G., Spectrometric Identification of Organic Compounds, 4th ed., John Wiley & Sons, Chichester England, 1991, Ch.3.

15 Witanowski, M., Webb, G.A., Nitrogen NMR, Plenum Press, London, 1973.

16 Sanders, J.K.M., Hunter, B.K., Modern NMR Spectroscopy, Oxford University Press, Oxford, 1987.

17 Gunther, H., NMR Spectroscopy, 2nd ed., John Wiley and Sons, Chichester England, 1994.

18 Kawashiro, K., Morimoto, S., Yoshida, H., *Bull. Chem. Soc. Jpn.* 1984, **57**, 1097.

19 Heinrich, N., Drewello, T., Burgers, P., Morrow, J., *J. Am. Chem. Soc.* 1992, **114**, 3776.

CHAPTER 7

SECONDARY DEGRADATION REACTIONS OF PNMMO AND THE ADDITION OF POTENTIAL STABILISERS TO PNMMO

7.1 THE ADDITION OF POTENTIAL STABILISERS TO PNMMO

Various potential stabilisers were added to untreated PNMMO in an attempt to reduce the rate of formation of both the formate ester and tertiary nitro species during thermal degradation. In addition 2-nitrodiphenylamine (2-NDPA), which has been subjected to only preliminary investigations by the DRA[1] but has been shown to reduce the amounts of all of the gases evolved from cured PNMMO during pyrolysis, was also tested; the effect of 2-NDPA on the rate of formation of both the formate ester and nitro species during pyrolysis of PNMMO was unknown and thus plots of the absorbances at 1729 and 1550 cm^{-1} versus time for the stabilised and unstabilised polymer were determined.

Our preliminary investigations moved away from classic antioxidants and examined the effect of additives such as 1,4-benzenedimethanol (BDM) and 1,2,3,4-tetrahydronaphthalene (THN) that might act as hydrogen donors. Recent work suggests that 1,4-benzenedimethanol may act both as an *in situ* hydrogenation agent and as an oxygen scavenger when used as a potential stabiliser in jet fuels[2]. Other publications document the stabilising affect of hydrogen donor additives in a wide range of polymers[3,4,5] and in aliphatic nitrate esters[6]. Thus, it was hoped that the potential hydrogen donor additives (BDM and THN) would resaturate carbon centred radicals formed during the thermolysis of PNMMO, resulting in a retardation of the formation of hydroperoxy and subsequent alkoxy groups.

THN appears to form a homogeneous mixture with PNMMO at room temperature and was added in 1.5 and 3 % by mass compositions to untreated, uncured PNMMO. BDM and 2-NDPA also appear to form a homogeneous mixture with untreated, uncured PNMMO after gradual heating and stirring in an oil bath at 90^0C for approximately 2 min. BDM was similarly added to PNMMO in 1.5 and 3 % by mass compositions whereas 2-NDPA was added to PNMMO in only 1.5 % by mass compositions. This concentration of 2-NDPA is the same as that commonly used by the DRA[1]. Ten samples (5.0 g) of each of these mixtures were placed in separate glass vials (17.5 cm^3) and heated in the oven at temperatures of 115, 128, 140, 147 and 160^0C. In addition, vials containing untreated, 'virgin' PNMMO were also placed in the oven. The vials were left in the oven for varying periods of time and, at set intervals, five vials containing each one of the five different mixtures and one vial containing the 'virgin' polymer were removed from the oven. This method of sampling ensured that the remaining samples were kept at a constant temperature.

At temperatures in excess of 160^0C the contents of the vials containing the additives were physically ejected spontaneously from their containers, leaving only carbonised remains. This temperature was slightly lower than the temperature of 165^0C required to produce the same effect in 'virgin' PNMMO, probably due to the increased gas evolution caused by decomposition of the respective stabiliser at this elevated temperature. Thus a full set of results could not be obtained at pyrolysis temperatures in excess of 160^0C.

Once removed from the oven, the contents were then again mixed thoroughly and solution IR spectra of weighed amounts of the pyrolysate were recorded. All solutions were prepared using identical masses of pyrolysate and $CHCl_3$. The absorbances at 1550 and 1729 cm^{-1} were plotted against pyrolysis time for the various temperatures. A suitable method for taking account of the percentage of additive present in the pyrolysate samples examined

could not be found. The resulting graphs which were plotted therefore include this inherent error. Experiments were repeated to ascertain the fluctuation in the final value of the absorbance at either 1729 or 1550 cm^{-1} for individual samples and this was found to be a maximum of 1.5 % for the absorbance at 1729 cm^{-1}. Figs.7.1A - H show the plots of carbonyl (1729 cm^{-1}) and nitro (1550 cm^{-1}) absorbance versus time for the additive-containing and untreated polymer heated at 115, 128, 140 and 147^{0}C. The plots obtained for the absorbances at 1550 and 1729 cm^{-1} for the samples containing either 1.5 % 2-NDPA or 3 % THN were nearly identical for every measurement taken and thus the IR data obtained for each of these samples are presented as a single plot in figs.7.1A - H. At 115, 128 and 140^{0}C fairly linear plots of carbonyl absorbance versus time are obtained for the additive-containing and untreated polymer. At 147^{0}C plots are non-linear and no particular trend is obvious. The plots obtained at 115, 128, 140 and 147^{0}C all show that THN and 2-NDPA have a greater influence on reducing carbonyl formation than BDM. PNMMO containing 1.5 % and 3 % by mass of 2-NDPA and THN respectively, consistently show a 25 - 30 % reduction in development of carbonyl absorbance.

Plots of absorbance at 1550 cm^{-1} versus pyrolysis time are non-linear. The rate of growth of this peak decreases as pyrolysis time increases in nearly all 15 plots obtained at 128, 140 and 147^{0}C. Conversely at 115^{0}C the equivalent plots are fairly linear. We propose that at temperatures greater than approximately 120^{0}C significant concentrations of the tertiary nitro species produced during thermal decomposition of PNMMO decompose via loss of NO_2. Consequently it appears that the concentration of the tertiary nitro species tends to a plateau value with increasing pyrolysis time at temperatures greater than 120^{0}C. At temperatures lower than 120^{0}C the formation of the nitro species is thought to occur to a far greater extent than its subsequent decomposition, thus generating more linear plots of

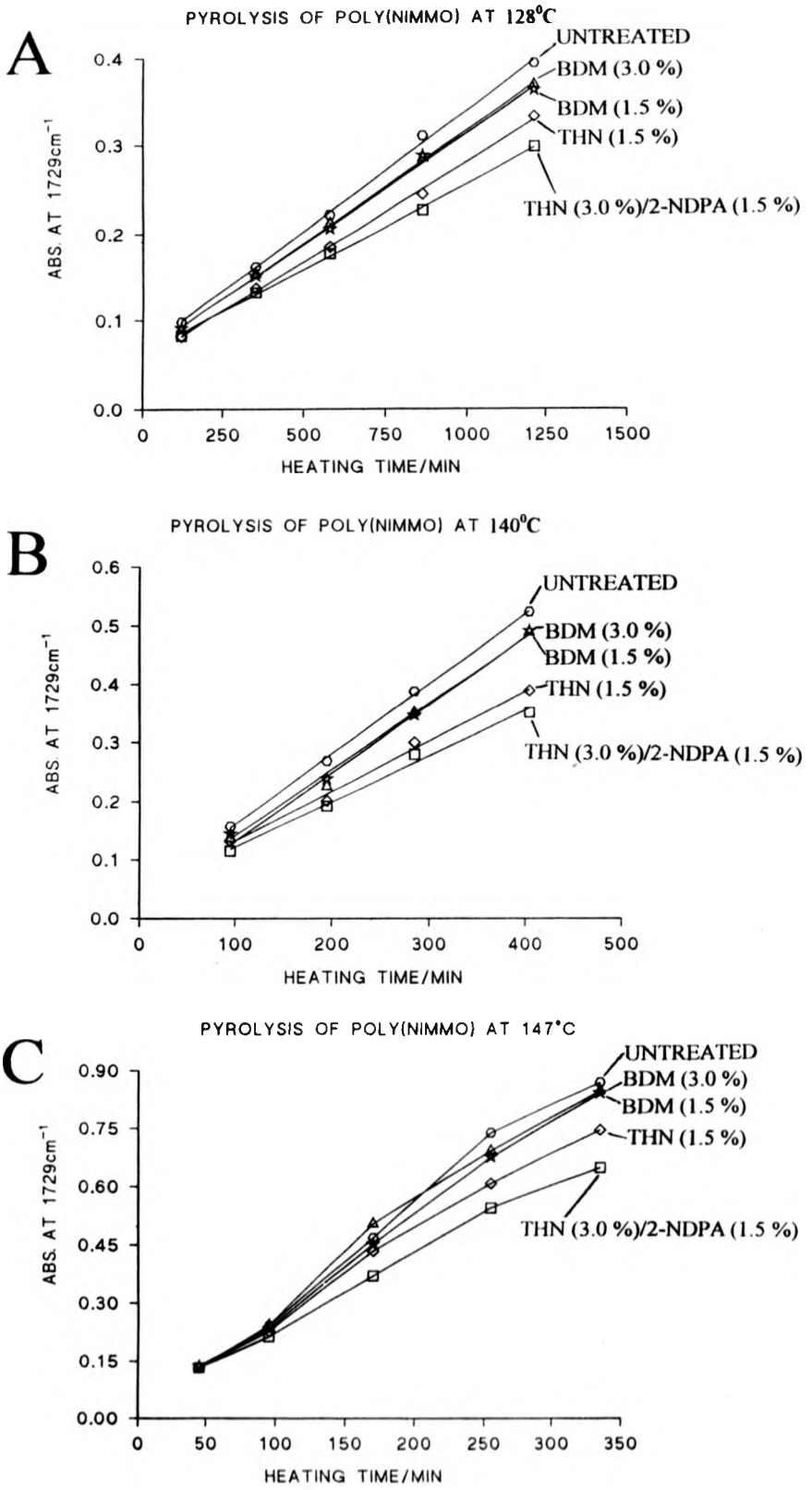

FIG 7.1A,B,C PLOTS OF CARBONYL ABSORBANCE VS. TIME FOR ADDITIVE-CONTAINING AND UNTREATED PNMMO HEATED AT VARIOUS TEMPERATURES

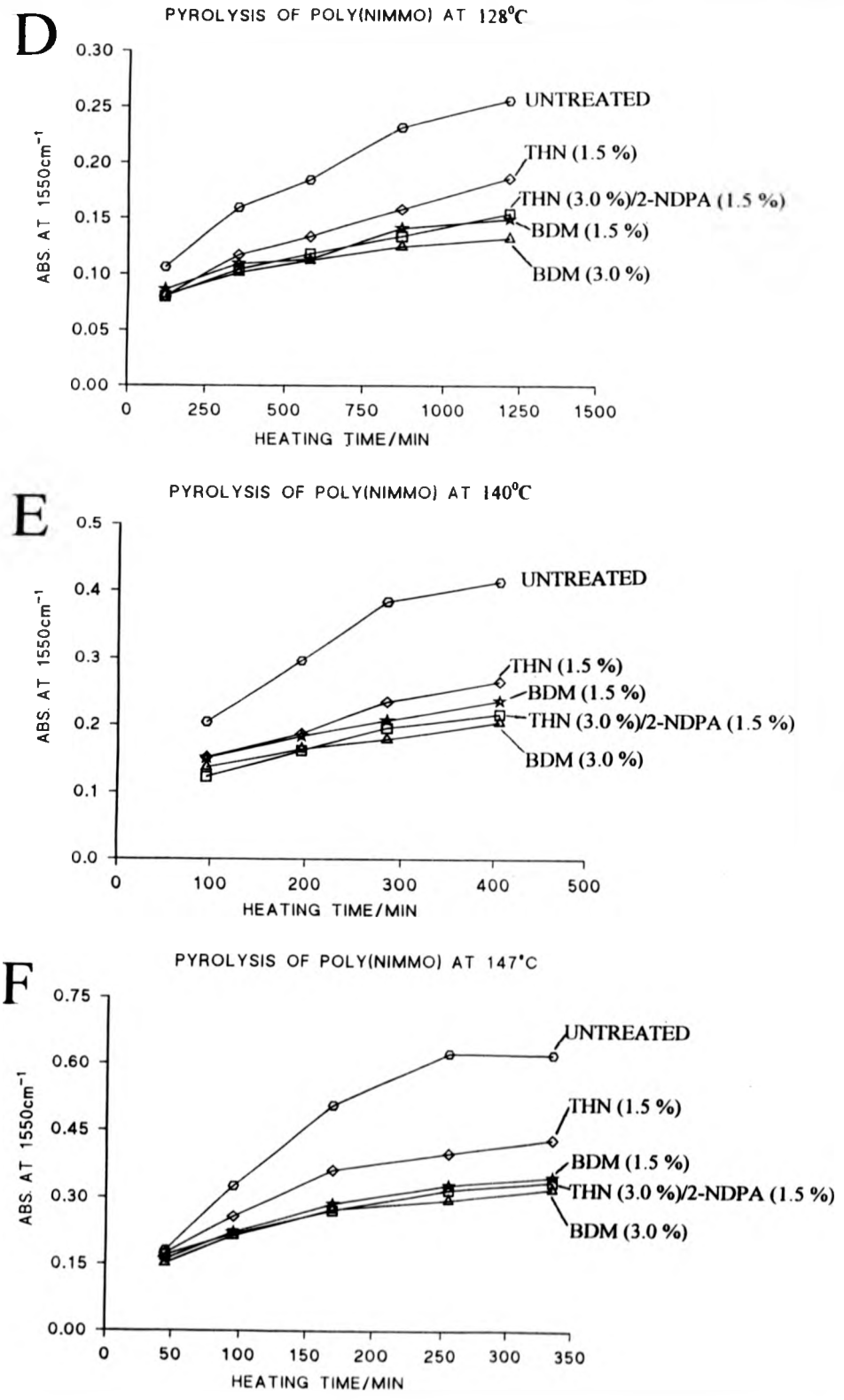

FIG 7.1D,E,F PLOTS OF NITRO (1550 cm^{-1}) ABSORBANCE VS TIME FOR ADDITIVE-CONTAINING AND UNTREATED PNMMO HEATED AT VARIOUS TEMPERATURES

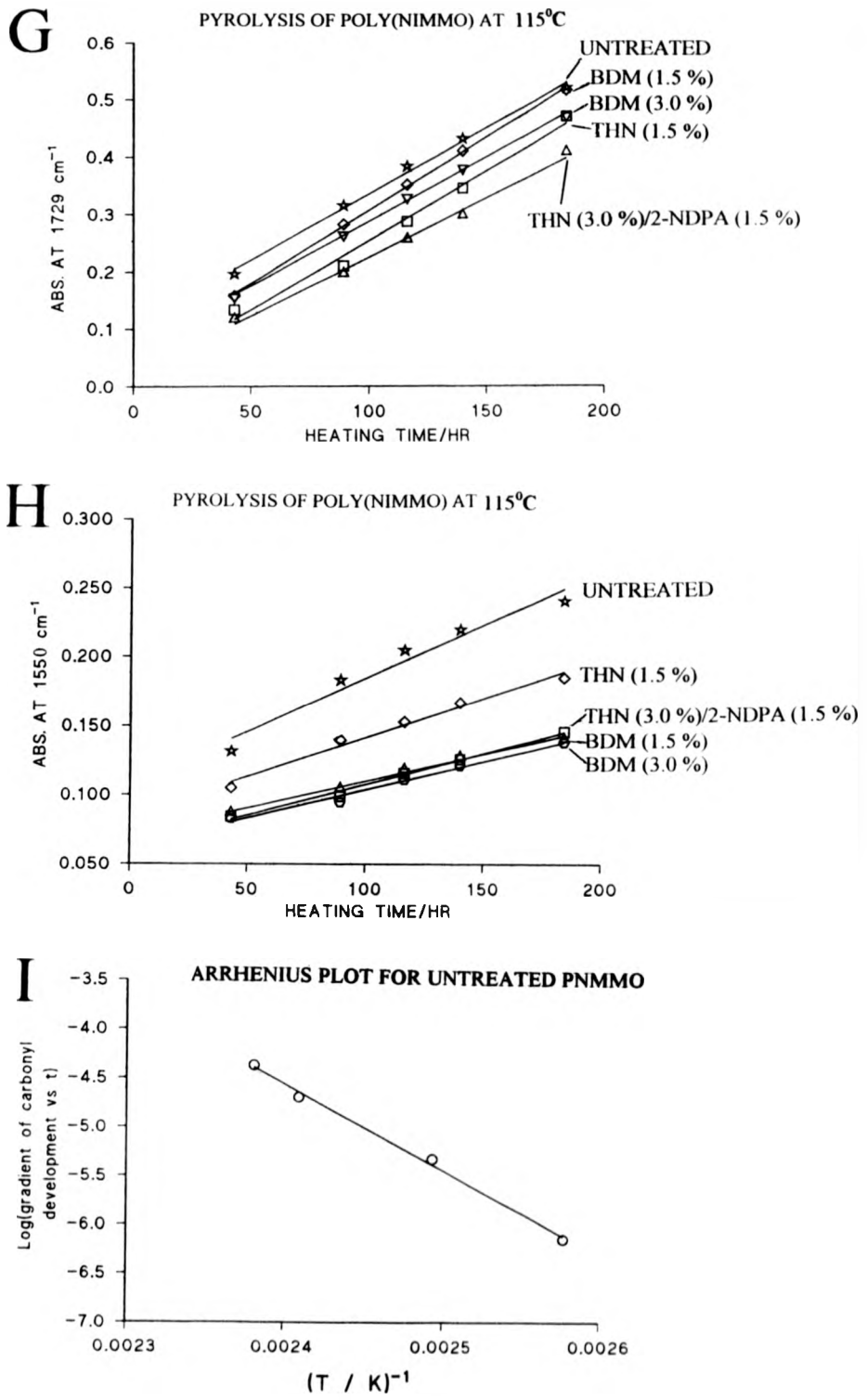

FIG 7.1G,H PLOTS OF CARBONYL AND NITRO ABSORBANCE VS TIME FOR ADDITIVE-CONTAINING AND UNTREATED PNMMO HEATED AT 115°C
FIG 7.1I(BOTTOM) ARRHENIUS PLOT OBTAINED FOR UNTREATED PNMMO

absorbance at 1550 cm^{-1} versus time. The additives appear to have a more substantial effect on reducing the development of the peak at 1550 cm^{-1} than at 1729 cm^{-1}. BDM (3 %) and BDM (1.5 %) induce 50 and 40 % reductions respectively in peak absorbance at 1550 cm^{-1} while THN (3 %) and 2-NDPA (1.5 %) induce approximately 45 % reductions at 1550 cm^{-1}. Consequently BDM is considered to be as equally effective as 2-NDPA in reducing the rate of formation of the nitro species, but less effective in reducing the rate of carbonyl growth. 2-NDPA is thus the most effective stabiliser of the three potential stabilisers examined but the stabilising capacity of the hydrogen donor additives in PNMMO has been demonstrated. 2-NDPA is thought to react with NO_2 as follows[7];

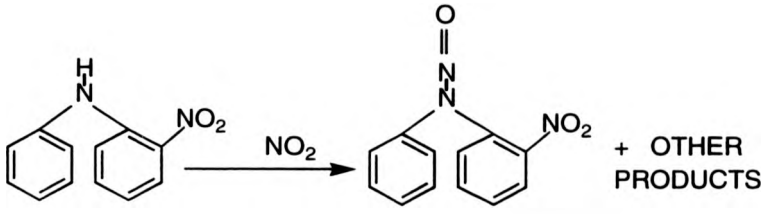

The mechanism of action of BDM and THN to reduce the rate of formation of the tertiary nitro species can only be presumed to occur via hydrogenation of evolved NO_2 to give HNO_2 or hydrogenation of the tertiary carbon-centred radical produced following the loss of NO_2 and subsequent loss of CH_2O from the nitrate ester side-chains in PNMMO during pyrolysis. The hydrogenation of the alkoxy radical produced after loss of NO_2 from the PNMMO side-chains is less likely due to its relatively high reactivity and energetically favourable loss of CH_2O.

Fig.7.1I shows the Arrhenius plot for PNMMO of log(gradient of carbonyl development versus time) against the reciprocal of temperature. The product-moment coefficient of correlation, r, was calculated to be -0.998 (-1 ≡ perfect negative correlation) thus showing that a strong degree of negative correlation exists between the data points and the 'best fit' line. The activation energy was calculated to be 170.4 ± 6 kJ mol^{-1}. As expected, this value is very close to the value for the bond dissociation energy of around 170 kJ mol^{-1} for the O-NO_2 bond. Gaseous methyl and ethyl nitrate exhibit 'normal' kinetic parameters, the observed activation energies (170 kJ mol^{-1}) being close to the O-NO_2 bond dissociation energies.

SEC chromatograms of all of the pyrolysed samples were also run. It was found that the molecular weight averages obtained from the chromatograms of the samples of pyrolysed PNMMO containing the additives (THN, BDM and 2-NDPA) were consistently higher in every sample than those of pyrolysed 'virgin' PNMMO. We attribute this to the findings of Coleman *et al.*[2] who propose that particularly BDM and possibly also THN may act as oxygen scavengers. Consequently loss of hydrogen from the PNMMO backbone may more likely result in a cross-linking reaction with another polymer radical as opposed to hydroperoxy formation, thus leading to a greater concentration of cross-linked material in the pyrolysed additive containing polymer as compared to the pyrolysed 'virgin' polymer.

7.2 EXPOSURE OF UNTREATED PNMMO TO GASEOUS NO_2 AND NO

Clearly, as shown by the gas-phase IR spectra obtained from the pyrolysis of PNMMO and from the activation energy obtained for PNMMO in section 7.1, significant quantities of NO_2(g) are generated during the pyrolysis of PNMMO. We have shown that an unknown proportion of this evolved NO_2 recombines with the tertiary carbon-centred radical

to generate the nitroalkane. Hiskey *et al.*[6] have used ^{15}N labelling experiments to show that the tert-butyl radical generated after loss of NO_2 and CH_2O from neopentanol nitrate does not exclusively combine with the NO_2 derived from the same parent neopentanol nitrate (see introduction). We propose that the relatively high viscosity of PNMMO most likely increases the probability that the tertiary carbon-centred radical does combine with the NO_2 derived from the same parent nitrate ester. However it appears likely that an unknown concentration of NO_2 may react with PNMMO in a number of different ways and thus the reaction of PNMMO with NO_2 at room temperature and elevated temperature is of consequence. The reaction of $NO_2(g)$ with polymers has received very little attention. The changes in the mechanical properties of nylon on exposure to $NO_2(g)$ at ambient temperature and pressure have been studied by Smith *et al.*[8] who propose that NO_2 may abstract hydrogen from the polymer chain to form nitrous acid. The newly formed polymer radical may then recombine with NO_2 or undergo chain scission or cross-linking reactions. The formation of HNO_2 during exposure of organic compounds to NO_2 has also been reported by March[9].

At ambient temperature and pressure NO_2 is a mixture of both NO_2 and its dimer N_2O_4 and possibly lesser quantities also of other nitrogen oxides. This was confirmed by gas-phase IR spectra of the gas released from our cylinder of NO_2 which showed absorbances predominantly for $NO_2(g)$ but also for $N_2O_4(g)$ (data not shown). Samples of PNMMO, PPO and PEO were placed in separate round bottomed flasks and both qualitative and quantitative experiments were performed as described in section 2.2.3. The quantitative experiments were performed using vacuum line apparatus and the gases were analysed via gas-phase IR spectroscopy before and after exposure to the respective polymer.

The gas phase IR spectrum of NO(g) showed no apparent impurities. As expected, due to its relatively low reactivity, NO(g) showed no apparent reaction with any of the three polymers. Analysis of the gas after exposure to the polymers for up to 24 h at room temperature showed no changes in the gas-phase IR spectrum. Similarly the solution IR spectra of the polymers showed no apparent changes. By contrast $NO_2(g)$ showed considerable reaction with all three polymers. Preliminary experiments were performed by exposing PNMMO to $NO_2(g)$ in air at room temperature over various lengths of time. Solution IR spectra of the resulting polymer showed considerable carbonyl formation and new absorptions in the region of 1710 - 1740 cm^{-1} were apparent. ^1H and ^{13}C NMR spectra of PNMMO obtained after 10 h exposure showed sharp new resonances around 9.5 and 202 ppm respectively. Although 2-D NMR experiments could not be performed due to the low intensity of these resonances, by a process of elimination they can, with a reasonable degree of certainty, be assigned to the hydrogen atom and carbonyl group present in an aldehyde. Carboxylic acids commonly show considerably different chemical shifts to those observed here and although ketones would be expected to show a carbonyl resonance around 200 ppm, no associated hydrogen resonance is expected around 9.5 ppm. We have shown in previous sections that PNMMO evolves significant quantities of formaldehyde on pyrolysis. To eliminate the possibility that these new resonances (9.5 and 202 ppm) were associated with formaldehyde, we recorded ^1H and ^{13}C NMR spectra of untreated PNMMO doped with paraformaldehyde and, neat paraformaldehyde in $CDCl_3$. In both cases a small proportion of the paraformaldehyde dissociates to yield formaldehyde and thus its associated ^1H and ^{13}C NMR resonances at 9.72 and 194.8 ppm respectively. The NMR shifts of formaldehyde in various solvents were also measured by Bercovici *et al.*[10] who found identical values to ours using $CDCl_3$ as a solvent. It appears therefore that the new resonances at 9.5 and 202 ppm in

the ^{1}H and ^{13}C NMR spectra which appear on exposure of PNMMO to $NO_2(g)$ cannot be attributed to formaldehyde. Other small molecules such as acetaldehyde and formic acid can also be eliminated on the basis of their chemical shifts. Consequently the new resonances are attributed to an aldehyde end group in PNMMO.

The NMR spectra of PNMMO exposed to $NO_2(g)$ for longer than 24 h show weak new resonances around 11.5 ppm in the ^{1}H NMR, strong new resonances around 177 ppm in the ^{13}C NMR spectra and the resonances attributed to the aldehyde disappear. We attribute the weak new resonances around 11.5 ppm to a carboxylic acid formed after extensive degradation of the polymer sample by NO_2 (presumably further oxidation of the aldehyde species may result in the formation of carboxylic acids). The resonances around 177 ppm consist of many peaks which may be associated with more than one carbonyl species, but we propose that the formation of ester species account for a significant proportion of these resonances. Ester species may be formed by the direct oxidation of the main chain methylene carbons in PNMMO; following alkoxy formation, a cage mechanism may then generate an ester. The mechanism of oxidation of PNMMO by $NO_2(g)$ proposed by us is shown at the end of this section. A new broad resonance is also visible around 7 ppm in the ^{1}H NMR spectrum of PNMMO exposed to $NO_2(g)$ and is seen to shift to lower field with increasing exposure (to NO_2) times. This resonance disappears on addition of D_2O to the $CDCl_3$ solution thus confirming the presence of an exchangeable hydrogen. Doping untreated PNMMO with HNO_2 or HNO_3 produces an exactly similar broad resonance in the ^{1}H NMR ranging from 6.0 ppm (0.05 g HNO_3/1.0 g PNMMO) to 8.6 ppm (0.2 g HNO_3/1.0 g PNMMO). The similar line shape, concentration effect and positive 'D_2O shake' result strongly suggest that the peak around 7 ppm in the ^{1}H NMR is attributable to HNO_2/HNO_3. A similar peak around 7 ppm in the ^{1}H NMR was also observed for samples of PNMMO

exposed to $NO_2(g)$ under anaerobic conditions although the relative concentration of HNO_2/HNO_3 was significantly less. This was presumably a consequence of the reduced effect of moisture under anaerobic conditions. Consequently the degradation of PNMMO using $NO_2(g)$ performed under aerobic conditions is most likely catalysed by the greater concentration of HNO_2/HNO_3 present. Absorptions for HNO_2/HNO_3 are also visible in the solution IR spectra of degraded PNMMO around 1350, 1660 and 3400 cm^{-1} [11,12].

Experiments under anaerobic conditions were performed using identical amounts of PNMMO and $NO_2(g)$ in each flask. One flask was left at room temperature for 12 h, while another similar flask was left for 12 h in an oven at 60^0C. Fig.7.2 shows the solution IR spectra, run using identical concentrations of polymer in $CDCl_3$, of the degraded polymer obtained from each flask. Clearly fairly extensive degradation of the sample has occurred after only 12 h exposure to $NO_2(g)$ and new absorptions are visible around 1740 and 1715 cm^{-1} in both samples, although to differing relative intensities, and additional absorptions are visible at 1560 and approximately 1660 cm^{-1} in the IR spectrum of the heated sample. The ^1H NMR spectra of both samples show new resonances around 9.5 and 11.5 ppm, previously assigned to the aldehyde and carboxylic acid protons. The ^{13}C NMR spectra show the corresponding carbonyl resonances around 202 and 177 ppm respectively. Like the previous spectra, the prominent new resonances around 177 ppm consist of many peaks most likely attributed predominantly to ester species due to the low intensity of the carboxylic acid protons in the ^1H NMR. The new band around 1740 cm^{-1} in the solution IR spectrum of degraded PNMMO is also consistent with an ester species. The absorption at 1560 cm^{-1}, only visible in the IR spectrum of the heated sample, appears in the region for the asymmetric stretch of nitroalkanes, and new absorptions in the ^{13}C NMR spectrum around 70 - 80 ppm are similarly indicative of the carbon α to the nitro group in a nitroalkane. IR

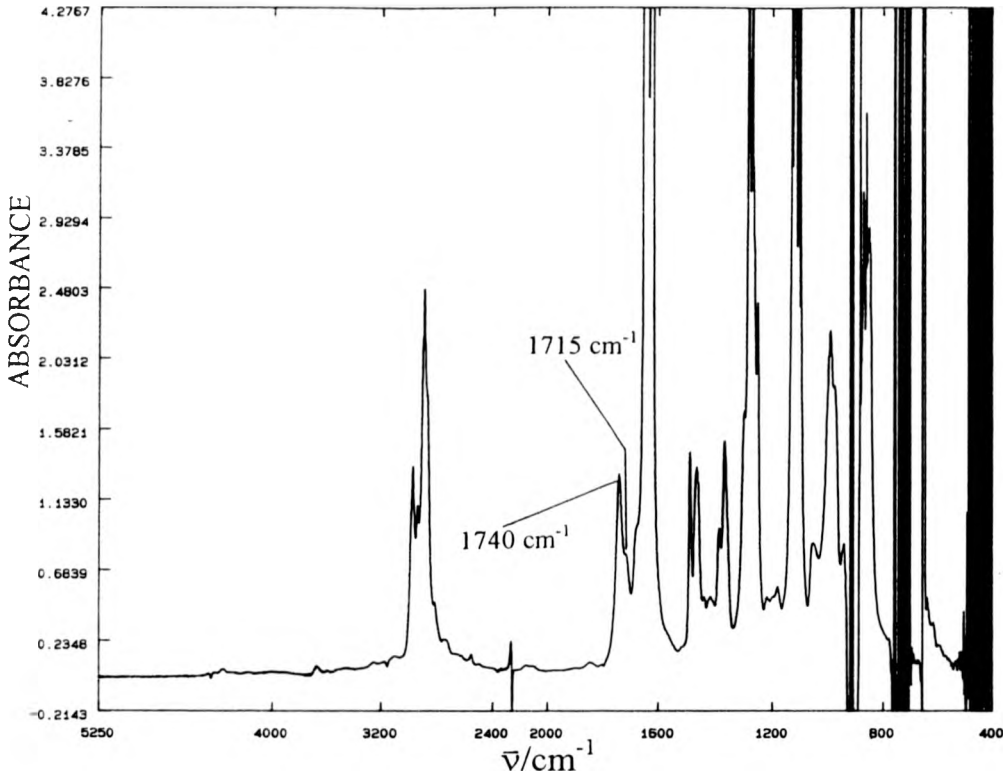
4.2767
3.8276
3.3785
2.9294
2.4803
2.0312
1.5821
1.1330
0.6839
0.2348
-0.2143
ABSORBANCE
1715 cm-1
1740 cm-1
5250
4000
3200
2400
2000
1600
1200
800
400
ν̄/cm-1

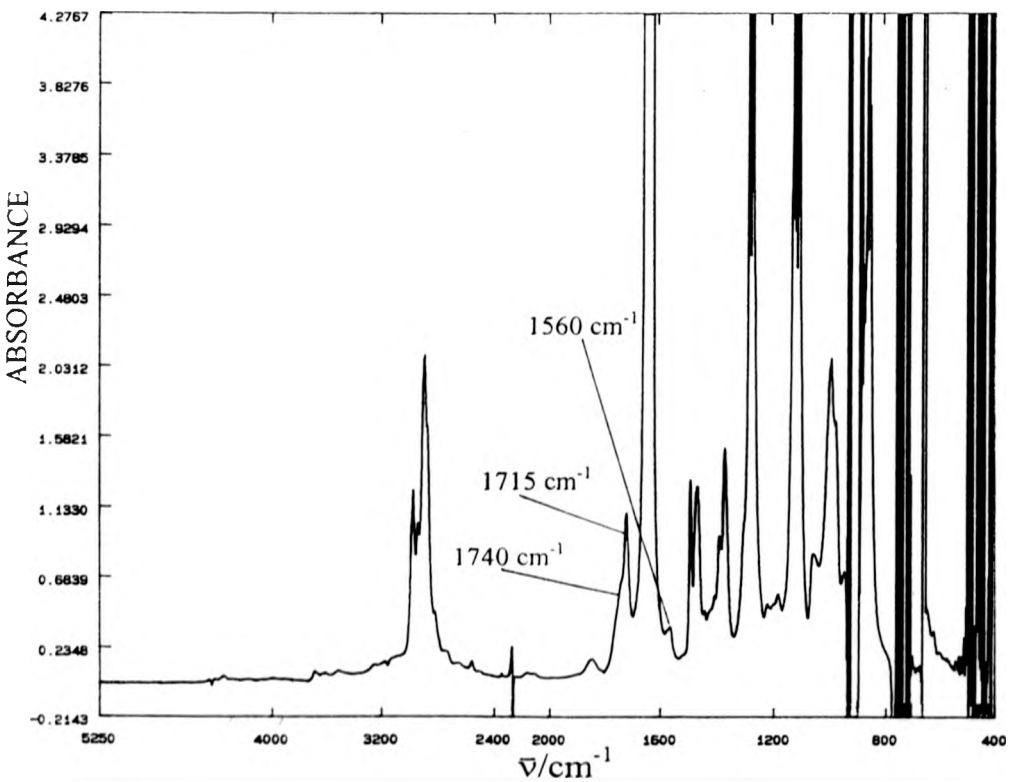
4.2767
3.8276
3.3785
2.9294
2.4803
2.0312
1.5821
1.1330
0.6839
0.2348
-0.2143
ABSORBANCE
1560 cm-1
1715 cm-1
1740 cm-1
5250
4000
3200
2400
2000
1600
1200
800
400
ν̄/cm-1

FIG.7.2A SOLUTION IR SPECTRUM OF PNMMO EXPOSED TO NO_2(g) FOR 12 h AT ROOM TEMPERATURE

FIG.7.2B SOLUTION IR SPECTRUM OF PNMMO EXPOSED TO NO_2(g) FOR 12 h AT 60^0C

difference spectra of the degraded sample show many new absorptions in the region 1400 - 1000 cm^{-1} and thus it is not possible to assign a symmetric absorption. The absorption at 1660 cm^{-1}, similarly only visible in the IR spectrum of the heated sample, appears in the region for both nitrate and nitroso species but cannot be positively assigned. Fig.7.3 shows the gas phase IR spectrum of the remaining gases obtained after exposure to PNMMO at 60^0C. Many new absorptions for NO, N_2O, CO_2 and CO are visible and the absorptions for NO_2 and N_2O_4 have significantly reduced in intensity. Presumably degradation of the polymer by either NO_2 or heat leads to the generation of CO_2 and CO. A control experiment was run to ensure that both N_2O and NO were formed as a result of reaction with the polymer and it was found that NO was produced but in far lower concentrations. It appears therefore that both NO_2 and N_2O_4 have reacted with PNMMO, resulting in the formation of NO and N_2O. Gas phase IR spectra of the gases obtained after exposure to PNMMO at room temperature showed much lesser quantities of CO, CO_2 and NO and thus it appears that both CO and CO_2 result predominantly from the thermal decomposition of PNMMO at 60^0C. It is difficult to draw definitive conclusions as to exactly which oxide of nitrogen generates which of the degradation products observed in the solution and gas phase IR spectra. At 160^0C and 1 atm, NO_2(g) exists nearly solely as NO_2(g) and virtually no dimerisation is observable[8]. However many attempts to expose PNMMO to NO_2(g) at temperatures in this range, thus eliminating the effects of N_2O_4, failed due to the large volumes of gas evolved from PNMMO and the inability to bubble gas through this highly viscous polymer. At temperatures in excess of 110^0C, sealed glass containers containing NO_2(g) and PNMMO ruptured and IR and NMR spectra of the resulting polymer contained so many new peaks that analysis was impossible.

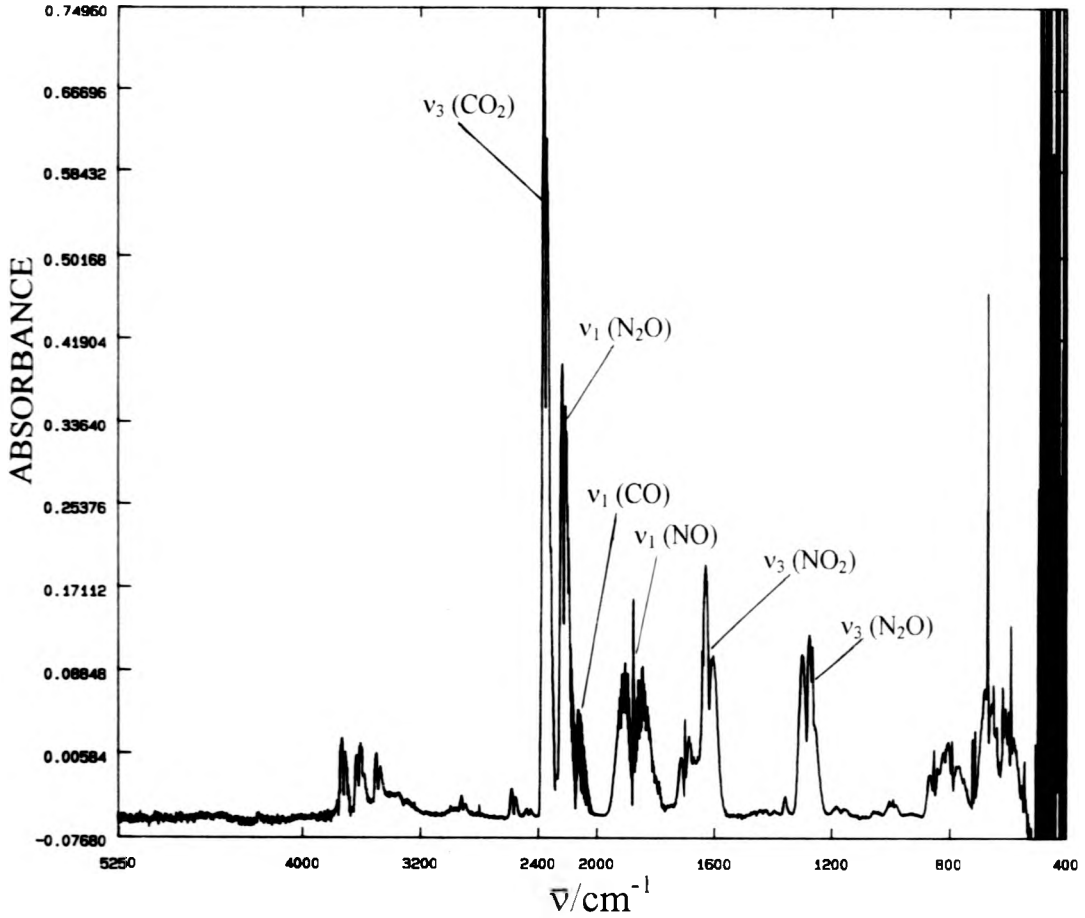

FIG 7.3 THE GAS PHASE IR SPECTRUM OF THE REMAINING GASES OBTAINED AFTER EXPOSURE TO PNMMO AT 60^0C

It is clear that the exposure of PNMMO to NO_2(g) produces a complex mixture of degradation products even after relatively short exposure times (12 h). It appears that at elevated temperature (60^0C) the reaction of NO_2(g) with PNMMO results in the formation of nitroalkane and possibly also nitroso and nitrate species in PNMMO not apparent at room temperature. The nitroalkane produced during thermal degradation of PNMMO absorbs at 1550 cm^{-1} in the IR. The asymmetric absorption of the nitro group increases in wavelength on moving from a nitro group attached to a tertiary carbon, to a nitro group attached to a primary carbon[1] and thus the absorption at 1560 cm^{-1}, attributed to the nitro species produced during exposure of PNMMO to NO_2(g) at 60^0C, is characteristic of a secondary or primary as opposed to a tertiary nitro species. Indeed the difference in wavelength of only 10 cm^{-1} between the tertiary nitro species at 1550 cm^{-1}, points to the assignment of a secondary as opposed to primary nitro species absorbing at 1560 cm^{-1}. We propose that the decomposition of the nitrate ester side-chains in the PNMMO sample exposed to NO_2(g) at 60^0C is negligible as compared to the abstraction of hydrogen by NO_2 from any one of the three methylene carbons in each monomer unit. Subsequent reactions of the secondary carbon-centred radical such as chain scission, cross-linking and recombination with NO_2, generating the absorption at 1560 cm^{-1} in the IR spectrum, may then occur. SEC chromatograms of the degraded polymer show an overall decrease in M_n and M_w suggesting that chain scission is favoured over cross-linking. Similar exposure of PPO to NO_2(g) also produced an absorption at 1562 cm^{-1} in the solution IR spectrum of degraded PPO.

As we have shown, the exposure of PNMMO to NO_2(g) for relatively short times (5 h) leads to the formation of an aldehyde exhibiting resonances at 202 and 9.5 ppm in the ^{13}C and ^{1}H NMR spectra respectively. These same peaks are observed, although only at relatively low intensity, during pyrolysis of PNMMO (see ^{13}C NMR spectrum of pyrolysed

PNMMO run at 100^0C, fig.5.6 and ^{1}H NMR spectrum, fig.5.4A). The preliminary stages of oxidation of PNMMO by NO_2(g) apparently produce the same aldehyde species observed during pyrolysis. Consequently we propose that the aldehyde generated during pyrolysis of PNMMO is a result partly of the reaction of evolved NO_2 with PNMMO. It is also possible that some aldehyde results as a direct consequence of pyrolysis. Thus during pyrolysis, formation of the aldehyde may occur via the following mechanism (for simplicity, only one monomer unit in the polymer chain is shown in the scheme);

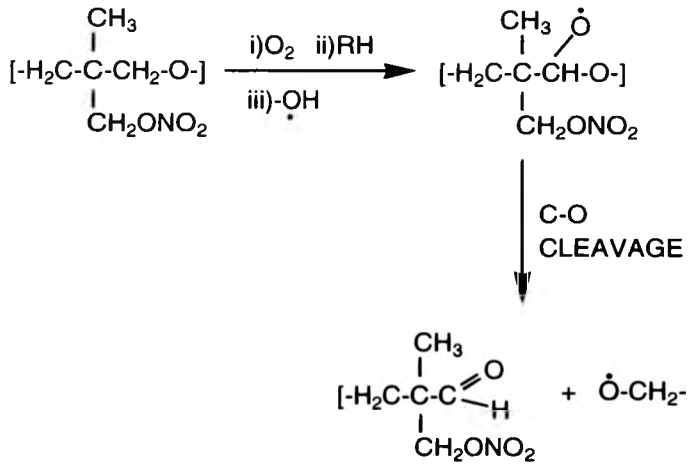

PROPOSED MECHANISM FOR THE FORMATION OF AN ALDEHYDE DURING PYROLYSIS OF PNMMO

Clearly the hydrogen resonance associated with the aldehyde around 9.5 ppm is expected to be a sharp singlet as no coupling with any of the nearest hydrogens four bonds distant is predicted and this is borne out in the ^{1}H NMR spectra of pyrolysed PNMMO (fig.5.4A) and PNMMO exposed to NO_2(g).

Presumably the abstraction of a hydrogen atom from the methylene side chains in PNMMO followed by hydroperoxy and subsequent alkoxy formation is also possible. The elimination of $\bullet NO_3$ may then generate an aldehyde with similar chemical shifts to that shown in the mechanism on the previous page.

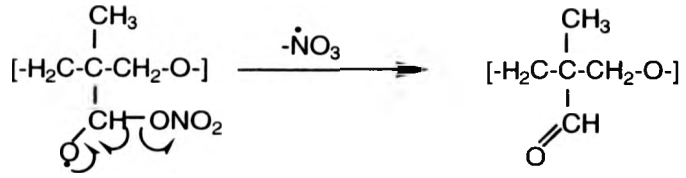

An alternative mechanism for the formation of the aldehyde during pyrolysis may involve the loss of NO_2 and the subsequent abstraction of hydrogen from the resulting alkoxy radical by NO_2 in a cage mechanism similar to that proposed to occur during pyrolysis of neopentanol nitrate[6]. Thus the formation of the aldehyde via oxidation at either the main chain or side chain methylenes appears possible. However, aldehyde formation via the main chain methylenes must result in the cleavage of the C-O bond in the main chain. Previous research concerning the photo- and thermal degradation of PEO[13,14,15] and PPO[15,16,17] and our research of both the photo- and thermal degradation of PPO indicates that C-O bond cleavage is negligible following alkoxy formation on the main chain methylenes in either PEO or PPO; consequently aldehyde formation is not observed during degradation of PEO or PPO. We can offer no explanation for this but to comment that it is not a direct result of the bond energies as the C-O bond energy is lower (ca. 12 kJ mol^{-1}) than the C-C bond energy[13]. Clearly due to the structural differences between PNMMO and both PPO and PEO, C-C bond cleavage may occur in the main chain of PNMMO following alkoxy formation to generate an aldehyde, but it appears more likely particularly considering

the degradation mechanisms of PEO and PPO, that aldehyde formation results from the oxidation of the side chain methylenes in PNMMO. It is noteworthy that we have excluded the possibility that the aldehyde species are formed as a result of the oxidation of the primary alcohol end groups in PNMMO owing to the relatively low abundance of end groups. Thus it was not thought that the end groups would contribute sufficiently to generate an observable resonance around 202 ppm in the ^{13}C NMR.

The oxidation of PNMMO by NO_2 may occur via a similar mechanism to that shown above where the oxygen originates from NO_2 as opposed to the air. Indeed, preliminary research has been performed very recently by Nishiguchi *et al.*[18] and also by Addison[19] to show that nitrogen dioxide transforms ketals to ketones in the presence of silica gel. The function of the silica gel is not completely understood, but it may act as site for the oxidation or may influence the oxidation by its acidic character. The conversion of the ketal to the ketone is proposed to occur via an intermediate nitrite which may eliminate NO to leave an alkoxy radical. We propose a similar mechanism for the oxidation of PNMMO by $NO_2(g)$. Thus following the abstraction of hydrogen from the methylene carbons in PNMMO by NO_2, additional NO_2 may then recombine with PNMMO to give a nitrite which may then eliminate NO to give an alkoxy radical. Subsequently the main chain methylenes can generate either an aldehyde, formate ester or ester (cage mechanism) whereas the side chain methylenes can generate only an aldehyde or an ester. Very minor peaks at ca. 8.1 ppm of much lower intensity as compared to those of the aldehyde around 9.5 ppm are visible in the ^{1}H NMR spectrum of PNMMO exposed to NO_2 at room temperature. These peaks are attributed to the previously assigned formate ester and their presence indicates that in addition to significant ester formation via a cage mechanism, oxidation of the main chain

methylenes by NO_2 also generates some formate ester via C-C bond scission adjacent to the alkoxy radical.

It is noteworthy therefore that the degradation of PNMMO during storage at room temperature may produce much larger quantities of ester and aldehyde as opposed to formate ester.

7.3 EXPOSURE OF PYROLYSED PNMMO TO GASEOUS NO_2

The evolution of NO_2(g) from PNMMO will presumably occur until decomposition of all the nitrate ester side chains has taken place. It is likely therefore that evolved NO_2 will react with the thermal degradation products, namely the formate ester and aldehyde, to generate further degradation species. A series of experiments were therefore performed to assess the extent of reaction, if any, of NO_2(g) with pyrolysed PNMMO. Qualitative experiments were performed in air at room temperature. Samples of pyrolysed PNMMO (10 h/145^{0}C) were exposed to NO_2(g) over various periods of time. Fig.7.4 shows the ^{1}H NMR spectra of pyrolysed PNMMO before and after exposure to NO_2(g). The peak attributed to the formate ester protons around 8.05 ppm has completely disappeared, as have the peaks around 4.2 ppm attributed to the methylene hydrogens β to the carbonyl group in the formate ester. As expected, a new singlet resonance is visible at 9.5 ppm due to aldehyde formation resulting from the reaction of NO_2 with PNMMO (see also inset showing the associated aldehyde resonance in the ^{13}C NMR). A new singlet is also visible at 8.01 ppm, not observed during exposure of untreated PNMMO to NO_2. This new singlet appears to increase in intensity with longer exposure times to NO_2 as the peak due to the formate ester hydrogen at 8.05 ppm decreases in intensity. Integration of these resonances shows that the new resonance at 8.01 ppm is present in a much lower concentration as compared to the

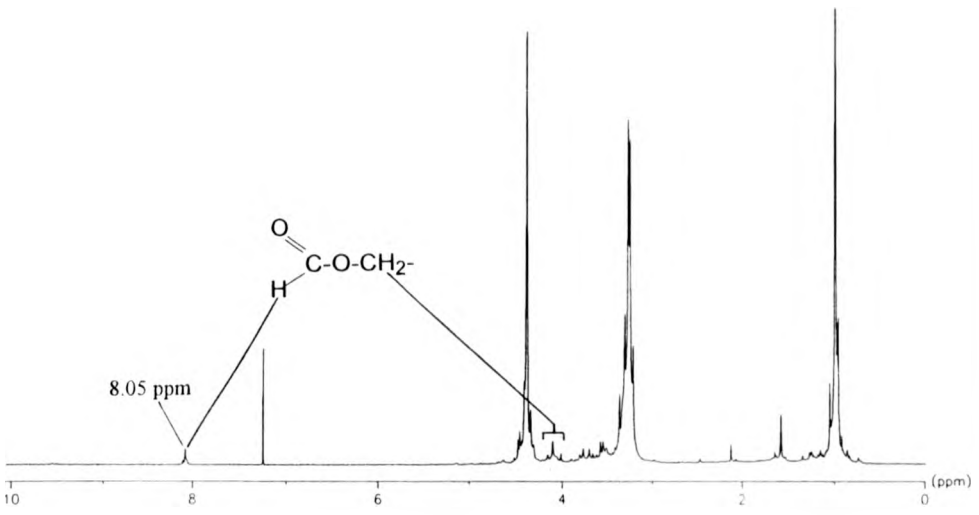

FIG.7.4A ^{1}H NMR SPECTRUM OF PYROLYSED (10 h/145^{0}C) PNMMO

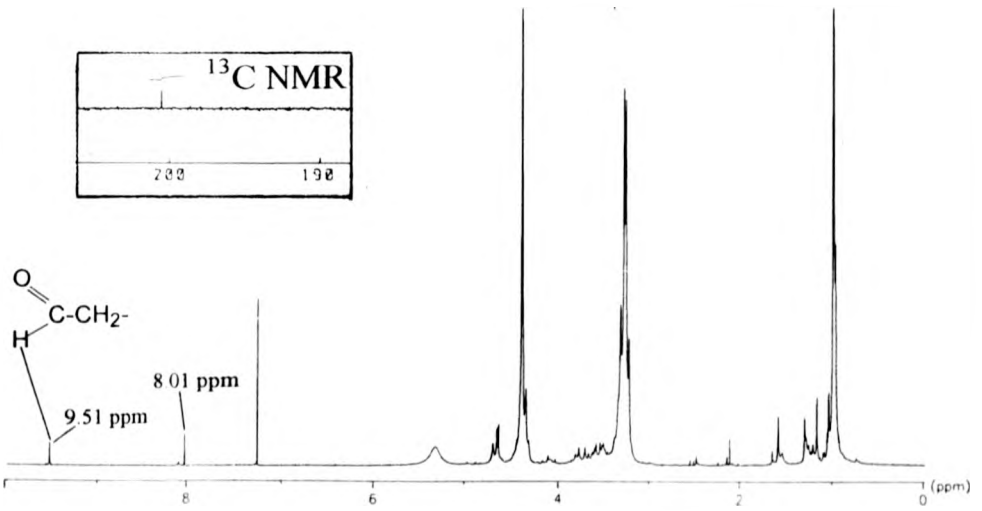

FIG.7.4B ^{1}H NMR SPECTRUM OF PYROLYSED (10 h/145^{0}C) PNMMO EXPOSED TO NO_2(g)

original formate ester hydrogens at 8.05 ppm. We tentatively propose therefore that the reaction of the formate ester with NO_2 occurs predominantly via the reaction scheme shown over the page, i.e. abstraction of the formate hydrogen, but hydrogen abstraction may also occur at an adjacent methylene carbon with subsequent recombination of NO_2 to produce a relatively low concentration of a new formate ester species with a slightly altered chemical shift (8.01 ppm). The solution IR spectra of pyrolysed PNMMO exposed to NO_2 also show a reduction in the carbonyl absorption around 1729 cm^{-1}, although new peaks are visible in the carbonyl region after long exposure to NO_2. It appears therefore that NO_2 reacts with the formate ester produced during pyrolysis resulting in an <u>apparent</u> reduction in the concentration of degradation species, although it is clear that different degradation species will result. The reaction of NO_2 with the formate ester may have been anticipated due to the reactivity of the formate ester proton. Presumably NO_2 abstracts this hydrogen as follows;

Subsequently the resulting carbon-centred radical most likely expels CO(g) or CO_2(g) to give either an alkoxy or another carbon-centred radical either of which will undergo further reaction. It is clear that this same hydrogen abstraction reaction shown above may occur during the pyrolysis of PNMMO, leading to a reduction in the concentration of formate ester produced during pyrolysis. Thus the formate ester may generate many secondary oxidation products during the pyrolysis of PNMMO.

7.4 PHOTOLYSIS OF UNTREATED, CURED AND UNCURED PNMMO

The predominant reactions which occur during the photo-oxidative degradation of all polymers are believed to be similar and these are clearly defined by Rabek[17]. Initiation is believed to proceed via the abstraction of hydrogen by either molecular oxygen or hydroxy radicals. The resulting polymer radical may then react with oxygen to generate a polymer peroxy radical which can further react to produce carbonyl species. The photo-oxidation of many polymers such as PE[20,21,22], PP[23,24], PEO[15] and PPO[15] has been studied and the rate of photo-oxidation has been shown to be dependent on both the wavelength and intensity of the irradiation source.

Clearly the aim of our work was to elucidate the degradation mechanisms of PNMMO with the eventual hope of finding a suitable stabiliser to prolong the polymer's shelf life. Consequently, all aspects of the degradation of PNMMO were of interest to us and in particular the photo-oxidative degradation which may play a significant role in the degradation process once PNMMO is exposed to ambient light, especially in sunny climates. Preliminary experiments were performed by coating thin films of neat untreated PNMMO on sodium chloride plates. The plates were mounted horizontally and films were irradiated in air using a 350 W xenon lamp. New IR bands were monitored simply by placing the sodium chloride plate in the IR spectrometer. However, many difficulties were associated with this apparently simple technique; only relatively small samples of PNMMO could be obtained for NMR analysis as the initial sample mass was only approximately 0.2 g. Other difficulties included the heating of the sample by the hot xenon lamp and the long photolysis times required to produce significant changes in the IR spectra of photolysed PNMMO. Preliminary experiments showed a new absorption at 1730 cm^{-1} in the solution IR spectra of neat samples of PNMMO photolysed in air. The absorption at 1730 cm^{-1} increases at a rate

similar to that for the formate ester absorption at 1729 cm^{-1} during pyrolysis at 110^0C and it was initially presumed that both absorptions were attributed to the carbonyl group in the formate ester. However, although the quantity of photolysate was too small for sufficient resolution in the carbonyl region of the ^{13}C NMR spectrum, ^1H NMR spectra (see fig.7.5) showed two new singlet resonances around 9.5 ppm, one of which was previously attributed to an aldehyde, and a triplet resonance around 9.7 ppm. It appears therefore that the degradation products, namely the aldehydes and the formate ester, both show carbonyl absorptions at approximately the same wavelength in the IR. Indeed, the carbonyl absorptions of various organic compounds substantiate this and show that both formate esters and aldehydes feature carbonyl absorptions in the range 1720 - 1735 cm^{-1}.[25,26] The presence of a ketone cannot however be dismissed without ^{13}C NMR analysis. Thus preliminary experiments suggested that three different species of aldehyde were produced during the initial stages of photolysis. Very minor peaks were also observed around 8.05 ppm, previously attributed to the formate ester. These results indicate that photolysis produces similar oxidation products to those observed during oxidation of PNMMO by $NO_2(g)$ although clearly more than one species of aldehyde is produced during photolysis whereas only a single resonance around 9.5 ppm was observed during exposure to $NO_2(g)$. Evidently photolysis can be considered to contribute significantly to the degradation process.

Clearly larger quantities of the photolysate were needed for analysis via NMR and SEC. A solution photolysis of a larger quantity of PNMMO was therefore conducted. PNMMO (10.0 g) was dissolved in 1,2-dimethoxyethane (250 cm^3) and photolysis was performed using a 220 W water-cooled Hanovia lamp. The solution was placed in a glass cylinder (500 cm^3). The bulb of the lamp was inserted into the cylinder so that the solution surrounded the bulb and the cylinder was placed on top of a magnetic stirrer so that the

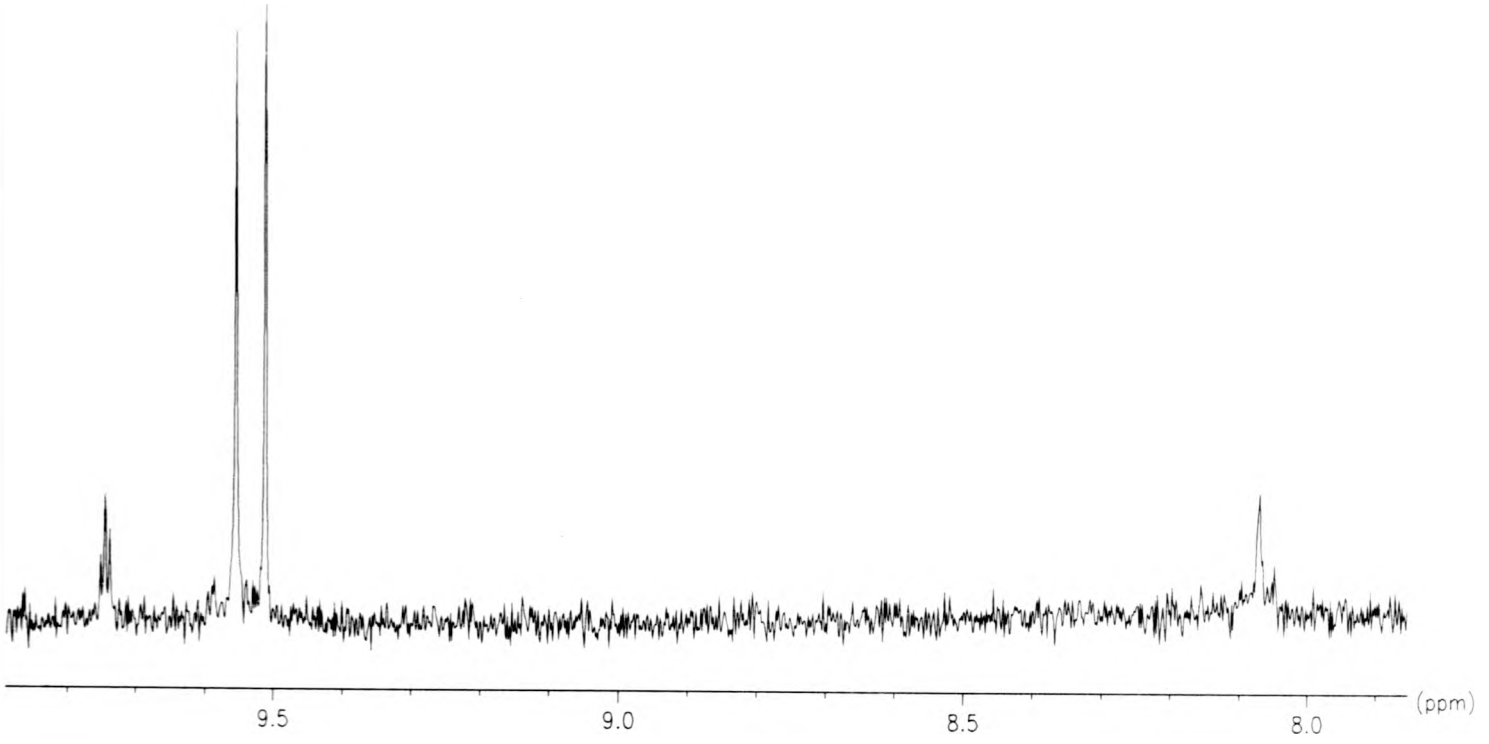

FIG.7.5 A PORTION OF THE ^{1}H NMR SPECTRUM OF PHOTOLYSED (350 W XENON LAMP) PNMMO

solution retained its homogeneity during photolysis. The solution was photolysed for a total of 459 h, during which samples were removed from time to time. 1,2-dimethoxyethane was removed using a rotary evaporator and both IR and NMR spectra were run in $CDCl_3$. Close monitoring of the temperature of the PNMMO solution during photolysis showed that it never exceeded 30^0C. This type of photolysis overcomes many of the difficulties associated with the photolysis of thin films of PNMMO (see previous page). However it is likely that the solvent, 1,2-dimethoxyethane, will also photodegrade to some extent. It was hoped that the degradation of the solvent would produce relatively low mass species which would be easily removed on the rotary evaporator and indeed this appeared to be borne out by experiment. The influence of the solvent, if any, on the degradation of PNMMO was unknown although it seemed possible that hydrogen transfer from the solvent molecules to polymer radicals may occur during photolysis.

Fig.7.6 shows the solution IR spectrum ($CDCl_3$) of photolysed (300 h) PNMMO obtained from the solution photolysis of PNMMO. The absorption attributed to the carbonyl group in the formate ester is clearly visible at 1729 cm^{-1}. This absorption increases in intensity during photolysis as does its associated C-O-C absorption around 1170 cm^{-1}. ^1H and ^{13}C NMR spectra of the photolysate are shown in fig.7.7 and clearly show significant new resonances for the formate ester at 161 and 8.1 ppm respectively. No new resonances are visible for the aldehyde around 9.5 ppm in the ^1H NMR. An additional new absorption is also visible at 1554 cm^{-1} in the solution IR spectrum of the photolysate. Clearly this absorption, which is only approximately one tenth as intense as the carbonyl absorption, appears at a very similar wavelength to that observed for the tertiary nitro species (1550 cm^{-1}) produced during pyrolysis of PNMMO. The formation of this nitro species entails the recombination of NO_2 and, because the viscosity of the polymer is reduced by the addition of solvent (1,2-dimethoxyethane), it is expected that the probability of recombination of

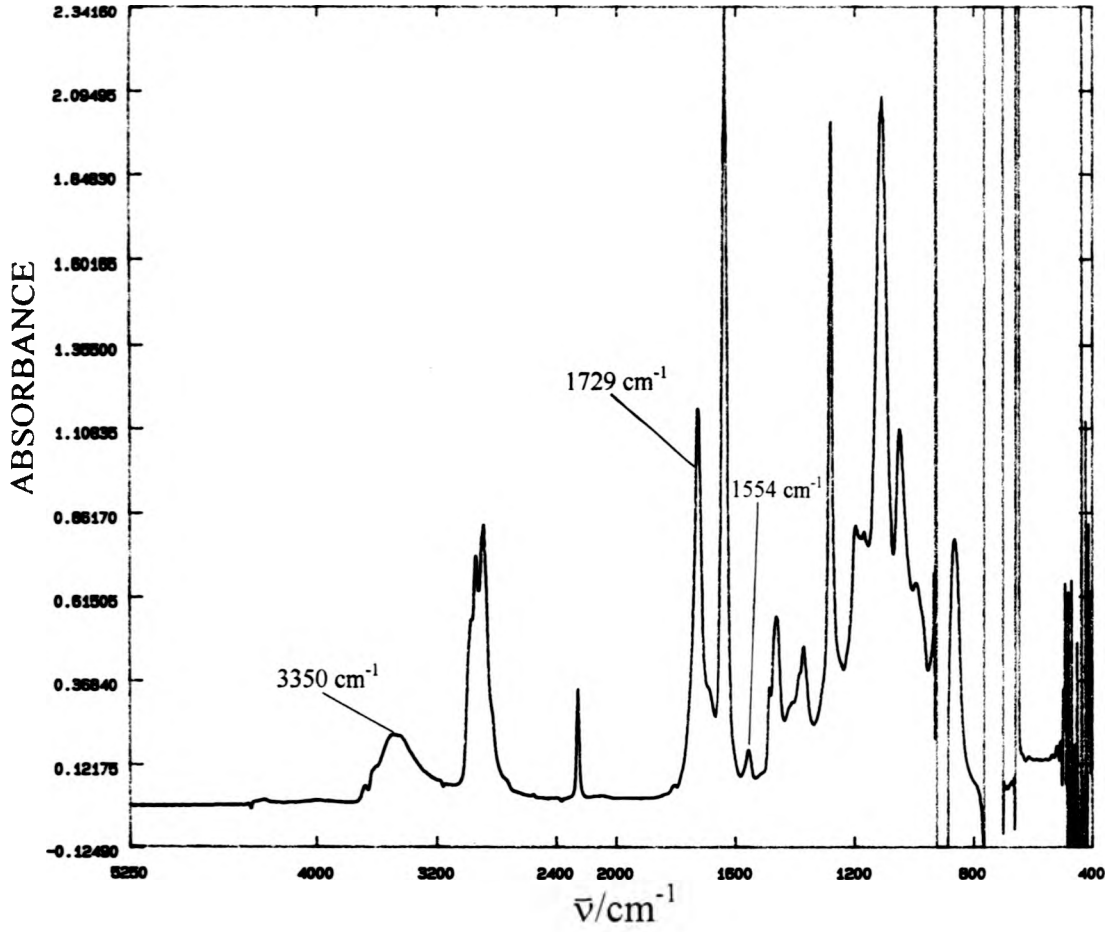

FIG.7.6 SOL^{N} IR SPECTRUM OF PHOTOLYSED (220 W HANOVIA LAMP) PNMMO

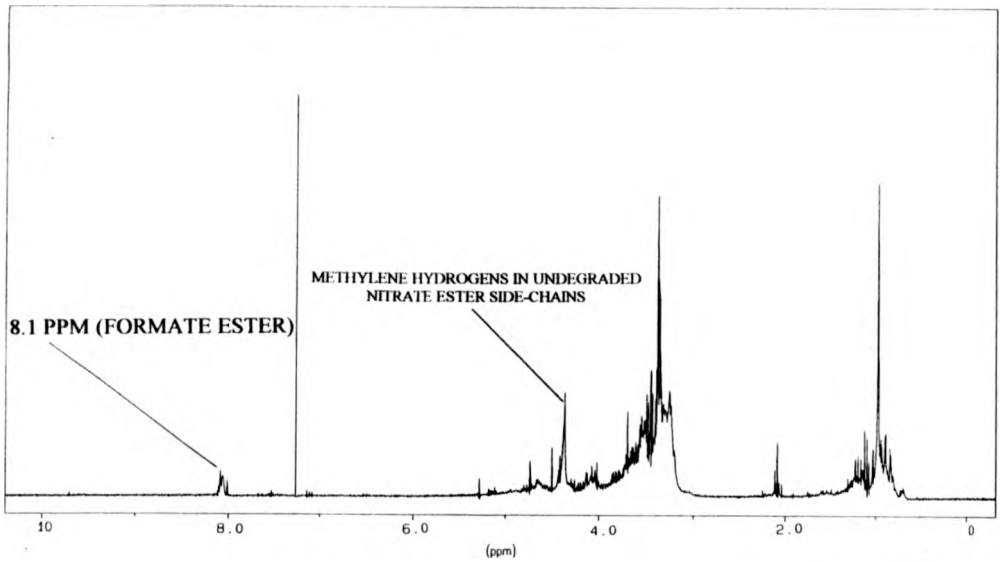

FIG.7.7A 250 MHz ^{1}H NMR SPECTRUM OF PHOTOLYSED (220 W HANOVIA LAMP) PNMMO

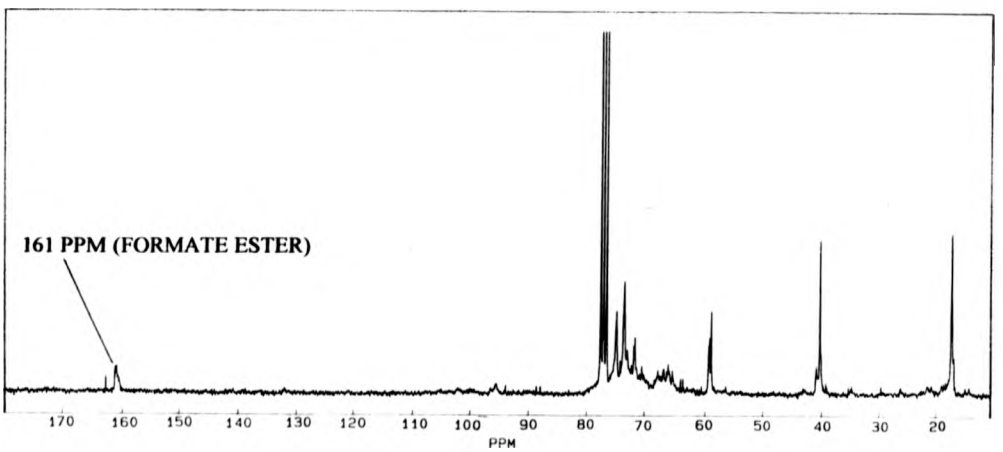

FIG.7.7B 250 MHz ^{13}C NMR SPECTRUM OF PHOTOLYSED (220 W HANOVIA LAMP) PNMMO

NO_2 will also be reduced (solvent cage); hydrogen abstraction or chain scission reactions may be more favourable. Consequently the significantly different intensities of the two absorptions at 1729 and 1554 cm^{-1} substantiates our previous assignment of the absorption at 1550 cm^{-1} to a nitro species. The difference of 4 cm^{-1} in the wavelengths of the absorption observed by pyrolysis (1550 cm^{-1}) and photolysis (1554 cm^{-1}) may be of consequence as the ^{13}C NMR spectrum of the photolysate shows new resonances around 95 ppm. Very weak new resonances are also visible around 89.0 ppm for the nitro carbon previously observed (at 89.0 ppm) in the ^{13}C NMR spectrum of pyrolysed PNMMO. The intensity of the IR absorption assigned to the nitro species in the IR spectrum of the photolysate is relatively low and thus its associated carbon resonance may not be visible in the ^{13}C NMR spectrum due to the low concentration of the nitro species present. However, it also appears possible that the extensive carbonyl formation in the photolysed sample may lead to an increase in the chemical shift of this nitro carbon. Indeed, the ^{1}H NMR spectrum of the photolysate clearly shows that extensive degradation of the nitrate ester side-chains has occurred and the resonance around 4.4 ppm attributed to the methylene hydrogens in the nitrate ester side-chains exhibits a significant reduction in intensity relative to the methyl and main chain methylene hydrogens. SEC chromatograms of the photolysed polymer show a 5 fold reduction in M_n after 350 h photolysis. Chain scission appears to be the dominant process and, in contrast to pyrolysis, no cross-linking associated with increased M_n is evidenced in the chromatograms. Rabek[17] comments that a reduction in M_n during photolysis of many polymers is often associated with a greater probability of chain scission and thus does not eliminate the possibility of cross-linking reactions occurring. Thus it appears that the photolysate consists of a large concentration of low molecular weight alcohol (3350 cm^{-1}) and alkyl- and formate- terminated species although clearly degradation is very extensive

and many other species may be present in lower concentrations. ESI mass spectra of the photolysate show a series of peaks not exceeding 1400 mus and centring around 600 mus. The photolysis of PNMMO results in a far more complex mixture of low-mass oligomers; there are considerably more peaks in the ESI spectrum of photolysed PNMMO as compared to untreated PNMMO, thus making the assignment of individual species very difficult using ESI.

The pyrolysis and subsequent analysis of cured PNMMO presented us with many difficulties. Solid phase NMR experiments could not be performed routinely as the apparatus was unavailable to us. IR analysis of films of cured untreated PNMMO greater in thickness than approximately 0.1 mm was also impossible as the IR spectra contained numerous intense unresolvable absorptions. However it was found that very thin films of PNMMO could be cured on sheets of PTFE and easily removed after curing. Subsequent IR analysis was possible but, due to the delicate nature of the resulting film, pyrolysis temperatures in excess of 100^0C caused rapid degradation and subsequent liquefaction or destruction of the film. Photolysis experiments using cured films of PNMMO were however more successful. The carbonyl region around 1730 cm^{-1} is unfortunately complicated by the presence of urethane linkages (-NH-C(O)-O) in the cured polymer. However IR difference spectra run by subtracting a spectrum of a cured untreated PNMMO film from a spectrum of a photolysed cured PNMMO film give some indication of new IR bands. Clearly this method is not ideal as small differences in film thickness lead to intense signals in the IR difference spectra but, by monitoring difference spectra over a period of 100 h photolysis, new absorptions at 1729 and 1550 cm^{-1} are clearly visible. It appears therefore that the main degradation species observed in the solution IR spectra of pyrolysed un-cured PNMMO at 1550 (tertiary nitro) and 1729 cm^{-1} (formate ester) are also observed for the cured polymer.

7.5 THERMOLYSIS OF PP260, PP330, PP340 AND P-GLYN

Only small quantities (less than 1.0 g) of each of these polymers were obtained from the DRA but very preliminary experiments were performed in an attempt to compare the rates of thermal degradation of PP260, PP330 and PP340 with PNMMO. PP260, PP330, PP340 and PNMMO are all structurally identical but differ in molecular weight (see experimental section). PP260, PP330 and PP340 all have M_w values around 3000 whereas PNMMO has an M_w of approximately 7500. As expected, thermal degradation of PP260, PP330 and PP340 generated similar absorptions to those of PNMMO at 1729 and 1550 cm^{-1} in the IR spectrum. However the rate of development of the carbonyl absorbance was consistently ca. 20 % greater for PP260, PP330 and PP340 as compared to PNMMO. Although viscosity measurements were not made, we attribute this increased carbonyl development to the greater oxygen diffusion rates in PP260, PP330 and PP340 due to their lower average molecular weights and thus lower viscosity. Similar observations were made during the thermal- and photo- oxidative degradation of LLDPE films and HDPE films[27]. LLDPE films consistently exhibited a greater rate of carbonyl development than the HDPE films due to the greater rate of oxygen diffusion into LLDPE. Increasing film thickness has also been observed to lead to lower oxidation rates in LDPE[28].

Untreated P-GLYN dissolved sparingly in $CDCl_3$ but became increasingly difficult to dissolve with increasing pyrolysis time. A suitable deuterated solvent was not found but a preliminary investigation of the pyrolysate was performed using IR and ^1H NMR spectroscopy as only small amounts of sample are required to obtain spectra. IR spectra showed that a similar carbonyl absorption to that observed during thermolysis of PNMMO was visible around 1730 cm^{-1} in the IR spectrum of P-GLYN and this was tentatively attributed to a formate ester. The absorption at 1550 cm^{-1} previously assigned to a nitro

species in PNMMO was not observed during thermolysis of P-GLYN, but an absorption was observed around 1570 cm^{-1}.

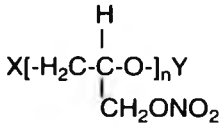

THE STRUCTURE OF P-GLYN

We cannot positively assign this absorption without further NMR investigation but its wavelength is indicative of the asymmetric stretch of a nitro group attached to a primary or secondary carbon. If the degradation of P-GLYN proceeds, like PNMMO, via loss of NO_2 and subsequent elimination of CH_2O, a secondary carbon-centred radical is generated as opposed to the tertiary carbon-centred radical in PNMMO. Clearly this explains the absence of an absorption at 1550 cm^{-1} in IR spectrum of pyrolysed P-GLYN.

The results of all the research concerning the analysis of degraded and undegraded PNMMO are summarised in chapter 9.

CHAPTER 7 REFERENCES

1 Bunyan, P., Cunliffe, A.V., Davis, A., Proc. Conference Int. Pyrotechnics (Sweden), 1991.

2 Coleman, M.M., Schobert, H.H., Song, C., *Chem. in Britain* 1993, **29**, 760.

3 Emanuel, N.M., *Russ. Chem. Rev.* 1991, **50**, 901.

4 Scott, G., *J. Appl. Polym. Sci.: Appl. Polym. Symp.* 1994, **55**, 3.

5 Pospisil, J., *Angew. Makromol. Chem.* 1994, **216**, 135.

6 Hiskey, M.A., Brower, K.R., Oxley, J.C., *J. Phys. Chem.* 1991, **95**, 3955.

7 Kuo, K.K., Summerfield, M., Fundamentals of Solid Propellant Combustion, American Institute of Aeronautics and Astronautics Inc., New York, 1984, Ch.4.

8 Smith, L.V., DeVries, K.L., *Polymer*, 1993, **34**, 546.

9 March, J., Advanced Organic Chemistry, 2nd ed., McGraw-Hill, London, 1977.

10 Bercovici, T., King, J., Becker, R.S., *J. Chem. Phys.* 1972, **56**, 3956.

11 Hall, R.T., Pimentel, G.C., *J. Chem. Phys.* 1963, **38**, 1889.

12 Cohn, H., Ingold, C.K., Poole, H.G., *J. Chem. Phys.* 1952, **20**, 4272.

13 Costa, L., Gad, A.M., Camino, G., Cameron, G.G., Qureshi, M.Y., *Macromol.* 1992, **25**, 5512.

14 Cameron, G.G., Ingram, M.D., Qureshi, M.Y., Gearing, H.M., *Eur. Polym. J.* 1989, **25**, 779.

15 Gauvin, P., Lemaire, J., *Makromol. Chem.* 1987, **188**, 1815.

16 Griffiths, P.J.F., Hughes, J.G., Park, G.S., *Eur. Polym. J.* 1993, **29**, 437.

17 Rabek, J.F., Polymer Photodegradation, Chapman and Hall, London, 1995.

18 Nishiguchi, T., Ohosima, T., Nishida, A., Fujisaki, S., *J. Chem. Soc., Chem. Commun.* 1995, 1121.

19 Addison, C.C., *Chem. Rev.* 1980, **80**, 21.

20 Cruz-Pinto, J.J.C., Carvalho, M.E.S., Ferreira, J.F.A., *Makromol. Chem.* 1994, **216**, 113.

21 Bigger, S.W., Scheirs, J., Delatycki, O., *J. Polym. Sci.: Part A: Polym. Chem.* 1992, **30**, 2277.

22 Skurat, V.E., Dorofeev, Y.I., *Makromol. Chem.* 1994, **216**, 205.

23 Lacoste, J., Vaillant, D., Carlsson, D.J., *J. Polym. Sci.: Part A: Polym. Chem.* 1993, **31**, 715.

24 Yang, C.Q., Martin, L.K., *J. Appl. Polym. Sci.* 1994, **51**, 389.

25 Bellamy, L.J., The Infrared Spectra of Complex Molecules, Vol.1, 3rd ed., Chapman and Hall, 1975, Ch.17.

26 Silverstein, R., Bassler, G., Spectrometric Identification of Organic Compounds, 4th ed., John Wiley & Sons, Chichester England, 1991, Ch.3.

27 Torikai, A., *Makromol. Chem.* 1994, **216**, 225.

28 Barr-Kumarakulasinghe, S.A., *Polymer*, 1994, **35**, 995.

CHAPTER 8

MASS SPECTRAL CHARACTERISATION OF THE THERMAL AND PHOTOLYTIC DEGRADATION OF PPO BY ESI AND MALDI

Poly(ethylene glycols) (PEGs) have been well characterised by ESI[1] and MALDI[2] mass spectrometry. PPO is well characterised by MALDI[2] but not nearly so well by ESI.

The structure and degradative mechanisms of PPO bear many resemblances to PNMMO. In view of this and the importance of PPO in polyurethane elastomers and foams[3] which undergo rapid oxidative degradation at elevated temperatures, we have sought to apply ESI and MALDI to the characterisation of the degradation pathways and products.

8.1 SEC ANALYSIS OF PPO

Figure 8.1 shows the size-exclusion chromatograms obtained for untreated (M_n = 2000) and pyrolysed PPO. All chromatograms were run using the same concentration of PPO. It is clear from figure 8.1 that chain scission is the predominant thermal degradation mechanism at 155^{0}C leading to a reduction in the M_n. After 92 h pyrolysis there is a nearly three fold reduction in the M_n and a two fold increase in the polydispersity. A small amount of cross-linked material is however apparent and is denoted by the shaded area in the chromatogram.

The same pyrolysis conditions produce an approximately two fold reduction in the M_n and a five fold increase in the polydispersity of PNMMO. There is significantly more cross-linked material present in the thermally degraded PNMMO samples as compared to the PPO samples. This is most likely a consequence of the higher viscosity of PNMMO and

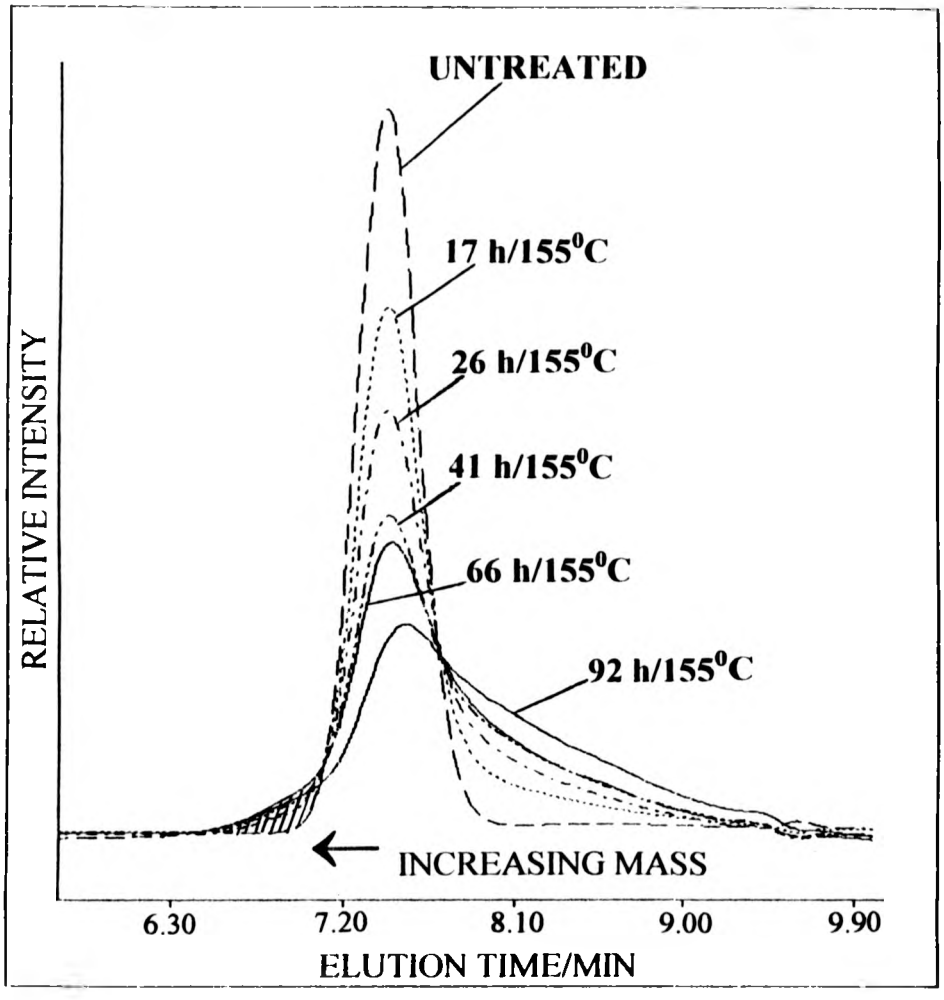

FIG.8.1 SEC CHROMATOGRAMS OF UNTREATED AND PYROLYSED (155°C) PPO

thus the lower rate of diffusion of oxygen into the polymer during pyrolysis as compared with PPO.

The SEC data generated an M_n value of 3000 for untreated PPO. This is substantially higher than the manufacturer's value of 2000. Indeed, it was consistently found that for PPO samples acquired from many different sources, the M_n value obtained by SEC varied significantly from the manufacturer's molecular weight specifications. This variation was different in all the samples and most significant when the polymer was polydisperse. Very minor impurities may be responsible for skewing the molecular weight determination, even though the SEC equipment has been calibrated with high purity standards[4] (the PPO chosen for our experiments thus had a narrow molecular weight distribution).

It is practically impossible to establish a proper calibration function for the pyrolysed samples due to the heterogeneity of chemical structures present. As compounds differing in structure and molecular weights may have the same hydrodynamic volume in THF, they will have the same retention volumes in the chromatograms so that complete separation of the mixtures cannot be achieved. Even so, the comparison of degraded and untreated samples can yield important information.

8.2.1 ESI ANALYSIS OF UNTREATED PPO

Untreated PPO was analysed by ESI using various salts to promote ionisation. NH_4Cl generated reproducible spectra with strong ion peaks and was therefore used consistently throughout the analysis of PPO. Fig.8.2 shows ESI spectra of untreated PPO recorded at cvs of 17, 45 and 84. All of the electrospray spectra show a distribution of singly charged ions due to NH_4^+ cationisation around 2000 mus denoted as series A^+. As expected, each species in series A^+ yields peaks at mass intervals of the monomer unit (58 mus).

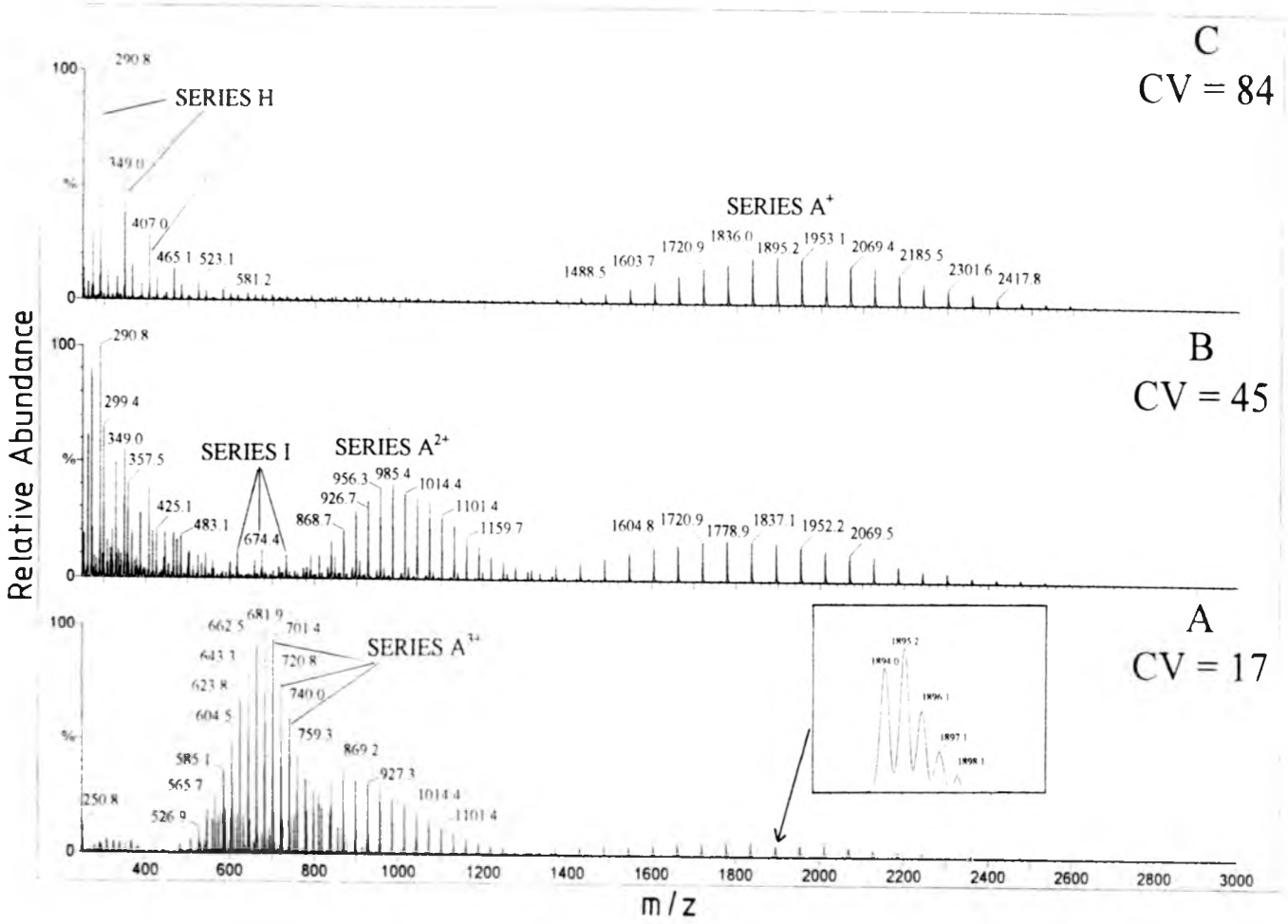
C
CV = 84
SERIES H
SERIES A+
B
CV = 45
SERIES I
SERIES A2+
A
CV = 17
SERIES A3+
Relative Abundance
m/z

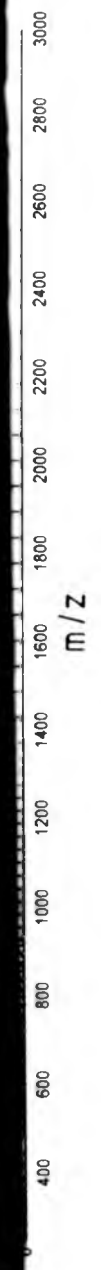

FIG.8.2 ESI SPECTRA OF UNTREATED PPO RECORDED AT CVS OF 17 (BOTTOM), 45 (MIDDLE) AND 84 (TOP) USING NH_4Cl TO PROMOTE IONISATION

Spectra run at a cv of 84 and greater show singly charged polymer ions only. A M_n value of 1935 mus was calculated from these spectra by subtracting 18 mus (NH_4^+) from the most intense ion peak. This is in close agreement with the manufacturer's value of 2000 mus.

Fig. 8.2B shows the ESI spectrum of PPO run at a cv of 45. A distribution of doubly charged ions around 1000 mus, denoted as series A^{2+} are apparent. As expected, each species in series A^{2+} displays peaks at mass intervals of one half the monomer unit (29 mus). Lowering the cv to 17 yields a distribution of triply charged ions around 700 mus, denoted as series A^{3+}. Similarly the separation of the peaks in series A^{3+} refers to one third the mass of the monomer unit (19.3 mus).

As the cv is decreased therefore, a greater concentration of doubly and then triply charged ions become apparent. In 1988, Loo *et al.*[5] demonstrated that the charge distribution for large molecules such as polypeptides was sensitive to a parameter which they termed the nozzle-skimmer voltage bias. This is the same as the cv. They found that decreasing the cv led to an increase in the abundance of more highly charged molecular ions. This effect of the cv is also well documented for PEGs[6] and proteins[5], and is attributed both to the greater ease of desolvation of multiply-charged species at low cv, and to the energetic collisions of multiply-charged solvated molecular ions in the nozzle-skimmer region. The fact that more-highly charged species are favoured at lower cv (less energetic collisions) is consistent with a CID process.

If we compare series A^+ in figures 8.2A (cv = 17) and 8.2B (cv = 45), it is evident that the mass distribution is skewed to lower mass as the cv is decreased. This same phenomenon is apparent for series A^{2+} in figures 8.2B (cv = 45) and 8.2C (cv = 84). It seems unlikely that a decrease in cv can lead to fragmentation. This result is logically attributed

therefore, to the higher stability and thus greater ease of cationisation of larger molecular weight species as compared to lower molecular weight species.

8.2.2 FRAGMENTATION AT HIGH CV

At a cv greater than 30, an unexpected spread of ions below 600 mus is evident in the untreated and pyrolysed samples (see fig.8.2). These ions appear particularly prevalent at a cv between 40 and 70. Selby *et al.*[7] suggest that protonation of polyglycols can occur at the oxygen atom during CID followed by subsequent C-O bond cleavage to produce a shorter polyglycol chain and a secondary cation. Loo *et al.*[5] have already shown that the influence of the cv can be attributed to a CID process and thus we propose that this protonation and cleavage reaction leads to the formation of these low molecular weight species at a cv greater than 30, thus

$$\mathrm{HO\text{-}[CH_2\text{-}CH(CH_3)\text{-}O]_x\text{-}CH_2\text{-}CH(CH_3)\text{-}\overset{\oplus}{O}H\text{-}[CH_2\text{-}CH(CH_3)\text{-}O]_yH}$$

$$\downarrow \quad \text{cv}>30$$

$$\mathrm{HO\text{-}[CH_2\text{-}CH(CH_3)\text{-}O]_x\text{-}CH_2\text{-}\overset{\oplus}{C}H(CH_3)} \quad \textbf{(H)} \qquad + \qquad \mathrm{HO\text{-}[CH_2\text{-}CH(CH_3)\text{-}O]_yH} \quad \textbf{(I)}$$

$$\text{RMM } 1+(58n) \qquad\qquad \text{RMM } 18+(58n)$$

Series I also exhibits H^+ (series J) adducts for $y = 6$ to $y = 11$. When x or $y = 5$ or less only H^+ adducts are detectable and similarly, for x or $y = 12$ and above, only NH_4^+ adducts are detectable. This is due to the relative stability of the two ions at the cv employed, the H^+ adduct presumably being formed by the removal of NH_3 from the NH_4^+ adduct.

Table 8.1 (over the page) shows the peak assignments for series A^{+}, A^{2+}, A^{3+}, H, I and J. In all cases except for series H and J, the entire series is not shown for the sake of brevity. All series show a well-defined ^{13}C isotopic splitting pattern (see inset to fig.8.2A).

TABLE 8.1

ASSIGNMENTS OF PRINCIPAL PEAKS IN THE ESI SPECTRUM OF UNTREATED PPO

Series A^+		**Series A^{2+}**	
$HO\text{-}[CH_2\text{-}CH(CH_3)\text{-}O]_nH.NH_4^+$		$HO\text{-}[CH_2\text{-}CH(CH_3)\text{-}O]_nH.(NH_4^+)_2$	
n	m/z	n	m/z
26	1545.5	26	781.6
27	1603.5	27	810.7
28	1661.8	28	839.7
29	1719.7	29	868.7
30	1778.0	30	897.8
31	1836.1	31	927.3
32	1894.0	32	956.2
33	1952.2	33	985.4
34	2010.2	34	1014.3
35	2068.4	35	1043.2

Series A^{3+}	
$HO\text{-}[CH_2\text{-}CH(CH_3)\text{-}O]_nH.(NH_4^+)_3$	
n	m/z
26	526.9
27	546.3
28	565.7
29	585.1
30	604.5
31	623.8
32	643.3
33	662.5
34	681.9
35	701.4

TABLE 8.1 (cont.)

ASSIGNMENTS OF PRINCIPAL PEAKS IN THE ESI SPECTRUM OF UNTREATED PPO

Series H	
$HO\text{-}[CH_2\text{-}CH(CH_3)\text{-}O]_x\text{-}CH_2\text{-}CH(CH_3)^{\oplus}$	
x	m/z
4	290.8
5	349.0
6	407.0
7	465.2
8	523.1
9	581.3
10	-

Series I		**Series J**	
$HO\text{-}[CH_2\text{-}CH(CH_3)\text{-}O]_yH.NH_4^+$		$HO\text{-}[CH_2\text{-}CH(CH_3)\text{-}O]_yH.H^+$	
y	m/z	y	m/z
4	-	4	250.9
5	-	5	308.9
6	383.9	6	366.9
7	442.1	7	425.1
8	500.1	8	483.1
9	558.1	9	541.2
10	616.3	10	599.4
11	674.3	11	657.2
12	732.4	12	-
13	790.5	13	-
14	848.5	14	-
15	906.5	15	-
16	964.6	16	-
17	1022.7	17	-

8.3.1 THE THERMAL DEGRADATION MECHANISMS OF PPO

We have studied the thermal degradation of PPO at 155^{0}C in air using SEC, solution IR spectroscopy, ^{1}H and ^{13}C NMR spectrometry and under anaerobic conditions using gas phase IR spectroscopy. Both the NMR and solution IR spectra of pyrolysed (in air) PPO closely resemble those of Griffiths *et al.*[3]; the main features being the gradual increase in intensity with increasing pyrolysis time of a broad new carbonyl resonance around 1726 cm^{-1} (1700 - 1760 cm^{-1}) in the solution IR spectrum and 3 new peaks in the ^{1}H NMR spectrum at 2.10, 2.18 and 8.17 ppm. The assignment of the resonances at 2.10, 2.18 and 8.17 ppm in the ^{1}H NMR to the protons in the structures CH_3-C(O)-O-, CH_3-C(O)-C and HC(O)-O- appears undisputed but, their mechanism of formation has been proposed to occur via generation of either the tertiary[3] or the secondary[8] hydroperoxide. Although these pathways differ in detail, it is not possible to distinguish between them from the masses of the resultant degradation species.

The thermal degradation of PPO has been studied using gas phase IR and ^{1}H NMR measurements by Griffiths *et al.*[3] and the photodegradation has been studied using solution IR by Lemaire *et al.*[8] Our work substantiates a hydroperoxide mechanism but shows that the scheme proposed by Lemaire *et al.*[8] giving oxidation predominantly at the secondary carbon better explains the relative product abundances observed by ESI and MALDI as compared to oxidation predominantly at the tertiary carbon proposed by Griffiths *et al.*[3]

Two possible mechanisms operating in parallel have been proposed by Griffiths *et al.*[3] based on hydroperoxide formation predominantly at the tertiary carbon atom. Both processes start with reaction with an oxygen molecule to give a tertiary hydroperoxide followed by its decomposition to an alkoxy radical and HO• (and hence H_2O). This tertiary hydroperoxide mechanism proposed by Griffiths *et al.*[3] is as follows.

$$HO\text{-}[CH_2\text{-}CH(CH_3)\text{-}O]_x\text{-}CH_2\text{-}C(CH_3)(\mathbf{OOH})\text{-}O\text{-}[CH_2\text{-}CH(CH_3)\text{-}O]_yH$$

$$\downarrow$$

$$HO\text{-}[CH_2\text{-}CH(CH_3)\text{-}O]_x\text{-}CH_2\text{-}C(CH_3)(\mathbf{O}\bullet)\text{-}O\text{-}[CH_2\text{-}CH(CH_3)\text{-}O]_yH$$

$$\mathbf{HO}\bullet + RH \rightarrow H_2O + R\bullet$$

Here RH is a polymer molecule and the R• radical leads to more hydroperoxide formation.

Mechanism 1 C-C bond cleavage adjacent to the alkoxy radical centre takes place to generate products B and C, followed by further peroxidation of product B.

(B)

$$HO\text{-}[CH_2\text{-}CH(CH_3)\text{-}O]_x\text{-}CH_2\bullet$$

(C)

$$(CH_3)C(\mathbf{O})\text{-}O\text{-}[CH_2\text{-}CH(CH_3)\text{-}O]_yH$$

(ACETATE ESTER)

$$\text{i)}+O_2 \quad \downarrow \quad \text{ii)}+RH$$

(D)

$$HO\text{-}[CH_2\text{-}CH(CH_3)\text{-}O]_x\text{-}CH_2OOH$$

$$+R\bullet$$

(E)

$$HO\text{-}[CH_2\text{-}CH(CH_3)\text{-}O]_x\text{-}C(O)H$$

(FORMATE ESTER)

$$+H_2O$$

Mechanism 2 C-O bond cleavage adjacent to the alkoxy group takes place to generate products F and G.

(F)

$HO\text{-}[CH_2\text{-}CH(CH_3)\text{-}O]_x\text{-}CH_2\text{-}C(O)CH_3$ $\quad \bullet O\text{-}[CH_2\text{-}CH(CH_3)\text{-}O]_yH$

i)+RH ↓

(G)

$HO\text{-}[CH_2\text{-}CH(CH_3)\text{-}O]_yH$

$+R\bullet$

Griffiths *et al*[3]. note that these two processes taken together give the observed acetate, formate and ketone end groups, but the acetate and formate are produced in equal amounts instead of the 2:3 ratio as found by NMR. However, they comment that more formate could result from breakdown of the less readily formed secondary hydroperoxide.

Table 8.2 gives the expected RMM of the species resulting from these two pathways, namely C, E, F and G (the original PPO molecule has an RMM of 18+(58*n*)).

TABLE 8.2

RMM OF THE THERMAL DEGRADATION PRODUCTS OF PPO

FRAGMENT	C	E	F	G
RMM	2+(58*n*)	46+(58*n*)	16+(58*n*)	18+(58*n*)

The mechanism of oxidation at the secondary carbon atom proposed by Lemaire *et al.*[8] is shown below. As with the oxidation at the tertiary carbon atom, two processes operating in parallel were proposed[8] and in addition, a cage recombination mechanism was also invoked. Although Lemaire *et al.*[8] propose that this secondary hydroperoxide mechanism predominates over the tertiary mechanism, no detailed scheme for this oxidation is presented. The mechanism we propose below bears many similarities with the thermal oxidation schemes proposed for PEO[9] and PP[10,11]. The alkoxy radical shown below may either undergo a cage recombination reaction to give the species labelled K or undergo a scission reaction as shown in pathways 1 and 2 (over the page).

$$HO\text{-}[CH_2\text{-}CH(CH_3)\text{-}O]_x\text{-}CH(\mathbf{OOH})\text{-}CH(CH_3)\text{-}O\text{-}[CH_2\text{-}CH(CH_3)\text{-}O]_yH$$

$$\downarrow$$

$$HO\text{-}[CH_2\text{-}CH(CH_3)\text{-}O]_x\text{-}CH(\mathbf{O}\bullet)\text{-}CH(CH_3)\text{-}O\text{-}[CH_2\text{-}CH(CH_3)\text{-}O]_yH$$

$$\downarrow$$

CAGE RECOMBINATION WITH HO•

$$\mathbf{(K)}$$

$$HO\text{-}[CH_2\text{-}CH(CH_3)\text{-}O]_x\text{-}C(\mathbf{O})\text{-}CH(CH_3)\text{-}O\text{-}[CH_2\text{-}CH(CH_3)\text{-}O]_yH \quad + H_2O$$

Pathway 1 C-C bond cleavage adjacent to the alkoxy radical centre takes place to generate products E and L.

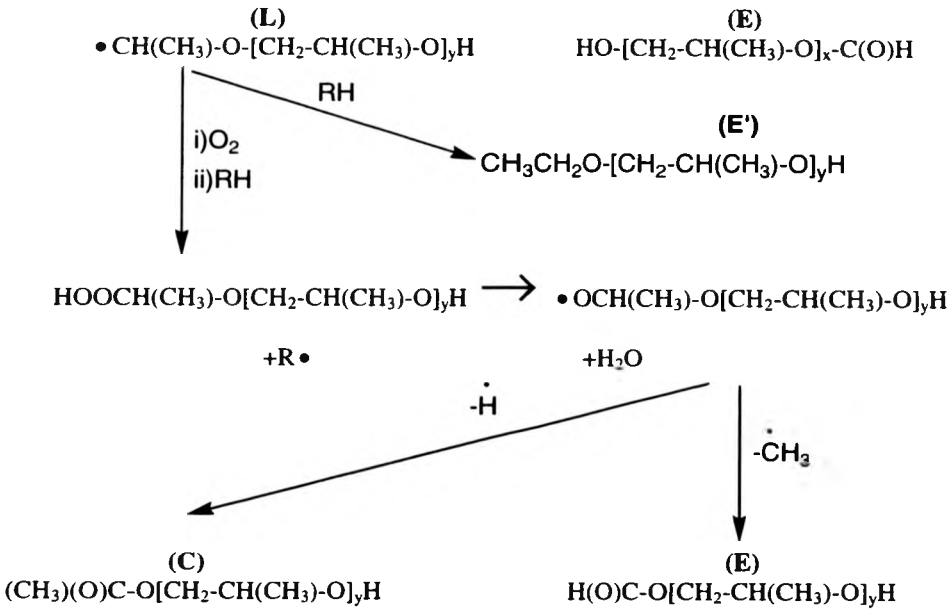

Pathway 2 C-O bond cleavage adjacent to the alkoxy group takes place to generate products F' and M.

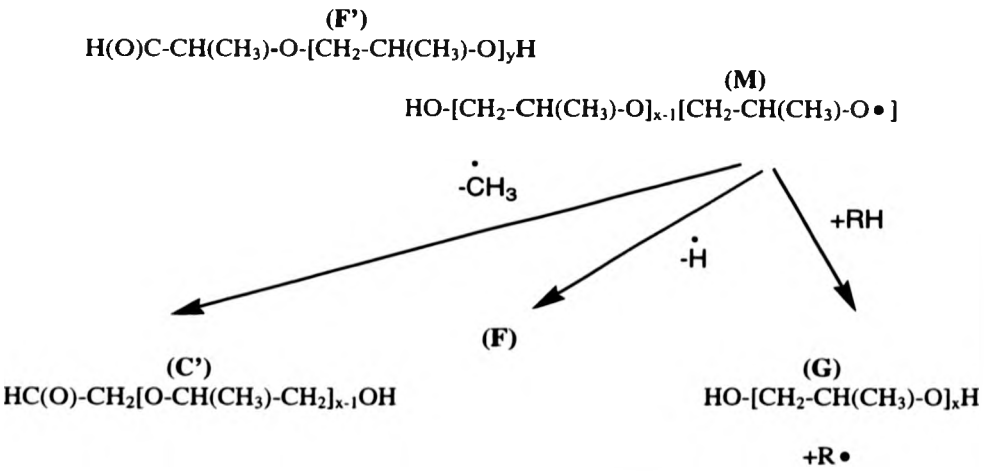

Clearly, the species labelled E and E' are structurally different but have similar masses and thus in our experiments it is not possible to distinguish between them from their masses; the same is true for C and C', F and F'. The scheme for the secondary oxidation mechanism shown above is not completely exhaustive and additional mechanisms are possible. However we propose that the mechanism above outlines the major decomposition pathways. ^{1}H NMR spectra of pyrolysed PPO show that the species labelled C' and F' are not produced in significant quantities as no new resonances are observed in the aldehyde region around 9 - 10 ppm.

8.3.2 ESI ANALYSIS OF PYROLYSED PPO

Electrospray spectra of untreated and pyrolysed (66 h/155^{0}C) PPO at a cv of 48 are shown in fig.8.3. Clearly the degradation of PPO has resulted in the development of a far more complex spectrum due to the production of degraded molecules : compare for example the region of series A^{2+} in fig.8.3A with the region of series A^{2+} in fig.8.3B.

Table 8.3 (over the page) shows the peak assignments for series C, E/E', F, G and K. In all cases the entire series is not shown for the sake of brevity.

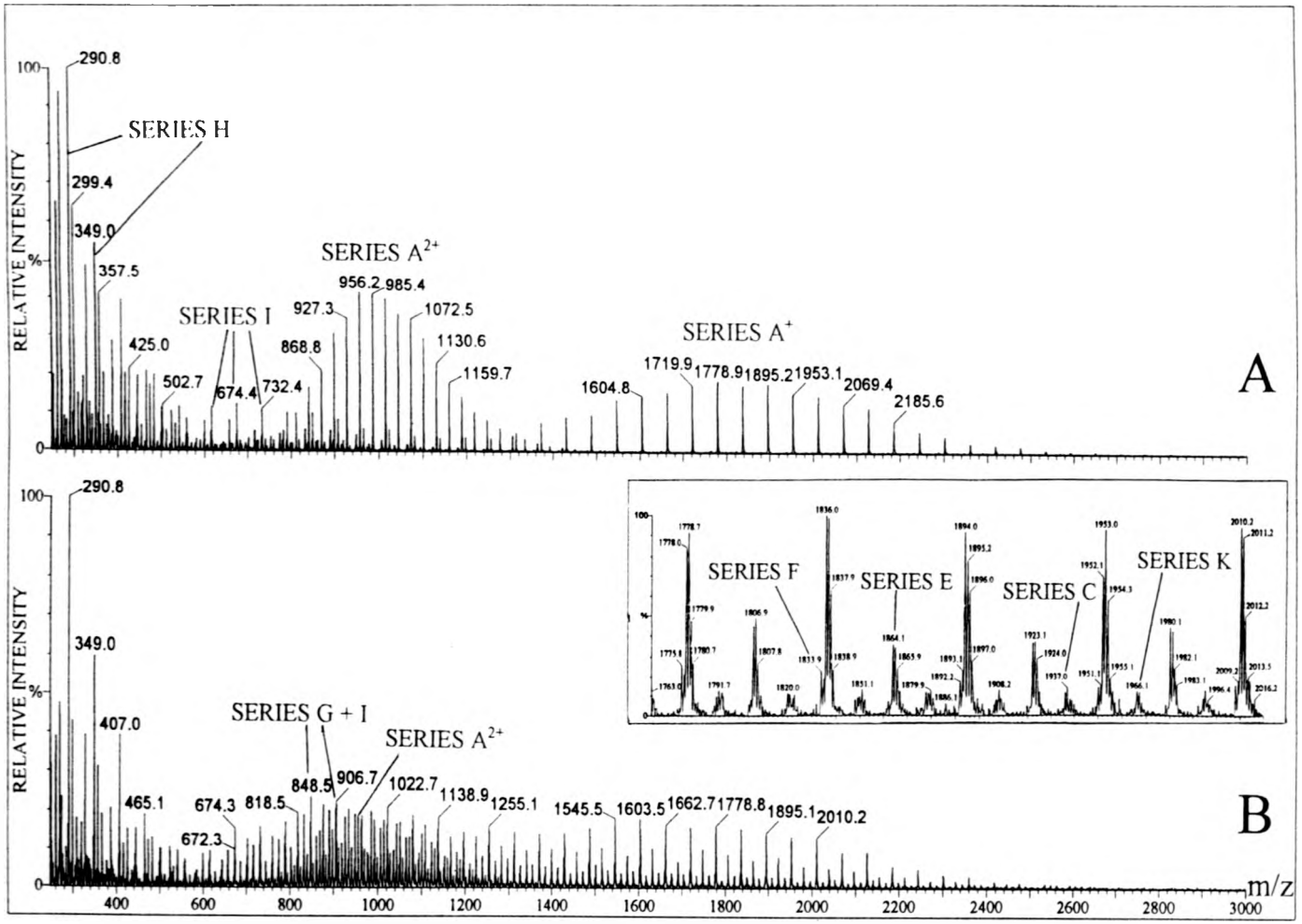
RELATIVE INTENSITY
100
%
0
290.8
SERIES H
299.4
349.0
357.5
425.0
502.7
674.4
732.4
SERIES I
927.3
SERIES A2+
956.2
985.4
1072.5
868.8
1130.6
1159.7
SERIES A+
1604.8
1719.9
1778.9
1895.2
1953.1
2069.4
2185.6
A
SERIES F
SERIES E
SERIES C
SERIES K
349.0
407.0
465.1
672.3
674.3
818.5
SERIES G + I
848.5
906.7
SERIES A2+
1022.7
1138.9
1255.1
1545.5
1603.5
1662.7
1778.8
1895.1
2010.2
B
m/z
400
600
800
1000
1200
1400
1600
1800
2000
2200
2400
2600
2800
3000

FIGS.8.3A,B ESI SPECTRA OF UNTREATED (A) AND PYROLYSED (B) PPO RECORDED AT A CV OF 48

TABLE 8.3

ASSIGNMENTS OF PRINCIPAL PEAKS IN THE ESI SPECTRUM OF DEGRADED PPO

Series C		**Series E and E'**	
C: $(CH_3)C(O)$-O-$[CH_2$-$CH(CH_3)$-$O]_yH.NH_4^+$		E: HO-$[CH_2$-$CH(CH_3)$-$O]_x$-$C(O)H.NH_4^+$ E': CH_3CH_2O-$[CH_2$-$CH(CH_3)$-$O]_yH.NH_4^+$	
y	m/z	x	m/z
26	1588.7	26	1573.9
27	1645.7	27	1632.0
28	1703.9	28	1690.0
29	1762.8	29	1748.0
30	1820.0	30	1806.0
31	1878.0	31	1864.1
32	1936.0	32	1922.1
33	1994.2	33	1980.1
34	2052.3	34	2038.1
35	2111.4	35	2096.2

Series F		**Series G**	
F: HO-$[CH_2$-$CH(CH_3)$-$O]_x$-$CH_2C(O)CH_3.NH_4^+$		HO-$[CH_2$-$CH(CH_3)$-$O]_yH.NH_4^+$	
x	m/z	y	m/z
26	1601.7	26	1545.7
27	1659.7	27	1603.7
28	1717.8	28	1661.7
29	1775.8	29	1719.9
30	1833.9	30	1778.0
31	1892.2	31	1836.0
32	1950.2	32	1894.0
33	2008.3	33	1952.1
34	2066.3	34	2010.2
35	2124.3	35	2068.4

TABLE 8.3 (cont.)

ASSIGNMENTS OF PRINCIPAL PEAKS IN THE ESI SPECTRUM OF DEGRADED PPO

Series K	
$HO\text{-}[CH_2\text{-}CH(CH_3)\text{-}O]_x\text{-}C(\mathbf{O})\text{-}CH(CH_3)\text{-}O\text{-}[CH_2\text{-}CH(CH_3)\text{-}O]_yH.NH_4^+$	
n	m/z
27	1617.8
28	1675.9
29	1733.9
30	1791.9
31	1850.0
32	1908.0
33	1966.0
34	2024.0
35	2082.1

Similarly with pyrolysed PPO, series H and I attributed to *in situ* fragmentation were clearly visible in the ESI spectra obtained at a cv>30 and particularly prominent around a cv of 50 (see fig.8.3).

Series K (32+58n) can only be attributed to oxidation at the secondary carbon atom, whereas all the other species (series C, E/E', F and G) can arise from oxidation at either the secondary or tertiary carbon atoms. The relatively high abundance of the ions due to series E suggests that oxidation at the secondary carbon atom predominates as three separate pathways exist for the formation of series E or species with the same mass as series E (series E') via C-C bond cleavage adjacent to the secondary alkoxy radical. Moreover the formation of the formate ester (series E) via the tertiary oxidation mechanism proposed by Griffiths *et al.*[3] appears less likely as the alkoxy radical generated may be expected to eliminate formaldehyde, which was not observed in the pyrolysis gases of PPO in our studies.

However significant quantities of acetaldehyde were observed in the gas-phase IR spectrum (see figs.8.4A,B) of the gases evolved from pyrolysed (100 - 170^{0}C) PPO in our studies and this similarly points to a major contribution from the secondary oxidation mechanism; the product L formed by C-C bond cleavage adjacent to the secondary alkoxy radical or the intermediate alkoxy radical formed by reaction of L with O_2 can both eliminate acetaldehyde. The elimination of acetaldehyde via the tertiary oxidation mechanism appears less likely on examination of the radical species generated.

Fig.8.3 shows that the relative abundance of the ions due to series C and F is clearly lower than that for series E. This is consistent with our secondary oxidation mechanism which shows that only one pathway exists for the formation of either series C or series F as compared with three pathways for the formation of series E or E'.

The presence of significant quantities of species attributed to series F and G in the ESI spectra of pyrolysed PPO suggests that the tertiary oxidation mechanism does contribute to the overall degradation process; the species associated with series F and G may also be formed via C-O bond cleavage adjacent to the secondary alkoxy radical, but we have shown that the absence of aldehyde species suggests that C-O bond cleavage is negligible. Consequently the tertiary oxidation mechanism cannot be ruled out but the ESI results do point to a major role of the secondary alkoxy radical as compared with the tertiary alkoxy radical advocated by Griffiths *et al.*[3]

Series I generated by *in situ* fragmentation and series G generated by thermal degradation coincide exactly with each other and with series A^+ and are therefore not easily identifiable when m/z is greater than 1400 mus as much unaltered PPO still remains. However, at lower mass, series I and G are easily recognisable. The relatively high abundance of the ions due to series I and G in fig.8.3B as compared with the ions due to

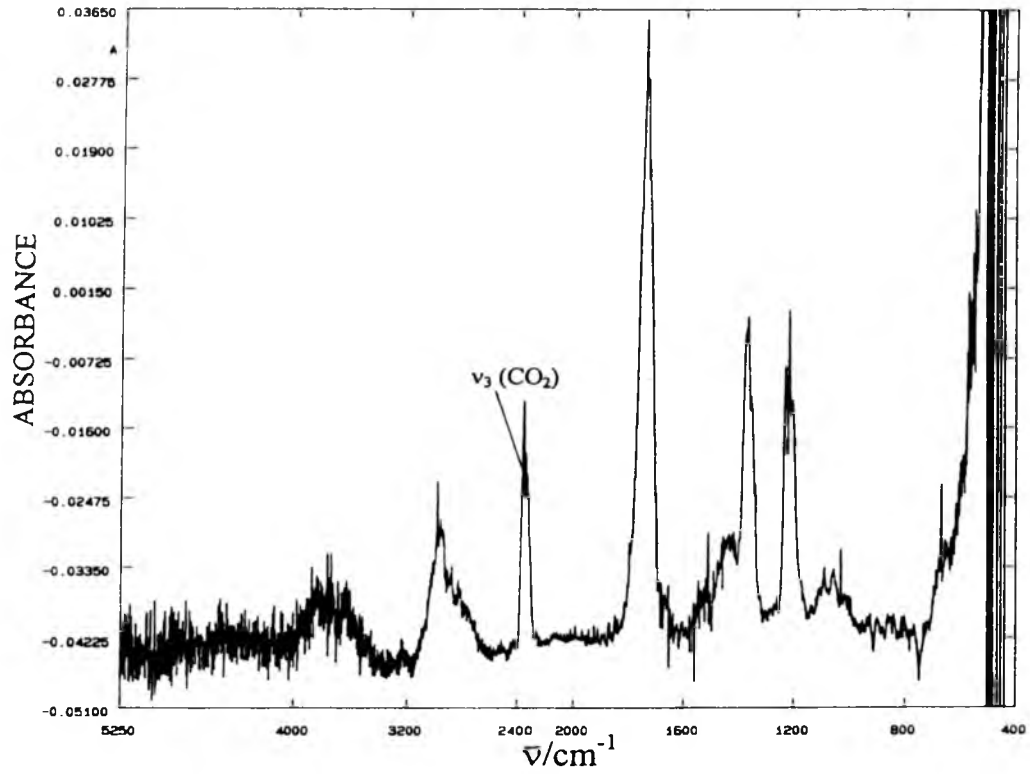
0.03650
A
0.02775
0.01900
0.01025
0.00150
-0.00725
-0.01600
-0.02475
-0.03350
-0.04225
-0.05100
ABSORBANCE
ν_3 (CO_2)
5250
4000
3200
2400
2000
1600
1200
800
400
$\bar{\nu}$/cm^{-1}

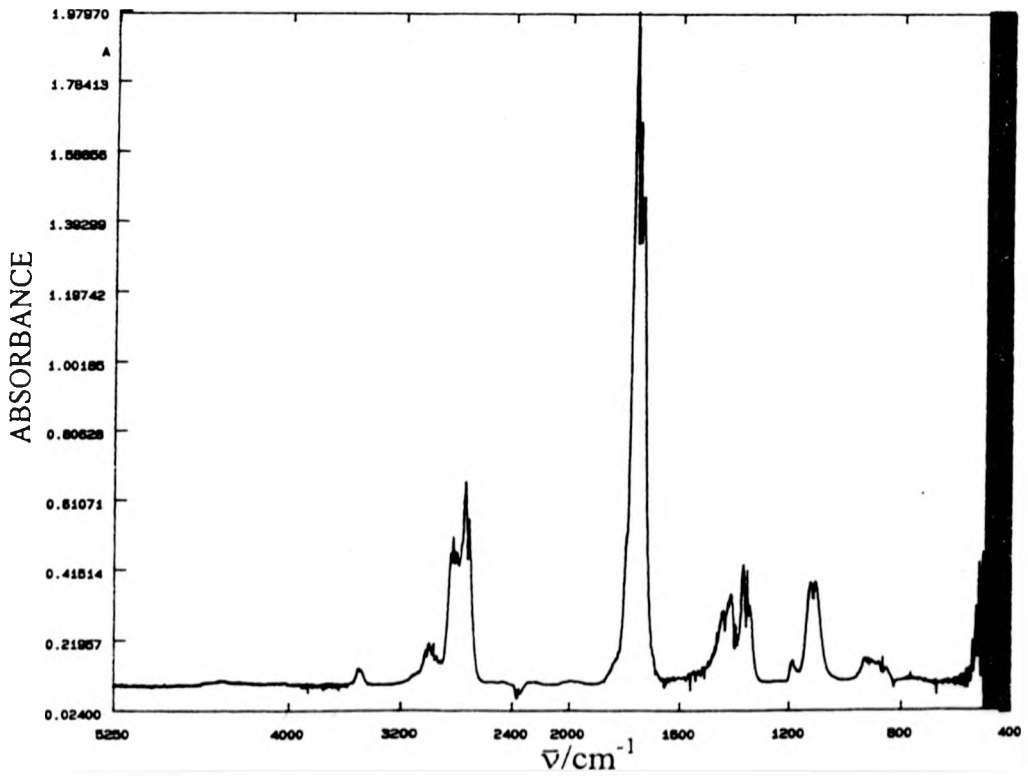
1.97970
A
1.78413
1.58856
1.39299
1.19742
1.00185
0.80628
0.61071
0.41514
0.21957
0.02400
ABSORBANCE
5250
4000
3200
2400
2000
1600
1200
800
400
$\bar{\nu}$/cm^{-1}

FIG.8.4A GAS-PHASE IR SPECTRUM OF THE GASES EVOLVED FROM PYROLYSED (155^{0}C) PPO

FIG.8.4B GAS-PHASE IR SPECTRUM OF A SAMPLE OF ACETALDEHYDE OBTAINED FROM ALDRICH CHEM. CO.

series I in fig.8.3A point to a relatively high concentration of series G. However species associated with series G may be formed via either the secondary or the tertiary oxidation mechanism and thus no inferences as to the mechanism of oxidation of PPO can be made from this observation.

The SEC chromatograms (fig.8.1) display a lower concentration of low mass (<1400 mus) degraded products as compared to the ESI spectra. This we believe is in part due to the fragmentation occurring *in situ* during ESI analysis, producing in particular series I, thus emphasising the concentration of thermally degraded products present at lower mass. The differing sensitivities of the two techniques also makes comparison difficult and may explain why the small concentration of higher mass material visible after approximately 6.6 min elution time in the SEC chromatograms is not visible in the ESI spectra. Other factors such as the stability of the ammonium ion adduct may also account for this difference. The ammonium ion adduct of this cross-linked material may have a far lower stability as compared to the other components of the mixture, thus explaining its non-appearance in the ESI spectrum. It is in fact probable that none of the components of this complex mixture are equally stable upon ion formation. This also makes it very difficult to assess the extent of degradation of the sample as ion intensities cannot be accurately compared without prior knowledge of the stability constants. Many difficulties will obviously be encountered during the analysis of such a complex mixture and this is clearly shown by the many differences between the ESI and SEC results.

8.4 MALDI ANALYSIS OF UNTREATED AND PYROLYSED PPO

For the analysis of compounds by MALDI, the correct choice of matrix is vital to the desorption process and the subsequent production of ions. MALDI is still a relatively new

technique and this desorption process is not yet fully understood. The role of the matrix is better recognised and it should fulfil certain requirements; (1) it must absorb the laser light (337 nm for the nitrogen laser used here), (2) it should not react chemically with the compound being analysed, (3) it should mix intimately with the analyte being used, and (4) it should be of relatively low volatility under the mass spectrometric vacuum conditions. Various matrices were tested with the pyrolysed and untreated PPO samples and although many fulfilled the requirements above only 2,5-dihydroxybenzoic acid (absorbing laser light at 337 nm) gave reproducible spectra with strong ion peaks. 3,5-dimethoxy-4-hydroxycinnamic acid (sinapinic acid) and 4-hydroxy-α-cyanocinnamic acid both absorb laser light at the same wavelength but failed to give ion peaks.

Untreated and pyrolysed PPO samples failed to give ion peaks at very low laser powers. As the laser power is gradually increased, there is a sudden appearance of ions. This phenomenon is well recognised and is termed the 'threshold irradiance'. There exists a small irradiance range above the threshold irradiance where reproducible molecular ion desorption becomes possible[13].

Fig.8.5 shows the MALDI mass spectra of pyrolysed (66 h/155°C) and untreated PPO recorded at high and low laser power using sodium chloride to promote ionisation. As with the ESI spectra, series A^+, C, E/E', F, G and K are easily recognisable. However multiply charged ions are not visible in the MALDI spectra.

The laser power was varied for every sample analysed. It was consistently found that increasing the laser power increased the concentration of degradation products appearing below approximately 1400 mus in the MALDI spectrum. This parallels the situation found with the ESI spectra where we suggest that *in situ* fragmentation occurs to produce series I at higher cv, thus emphasising the concentration of thermal degradation products.

PAGINATION ERROR

P264

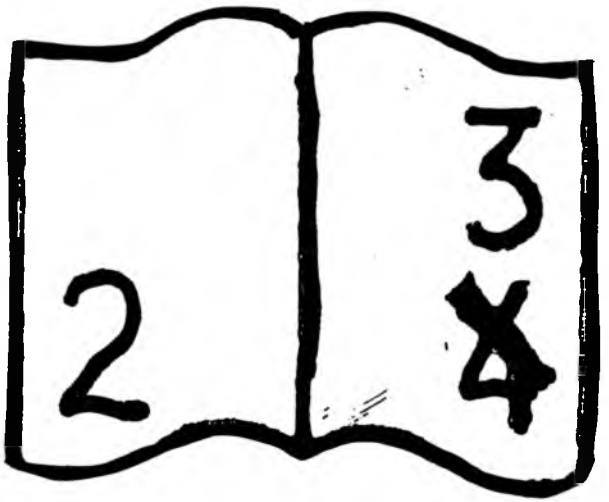

Fragmentation of this type was seen only to a very minor extent in the untreated samples and only when the laser power was at a maximum. A more obvious skewing of the main distribution towards lower mass is however apparent in the degraded samples at high laser power. Creel[12] suggests that a loss of detector sensitivity may sometimes account for these phenomena. Thus the microchannel plate array detector can be swamped by a large number of low-mass ions. If the detector does not recover sufficiently, the high-mass ions may be detected at a lower signal strength, resulting in a skewed mass distribution with concomitant mass average errors. This would explain the more variable mass distribution in the degraded samples where a higher concentration of low-mass ions exist as compared to the undegraded samples. This phenomenon of the loss of detector sensitivity is thought to account for figure 8.6. The spectrum of pyrolysed PPO (66 h/155°C) was recorded at high laser power and averaged over 200 laser shots (fig.8.6B). The top spectrum (fig.8.6A) shows one of these 200 spectra. No ions are visible above 1500 mus and clearly this is not a representative spectrum of the mixture as a whole, demonstrating that the results obtained at high laser power are unreliable. 'Single-shot' spectra acquired at low laser power were always identical to the averaged spectrum and show good agreement with the polymer distribution pattern observed by SEC.

Non-homogeneous mixing of the matrix and analyte could also produce similar mass discrepancies, as documented for poly(methyl methacrylate)[14]. The laser energy is absorbed directly by the analyte (PPO) as opposed to indirectly from the matrix, thereby increasing the possibility of fragmentation.

The inset to fig.8.6A shows an enlarged portion of the spectrum of pyrolysed PPO. The peaks are not nearly so well resolved as those in the ESI spectrum and no ^{13}C isotopic

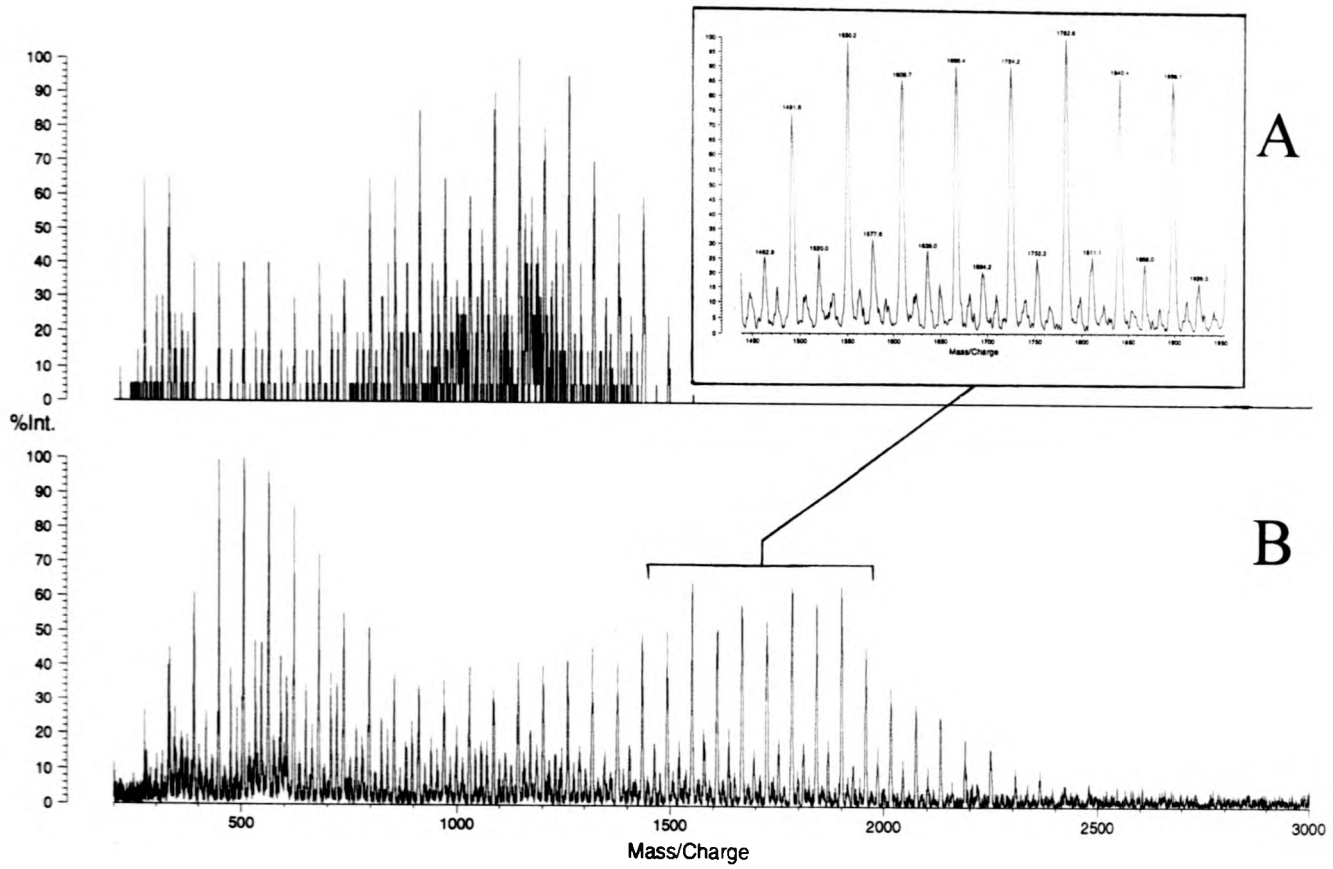

FIG 8.6 MALDI SPECTRUM OF PYROLYSED (66 h/155^{0}C) PPO AVERAGED OVER 200 LASER SHOTS (BOTTOM) AND THE MALDI SPECTRUM OF PYROLYSED PPO OBTAINED USING A SINGLE LASER SHOT (TOP)

pattern is apparent. This resolution difference between the two mass spectrometric techniques is thought to be due to their differing sensitivities.

The MALDI spectra became gradually more difficult to obtain with increasing pyrolysis times of the PPO samples and it was necessary to increase the laser power to achieve ion formation. Increased laser power leads to increased *in situ* fragmentation of the polymer and thus less reliable results. Possibly the degraded fraction was less easily desorbed and thus the polymer mixture became less amenable to MALDI analysis. This same phenomenon was not observed during ESI analysis.

In conclusion, the degradation pathways involving C-C and C-O cleavage adjacent to the alkoxy radical centre suggested for PPO from ^{1}H NMR measurements on the bulk material were confirmed by characterisation of all of the immediate products of decomposition, namely C, E/E', F, G and K by ESI and MALDI experiments for each individual component of the PPO sample. The mass spectrometric measurements also give an indication of the extent of pyrolysis and point towards a major role of the secondary alkoxy radical as compared with the tertiary alkoxy radical. High cv's in ESI and high laser power in MALDI can lead to additional degradation of the PPO sample, but these can be avoided by using milder conditions. ESI appears to be the most suitable technique for the analysis of the degraded PPO samples. Analysis of highly degraded samples was more facile and unlike the MALDI experiments, conditions could be found where *in situ* fragmentation was kept to a minimum.

8.5 THE ANALYSIS OF PHOTOLYSED PPO

Neat PPO was photolysed for 2000 h inside a uv baking tank. The IR and NMR spectra obtained for the photolysed polymer were similar to those for the thermally degraded polymer.

8.5.1 SEC ANALYSIS OF PHOTOLYSED PPO

It is clear from SEC chromatograms (data not shown) that chain scission is the predominant photolysis mechanism leading to a reduction in the M_n. After 2000 h photolysis there is a 3 fold reduction in the M_n and a 2 fold increase in the polydispersity.

8.5.2 ESI ANALYSIS OF PHOTOLYSED PPO

Figure 8.7 shows the ESI spectrum of photolysed (2000 h) PPO at a cv of 45. NH_4Cl was used to promote ionisation. A polymer distribution centring around 800 mus is observed and no ions are visible above 2000 mus. These results closely compare with the data obtained by SEC.

The ESI spectrum of photolysed PPO shows that the photolysis products are the same as the pyrolysis products (see inset to fig.8.7). Photolysis over 2000 h has led to the decomposition of nearly all the original polymer (compare with fig.8.2, ESI spectra of untreated PPO). Although the photolysis of PPO (2000 h) has resulted in a seemingly more extensively degraded polymer sample as compared to the pyrolysed samples (92 h/155^{0}C), longer pyrolysis times will presumably produce equally degraded samples. All of the peaks in the spectrum of photolysed PPO can be assigned to the decomposition products shown in section 8.3.1. The assignment of these peaks is facilitated as multiply charged ions are not observed. This is thought to be due to the shorter chain length of the photolysed polymer.

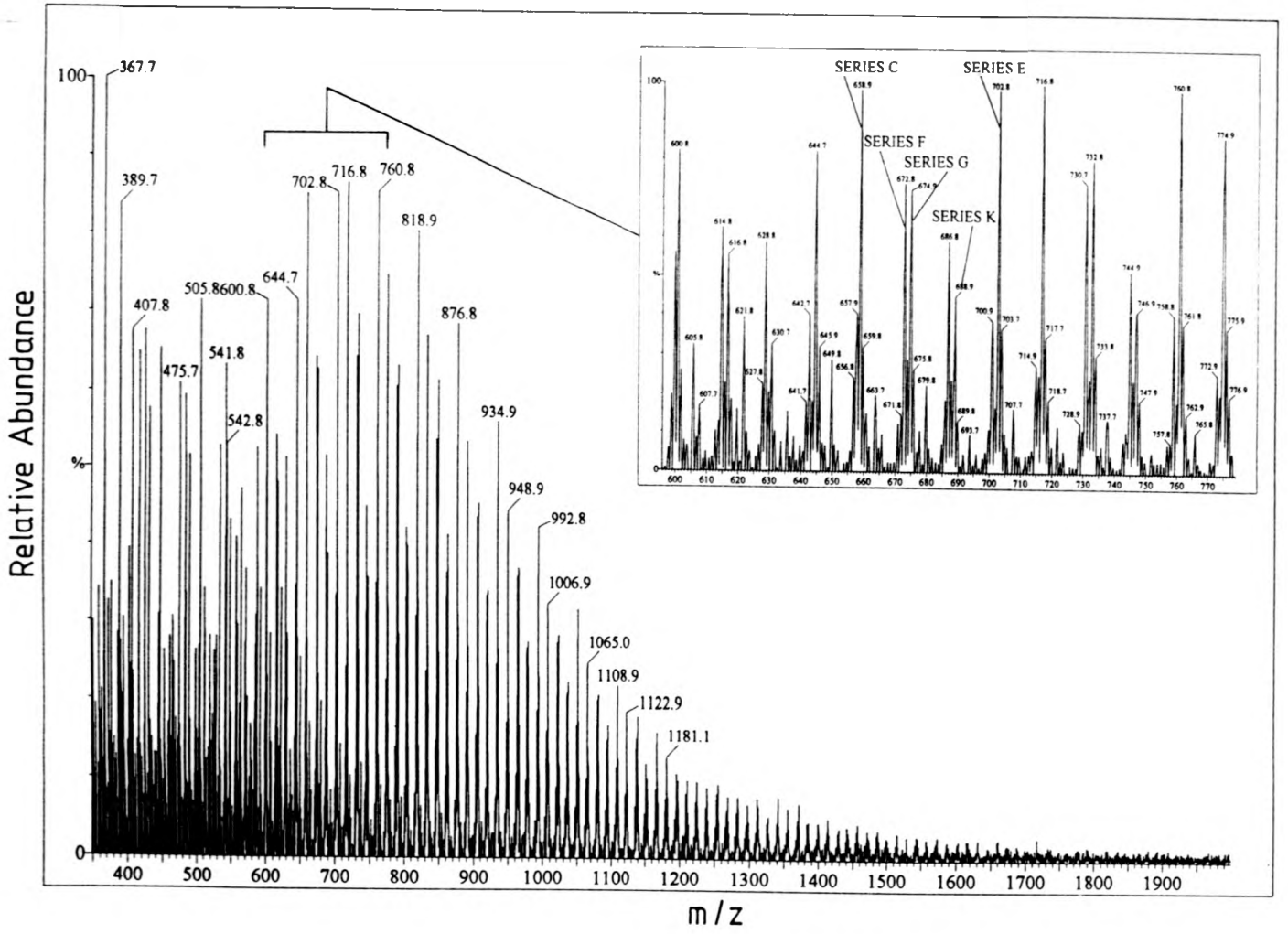
Relative Abundance
100
%
0
367.7
389.7
407.8
475.7
505.8
541.8
542.8
600.8
644.7
702.8
716.8
760.8
818.9
876.8
934.9
948.9
992.8
1006.9
1065.0
1108.9
1122.9
1181.1
400
500
600
700
800
900
1000
1100
1200
1300
1400
1500
1600
1700
1800
1900
m / z
SERIES C
SERIES E
SERIES F
SERIES G
SERIES K
600
610
620
630
640
650
660
670
680
690
700
710
720
730
740
750
760
770

FIG.8.7 ESI SPECTRUM OF PHOTOLYSED PPO (2000 h) OBTAINED USING NH_4Cl TO PROMOTE IONISATION

Thus, the ability of the polymer to accept multiple charges decreases as the chain length decreases. Wong *et al.*[15] also document this phenomenon for PEGs with molecular weights up to 17 500 mus.

It is clear from the ESI spectra of photolysed PPO that series K, previously assigned to the species with a mass of 32+58n mus, incorporates two separate species appearing at 30+58n and 32+58n. Similarly, additional species are apparent with masses 2 mus greater or less than those for the species attributed to series C, E, F and G. Clearly however extensive photolysis of PPO will result in a very complex mixture of degradation products as the species due to series C, E/E', F G and K will undergo further oxidation making the assignment of individual species very difficult. CID experiments were carried out to determine the structure of individual species but these were unsuccessful as the accuracy of the CID technique is limited. Thus the selection (for CID) of a single ionic species with mass X is impossible if significant concentrations of species with a mass of $X \pm 2$ mus are present as for the photolysis products of PPO. Analysis of individual ions by CID is further complicated by the presence of ions with nearly identical masses such as E and E' for which accurate mass measurements of up to 4 d.p. are required for their differentiation.

Thus, the ability of the polymer to accept multiple charges decreases as the chain length decreases. Wong *et al.*[15] also document this phenomenon for PEGs with molecular weights up to 17 500 mus.

It is clear from the ESI spectra of photolysed PPO that series K, previously assigned to the species with a mass of 32+58n mus, incorporates two separate species appearing at 30+58n and 32+58n. Similarly, additional species are apparent with masses 2 mus greater or less than those for the species attributed to series C, E, F and G. Clearly however extensive photolysis of PPO will result in a very complex mixture of degradation products as the species due to series C, E/E', F G and K will undergo further oxidation making the assignment of individual species very difficult. CID experiments were carried out to determine the structure of individual species but these were unsuccessful as the accuracy of the CID technique is limited. Thus the selection (for CID) of a single ionic species with mass X is impossible if significant concentrations of species with a mass of $X \pm 2$ mus are present as for the photolysis products of PPO. Analysis of individual ions by CID is further complicated by the presence of ions with nearly identical masses such as E and E' for which accurate mass measurements of up to 4 d.p. are required for their differentiation.

CHAPTER 8 **REFERENCES**

1 Nohmi, T., Fenn, J.B., *J. Am. Chem.Soc.* 1992, **114**, 3241.

2 Bahr, U., Andreas, D., Karas, M., Hillenkamp, F., Giessmann, U., *Anal. Chem.* 1992, **64**, 2866.

3 Griffiths, P.J., Hughes, J.H., Park, G.S., *Eur. Polym. J.* 1993, **29**, 437.

4 Compana, J.E., Sheng, L.-S., Shew, S.L. Winger, B.E., *Trends Anal. Chem.* 1994, **13**, 239.

5 Loo, J.A., Udseth, H.R., Smith, R.D., *Rapid Commun. Mass Spectrom.* 1988, **2**, 207.

6 McEwen, C.N., Larsen, B.S., Simonsick, W.J., *Abstracts 42nd ASMS Conference on Mass Spectrometry*, Chicago, 1994, 317.

7 Selby, T.L., Wesdemiotis, C., Lattimer, R.P., *J. Am. Soc. Mass Spectrom.* 1994, **5**, 1081.

8 Lemaire, J., Gauvin, P., *Makromol. Chem.* 1987, **188**, 1815.

9 Costa, L., Gad, A.M., Camino, G., Cameron, G.G., Qureshi, M.Y., *J. Am. Chem.Soc.* 1992, **25**, 5512.

10 Yang, C.Q., Martin, L.K., *J. Appl. Polym. Sci.* 1994, **51**, 389.

11 Lacoste, J., Vaillant, D., Carlsson, D.J., *J. Polym. Sci.: Part A: Polym. Chem.* 1993, **31**, 715.

12 Creel, H.S., *TRIP*. 1993, **1**, 1993.

13 Karas, M., *Analusis*, 1992, **20**, 31s.

14 Corless, S., Tetler, L.W., Parr, V., Wood, D., *Abstracts 42nd ASMS Conference on Mass Spectrometry, Chicago*, 1994.

15 Wong, S.F., Meng, C.K., Fenn, J.B., *J. Phys. Chem.* 1988, **92**, 546.

CHAPTER 9 CONCLUSIONS AND FUTURE WORK

9.1 UNTREATED PNMMO

ESI mass spectra of untreated PNMMO show that it contains a series of low-mass cyclic and linear oligomers incorporating up to 22 monomer units. Oligomers of higher mass appear not to be detectable by ESI mass spectrometry and this is attributed to their lack of solubility in the THF/MeOH and DMF/THF solvent systems. The relative abundances of the cyclic oligomer ions in the spectra are affected by various factors such as the cv and to some extent the solvent system used but the governing influence is the size of the alkali metal cation used to promote ionisation. The influence of the cation size was confirmed by molecular modelling calculations for the Na^+ adducts of the cyclic tetramer and pentamer.

The cyclic and linear oligomers were separated from each other using column chromatography and the cyclic species were individually characterised by ESI, SEC and ^{13}C NMR spectroscopy. ^{13}C NMR spectroscopy can be used to distinguish between the cyclic tetramer and the higher cyclic homologues due to the relatively high symmetry of the cyclic tetramer ring. A combination of SEC, ESI and NMR measurements of the eluted fractions showed that the relative concentration of the cyclic tetramer in untreated PNMMO is approximately twenty times that of any of the other cyclic homologues. The relative concentrations of the various cyclic species present in each fraction were determined by NMR and SEC measurements and a direct comparison was made with the relative ion abundances of the cyclic adducts in the ESI spectrum. This comparison showed that the relative ion abundances differed substantially from the relative concentrations of cyclic species present as determined by SEC and NMR and thus confirmed that the cyclic adducts

differed in their relative stabilities depending on the size of the cyclic ring and the cation used to promote ionisation.

The masses of individual low-mass linear oligomers show that they contain the expected hydroxy and ethoxy end-groups and in addition they also contain the $O(CH_2)_4OH$ end-group. Various combinations of these three end-groups are present in the low-mass linear oligomers. Furthermore a single series of linear oligomers was also identified in PNMMO for which the end-group could not be identified. CID experiments failed to yield any relevant structural information concerning this unidentified end-group.

CID experiments performed on the cyclic tetramer showed that it fragmented initially via either loss of HNO_2 and CHO• to eliminate a single nitrate ester side chain or via elimination of a fragment with a mass equal to that of the PNMMO monomer unit. Subsequent fragmentations involved similar pathways to yield a complex series of daughter ions.

Extensive research was performed to find the appropriate conditions for the analysis of PNMMO by MALDI mass spectrometry. Many different matrices and salts were tested and although ion peaks were occasionally detected, the spectra obtained were unreproducible.

9.2 THE PYROLYSIS OF PNMMO

PNMMO was pyrolysed at temperatures in excess of 90^0C and subject to a wide variety of physical techniques. PNMMO darkens in colour and becomes gradually more viscous with increasing pyrolysis times. SEC chromatograms show that both chain scission and cross-linking reactions occur during the pyrolysis of PNMMO. Thermal degradation results in the gradual increase in intensity of two main new absorptions around 1729 and

1550 cm^{-1} in the solution IR spectrum of PNMMO. The band at 1729 cm^{-1} is attributed to the carbonyl group in a formate ester and the formate proton and carbonyl carbon associated with this compound are clearly visible in the ^{1}H and ^{13}C NMR spectrum at 8.1 and 162 ppm respectively and can be cross-correlated by 2-D NMR. The formation of a formate ester species is consistent with the oxidation of the main chain methylenes to form a secondary alkoxy radical which undergoes C-C bond scission adjacent to the alkoxy radical;

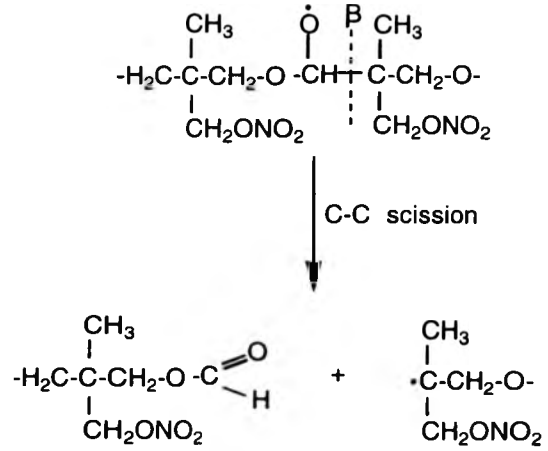

This oxidation mechanism is found to bear many similarities with those of other polyethers such as PEO and PPO which similarly form secondary alkoxy radicals and undergo C-C bond scission. Tertiary alcohols formed during the pyrolysis of PNMMO are proposed to originate from the oxidation of the tertiary carbon-centred radical shown above.

400 MHz ^{1}H and ^{13}C NMR spectra of pyrolysed PNMMO show very low intensity resonances around 9.5 and 205 ppm respectively, indicating that relatively small amounts of aldehyde species are also produced during pyrolysis. Aldehyde species may result from the

oxidation of the main chain or side chain methylenes and it is not clear which of these mechanistic routes leads to aldehyde formation. If the oxidation site is the main chain methylenes then the secondary alkoxy radical shown in the scheme above does undergo some C-O bond scission adjacent to the alkoxy radical to generate an aldehyde but to a much lesser extent than C-C bond scission. Alternatively if the oxidation site is the side chain methylenes then the loss of NO_2 and subsequent abstraction of a hydrogen atom from the resulting alkoxy radical by NO_2, via a cage mechanism, generates an aldehyde.

The new absorption at 1550 cm^{-1} in the IR spectrum of pyrolysed PNMMO is attributed to the asymmetric stretch of a nitro group attached to a tertiary carbon. The symmetric stretch, which can only be observed in IR difference spectra, is weak due to various factors such as the splitting of this absorption by the methyl group β to the nitro moiety. We propose that this nitro species is formed by the recombination of NO_2 following the loss of NO_2 and subsequent elimination of CH_2O from the PNMMO side chains;

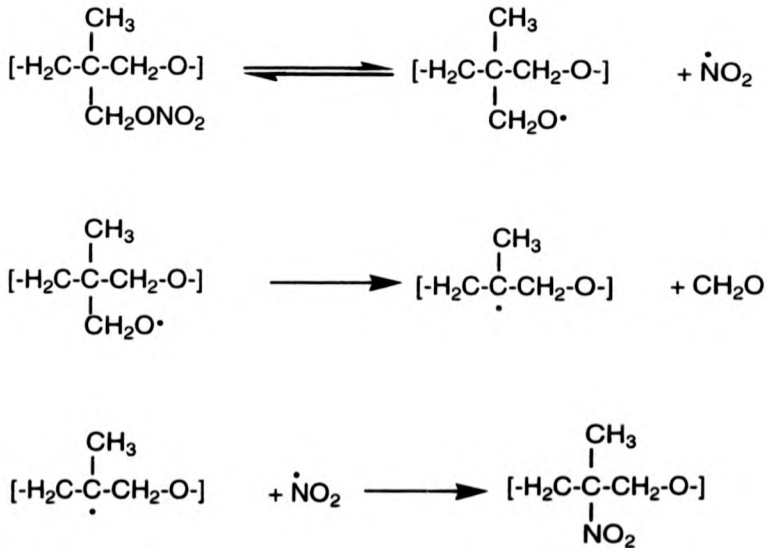

Numerous chromatographic separations of pyrolysed PNMMO eventually yielded a single fraction of the nitro species of sufficient purity and quantity for analysis. The assignment of this tertiary nitroalkane was then confirmed by ESI mass spectrometry and spectroscopic characterisation of this fraction. ^{13}C NMR measurements confirmed that this nitro species was attributable to a compound formed by the decomposition of the cyclic tetramer where one of the four nitrate ester side chains had decomposed, as shown in the scheme above, to generate a nitro group attached to a tertiary carbon. CID experiments showed that the nitro species eliminated HNO_2 which is consistent with a tertiary nitroalkane.

Our degradation mechanism for the formation of the tertiary nitroalkane in PNMMO bears many similarities with the findings of Hiskey *et al.*[1] who proposes that neopentanol nitrate thermally degrades via a similar mechanism to yield the tertiary nitroalkane, 2-methyl-2-nitropropane.

Our degradation mechanism for the formation of the nitroalkane in PNMMO was substantiated by the presence of significant amounts of $CH_2O(g)$ in the pyrolysis gases of PNMMO and the detection of a gradually increasing concentration of a nitroxide radical during pyrolysis of PNMMO. We propose that the nitroxide radical is generated by the reaction of the newly formed tertiary nitroalkane with alkyl polymer radicals.

Although the gradual increase in intensity of an absorption around 1550 cm^{-1} was generally observed in the IR spectrum of pyrolysed PNMMO during pyrolysis, the position of this new band was found to vary depending on the experimental conditions. Thus an absorption was observed around 1572 cm^{-1} during the pyrolysis of thin films of PNMMO and this band eventually merged with the band around 1550 cm^{-1} to give a net absorption at 1550 cm^{-1}. Photolysis produced an absorption around 1562 cm^{-1} and the position of this

band was also found to vary according to the photolysis conditions. Thus it appears that more than one nitro species is produced and indeed, absorptions around 1550 cm^{-1} in the IR spectrum could also be associated with nitroso species. Nitrogen monoxide (NO) could be formed by the reduction of $NO_2(g)$ by $CH_2O(g)$, both of which are formed in significant quantities during the pyrolysis of PNMMO, or NO may result from the decomposition of the tertiary nitroalkane. Nitroso species can then be produced by the recombination of NO with carbon-centred radicals in PNMMO. However, both primary and secondary nitroso species are generally very unstable and undergo dimerisation. Tertiary nitroso species are somewhat more stable than primary or secondary nitroso species but they are generally either blue in colour or if they are sterically hindered they undergo dimerisation[2]. Thus it appears that the formation of nitroso species during the pyrolysis of PNMMO is less likely than the formation of both primary and secondary nitro species. Consequently the latter nitro species may account for the appearance of more than one absorption due to the asymmetric stretch of the nitro group around 1550 - 1575 cm^{-1} in the IR spectrum and often more than one resonance around 90 ppm in the ^{13}C NMR spectrum due to the carbon atom directly attached to the nitro group.

9.3 SECONDARY REACTIONS OF PNMMO

PNMMO was found to react with $NO_2(g)$ at 60^0C to generate a complex mixture of degradation products. These were found to consist predominantly of nitro species, esters and aldehydes but relatively small quantities of formate ester were also detected.

1,2,3,4-tetrahydronaphthalene (THN) and 1,4-benzenedimethanol, well-known for their hydrogen donating ability, were found to induce ca. 45 % reductions in the formation of nitroalkanes and ca. 25 % reductions in carbonyl formation when present in 3 % by mass

concentrations. However when present in a similar mass concentration, 2-nitrodiphenylamine consistently induced the greatest reductions in both nitro (50 %) and carbonyl (30 %) formation.

9.4 THE PYROLYSIS AND PHOTOLYSIS OF PPO

Both ESI and MALDI spectra were obtained for untreated and degraded PPO. Well resolved ESI spectra were obtained using a 50 : 50 mixture of THF and MeOH as a solvent and NH_4Cl to promote ionisation. ESI spectra of untreated and degraded PNMMO showed that a relatively small amount of *in situ* degradation did occur but that this could be kept to a minimum by using a low cv (< 30). MALDI spectra of untreated and degraded PNMMO showed that *in situ* degradation only occurred using high laser power and as for ESI this degradation was kept to a minimum by using appropriate experimental conditions such as low laser power. Various new series of peaks were observed in the ESI and MALDI mass spectra of degraded PPO and these were assigned to the degradation products of PPO on the basis of oxidative schemes proposed by us. The photo- and thermo- oxidative degradation of PPO were found to proceed predominantly via the secondary hydroperoxide although some contribution from the tertiary hydroperoxide was also proposed to occur.

9.5 FUTURE WORK

We have clearly established that both MALDI and ESI mass spectrometry provide important results concerning the degradation products and pathways of PPO. We propose that these experiments can be extended to the analysis of other polyether polymers such as PEO which will dissolve in similar solvents and can be analysed using similar experimental conditions as for PPO.

The usefulness of CID was clearly demonstrated for the analysis of the fractions obtained from the column chromatography of pyrolysed PNMMO. Further experiments involving the chromatographic separation of pyrolysed PPO and the ESI/CID analysis of the fractions may provide valuable structural information concerning the degradation products of PPO, some of which are indistinguishable by mass spectrometry owing to their similar masses.

Clearly an ideal solvent/salt system was not found for the analysis of PNMMO by ESI. Further research would involve the testing of many other solvent/salt systems in an attempt to promote ion formation from higher mass polymer molecules. The analysis of the thermal degradation products of PNMMO could then be attempted as for PPO. Further research is also required to find the appropriate conditions for the analysis of PNMMO by MALDI.

^{14}N NMR analysis of pyrolysed PNMMO produced inconclusive results. The resonances observed were either too weak or too broad to provide valuable structural information concerning the pyrolysate. Similar problems have been encountered by many other authors who demonstrate that ^{15}N is often a far superior nucleus for the structural analysis of many compounds. Consequently, further experiments would involve ^{15}N labelling of untreated PNMMO in an attempt to characterise the nitrogen-containing species formed during the degradation of PNMMO.

CHAPTER 9 REFERENCES

1 Hiskey, M.A., Brower, K.R., Oxley, J.C., *J. Phys. Chem.* 1991, **95**, 3955.

2 Sidgwick, N.V., The Organic Chemistry of Nitrogen, 2nd ed., Taylor, T.W.J., Baker W., 1949.

APPENDIX: PUBLISHED WORK

PUBLISHED PAPERS NOT FILMED FOR COPYRIGHT REASONS

End of Book

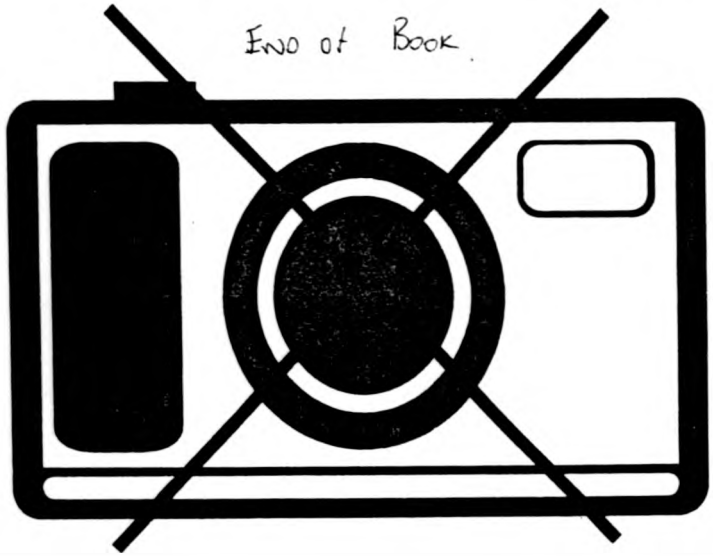

DX
199313